Author: Čubrović, Mihailo
Title: Holography, Fermi surfaces and criticality
Issue Date: 2013-02-27

Holography, Fermi surfaces and Criticality

Proefschrift

ter verkrijging van
de graad van Doctor aan de Universiteit Leiden,
op gezag van Rector Magnificus
Prof. mr. C. J. J. M. Stolker,
volgens besluit van het College voor Promoties
te verdedigen op woensdag 27 februari 2013
te klokke 13.45 uur

door

Mihailo Čubrović

geboren te Belgrado, Servie in 1985

Promotiecommissie

Promotor:	prof. dr. J. Zaanen (Universiteit Leiden)
Co-promotor:	dr. K. Schalm (Universiteit Leiden)
Overige leden:	prof. dr. E. R. Eliel (Universiteit Leiden)
	prof. dr. H. Liu (Massachusetts Institute of Technology)
	prof. dr. E. Verlinde (Universiteit van Amsterdam)
	prof. dr. C. W. J. Beenakker (Universiteit Leiden)
	prof. dr. J. M. van Ruitenbeek (Universiteit Leiden)

Casimir PhD Series, Delft-Leiden, 2013-01
ISBN 978-90-8593-099-0

This work is part of the research programme of the Foundation for Fundamental Research on Matter (FOM), which is part of the Netherlands Organization for Scientific Research (NWO).

Dit werk maakt deel uit van het onderzoekprogramma van de Stichting voor Fundamenteel Onderzoek der Materie (FOM), die deel uit maakt van de Nederlandse Organisatie voor Wetenschappelijk Onderzoek (NWO).

Contents

Chapter 1

Introduction

1.1 Holographic principle: the idea

Reductionism lies at the heart of physics. Much of the history of physics can be understood as striving for reduction in the number of basic principles and thus explaining seemingly disparate phenomena starting from the same core idea. Indeed some of the key scientific revolutions can be formulated in terms of unifying previously distinct areas of study: Newtonian mechanics bridges the gap between statics and dynamics, Maxwell electrodynamics connects electricity and magnetism, Boltzmann's kinetics unites mechanics and statistical physics. General relativity has unified gravity with mechanics while quantum field theory brought a unified look at quantum mechanics, electrodynamics and statistical physics. Finally, in the last decades we are witnessing the attempts at unifying all of physics within string theory. Looking for analogies between different systems has certainly proven to be one of the deepest principles in the search for fundamental laws of nature.

The presumed approach of the Theory of Everything through the advent of string theory (if it indeed turns out to lead to the Theory of Everything) in parallel with the standing fundamental problems of many-body and collective physics – such as unconventional superconductivity and quark confinement – has actualized the problem of emergence versus reductionism. We are facing the question of how the reduction to the few fundamental principles might help us with resolving the problems which obviously come from a complicated interplay of an enormous number of degrees of freedom. One could even wonder if extremely complex systems are within the reach of microscopic models at all – after all, we know that hydrodynamics is not within the reach of the single-molecule description. Such a question, in its full generality, is hard to address, and the answer almost certainly varies – systems which do not at all have a single dominant energy scale might well be out of reach. On the other hand, successful explanations of collective phenomena such as Mott insulators, or the energy cascade in turbulence do give a hint that reduction to the basic principles can be fruitful even if these principles live on the scales which are many orders of magnitude smaller.

All of the above prompts us to rethink the quest for reduction and analogies as formulated in the first paragraph. We might look for direct analogies between fundamental and emergent phenomena. If Maxwell's equations connect the two elementary constituents of electromagnetic interaction, are we able to find a theory which connects a fundamental interaction to an emergent phenomenon? Putting it bluntly, is there an analogy between the simple and the complicated? This thesis is an attempt to contribute to the answer in a specific setting – strongly correlated fermions – where the "complex" side of the duality is likely unreachable by "ordinary means"[1] and the fundamental side is a string theory through a mapping known as holography.

Holography is an idea aimed at providing a unified description of quantum mechanics and gravity. It was coined from a disparity between the thermodynamically calculated black hole entropy and the naive guess from dimensional analysis. Understood as information content of a physical system, entropy is expected to be an extensive quantity, proportional to the volume (measure) of the system. Nevertheless, the famous semiclassical Hawking-Bekenstein result for the entropy of a neutral non-rotating (Schwarzschild) black hole [9] predicts it as proportional to the surface

[1] It is known [109] that the problem of interacting fermions is NP complete. At this place we briefly remind what this means. A problem is said to belong to the NP class if an algorithm exists which *checks* a proposed solution in polynomial time, but no algorithm is known which *finds* a solution in polynomial time. An example could be an equation such that plugging in a given candidate solution and checking if it satisfies the equation can be done in polynomial time, but no polynomial algorithm is known to compute the solution starting from the equation only. Notice that we do not know if such an algorithm really does not exist, or we are simply unable to find it yet (this question is the famous unsolved $P = NP$ problem). NP complete problems are a subclass of NP problems, such that an algorithm that solves an NP problem polynomially could be modified in a certain way to solve *all* NP problems in polynomial time.

area:

$$S = \frac{Ac^3}{4G\hbar} \tag{1.1}$$

Informally, all information about the black hole is stored on a lower-dimensional object, suggesting that a complete description of the black hole in D dimensions can be obtained by looking at the correctly chosen degrees of freedom on a $D-1$-dimensional manifold. This is the logic behind the arguments by 't Hooft [122] and Susskind [107]. The foundation of this principle is that it connects the concept of gravity to the quantum-mechanical concept of entropy as counting the states of the system.

The second, more technical key concept in holography is the idea of dualities, mathematically equivalent but different descriptions of the same phenomena – thus providing a bridge between different formalisms or even altogether different physical systems. The idea of duality can be given a very precise and familiar meaning. Formally, it is just a canonical transformation of the action. Well-known examples are the vortex duality for charged scalar fields and electric-magnetic duality in $U(1)$ gauge theory [71]. In the vortex case, the physical picture is that of changing the viewpoint of what is an elementary excitation. If it is the linearly dispersing plane wave, then the vortices then appear as defects where the phase of the charged field winds for a full circle. But if we dualize, then vortices are the elementary excitations and plane waves are complex vortex combinations. The duality can be captured by a Legendre transformation of the action:

$$S = \int d^3x \partial_\mu \Phi \partial^\mu \Phi \mapsto S_{dual} = \int d^3x \left(a_\mu a^\mu - \partial_\mu \Phi a^\mu \right). \tag{1.2}$$

Here, Φ is the charged scalar field which lives in two space dimensions, while its gradient $\partial^\mu \Phi$ maps to the vortex field a^μ. We can thus reexpress the action in terms of a^μ: the physics must remain the same but that does not change the fact that some phenomena are much easier to see in one or in the other language. Similar is the wisdom behind the electric-magnetic duality, where the physical observables, i.e. elements of the field strength tensor, transform into each other, again by adding a bilinear term (linear in both old and new components) to the action.

As an idea which connects quantum theories with gravity, holography finds its natural language in the formalism of string theory, where it arises as a duality transformation of the strings themselves. It is within string theory and M theory that a precise realization of the abstract holographic principle was found. One reason is simply that it offers a coherent framework in which we can study the gravity at various energy scales– from the low-energy description of general relativity to the nonperturbative regime where the string effects dominate.

In string theory language, the duality becomes the equivalence of the open and closed string descriptions. The higher-dimensional, gravitational system is given by the excitations of the closed string. Its lower-dimensional dual gauge field description is given by the excitations on the open strings. In the next section we will present a more detailed explanation of this construction, known as the *AdS/CFT correspondence* [81, 38, 114]. However, in this introductory chapter we will not assume any prior knowledge of string theory on the side of the reader. We will stay away from extensive use of string-theoretical language and results and formulate AdS/CFT in terms of gauge theory and general relativity, with only qualitative discussion of the underlying specifically stringy constructions (branes, open strings between branes, string dualities, etc).

1.2 Realization: AdS/CFT correspondence

We do not intend to give anything like a comprehensive tutorial on AdS/CFT in this (or any subsequent) chapter, we will merely wet the reader's appetite to look for the original references if interested; most of the thesis can be followed without a detailed understanding of the foundations of AdS/CFT. The first explicit realization is due to Maldacena [81]. Here we have a Type IIB superstring theory in a configuration describing a stack of parallel D3 branes (planar objects extending along three spacetime dimensions) at some distance r from each other. The interbrane distance r also determines the "elastic energy" of the open strings which stretch between the branes and carry the gauge fields from a $U(N)$ multiplet: the energy is proportional to r/α', where α' is the string tension. Consider now the limit of coincident branes, when $r \to 0$ but with $r/\alpha' = \text{const.}$. In the closed string description, the metric of a stack of coincident D3 branes factors out into the product of AdS space and a sphere: $\mathrm{AdS}_5 \otimes S_5$. The open string description is a very special, highly symmetric QFT – a conformal field theory (CFT). The idea is that the more restricted and special the field theory, the easier it is to relate it to gravity. This certainly does hold for a conformal field theory (CFT), where the very high symmetry severely constraints behavior of correlation functions. CFT has a central place in modern high and low energy physics – allowing exact calculation of correlation functions in two dimensions and strong results on RG flow (c-theorem [120]) and scaling [24]. In low energy physics they describe the quantum critical systems [15] lying at the heart of the description of phase transitions and strongly competing interactions. The $\mathcal{N} = 4$ supersymmetric Yang-Mills in four spacetime dimensions is such a CFT – despite the many fields involved, its behavior is simple due to conformality, and it has given us the first example of a holographic duality.

This explicit example allows for a quantitative connection between the gauge theory and the supersymmetric theory in AdS geometry. The connection is provided by the fact that the radius of AdS space is proportional to $(gN)^{1/4}$. The supergravity solution can be trusted if $gN \gg 1$ and $N \gg 1$. Remember that this means that the field theory is strongly coupled *and* can be expanded in the inverse number of colors. The lower-dimensional, field theory side in this and similar (early) setups of AdS/CFT are generically non-Abelian gauge theories, either Yang-Mills or its supersymmetric version, motivating another frequently used name for AdS/CFT: *gauge/gravity duality*.

To turn the above discussion into a precise duality, one needs a relation between the partition functions (on-shell actions) of the gauge theory and supergravity. To this end it is critical to determine the boundary conditions for the supergravity fields living in AdS – when they reach the branes, they are coupled to the fields living on them. This was done in the follow-up work by Gubser, Klebanov and Polyakov [38] as well as Witten [114].

1.2.1 Warmup: symmetries

Let us study the closed string (gravity) side first. The formulation of a field theory on AdS spaces is not quite trivial: AdS geometry possesses some troublesome properties such as closed timelike curves and the existence of a boundary at infinity. Informally, anti de Sitter (AdS) space is an open (hyperbolic) equivalent of the perhaps more familiar de Sitter (dS) space. The latter is the solution to the Einstein equations in the vacuum with a positive cosmological constant [2]. The latter can be thought of as a mysterious form of matter with equation of state $p = -\rho$. It has negative pressure: it expands as it cools down, just like our universe. It is thus a cosmological model in the approximation of "empty Universe" where the presence of matter is negligible and the geometry is dictated by the cosmological constant. In AdS space, on the other hand, the cosmological constant is negative, i.e. it behaves as (positive) pressure of regular matter. Because the matter is cosmological, it cannot clump and one finds a static (time-independent) solution. The Einstein-Hilbert action that describes the anti de Sitter space in $D+1$ spacetime dimensions is:[2]

$$S = \int d^{D+1}x(R - \Lambda) \tag{1.3}$$

where R is the scalar curvature while $\Lambda < 0$. As the only dimensionful factor, Λ can be rescaled at will depending on the choice of the unit of length. By convention, we write $\Lambda = -D(D-1)/L^2$ where L has the meaning of AdS radius. This means that the solution can be embedded into a $D+2$-dimensional flat space as a sphere:

$$t^2 - z^2 - y_i y^i = L^2. \tag{1.4}$$

A natural coordinate patch covers half of the space:

$$ds^2 = \frac{r^2}{L^2}(-dt^2 + dx_i dx^i) + \frac{L^2 dr^2}{r^2}. \tag{1.5}$$

The radial coordinate r stretches from 0, called the interior, to infinity, called the AdS boundary. AdS is the maximally symmetric solution to Einstein equations. An extremely useful way to think about AdS_{D+1} is s a hyperboloid embedded in a $D+2$-dimensional flat spacetime with signature $(+,\ldots+,-,-)$. The embedding in a spacetime with $D+2$ dimensions helps to see that the total geometric symmetry group of AdS space is $SO(D,2)$. The global and local geometry of AdS space are sketched in Fig. 1.1: what globally looks as the usual double hyperboloid (but in Minkowskian as opposed to Euclidean spacetime) locally becomes a patch of isotropic space of "decreasing size" as we move further and further, until at infinity all lengths scale to zero.

One can now motivate the correspondence starting from the symmetry arguments. It is well known that a CFT in D dimensions (one timelike and $D-1$ spacelike dimension) also obeys the $SO(D,2)$ symmetry [24]. Informally, the conformal symmetry is just the symmetry associated to

[2] In this thesis, unless specified otherwise the dimensionality of spacetime is always $D+1$, the flat space coordinates in D dimensions are denoted by (t, y_i) $(i = 1\ldots D)$ and the metric signature follows the convention $ds^2 = -dt^2 + dy_i dy^i$.

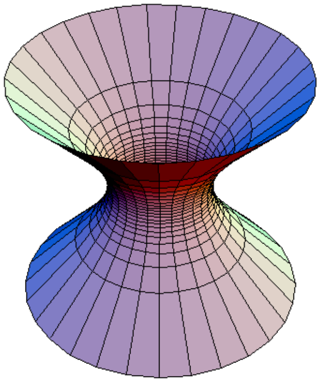

Figure 1.1: Sketch of AdS geometry. Globally it looks like a double hyperboloid but if we take a small patch it becomes very much like Minkowski space in which distances decrease as we move toward infinity. Counterintuitively, local AdS is completely isotropic and has spherical symmetry.

length rescaling, i.e. changing the scale combined with rotations. Conformal field theories are thus closely related to the concepts of self-similarity, fractality and scale-free objects but more general: the scale invariance is continuous, not discrete as in fractals, and it can be broken due to quantum effects – anomalies, like any other physical symmetry. A closer inspection reveals that the exact conformal representation of $SO(D, 2)$ is already geometrically encoded in AdS in a special limit – its boundary transforms in the same way. If one would "extend" the AdS space by "gluing" some fields on its D-dimensional boundary, these fields ought to be redefinable as representations of the conformal group.

As a result, the CFT can be understood as the boundary degrees of freedom of a field theory in AdS. Emphatically, however, this is *not* enough for a duality, and does not yet encapsulate the idea of AdS/CFT. We need more – not just that AdS space in the near-boundary limit becomes conformal invariant but that *the fields* in AdS in the near-boundary limit also encapsulate the behavior of a conformal field.

1.2.2 Enlightenment: the duality relation

This idea finds its precise formulation in the concept of duality introduced earlier. The quantum theory is dual to gravity, thus *the operators in field* *theory are sourced by the fields on the gravity side.* More precisely, the generating functional for the correlation functions in field theory is identified with the minimum of the supergravity action, satisfying specific boundary conditions at the AdS boundary. The precise boundary conditions and the crucial point of AdS/CFT, known as the GKPW (Gubser-Klebanov-Polyakov-Witten) prescription. The prescription addresses the boundary conditions mentioned at the beginning of this section and was proposed in [38, 114]. The conformal and the gravity side are connected through their partition functions as

$$Z_{bnd}(J) = Z_{bulk}(\Phi|_{\partial \mathrm{AdS}} = J) \tag{1.6}$$

where Z_{bnd} and Z_{bulk} are the partition functions on each side, and we have employed Φ as a generic notation for all fields living in the bulk and J are their boundary values, acting as sources. In the classical gravity limit, i.e. for a large N strongly coupled field theory, Z_{bulk} is evaluated simply by plugging in the classical solutions to the equations of motion into the gravity-matter action (in other words, it is the on-shell action). Schematically, this looks like

$$Z_{bulk} = e^{-S(\Phi)}|_{\Phi(r\to\infty)=J} = \langle e^{\phi J}\rangle_{\mathrm{CFT}} \tag{1.7}$$

where S is the classical gravity action, and in the second equality we have expressed the partition function at the boundary as the generating function of the field theory correlators. The boundary operator ϕ sees the boundary values $\Phi(r \to \infty) = J$ precisely as sources: treating Z_{bulk} in (1.7) as an effective action for ϕ, we can apply the textbook rule to calculate their correlation functions:

$$\langle \phi(y_1)\phi(y_2)\dots\phi(y_n)\rangle = \lim_{r\to\infty} \frac{\partial^n e^{-S}}{\partial\Phi(r,y_1)\partial\Phi(r,y_2)\dots\partial\Phi(r,y_n)}$$

This is the essence of applying holography in practice: we do not know how to write Z_{bnd} in terms of boundary fields explicitly, but we can use it as the generating functional of the correlation functions, and thus gain qualitative insight into the system.

The precise translation of the bulk physics into the boundary is thus achieved by analyzing the $r \to \infty$ limit of various bulk quantities. This is the quantitative basis to constructing the *holographic dictionary* which makes possible numerous practical applications of AdS/CFT. In the next chapter we will introduce dictionary entries such as temperature, chemical

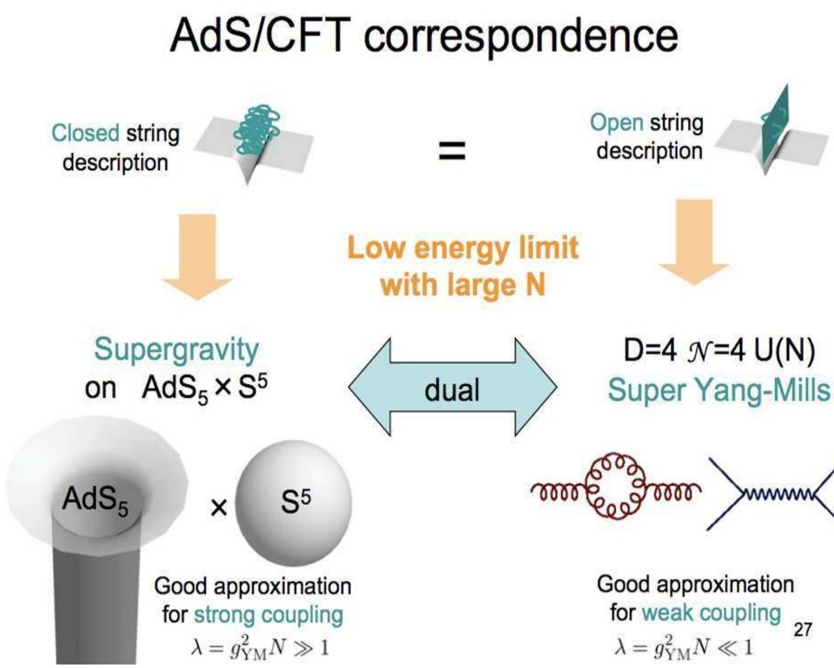

Figure 1.2: Pictorial resume of AdS/CFT: the duality is rooted in the notion of open-closed string duality. On the level of coupling constants it is also a weak-strong duality. Closed string coupling g is related to the coupling g_{YM} of the Yang-Mills theory on open strings as $g^2_{YM} = g$. The small parameter in the perturbative expansion for the closed string interactions is the combination $\lambda \equiv gN$. Sending the closed string coupling to zero ($g \to 0$) at constant λ we get classical strings in $\mathrm{AdS}_5 \otimes \mathbb{S}_5$ while the Yang-Mills theory on open strings reaches the large N limit ($N \to \infty$). Taking also the limit $\lambda \to 0$, the classical type IIB string theory becomes type IIB SUGRA.

potential, electromagnetic field, conformal dimension... It is the main link between the formalism of holography and more familiar low-energy QFT physics.

From a more general viewpoint, AdS/CFT was historically important as a facet of the second superstring revolution, which found numerous dualities between string theories with different coupling constants or geometric properties. Here, the control parameter is the combination $1/gN$ of the string coupling $g = g_{YM}^2$ and the number of colors N. In order to trust the supergravity limit we need $gN \gg 1$, but this is precisely the strongly coupled regime of the gauge theory. Therefore, AdS/CFT is an example of a weak-strong duality. Such dualities are known as S-dualities. Formally, these relate a theory with coupling constant g to a theory with coupling $1/g$. While AdS/CFT does not quite follow this pattern, as the control parameter is not g but gN, it remains a relation between strongly and weakly coupled systems. Needless to say, this gives it a great deal of practical utility: when one side becomes intractable due to string interactions, the other one becomes better and better controlled.

1.2.3 Some general remarks

We will conclude this section with some speculations on broader implications of holography on string theory and other areas. Even though the general holographic principle is essentially a gravity/quantum field theory duality, its full realization in the form of AdS/CFT is a decidedly string-theoretical result, which follows from the near-brane geometry and the action of that solution in a specific brane configuration. In other words, the 't Hooft-Susskind principle states more than AdS/CFT – it states than any physical system with gravity is equivalent to a lower-dimensional system without gravity. One might now wonder if this is indeed so, if holography is in fact a fundamental principle itself, independent of string theory, and a property of gravity and field theory as we know them. There is no answer yet on this central question. At the very least, what one can try is to apply the precise results of AdS/CFT (dictionary entries) to geometries which do not follow from string theory. As long as the geometry looks like AdS at long distances, numerous attempts so far give encouraging results.[3] The non-string AdS spaces give us more freedom: we can work in any number of dimensions, with any field content. The price to

[3] It is much less clear and much more complicated to generalize it to non-AdS spaces, including flat space. This is another important problem to work on. The natural guess is that the correspondence can be generalized to arbitrary geometries and arbitrary field theories. Reasons that require an asymptotically AdS geometry and the difficulties involved in constructing a flat space holography are beyond the scope of this Introduction and indeed this thesis. Roughly speaking, in flat spacetime there seem to be too many degrees of freedom on the gravity side to match to a lower-dimensional QFT; AdS asymptotics puts some rather stringent constraints on the dynamics of gravitational field. The extension beyond AdS is certainly a central fundamental question for the future of holography.

pay is, of course, that we cannot at the present be sure about the consistency of such attempts. This approach is known as *bottom-up* as opposed to the *top-down* string approaches. In this thesis we will mostly use the bottom-up logic, for both practical and conceptual reasons.

In this place it is appropriate to discuss the status of AdS/CFT as a confirmed result versus a conjecture. Though it is widely accepted (e.g. [25]), a rigorous proof is lacking. Nevertheless, the evidence in favor of AdS/CFT is very solid: it has passed numerous non-trivial tests where observables whose forms do not depend on the coupling constant were computed on both sides and compared [2].

1.2.4 Holography outside high-energy theory

The manifestation of holography as a duality has given rise to a completely different research pursuit from the understanding of black holes. Holography can also be used as a tool to understand systems at strong coupling, where the conventional perturbative methods of field theory fail. So far AdS/CFT has established itself as an approach to quantum chromodynamics (QCD) and to condensed matter theory (CMT), the corresponding fields being known as AdS/QCD and AdS/CMT. The power of holography is that it allows us to study previously inaccessible strongly coupled systems. In AdS/QCD, the focus of most work done so far was on describing the confinement transition and studying the quark-gluon plasma at intermediate energies, when neither perturbative QCD nor effective low-energy theories work well (this regime is primarily tested in heavy ion collisions). The latter line of research has produced perhaps the most important result of applied holography so far, the universal viscosity bound, stating that any isotropic equilibrium fluid has an inherent shear viscosity to entropy ratio

$$\frac{\eta}{s} \geq \frac{1}{4\pi} \tag{1.8}$$

The quark-gluon plasma studied in the RHIC accelerator exhibit a viscosity remarkably close to the bound (1.8).

The main approaches exist in AdS/CFT. The first is a top-down approach which constructs a Yang-Mills theory akin to QCD from brane intersections, following closely the early ideas of Witten [114, 115] where the whole endeavor of AdS/CFT is put in the context of specifically gauge/gravity duality, i.e. understanding the dynamics of Yang-Mills fields. The second is a bottom-up scheme where the four-dimensional

QCD is dual an asymptotically AdS_5 space where confinement is modeled by "thinning out" (suppressing exponentially) the amplitudes of fields in the IR. This is done using the insight that the extra dimension in AdS corresponds to the scaling flow in field theory with the near boundary behavior encoding the UV asymptotics. In this case, the RG flow interpretation is that the confinement of low-energy excitations corresponds to suppressing the dynamics in deep interior.

The second claim to fame for AdS/CFT is its application to condensed matter theory. Here, the problems of strong correlations and competing orders show their best (or rather, worst) side. It is thus extremely exciting to see how they dualize in gravity. However, since the phenomenology of condensed matter systems is much richer, and removed even further from the microscopic Hamiltonian, it becomes important to build the model in an appropriate way: to start from the solid and robust features (symmetries, degrees of freedom, extreme limits when some fields decouple or become exactly soluble) rather than engineer the gravity dual in order to get this or another specific phenomenon. The field started with a holographic calculation of transport properties of certain strongly coupled systems [59] and took off with the crucial work of Hartnoll, Horowitz and Herzog on holographic superconductors [47]. Despite the by now universally accepted name, the model in question is not actually a superconductor at all but a boson at finite density which breaks the global phase symmetry by condensing, akin to a superfluid. Nevertheless, precisely as it stands it is a very important proof of concept: this is the simplest possible case of the Landau-Ginzburg picture of order, and thus the obligatory starting point of any candidate theory for description of many-body systems. Holographic superconductors have taken the *bosonic* AdS/CMT to perfection and have been the arena in which many of the universal results and dictionary entries have been obtained.

1.3 The arena: fermions in organized matter

This thesis will focus on AdS/CFT applied to strongly coupled fermion matter. Experimental condensed matter physics has discovered numerous materials which cannot be understood from the weakly coupled perspective. Strongly coupled fermions are thus an experimental reality, and developing general methods to study them is of central importance for understanding the observed phenomena in condensed matter. In AdS/CFT, precisely the strong coupling regime in field theory is easy to understand on the gravity side, as it corresponds to classical (super)gravity. We will now argue that such holographic description of the strongly coupled physics is especially valuable precisely for fermion systems, as conventional field-theoretical methods are far less helpful for fermions then for bosons.

We have a number of nearly equivalent ways to describe the simple observation that fermions and bosons differ in their behavior. Antisymmetry of fermionic wave functions, the Pauli principle, fermion sign problem and kinematic correlations (i.e., Slater determinants) are all about the fact that the antisymmetry of fermionic states reduces the number of available configurations, acting as a constraint on dynamics and introducing an effective interaction (or correlation) even in absence of any explicit interacting potential. While a non-interacting Fermi gas can still be solved by explicitly taking into account the antisymmetry of states when constructing thermodynamical potentials, presence of interactions spoils the picture: antisymmetry acts as a constraint, and solving an interacting system in the presence of such a constraint becomes a hopeless task. A common way to phrase the problem is the "fermion sign" viewpoint, reviewed e.g. in [119]: it refers to the negative contributions to the fermionic partition function, meaning that it cannot be regarded as a sum of probability amplitudes as for bosons and classical particles.[4]

The fermion signs are simply the minus signs in the density matrix of a fermion system. This is a direct consequence of antisymmetry of the fermionic wave function. For a system of free fermions we can write the wave function exactly; the outcome is the Slater determinant where the odd permutations contribute with a minus sign. Antisymmetry, however, does not depend on interactions in the system and the sign picture will be exactly the same. A technical way to see the trouble with fermion signs is analysis of the fermionic path integral. It is enough to remember the basic rule of constructing the partition function for a system of fermions in compact Euclidean time with period β, thus accounting for finite tem-

[4]Besides condensed matter, another area where the sign problem is well-known is Quantum Chromodynamics (QCD). There, the sign problem arises in a seemingly different but in essence equivalent form: the presence of finite density (and thus chemical potential) makes the Euclidean Hamiltonian non-Hermitian, and thus the partition function complex. The negative vs. complex dichotomy is that of real vs. imaginary time, but in both cases it is the fermionicity of the Hamiltonian which gives rise to problems at finite density, and both negative and complex partition function give us the same pain: absence of probabilistic interpretation.

perature $T = 1/\beta$. Remember that partition function equals the integral of the trace of the density operator:

$$Z = \mathrm{Tr} e^{-\beta H} = \int d^{ND}\mathbf{x}\rho(\mathbf{x}, \mathbf{x}; \beta) \tag{1.9}$$

where the density operator is $\rho(\mathbf{x}_1, \mathbf{x_2})$ and $\mathbf{x}$ denotes the set of coordinates of all particles in a D-dimensional system with N fermions. Now for a system of indistinguishable particles ρ is a sum over of all permutations Π of the particles, as any two particles can be exchanged without changing the system physically. This gives

$$\rho(\mathbf{x}, \mathbf{x}; \beta) = \frac{1}{N!} \sum_{\Pi} (\pm 1)^{|\Pi|} \rho(\mathbf{x}, \Pi\mathbf{x}; \beta) \tag{1.10}$$

Here, the sum is over all permutations Π of the particles, and $|\Pi|$ is the parity (symmetry/antisymmetry) of the permutation. For bosons all terms are positive and one can define a measure based on the density matrix ρ_+. For fermions, however, odd permutations carry a negative contribution. The partition function is, of course, always positive, but we see that individual contributions to the density matrix are not. This in turn means that fermions are never classical: unlike for bosons, quantum statistics brings a discontinuity from classical Euclidean field theory and its path integral formulation. The effective action for bosonic expectation values is just the celebrated Ginzburg-Landau theory or one of its many derivations. Nothing like it exists for fermionic operators.[5] Consequently, despite decades of research of strongly correlated fermions, the actual methodologically sound knowledge we have on this topic is very limited. A measure of the difficulty of the sign problem is the realization of Troyer and Wiese [109] that it is NP complete.

What, then, are the things we do know?

1. *Free Fermi gas.* One example is obvious: the free Fermi gas is exactly soluble. It is not really free, as kinematic correlations are introduced by the statistics, however we know that the Slater determinant accounts for them exactly.

[5] While the expectation value of a fermionic operator is trivially zero, we typically want to compute operator products. Density, correlation functions, transport coefficients etc. are all of this form. However, working with fermion operator products is no easier than working with single fermions.

2. *Fermi liquid.* The second example is the breakthrough of Landau in understanding normal metals in terms of Fermi gases [73]: the Fermi liquid paradigm. The logic is well-known: a gas of particles with infinite lifetimes turns into a gas of quasiparticles with finite but long lifetimes. Everything remains the same as for a free gas, except that all parameters undergo renormalization. The crucial requirement is that the ground state of the interacting system have a nonzero overlap with the ground state in the non-interacting limit. In other words, Fermi liquid is so much akin to a Fermi gas simply because it is adiabatically connected to it. Subsequent, more rigorous studies of the Fermi liquid have confirmed this basic picture (see [5] and references therein). The mathematical foundation of Landau's Fermi liquid insight is provided by the RG formalism for fermions given in [88, 100] and has the form of a functional RG which starts from a weakly interacting theory at intermediate scales and introduces interactions perturbatively in the effective action. Being a weak coupling expansion, it does not have sign problems. However the perturbative treatment does make it hard to treat non-perturbative phenomena e.g. a superconducting instability within this approach.

3. *Fermions in* $(1+1)d$. A special case which is in principle completely known is that of fermions in one spatial dimensions. While fashionable these days, and certainly capable of displaying very intricate behavior of correlation functions and transport properties (see e.g. [110]), one-dimensional fermions are completely demystified by bosonization: in one space dimension, any fermion system can be bosonized in infinitely many ways (the most typical situation is the spin-charge separation) and then solved through usual field theory methods. The reason is that statistics cannot really be defined in $1+1$ dimension: the manifold of possible Slater determinant states coincides with the manifold of nodeless wave functions.

4. *Miscellanea.* Finally, there is a small number of exactly soluble interacting fermion models in higher dimension, such as exact wave functions for Fractional Quantum Hall states [74]. These are however of very little significance for the broader sign problem, being rather special non-generic.

The inescapable conclusion is that, if we want to avoid the strange ad hoc models of the point (4), everything we know is either to bosonize or to hope that the system studied is adiabatically connected to a non-interacting Fermi gas, at least in the IR. The vast field of strongly correlated electrons armed with various field-theoretical techniques [34, 110] is as it stands incapable of constructing (through controlled, justifiable approximations) *novel ground states* of fermion matter. The list of celebrated experimental puzzles, from unconventional superconductors [118, 42] to heavy fermions [80], all likely novel ground states qualitatively different from normal Fermi liquids, is therefore in desperate need of a theoretical paradigm that will not depend on non-interacting or bosonic physics.

We are now able to formulate a sharp question underlying all of strongly correlated electron systems: *Is there a stable state of electrons at finite density which cannot be adiabatically continued to Fermi gas?* This is perhaps the closest it comes to formulating the motivation for this thesis in one sentence. A solution we propose here is to use the power of holography.[6]

This is not just an academic question. The importance of strongly correlated electron physics is its manifest necessity to explain a multitude of experimental findings amidst experimental evidence in favor of distinctly non-Fermi liquid phases of fermionic matter. The most famous are certainly high temperature superconductors, cuprates and pnictides being the leading members of this heterogenous group. The superconducting order at relatively high temperatures is almost the least important of the many unusual properties. A glance at the phase diagram of cuprates (Fig. 1.3) reveals how the doping of external charge carriers turns the system from the familiar normal metal, i.e. Fermi liquid phase into a non-Fermi liquid, universally known in condensed matter physics as strange metal, continuing on into the pseudogap. The pseudogap region is also mysterious, but thought to display some kind of long-range order. Dozens of exotic order parameters were proposed to explain this novel ground state: stripes, current loops, exotic spin ordering and others [118]. Many of them

[6] As a side remark, we refer the reader to [119, 72] for a possible geometric interpretation of the "fermionic constraint" which allows one to treat the problem of fermionicity by looking at certain global (topological) properties of the many-particle wave function and the path integral. The key result is the proof [13] that the signful path integral can be turned into ordinary bosonic path integral but with an additional constraint. For us, it is the morale and not the details which is important: it provides a construction which explicitly reduces fermion dynamics to boson dynamics with constraints. While AdS/CFT handles fermions in a somewhat different way, essentially trading the fermionic physics for curved space, it might be an indication that in the end all fermionicity can be bosonized by adding additional constraint structure to dynamics.

have some degree of experimental support [118]. We also do not understand how the advent of the strange metal is related to superconductivity itself.

A possible unifying point for these phenomena in unconventional superconductors and heavy fermions (as well as some other materials) is quantum criticality [95, 15], developed mainly by Sachdev. Its basic idea is that quantum fluctuations can mimic the effects of temperature on the order parameter of some ordered phase. The outcome is that the ordered phase becomes unstable and vanishes at a critical point at zero temperature. In place of temperature, the control parameter is typically some quantity which governs the competition between two ordered phases at $T = 0$, e.g. coupling strength or doping. The phase diagram of a system with a quantum critical point typically looks as in Fig. 1.3(A), quite similar to the phase diagram of real-world cuprates in Fig. 1.3(B) – above the critical point one has a characteristic quantum critical "cone", the regime in which the quantum critical point influences the physics even at relatively high temperatures. This is an important difference with respect to finite temperature critical points: in the latter case, the scale invariance inherent to criticality is only felt in a narrow window around $T = T_c$, while quantum critical behavior can be detected even by measurements significantly above $T = 0$. Systems with a quantum critical point are mainly recognized for exhibiting remarkable scaling laws [111]. Of course, quantum criticality immediately brings associations on CFT and makes a great starting point for a holographic investigation. Notice the inverted epistemology of holography compared to conventional methods: normally, we would start from the Fermi liquid phase and try to build up interactions that drive it to the critical point. In AdS/CFT, we can start from the quantum critical point where the theory is very strongly coupled and completely encapsulated in the scaling relations, with particles being nonexistent, and the challenge is to see how the system picks a ground state away from criticality. This is the essence of AdS/CMT: we know most in AdS/CFT precisely in the situation when we know least in conventional CMT.

This in turn makes CFT an important tool for description of such systems – scale invariance of the quantum critical phase is almost equivalent to conformal invariance. Therefore, if the universal ingredient in transitions from Fermi liquid non-Fermi liquid systems is quantum criticality, then the CFT and its gravity dual in AdS present a natural starting point.

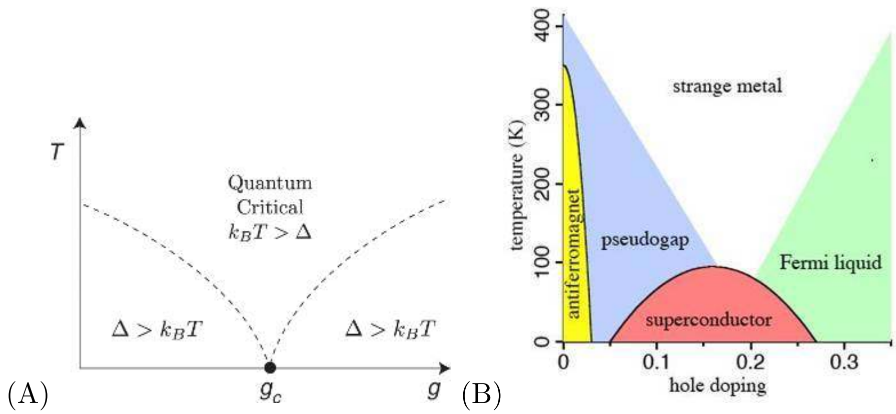

Figure 1.3: (A) Sketch of the phase diagram of cuprates. Normal metal phase turns into a non-Fermi liquid at critical doping, which presumably corresponds to a quantum critical point. The zoo of exotic orderings resides in the strange metal phase, which partially overlaps with the superconducting region. The properties of the strange metal remain mystifying, and might constitute a prime example of a stable non-Fermi liquid ground state. In (B) (adopted from [95]) we see schematically how the quantum critical point influences the physics at finite temperature: when the temperature energy scale k_BT is larger than some characteristic energy scale Δ of the system, we are in the quantum critical ”cone” where the physics is governed by the scaling laws imposed by the quantum critical point.

1.4 Outline

Our first goal will be to find the gravity dual for the Fermi surface which will be as general as possible and not hinge on existence of quasiparticles. The minimal ingredients we need are fermions, temperature and chemical potential. Our holographic dictionary translates this into a charged black hole plus the Dirac equation for the fermions. This is done in the next chapter. A Fermi surface should reveal itself in the spectrum of perturbations. We will study in detail the momentum and energy distributions of the spectral weight and conclude a great deal about the quantum critical fermions in this way. This chapter is adapted from [17] and includes the formalism for calculating the spectrum in a separate section (originally the Supplementary material of the paper). Chapter 4 [18] studies fermionic instabilities, giving dictionary entries for fermion density and Fermi liquid itself, within a model we call black hole with Dirac hair. Chapter 5 [19] is the beginning of the study of the phase diagram of holographic fermions. In this chapter, we compare the Dirac hair model to the electron star model by Hartnoll et al [51] and show how one can interpolate between the two, corresponding to stable quasiparticles with different properties in field theory. In chapter 6 [83] we will study the actual phase diagram of holographic fermions by a full quantum-mechanical formulation of electron star and Dirac hair. and finally address the question – can we see novel phases from AdS/CFT? Chapter 7 sums up the conclusions.

Chapter 2

The holographic dictionary

2.1 The basic entries

We are now ready to consider the theoretical background of our work and to work out in some detail the results we will use. This essentially corresponds to constructing the detailed dictionary entries and formulate rules for the boundary terms in the action. We start with pure AdS space (we will need more later, to introduce temperature). We will work on the Poincaré patch of AdS space rather than global AdS. For most of the calculations it is much more appropriate to use the dimensionless inverse of the r coordinate:

$$z \equiv \frac{L}{r} \tag{2.1}$$

While the radial distance goes from $r = 0$ in the interior to infinity, now $z = 0$ corresponds to the boundary while $z = \infty$ is the deep interior. We might have a situation where there is a lowest bound on r, e.g. the position of a black hole horizon r_h (and there will be, if the temperature is finite). Then the deep IR is at $z_h = L/r_h$ instead of infinity. The AdS_{D+1} metric in z coordinate is

$$ds^2 = \frac{1}{z^2}\left(-dt^2 + \sum_{i=1}^{D-1} dx_i^2 + dz^2\right). \tag{2.2}$$

Deformations away from AdS space are allowed as long as the small z asymptotics (AdS boundary) is unchanged. We will only consider equilibrium physics in this thesis, which corresponds to stationary and homogenous geometries. We will also only consider isotropic systems, i.e.

isotropic geometries in the bulk. This makes all components of the metric depend only on z and allows at most two free functions parametrizing deformations from AdS. We can therefore write the most general metric as

$$ds^2 = \frac{1}{z^2}\left(-f(z)h(z)dt^2 + \sum_{i=1}^{D-1} dx_i^2 + \frac{dz^2}{f(z)}\right) \tag{2.3}$$

where we recognize $f(z)$ as the red shift factor (warp function). For AdS asymptotics we must have $f(z) = 1 + O(z)$ and $h(z) = 1 + O(z)$ for $z \to 0$. General stability conditions also make both f and h everywhere non-negative. Finally, $f(z_h) = 0$ indicates the existence of a horizon at $z = z_h$.

2.1.1 Thermodynamics

Finite temperature

The basis of the dictionary is given by the identification of the partition functions given in (1.6). The first new dictionary entry we introduce is temperature, originally proposed by Witten in [115]. It is a direct consequence of the basic fact that temperature enters kinematics of a field theory by imposing periodicity of Euclidean time. Consider first an AdS space in imaginary time. A well-known (but not unique) solution with periodic Euclidean time $\tau \equiv it$ is the Schwarzschild black hole. This solution corresponds to metric (2.3) with $h = 0$ and

$$f(z) = 1 - \frac{4\pi M}{D\pi^{D/2}\Gamma(D/2+1)} z^D, \tag{2.4}$$

where M is the black hole mass. This solution is only defined up to the horizon at z_h, the outermost (smallest z) radial slice where the red shift function vanishes: $f(z_h) = 0$. It is only smooth if the time is periodic with the period

$$\frac{1}{T_{BH}} \equiv \beta = \frac{z_h}{2\pi} \tag{2.5}$$

where T_{BH} is the Hawking temperature of the black hole. Since the spacetime coordinates (t, x) are directly identified in the dictionary, the compactification of imaginary time retains the same meaning in the boundary theory: $T_{BH} = T_{bnd}$. Notice that the temperature in field theory equals the temperature of the black hole and *not the temperature of the bulk*, as the latter is always zero. This is of more than academic interest as it means that the bulk fields live at $T = 0$ and should be treated by the usual field theory and not thermal field theory.

Free energy

The next dictionary entry, especially important when dealing with exotic systems where very few principles are known to hold, is that of free energy of the field theory, as the laws of thermodynamics are general enough that they can always be used as the starting point. This directly follows from the relation of free energy $\mathcal{F}_{bnd}$ to partition function Z_{bnd} as the defining equality:

$$e^{-\beta\mathcal{F}_{CFT}} = \langle Z_{CFT}\rangle_{\mathrm{CFT}}. \tag{2.6}$$

According to GKPW formula, the right-hand side equals the bulk on-shell action with appropriate boundary conditions. We thus find:

$$e^{-\beta\mathcal{F}_{CFT}} = \langle e^{-\int d\tau\mathcal{L}_{bulk}+S_{bnd}}\rangle_{\mathrm{AdS}} \tag{2.7}$$

where we have included the possibility of boundary interactions on the gravity side. In classical gravity, i.e. for large N and large gN the bulk expectation value is obtained simply by plugging in the on-shell solutions into $S_{bulk} + S_{bnd}$. Taking into account (2.5) we get the factor of β in the exponent of Z_{bulk} too, so

$$\mathcal{F}_{CFT} = S_{bulk}(\Phi_{\mathrm{on-shell}}) + S_{bnd}(\Phi_{\mathrm{on-shell}}). \tag{2.8}$$

This simple but very important rule was given in [115]. Then we can follow all the usual thermodynamic identities to find other thermodynamic potentials, as well as their derivatives. Notice again that we cannot equate $\mathcal{F}_{CFT}$ to any *thermodynamic* quantity in the bulk, as the latter is at zero temperature.

2.1.2 Sources and expectation values

Scalar field

The observables of a CFT have correlation functions of their operators $\mathcal{O}$, carrying certain quantum numbers. These correlation functions are formally generated in the standard way by taking functional derivatives of

$$\langle\mathcal{O}\mathcal{O}\ldots\mathcal{O}\rangle = \frac{\delta^n}{\delta^n\Phi_0}\langle e^{\int\Phi_0\mathcal{O}}\rangle_{\mathrm{CFT}}. \tag{2.9}$$

Recalling our duality discussion, we should identify the source Φ_0 with a field in AdS $\Phi(x)$ restricted to the boundary where conformal symmetries are realized, relating $\lim_{z\to 0}\Phi(z)$ to Φ_0. The boundary conditions should ensure that the source is the leading (non-normalizable) component of the solution at the boundary. Let us see how such a procedure works for a scalar field and for a gauge field. The results to follow are mostly from [114, 115] with some slight refinements summarized in [2, 25]. In this case the bulk action and the equations of motion are trivially

$$S_{bulk} = -\int d^D x \left(D^\dagger_\mu \Phi D^\mu \Phi + m^2 \Phi^2 \right) \tag{2.10}$$

$$\left(z^{D-1}\partial_z z^{1-D}\partial_z + k^2 - \frac{m^2}{z^2} \right) \Phi = 0 \tag{2.11}$$

We are looking for a solution which remains finite at the boundary $z \to 0$. Making a power-law ansatz $\Phi \sim z^\alpha$, we find that exponents of the near-boundary asymptotic of the field Φ are $\Delta_\pm = D/2 \mp \sqrt{(D/2)^2 + m^2}$. Here, Δ_- corresponds to the leading and Δ_+ to the subleading branch. One can actually find the exact solution in the whole AdS space in terms of modified Bessel functions, giving general solution of the form

$$\Phi(z) = \Phi_S z^{D/2} K_{\Delta - D/2}(kz) + \Phi_R z^{D/2} I_{\Delta - D/2}(kz) \tag{2.12}$$

where K and I are modified Bessel functions of first and second kind, respectively and

$$\Delta = \Delta_+ = D/2 + \sqrt{\left(\frac{D}{2}\right)^2 + m^2}. \tag{2.13}$$

The normalizable solution is proportional to Φ_R while the non-normalizable one is the Φ_S branch. Therefore, according to the dictionary, Φ_R is the response (expectation value) and Φ_S the source. Consider now the one-point function $\langle O \rangle$. The variation of the bulk action for such a configuration is found by substituting the solution into S_{bulk}:

$$\delta S_{bulk} = \int_0^\infty dz \int d^D x \sqrt{-g} 2\delta\Phi (D^\dagger_\mu D^\mu - m^2)\Phi - 2\int d^D x \sqrt{-h}\delta\Phi \partial_z \Phi|_{z=0} \tag{2.14}$$

where h is the induced metric on the boundary. The first term vanishes for the solution of (2.11). For the second term the characteristic AdS/CFT steps come. First, we see that the bulk action in general diverges at the UV boundary $z \to 0$ and needs to be regularized. The last, divergent part of (2.14) can be removed by the boundary counterterm

$$S_{bnd} = \int d^D x \sqrt{-h} \Phi^2 \tag{2.15}$$

This is exactly the Dirichlet term familiar from elementary analysis: its meaning is to fix the boundary data Φ_0. So consistency if the bulk theory *requires* it to be reconstructible from the boundary.

At second order we find the two-point correlator for the boundary field $\mathcal{O}$

$$\langle \mathcal{O}(\mathbf{x}_1)\mathcal{O}(\mathbf{x}_2)\rangle = \frac{\partial^2 S}{\partial\Phi(x_1)\partial\Phi(x_2)} \sim \frac{\text{const.}}{|x_1 - x_2|^{2\Delta}} \tag{2.16}$$

with Δ defined in (2.13). Therefore, the seemingly arbitrary definition of Δ in (2.12) is chosen to match the conformal dimension of the boundary field. We see that the operator $\mathcal{O}$ scales in accordance with the predictions of CFT with conformal dimension Δ. Also if additional terms asuch as interactions are added in the bulk, it is clear that the UV asympotics will still be determined by m, or else (if the additional terms are irrelevant at the boundary) the asymptotic AdS geometry will be unstable. So another dictionary entry is that *conformal dimension in field theory is determined by the bulk mass of the field.*

Gauge fields, field strengths and densities

The procedure above is readily generalized to gauge fields. In this thesis we will need only the Abelian $U(1)$ field so we focus on that. Let us start from the well known Maxwell action. By partial integration, bulk action evaluates to

$$S = -\frac{1}{4}\int_0^\infty dz \int d^D x \sqrt{-g} F_{\mu\nu}F^{\mu\nu} = \frac{1}{2}\lim_{z_0 \to 0}\int d^D x \sqrt{-g} F_{\mu\nu}A^\mu n^\nu|_{z_0} + \\ + \int_0^\infty dz \int d^D x \sqrt{-g} A_\nu \partial_\mu F^{\mu\nu} \tag{2.17}$$

where n^ν is the unit normal vector to the boundary. To cancel the boundary contribution we precisely need the von Neumann term $S_{ct} = \int d^D x \sqrt{-h} F_{\mu\nu} A^\mu$ that fixes the field strength at the boundary. Now that we have the boundary action, we can proceed to find the dictionary entries. The solution to the Maxwell equations near the AdS boundary is a linear function in z. For the component A_0 we can write

$$A_0 = A_0^{(0)} + A_0^{(1)} z + O(z^2), \tag{2.18}$$

so the leading term, $A_0^{(0)}$, is the source and $A_0^{(1)}$ is the response. The boundary action is $S_{bnd} = -A_0^{(0)} A_0^{(1)} + \ldots$: the leading and subleading term are linearly coupled to each other. It becomes clear that $A_0^{(1)}$ can be identified with negative charge density ρ while its source $A_0^{(0)}$ has the meaning of chemical potential μ (i.e. background scalar potential). For a spatial component of the gauge field, we can write

$$A_i = A_i^{(0)} + A_i^{(1)} z + O(z^2) \tag{2.19}$$

and equate the subleading term $A_i^{(1)}$ to the current J_i while $A_x^{(0)}$ is its source. Therefore, we arrive at the conclusion that the subleading and leading term of the bulk gauge field encode the current density and its source, i.e. background $U(1)$ field. We can rephrase this conclusion in terms of electric and magnetic field strengths in the bulk if we assume spacetime homogeneity. In this case transverse electric field is simply $E_i = -i\omega A_i$ and the radial magnetic field is $B_i = i\epsilon_{ijk} k_j A_k$. We can now say that the bulk radial electric field stands for the charge density while the radial magnetic field in the bulk is the magnetic field at the boundary. For the transverse fields, we get that transverse bulk electric field encodes for the electric field at the boundary, while transverse bulk magnetic field stands for spatial current on field theory side.[1] Notice that the fields at the boundary obey *global* rather than gauge currents. This is an important property of the dictionary: gauge symmetry in the bulk becomes a local symmetry at the boundary. Another manifestation of this principle is the $SO(D-1)$ rotational invariance in field theory. In AdS, $SO(D-1)$ is a gauge symmetry, a consequence of diffeomorphism

[1] This fails for the component A_z. Obviously, since the radial coordinate does not exist on field theory side, A_z cannot be dual to any component of the current. In fact, it has no physical sense at all and one should put $A_z = 0$ in holographic setups. To see this, remember that nonzero radial gauge field implies a nonzero radial flux through the boundary. This would violate the RG flow interpretation of the radial direction – we do not know how to interpret radial flow of *matter* along z. For that reason we always put $A_z = 0$.

invariance, in the sense that an $SO(D-1)$ rotation transforms AdS space into itself but in different coordinates.

There is a way to use AdS/CFT in the canonical ensemble using the method of alternative quantization for the gauge field. From (2.19), we see that the leading term has the same asymptotics as the derivative of the subleading term. By a Legendre transform we can thus swap the roles of $F_{\mu\nu}$ and A_μ in the boundary term and regard J_μ as fixed instead of the source E_μ. For example, suppose the gauge field has the form $A = A_0 dt$. Then the boundary action is $S_{ct} = \mu\rho + \ldots$: the two coefficients are linearly coupled to each other, and we can identify $a_0 \mapsto \mu, b_0 \mapsto \rho$: *leading and subleading term in the gauge field component A_0 correspond to chemical potential and charge density in field theory.*

2.2 Holographic superconductors: a tutorial

In this subsection we will present a worked-out example where the general formalism of holography is applied on perhaps the simplest possible nontrivial system: a charged scalar boson coupled to the $U(1)$ Maxwell field and gravity. This is the famous holographic superconductor model, proposed in 2008 by Hartnoll, Horowitz and Herzog [47, 46], and Gubser [40]. It is immediately clear that the term superconductor is not quite satisfying: not only are there no fermionic degrees of freedom but the $U(1)$ symmetry is global and not gauged, thus more akin to the situation in a superfluid. Nevertheless, it is the most famous application of AdS/CFT on complex systems, encapsulating all important elements.

Let us first recall the effective Landau-Ginzburg theory of superconductivity. There, one replaces the microscopic treatment of Cooper pairs by an effective theory for the charged bosonic order parameter Φ. One then constructs the free energy in the vicinity of the transition point in accordance with general symmetry requirements. The result is a phenomenological action which can describe the dependence of the pair density on temperature near the critical point, as well as the Higgsing phenomenon, i.e. breaking of the gauge $U(1)$ symmetry by the condensate. Since the holographic description will take $U(1)$ to be a global rather a local symmetry, This last ingredient is missing in the holographic version. The holographic superconductivity an important breakthrough. Not only does it give an example on how to treat in principle the condensation of any order parameter holographically, but it does so in a novel way: directly from a critical system and this is reflected in non-standard transport properties which reproduce the experimental results for superconducting materials.

Following the original papers, we specify to the case of $D = 3$ in this section. The bulk action is easy to write from the symmetry requirements:

$$S_{bulk} = \int dz \int d^3x \left[R + 6 - \frac{1}{4} F_{\mu\nu} F^{\mu\nu} - D^\dagger_\mu \Phi D^\mu \Phi - m^2 \Phi^2 - V_{int}(|\Phi|) \right] \tag{2.20}$$

where the covariant derivative is

$$D_\mu = \partial_\mu - iqA_\mu \tag{2.21}$$

and the potential V_{int} can be an arbitrary function in the bottom-up setup. We will opt for the simplest case and set it to zero. At finite temperature nothing changes dramatically upon introducing a finite potential. The ansatz (2.3) can be used for the metric. For simplicity, let us assume spherical symmetry, isotropy and an electric-only configuration of the Maxwell field for now, writing

$$A = A_0(z) dt \tag{2.22}$$

The 00 and zz components of the Einstein equations read:

$$3f - z\partial_z f - 3 = \frac{1}{2} \left((\partial_z \Phi)^2 - V + (\partial_z A_0)^2 + q^2 \Phi^2 A_0^2 \right) \tag{2.23}$$

$$3f - z\partial_z f - 3zf \frac{\partial_z h}{h} - 3 = \frac{1}{2} \left((\partial_z \Phi)^2 + V + (\partial_z A_0)^2 + q^2 \Phi^2 A_0^2 \right) \tag{2.24}$$

while the Maxwell equation for F_{0z} reads

$$\partial_z \left(\frac{1}{\sqrt{h}} \partial_z A_0 \right) = 2q^2 \frac{\Phi^2}{z^3 \sqrt{fh}}. \tag{2.25}$$

The ii component of Einstein equations can be shown to be a linear combination of the remaining two and can be left out. The equations for this simple system are clearly quite involved. This is typical for the bulk physics of holographic systems: the full solution has to be obtained numerically, while analytical estimates can be made in the near-horizon and near-boundary limit. The former is of importance for the phase diagram and analysis of the condensate formation. We will discuss it after we solve a more basic question: how to impose the boundary conditions and calculate the quantities on the field theory side? To that end, we can use the results obtained earlier for the near-boundary asymptotics of the scalar field – it turns out that coupling to the gauge field is always a subleading term for $z \to 0$ and does not change the asymptotics. Schematically, the near-boundary solution is therefore

$$\Phi(z \to 0) = \Phi^{(1)} z^{3-\Delta} + \Phi^{(2)} z^{\Delta}. \tag{2.26}$$

The boundary action is important for the calculation of free energy at the boundary. The scaling dimension is set by the bulk mass; as before, we have $\Delta = D/2 + \sqrt{D^2/4 + m^2}$. According to the dictionary, $\Phi^{(2)}$ sources the boundary field while $\Phi^{(1)}$ is its VEV. For a solution that holographically encodes spontaneous symmetry breaking, we must seek for a spontaneously generated VEV without a source for the scalar and gauge field:[2]

$$S^{(1)}_{bnd-\Phi} = \oint d^3x \sqrt{-h}\Phi^2|_{z\to 0} \tag{2.27}$$

For completeness we give also the boundary action for the metric and the gauge field. This is the Hawking-Gibbons term for the metric and imposing the chemical potential $\mu = A_0(z_0)$ through a Dirichlet boundary condition for A_0. This gives altogether:

$$S_{bnd} = \oint d^3x \sqrt{-h} \left(-2K + 4 + A_0 \partial_z A_0 + \Phi^2\right). \tag{2.28}$$

2.2.1 Scalar condensate and phase transitions

In the presence of a nonzero electrostatic potential the scalar has an effective negative mass: $-m^2_{eff}\Phi^2 \sim -q^2 f h A_0^2 \Phi^2/z^2$. For a large enough charge q, it is reasonable to expect the scalar order parameter to condense. This is precisely what happens. Note that this means that the spontaneous breaking of the global $U(1)$ invariance in field theory is described by the spontaneous breaking of a local symmetry in the bulk, i.e. Higgsing in the bulk. Upon solving the equations of motion (2.23-2.25) with appropriate boundary conditions, one is able to find a solution with non-vanishing scalar field. On the field theory side, the operator dual to Φ will condense,

[2] We can also employ the alternative quantization, where the subleading term becomes the source. Fixing the subleading term however is not enough to cancel the divergence, and we need to add an explicit counterterm so the boundary action becomes $S^{(2)}_{bnd-\Phi} = \oint d^3x\sqrt{-h}(\Phi^2 + 2\Phi n_z \partial^z \Phi)$.

breaking now the global $U(1)$ symmetry.[3] Solving the system (2.23-2.25) numerically, one obtains the dependence of the condensate value $\langle\Phi\rangle$ on temperature. The result is a textbook order-disorder transition with the *mean field* scaling of the condensate with temperature:

$$\langle\Phi_{1,2}\rangle \propto \left(1 - \frac{T}{T_c}\right)^{\beta_{1,2}}. \tag{2.29}$$

One can then proceed to calculate the free energy which indeed reveals the existence of a second order phase transition, and with mean field exponents, thus reproducing the predictions of the Landau-Ginzburg theory. This finding encapsulates the essential features of holographic superconductivity – a scalar with arbitrary mass Higsses in the bulk leading to a global order-disorder transition on the field theory side.

Hartnoll et al have proceeded to compute conductivities [47] and found excellent qualitative agreement with experiment. In the standard quantization, Φ_1 condenses and backreacts on the gauge field. We can then compute the conductivity of the system as the ration of the current and the external field – the corresponding bulk quantities are the subleading and the leading term of a spatial component of the gauge field. The resulting curve looks like that of conventional BCS superconductors. Doing the same in alternative quantization, for Φ_2 (see the footnote on this page), one finds that conductivity mimics the one seen in unconventional superconductors. This was the first triumph of AdS/CMT in approaching the experiment [45].

Remarkably, a neutral scalar can also condense. The above mechanism clearly cannot be the cause of the formation of neutral hair. What is the mechanism here? The explanation lies in the generalization of the tachyonic instability to AdS known as the Breitenlohner-Freedman (BF) bound [25, 47, 46] and the geometry of the charged black hole. The BF bound is the value for which the square root in Δ becomes imaginary. In $D+1$ dimension it reads:

$$m^2 < m^2_{BF} = -\frac{D^2}{4L^2} \tag{2.30}$$

[3] For low masses, the scalar field has two quantizations with the non-standard alternative quantization similar to the Legendre transform to the canonical ensemble as described earlier. The two possible choices for the boundary conditions – fixing the VEV versus fixing the source – lead to two different field theories, with different properties.

where L is the radius of the space. In AdS$_4$ the BF value is thus $-9/4L^2$. In the presence of non-zero chemical potential, this system has a different geometry in deep interior dual to the IR of a CFT. The near-horizon region of the charged black hole has the geometry AdS$_2 \otimes \mathbb{R}^2$: it is a direct product of the $x-y$ plane and a *two-dimensional* AdS space, distinct from the AdS$_4$ where the system as a whole lives. AdS$_2$ has the BF bound $m^2 < m^2_{BF}$. Dimension is reduced from $D+1=4$ to $D+1=2$ but the radius of the AdS$_2$ is smaller than the radius of AdS$_4$: $L_2 = L/\sqrt{6}$. Therefore, the BF bound in the interior is $m^2 < -6/4L^2$. This means that there is a window of the values of m where $m^2_{\mathrm{AdS4}} < m^2 < m^2_{\mathrm{AdS2}}$, so a scalar which is stable in AdS$_4$ will still condense in AdS$_2$ [47]. The field theory meaning of this effect is the breaking of the discrete (Ising) $\mathbb{Z}_2$ gauge symmetry. This is a truly novel result of the holographic theory. The fact that the physics on field theory side can be explained by analyzing near-horizon geometry is an important lesson we will take from this review section.

2.3 Holographic dictionary for fermions

We now proceed to the object of this thesis: fermions. The essential problem for fermions is the well-known fact the Dirac fermion is a constrained system: the equations of motion are of first order, only half of the components of Dirac field are independent degrees of freedom while the rest are uniquely determined by them. The sign problem does *not* plague holography at least at the leading (tree) level. This is because the quasiparticle picture is preserved in the bulk, in the sense that we will consider weakly interacting fermions coupled to external fields only. Besides, we know that two-point correlation functions and expectation values (densities) are dual to tree-level objects in the bulk, thus one does not need to face the loop effects where the fermionicity strikes harder.[4]

[4]Occasionally, it is laconically claimed that the fermion sign problem is eliminated by holography as in the limit of classical gravity/large N strongly coupled field theory the bulk physics is classical. This is not entirely true: while *gravity* is treated classically in this limit as the gravitational constant $\kappa_{D+1} \to 0$, this does not tell us anything about the matter fields. Indeed, these in general require the same QFT treatment no matter if we take classical gravity limit, SUGRA limit or neither.

2.3.1 Equations of motion

While already the original AdS/CFT works include fermions as the field theory side is supersymmetric, it was not *a priori* clear how to construct dictionary entries for a fermionic observable in field theory. This problem was addressed in [84, 7, 56]. A more systematic rephrasing of the solution, which takes the viewpoint of holographic regularization, was given in [16]. We will mainly follow the reasoning of the latter reference as it is the most logically coherent exposition of the problem. Whereas the boundary action S_{bnd} needed to be picked by hand in earlier formulations, [16] shows that it follows logically from the requirement that the theory should be regular in the UV.

Kinematics and holography

Let us first discuss the kinematics of Dirac fermion; we have already announced that this will be the main source of trouble. The Dirac algebra in full AdS space ($D+1$-dimensional) is represented by gamma matrices Γ_μ, $\mu = 0, \ldots D$, and $\Gamma_D \equiv \Gamma_z$. The restriction of this representation to D dimensions, i.e. on the boundary, we will denote by γ_μ ($\mu = 0, \ldots D-1$). Recalling the table of the representations of Dirac algebra in various dimensions, we find that in odd number of dimensions $D+1$, i.e. for D even, there is a single spinor representation, whereas for D odd there are two irreducible representations of the Dirac algebra. We will mainly deal with this case in the thesis. In this case, Ψ is a bispinor and we can decompose it into two spinors $\Psi_\pm$. The choice of projection operator $\Pi_\pm$ is non-unique. In holography there is a natural choice which preserves all symmetries in the boundary theory: projection on the radial direction. Thus the projectors are $\Pi_\pm = (1 \pm \Gamma_z)/2$.

Dynamics

We are now ready to write the Dirac equation. We can always write it as a pair of coupled equations for $\Psi_\pm$. As we know, the Dirac equation reads

$$(\not{D} - m)\Psi = 0. \tag{2.31}$$

The covariant derivative includes the coupling to any gauge fields present and to the metric through the spin connection:

$$\not{D} = e^\mu_a \left(\partial_\mu + \frac{1}{8}\omega^{bc}_\mu [\Gamma_b, \Gamma_c] - iqe^\mu_a A_a \right). \tag{2.32}$$

From now on, we will denote the local tangential coordinates by Latin indices and the metric coordinates by Greek indices. The inverse vielbein is e^μ_a. From now on we will study a fermion in the homogenous background coupled to isotropic A_0 gauge field, describing a field theory at finite density. Taking into account homogeneity and isotropy of the system in transverse direction, we can partially Fourier-transform so that the derivative becomes $\partial_\mu \mapsto (-i\omega, ik, \partial_z)$. The spin connection, given in general by $\omega_\mu^{bc} = e^b_\nu \partial_\mu e^{\nu c} + e^b_\nu e^{\sigma c}\Gamma^\nu_{\sigma\mu}$, has only two nonzero components, ω_0^{0z} and ω_i^{iz}:

$$\begin{aligned}\omega_0^{0z} &= e^0_0 e^{zz}\Gamma^0_{z0} = \frac{1}{2}e^0_0 e^{zz} g^{00}\partial_z g_{00} = e^{zz}\partial_z e^0_0 \\ \omega_i^{iz} &= e^i_i e^{zz}\Gamma^i_{zi} = \frac{1}{2}e^i_i e^{zz} g^{ii}\partial_z g_{ii} = e^{zz}\partial_z e^i_i,\end{aligned} \tag{2.33}$$

Note that they can be formally written as total derivatives and as a consequence they can be absorbed in the redefinition of the fermion field in the following way. The equation of the form

$$\Gamma^z e^z_z \left[\partial_z + \partial_z\left(e^0_0 + (D-1)\, e^i_i\right)\right]\Psi + (\ldots)\Psi = 0, \tag{2.34}$$

where $(\ldots)$ denotes all terms containing no radial derivatives, can be rewritten as $\Gamma^z e^z_z \partial_z \psi + (\ldots)\psi = 0$ upon rescaling the Dirac field as

$$\Psi \mapsto \psi \equiv \Psi\sqrt{g_{00}\left(g_{ii}\right)^{D-1}} = \Psi\sqrt{-g g^{zz}}. \tag{2.35}$$

This rescaling works generally for single parameter metrics. From now on throughout this chapter we will use the rescaling (2.35) and work with ψ and $\psi_\pm$ instead of Ψ and $\Psi_\pm$.

With the rescaling for the Dirac field, we can write the Dirac equation for ψ

$$\left[e^z_z \partial_z - \Gamma^z(iqe^\mu_0 A^0 + m)\right]\psi = 0. \tag{2.36}$$

Next we decompose the equation into the equations for $\psi_\pm$. The result can be written as:

$$(\partial_z + e^{zz} m)\psi_\pm \pm \mathcal{T}\psi_\mp = 0 \tag{2.37}$$

where $\mathcal{T}$ is the transverse covariant derivative rescaled by the vielbein e^z_z:

$$-i\mathcal{T} = e^z_z e^{00}\gamma_0(-\omega + qA_0) + e^z_z e^{ii}\gamma_i k_i. \tag{2.38}$$

Starting from the Dirac equation (2.38), we can eliminate either ψ_+ or ψ_- and readily derive a second order equation of motion for $\psi_\pm$. Using that $\mathcal{T}\mathcal{T} = -T_0T^0 + T_iT^i \equiv \mathcal{T}^2$, we can invert $\mathcal{T}$ to rewrite

$$\frac{\mathcal{T}}{\mathcal{T}^2}\left(\partial_z + e_z^z m\right)\psi_+ = -\psi_- \tag{2.39}$$

and use the ψ_- equation to obtain

$$\left(\partial_z - me_z^z\right)\frac{\mathcal{T}}{\mathcal{T}^2}\left(\partial_z + me_z^z\right)\psi_+ = -\mathcal{T}\psi_+. \tag{2.40}$$

This finally brings us to the second-order form of the Dirac equation, for the spinor ψ_+. Denoting it as

$$\left(\partial_{zz} + \mathcal{P}\partial_z + \mathcal{Q}_+\right)\psi_+ = 0 \tag{2.41}$$

we have for the coefficients

$$\begin{aligned}\mathcal{P}(z) &= -[\partial_z, \mathcal{T}]\frac{\mathcal{T}}{\mathcal{T}^2}\\ \mathcal{Q}_+(q,m,\omega,k;z) &= -2me_z^z + (\partial_z me_z^z) - [\partial_z,\mathcal{T}]\frac{\mathcal{T}}{\mathcal{T}^2}me_z^z + \mathcal{T}^2\end{aligned} \tag{2.42}$$

For the second component ψ_- we get the same equation but with $\mathcal{Q}_- = \mathcal{Q}_+(-q,-m,-\omega,-k)$.

Of course, the second order equation implies the Dirac equation but is not equivalent to it. The necessary and sufficient condition for ψ_+, the solution of (2.41), to be also the solution to (2.37), reads

$$\psi_- = \frac{1}{\mathcal{T}}\left(\partial_z + me_z^z\right)\psi_+. \tag{2.43}$$

It is instructive to solve the simplest case: that of pure AdS with no gauge fields. The field is rescaled as $\psi = \Psi/z^{(D+3)/2}$, and the second order equation for ψ_+ becomes

$$\left(\partial_{zz} - \frac{2m}{z} - \frac{m}{z^2}\right)\Psi_+ = 0 \tag{2.44}$$

which we readily recognize as the Bessel equation. It yields the following general solution:

$$\psi_+(z) = \frac{1}{z}\left(\psi_0^{(1)}K_{m+1/2}\left(kz\right) + \psi_0^{(2)}K_{m-1/2}\left(kz\right)\right), \tag{2.45}$$

where $K_{m\pm 1/2}$ are modified Bessel functions of the second kind. The near boundary asymptotics of the non-rescaled field Ψ_+ behaves as $\Psi_+ = \Psi_+^{(1)} z^{D/2-m} + \Psi_+^{(2)} z^{D/2+m}$. Clearly, $\Psi_+^{(1)}$ is always the leading, source term. But what is the response? Naively, it can be $\Psi_+^{(2)}$ as the subleading term. In the boundary action (2.48) we have however Ψ_- coupled linearly to the source Ψ_+ (which, with appropriate boundary conditions, becomes $\Psi_+^{(1)}$). Therefore, the response is Ψ_- with appropriate boundary asymptotics. Dirac equation tells that $\Psi_-^{(1)} \propto \Psi_+^{(2)}$ so we conclude that the response is $\Psi_-^{(1)}$.

2.3.2 Boundary action

Let us start again from the minimal bulk action for Dirac fermions coupled to gravity and possibly gauge fields:

$$S_{bulk} = S_{grav} + \int d^{D+1}x\sqrt{-g}\bar{\Psi}(\not{D} - m)\Psi + \ldots, \tag{2.46}$$

where $(\ldots)$ stand for any additional fields in the system. It is assumed that these will not change the UV behavior of fermions nor the AdS asymptotics of the background; they might change the background and thus also the fermionic behavior in IR but we will simply assume a given fixed IR whatever might be the fields which produce it. The issue is how to implement the dictionary. The Dirac action is famously proportional to Dirac equation and thus vanishes on shell. We have seen this also in the scalar sector however. The resolution is the existence of a boundary action, which in fact encodes the full holographic partition function. The objective is to construct it here for fermions. To do so, let us find the variation of the bulk part (disregarding again the parts we know: gravity and bosons). Since we work in a spacetime with a boundary, there will generically be a boundary contribution. Employing partial integration in (2.46) and varying with respect to ψ, we get:

$$\begin{aligned} \delta S_{bulk} = \delta \int d^{D+1}x\sqrt{-g}\bar{\psi}(\not{D} - m)\psi = \\ = \int d^D x\sqrt{-h}\bar{\psi}\delta\psi|_{z_0}^{z_h} - \int d^{D+1}x\sqrt{-g}(-\not{D} - m)\bar{\psi}\delta\psi. \end{aligned} \tag{2.47}$$

The second, bulk term vanishes on shell as it is proportional to the equation of motion. The first, boundary term does not vanish however. It is to be evaluated on the boundary of AdS in UV and at z_h in IR.[5] In terms of the radial projections, it reads

$$\delta S = \frac{1}{2} \int d^D x \sqrt{-h} \left(\bar{\psi}_+ \delta \psi_- + \bar{\psi}_- \delta \psi_+ \right). \tag{2.48}$$

We know from general rules of AdS/CFT that one of the components of ψ will be the source and the other the response, and in the previous subsection we have seen that the leading component of ψ_+ is larger (i.e. decays slower) at the boundary than the leading component of ψ_-. We can therefore pick ψ_+ to be the source. This means that ψ_+ is fixed at the boundary and its variation is zero: $\delta\psi_+ = 0$. The variation of the action now reduces to the first term in (2.48). To cancel ad we can add a counterterm reading

$$S_{ct} = \frac{1}{2} \int d^D x \sqrt{-h} (\bar{\psi}_+ \psi_- + \bar{\psi}_- \psi_+) \tag{2.49}$$

and the whole action is given by $S = S_{bulk} + S_{ct}$, so $S_{bnd} \equiv S_{ct}$: the whole boundary contribution can be understood as the counterterm which regularizes the action, eliminating UV divergences and making the on-shell solution satisfy the Dirac equation in the bulk.

For the steps to follow it is convenient to introduce the bulk-to-boundary propagator $\mathcal{G}_\pm(z)$ and to express the solution in terms of $\mathcal{G}_\pm$. The bulk-to-boundary propagator satisfies the equation of motion [114]:

$$(\not{D} - m) \, \mathcal{G}(z) = \delta(z) \tag{2.50}$$

i.e. it is a response to a Dirac delta function source at the boundary. We can now express the solution to Dirac equation in terms of $\mathcal{G}_\pm$ and $\chi_\pm$. The expression for $\psi_\pm$ reads

$$\psi_+ = \mathcal{G}_+^{-1}(z_0) \mathcal{G}_+(z) \chi_+, \quad \psi_- = \mathcal{G}_+^{-1}(z_0) \mathcal{G}_-(z) S \chi_- \tag{2.51}$$

where $S = \lim_{z \to 0} \mathcal{T}/\not{\mathcal{T}}$. Namely, at the boundary the energy-momentum dependence can be shown to drop from the factor $\mathcal{T}/\not{\mathcal{T}}$, leaving only a constant matrix (which of course depends on the representation of gamma matrices, hence we do not specify it here). The convenience of the above representation of ψ is that all z dependence of ψ is encoded in the bulk-to-boundary propagators. Substituting (2.51) into the boundary action, we

[5] The latter is a single point if $z_h \to \infty$ or a slice in the transverse direction if z_h is finite.

obtain an expression for the full on-shell action in terms of the solutions $\mathcal{G}_\pm(z)$:

$$S^{on-shell} = \int_{z=z_0} \frac{d\omega d^2k}{(2\pi)^3} \sqrt{-h}\bar{\chi}_+ \mathcal{G}_-(z_0)\mathcal{G}_+^{-1}(z_0)\chi_+. \tag{2.52}$$

The two-point correlator in field theory is therefore

$$G(\omega, k) = \mathcal{G}_-(z_0)\mathcal{G}_+^{-1}(z_0). \tag{2.53}$$

What this illustrates is that the subleading component of Ψ_- is the response to the leading component of Ψ_+. This will be the starting point of the work done in most of Chapter 3 and 4.

2.4 The remainder of the thesis

Having discussed the larger context in the first chapter and the theoretical foundations and previous work on the topic of our research in this, second chapter, we have finished introducing the formal framework of our work. We now outline the work done in this thesis on specific problems with fermion systems. We will use the power of holography to describe strongly coupled systems from a new fundamental perspective, to circumvent the sign problem. We stay exclusively with bottom-up setups. The first reason is their obvious simplicity as compared to top-down constructions which become particularly complicated if fermions are included. A deeper reason is that the conceptual aspects we consider such as the dictionary entry for a Fermi surface, or for a Fermi liquid state, or pathways through which Fermi liquids are destroyed – are not expected to depend much on the exact string action.

Another compromise with consistency that we have to decide about is the choice between self-consistent calculations, with backreaction, versus probe limit calculations. We start from the probe limit and afterwards include backreaction, first on gauge field and then also on geometry. Of course, probe limit suffices at small fermion density, when the backreaction is anyway small, but becomes less and less satisfactory as the density increases. The field theory interpretation is that backreaction probes the stability of the system – unstable quantum critical matter is described by the probe limit calculations, but to arrive at stable phases we need to backreact. In particular, the Fermi-liquid-like phase (which we know empirically to be very stable) requires backreaction.

In Chapter 3 we address the critical theory governing the zero temperature quantum phase transition between strongly renormalized Fermi-liquids as found in heavy fermion intermetallics and possibly high T_c superconductors. From the solutions of Dirac equation in the probe limit in the AdS-RN background, we obtain the spectral functions of fermions in the field theory. By increasing the fermion density away from the relativistic quantum critical point, we observe multiple Fermi surfaces, some of them of distinctly non-Fermi liquid nature while others have some features of the Fermi liquid. Tuning the scaling dimensions of the critical fermion fields we find that the quasiparticle disappears at a quantum phase transition of a purely statistical nature, not involving any symmetry change. The resulting phase has no Fermi surfaces at all.

In Chapter 4 we extend our work by backreacting on gauge field. We provide evidence that the bulk dual to a strongly coupled charged Fermi-liquid-like system has a non-zero fermion density in the bulk. We then calculate density explicitly in the small density approximation, a model we call black hole with Dirac hair. Then we show that the pole strength of the stable quasiparticle characterizing the Fermi surface is encoded in the spatially averaged AdS probability density of a single normalizable fermion wave function in AdS. Recalling Migdal's theorem which relates the pole strength to the Fermi-Dirac characteristic discontinuity in the number density at Fermi energy, we conclude that the AdS dual of a Fermi liquid is described by occupied on-shell fermionic modes in AdS. Encoding the occupied levels in the total spatially averaged probability density of the fermion field directly, we show that an AdS Reissner-Nordström black hole in a theory with charged fermions has a critical temperature, at which the system undergoes a first-order transition to a black hole with a non-vanishing profile for the bulk fermion field. Thermodynamics and spectral analysis support that the solution with non-zero AdS fermion-profile is the preferred ground state at low temperatures.

In Chapter 5 we continue our study of self-consistent (backreacted) models and move toward constructing the full phase diagram of the Dirac-Maxwell-Einstein system and its field theory dual. We compare our Dirac hair model with the electron star model of Hartnoll et all [51], and argue that the electron star and the AdS Dirac hair solution are two limits of the free charged Fermi gas in AdS. Spectral functions of holographic duals to probe fermions in the background of electron stars have a free parameter that quantifies the number of constituent fermions that make up the charge and energy density characterizing the electron star solution. The strict electron star limit takes this number to be infinite. The Dirac hair solution is the limit where this number is unity. This is evident in the behavior of the distribution of holographically dual Fermi surfaces. As we decrease the number of constituents in a fixed electron star background the number of Fermi surfaces also decreases. An improved holographic Fermi ground state should be a configuration that shares the qualitative properties of both limits.

We construct such configuration in Chapter 6. We employ a model which combines the (semiclassical) WKB approximation and its Airy correction with the quantum corrections based on Dirac equation. At high temperatures, the system exhibits a first order thermal phase transition to a charged AdS-RN black hole in the bulk and the emergence of local quantum criticality on the CFT side. This restores the intuition that the transition between the critical AdS-RN liquid and the finite density Fermi system is of van der Waals liquid-gas type. At zero temperature, we find a Berezhinsky-Kosterlitz-Thouless transition from Fermi-liquid-like finite density phase with a sharp Fermi surface to zero density AdS-Reissner-Nordström but in the regime without Fermi surfaces. This suggests that it is indeed the Fermi surface which drives the instability of the AdS-RN quantum critical phase. Based on these findings, we construct the three-dimensional phase diagram, with temperature, conformal dimension and fermion charge.

Even though we have not answered some of the questions we started from, in particular the question of what is the holographic dual to a textbook Landau Fermi liquid and how it is destroyed by strong interactions, we have obtained a qualitative model of how stable Fermi-liquid-*like* quasiparticles become unstable at a quantum critical point and give rise to novel phenomena. These phenomena could not be obtained in a perturbative approach and they illustrate the power of AdS/CFT and its ability to make specific predictions on strongly correlated fermions. These predictions have not been tested experimentally so far. Because of many simplifying assumptions and the lack of ability to construct a microscopic Hamiltonian on the boundary, our results are unlikely to be a good quantitative description of any realistic system. Nevertheless, they make some remarkable qualitative predictions which can be expected to hold also in real-world materials, due to the universality associated to quantum critical behavior. The coming years will surely determine whether the novel physics on display in AdS/CMT is a part of the real world.

Chapter 3

Charged black hole and critical Fermi surfaces [17]

Quantum many-particle-physics lacks a general mathematical theory to deal with fermions at finite density. This is known as the "fermion-sign-problem": there is no recourse to brute force lattice models as the statistical path integral methods that work for any bosonic quantum field theory do not work for finite density fermi-systems. The non-probabilistic fermion problem is known to be of exponential complexity [109] and in the absence of a general mathematical framework all that remains is phenomenological guesswork in the form of the Fermi-liquid theory describing the state of electrons in normal metals and the mean-field theories describing superconductivity and other manifestations of spontaneous symmetry breaking. This problem has become particularly manifest in quantum condensed matter physics with the discovery of electron systems undergoing quantum phase transitions that are reminiscent of the bosonic quantum critical systems [95] but are governed by fermion statistics. Empirically well documented examples are found in the 'heavy fermion' intermetallics where the zero temperature transition occurs between different Fermi-liquids with quasiparticle masses that diverge at the quantum critical point [117]. Such fermionic quantum critical states are believed to have a direct bearing on the problem of high T_c superconductivity because of the observation of quantum critical features in the normal state of optimally doped cuprate high T_c superconductors [111, 116].

A large part of the "fermion-sign-problem" is to understand this strongly coupled fermionic quantum critical state. The emergent scale invariance and conformal symmetry at critical points is a benefit in isolating deep questions of principle. The question is how does the system get rid off the scales of Fermi-energy and Fermi-momentum that are intrinsically rooted in the workings of Fermi-Dirac statistics [99, 72]? Vice versa, how to construct a renormalization group with a relevant 'operator' that describes the emergence of a statistics controlled (heavy) Fermi liquid from the critical state [117], or perhaps the emergence of a high T_c superconductor? We will show that a mathematical method developed in string theory has the capacity to answer at least some of these questions.

3.1 String theory for condensed matter

We refer to the AdS/CFT correspondence: a duality relation between classical gravitational physics in a $d+1$ dimensional 'bulk' space-time with an Anti-de-Sitter (AdS) geometry and a strongly coupled conformal (quantum critical) field theory (CFT) with a large number of degrees of freedom that occupies a flat or spherical d dimensional 'boundary' space-time. Applications of AdS/CFT to quantum critical systems have already been studied in the context of the quark-gluon plasma [104, 41], superconductor-insulator transitions [59, 46, 40, 47] and cold atom systems at the Feshbach resonance [103, 8, 1] but so far the focus has been on bosonic currents (see [45, 49] and references therein). Although AdS/CFT is convenient, in principle the groundstate or any response of a bosonic statistical field theory can also be computed directly by averaging on a lattice. For fermions statistical averaging is not possible because of the sign-problem. There are, however, indications that AdS/CFT should be able to capture finite density fermi systems as well. Ensembles described through AdS/CFT can exhibit a specific heat that scales linear with the temperature characteristic of Fermi systems [69], zero sound [69, 65, 70] and a minimum energy for fermionic excitations [93, 101].

To address the question whether AdS/CFT can describe finite density fermi-systems and the Fermi liquid in particular, we compute the single charged fermion propagators and the associated spectral functions that are measured experimentally by angular resolved photoemission ("AdS-to-ARPES") and indirectly by scanning tunneling microscopy. The spectral functions contain the crucial information regarding the nature of the fermion states. These are computed on the AdS side by solving for the on-shell (classical) Dirac equation in the curved AdS space-time background with sources at the boundary. A temperature T and finite $U(1)$ chemical potential μ_0 for electric charge is imposed in the field theory by studying the Dirac equation in the background of an AdS Reissner-Nordstrom black hole. We do so expecting that the $U(1)$ chemical potential induces a finite density of the charged fermions. The procedure to compute the retarded CFT propagator from the dual AdS description is then well established [104, 49]. Compared to the algorithm for computing bosonic responses, the treatment of Dirac waves in AdS is more delicate, but straightforward; details are provided in the final section of this chapter. The equations obtained this way are solved numerically and the output is the retarded single fermion propagator $G_R(\omega, k)$ at finite T. Its imaginary part is the single fermion spectral function $A(\omega, k) = -\frac{1}{\pi}\mathrm{Im}\mathrm{Tr}(\, i\gamma^0 G_R(\omega, k))$ that can be directly compared with ARPES experiments.

The reference point for this comparison is the quantum critical point described by a zero chemical potential ($\mu_0 = 0$), zero temperature ($T = 0$), conformal and Lorentz invariant field theory. Here the fermion propagators $\langle \bar{\Psi}\Psi \rangle \equiv G(\omega, k)$ are completely fixed by symmetry to be of the form (we use relativistic notation where $c = 1$)

$$G^{CFT}_{\Delta_\Psi}(\omega, k) \sim \frac{1}{(\sqrt{-\omega^2 + k^2})^{d-2\Delta_\Psi}} \tag{3.1}$$

with Δ_Ψ the scaling dimension of the fermion field. Through the $\mathrm{AdS}_{d+1}/\mathrm{CFT}_d$ dictionary Δ_Ψ is related to the mass parameter in the $d+1$-dimensional AdS Dirac equation. Unitarity bounds this mass from below in units of the AdS radius $mL = \Delta_\Psi - d/2 > -1/2$ (we set $L = 1$ in the remainder). The choice of which value to use for m will prove essential to show the emergence of the Fermi liquid. The lower end of the unitarity bound $m = -1/2 + \delta$, $\delta \ll 1$, corresponds to introducing a fermionic conformal operator with weight $\Delta_\Psi = (d-1)/2 + \delta$. This equals the scaling dimension of a nearly free fermion. Despite the fact that the underlying CFT is strongly coupled, the absence of a large anomalous dimension for a fermion with mass $m = -1/2 + \delta$ argues that such an operator fulfills a spectator-role and is only weakly coupled to this CFT. We will therefore use such values in our calculations. Our expectation is that the Fermi liquid, as a system with well-defined quasiparticle excitations, can be described in terms of weakly interacting long-range fields. As we increase m from $m = -1/2 + \delta$, the interactions increase and we can expect the quasi-particle description to cease to be valid beyond $m = 0$. For that value $m = 0$, and beyond $m > 0$, the naive scaling dimension $\Delta_{\mathcal{O}}$ of the fermion-bilinear $\mathcal{O}_{\Delta_{\mathcal{O}}} = \bar{\Psi}\Psi$ is marginal or irrelevant and it is hard to see how the ultra-violet conformal theory can flow to a Fermi-liquid state, assuming that all vacuum state changes are caused by the condensation of bosonic operators. This intuition will be borne out by our results: when $m \geq 0$ the standard Fermi-liquid disappears. A similar approach to describing fermionic quantum criticality [79] discusses the special case $m = 0$ or $\Delta_\Psi = d/2$ in detail; other descriptions of the $m = 0$ system are [76, 91].

3.2 The emergent Fermi liquid

With an eye towards experiment we shall consider the AdS$_4$ dual to a relativistic CFT$_3$ in $d = 2 + 1$ dimensions; see the last section of this chapter. As we argue there, we do not know the detailed microscopic CFT nor whether a dual AdS with fermions as the sole U(1) charged field exists as a fully quantum consistent theory for all values of $m = \Delta_\Psi - d/2$, but the behavior of fermion spectral functions at a strongly coupled quantum critical point can be deduced nonetheless. Aside from Δ_Ψ, the spectral function will depend on the dimensionless ratio μ_0/T as well as the $U(1)$ charge g of the fermion; we shall set $g = 1$ from here on, as we expect that only large changes away from $g = 1$ will change our results qualitatively. We therefore study the system as a function of μ_0/T and Δ_Ψ. We have drawn our approach in Fig. 3.1B: first we shall study the spectral behavior as a function of μ_0/T for fixed $\Delta_\Psi < 3/2$; then we study the spectral behaviour as we vary the scaling dimension Δ_Ψ from 1 to 3/2 for fixed μ_0/T coding for an increasingly interacting fermion. Note that our set-up and numerical calculation necessitate a finite value of μ_0/T: all our results are at non-zero T.

Our analysis starts near the reference point $\mu_0/T \to 0$ where the long range behavior of the system is controlled by the quantum critical point (Fig. 3.1A). Here we expect to recover conformal invariance, as the system forgets about any well-defined scales, and the spectral function should be controlled by the branchcut at $\omega = k$ in the Green's function (Eq.1) : (a) For $\omega < k$ it should vanish, (b) At $\omega = k$ we expect a sharp peak which for $\omega \gg k$ scales as $\omega^{2\Delta_\Psi - d}$. Fig. 3.2A shows this expected behavior of spectral function for three different values of the momentum for a fermionic operator with weight $\Delta_\Psi = 5/4$ computed from AdS$_4$.

Turning on μ_0/T holding $\Delta_\Psi = 5/4$ fixed, shifts the center location of the two branchcuts to an effective chemical potential $\omega = \mu_{eff}$; this

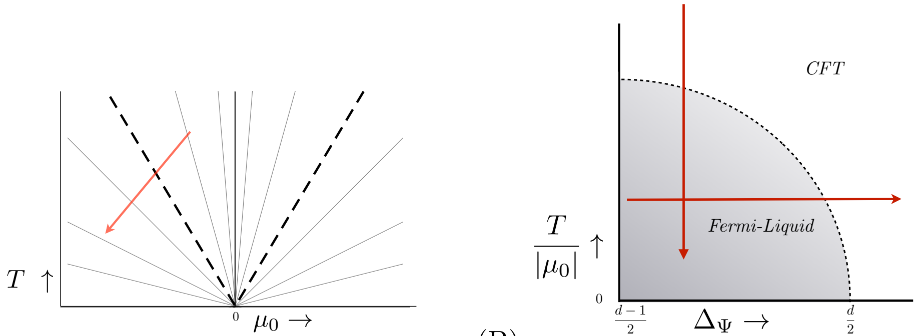

(A) (B)

Figure 3.1: The phase diagram near a quantum-critical point. Gray lines depict lines of constant μ_0/T: the spectral function of fermions is unchanged along each line if the momenta are appropriately rescaled. As we increase μ_0/T we crossover from the quantum-critical regime to the Fermi-liquid. (B) The trajectories in parameter space $(\mu_0/T, \Delta_\Psi)$ studied here. We show the crossover from the quantum critical regime to the Fermi liquid by varying μ_0/T keeping Δ_Ψ fixed; we cross back to the critical regime varying $\Delta_\Psi \to d/2$ for μ_0/T fixed. The boundary region is not an exact curve, but only a qualitative indication.

bears out our expectation that the $U(1)$ chemical potential induces a finite fermion density. While the peak at the location of the negative branchcut $\omega \sim \mu_{eff} - k$ stays broad, the peak at the other branchcut $\omega \sim \mu_{eff} + k$ sharpens distinctively as the size of μ_0/T is increased (Fig. 3.2B). We shall identify this peak with the quasiparticle of the Fermi liquid and its appearance as the crossover between the quantum-critical and the Fermi-liquid regime. The spectral properties of the Fermi liquid are very well known and display a number of uniquely identifying characteristics [77, 98]. If this identification is correct, all these characteristics must be present in our spectra as well.

1. The quasiparticle peak should approach a delta function at the Fermi momentum $k = k_F$. In Fig. 3.2B we see the peak narrow as we increase k, peak, and broaden as we pass $k \sim k_F$ (recall that $T = 0$ is outside our numerical control and the peak always has some broadening). In addition the spectrum should vanish identically at the Fermi-energy $A(\omega = E_F, k) = 0$, independent of k. This is shown in Fig. 3.2C.

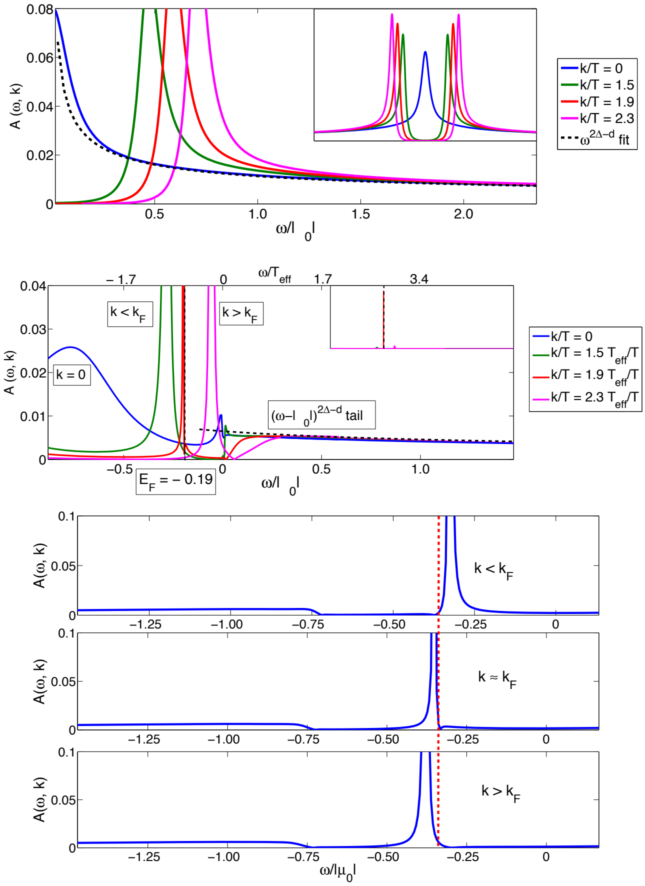

(A) (B) (C)

Figure 3.2: (A) The spectral function $A(\omega, k)$ for $\mu_0/T = 0.01$ and $m = -1/4$. The spectral function has the asymptotic branch cut behavior of a conformal field of dimension $\Delta_\Psi = d/2 + m = 5/4$: it vanishes for $\omega < k$, save for a finite T tail, and for large ω scales as $\omega^{2\Delta_\Psi - d}$. (B) The emergence of the quasiparticle peak as we change the chemical potential to $\mu_0/T = -30.9$ for the same value $\Delta_\Psi = 5/4$. The three displayed momenta k/T are rescaled by a factor T_{eff}/T for the most meaningful comparison with those in (A). The insets show the full scales of the peak heights and the dominance of the quasiparticle peak for $k \sim k_F$. (C) Vanishing of the spectral function at E_F for $\Delta_\Psi = 1.05$ and $\mu_0/T = -30.9$. The deviation of the dip-location from E_F is a finite temperature effect. It decreases with increasing μ_0/T.

2. The quasiparticle should have linear dispersion relation near the Fermi energy with a renormalized Fermi velocity v_F different than the underlying relativistic speed $c = 1$. In Fig. 3.3 we plot the maximum of the peak ω_{max} as a function of k. At high k we recover the linear dispersion relation $\omega = |k|$ underlying the Lorentz invariant branchcut in Eq.1. Near the Fermi energy/Fermi momentum however, this dispersion relation changes to a slope v_F given by the limit $\lim_{\omega \to E_F, k \to k_F} (\omega - E_F)/(k - k_F)$ clearly less than one. Importantly, it appears that the Fermi Energy E_F is not located at zero-frequency.[1] Recall, however, that the AdS chemical potential μ_0 is the bare $U(1)$ chemical potential in the CFT. This is confirmed in Fig. 3.3 from the high k behavior: its Dirac point is μ_0. On the other hand, the chemical potential felt by the IR fermionic degrees of freedom is renormalized to the value $\mu_F = \mu_0 - E_F$. As is standard, the effective energy $\tilde{\omega} = \omega - E_F$ of the quasiparticle is measured with respect to E_F.

3. At low temperatures Fermi-liquid theory predicts the width of the quasiparticle peak to grow quadratically with temperature. Fig. 3.4A, 3.4B show this distinctive behavior up to a critical temperature $T_c/\mu_0 \sim 0.16$. This temperature behavior directly follows from the fact that imaginary part of the self-energy $\Sigma(\omega, k) = \omega - k - (\mathrm{Tr} i\gamma^0 G(\omega, k))^{-1}$ should have no linear term when expanded around E_F: $\mathrm{Im}\Sigma(\omega, k) \sim (\omega - E_F)^2 + ...$ This is shown in Fig. 3.4C, 3.4D.

These results give us confidence that we have identified the characteristic quasiparticles at the Fermi surface of the Fermi liquid emerging from the quantum critical point.

Let us now discuss how this Fermi-liquid evolves when we increase the bare μ_0 (Fig. 3.5). Similar to the fermion chemical potential μ_F, the fundamental control parameter of the Fermi-liquid, the fermion density ρ_F, is not directly related to the AdS μ_0. We can, however, infer it from the Fermi-momentum k_F that is set by the quasiparticle pole via Luttinger's theorem $\rho_F \sim k_F^{d-1}$. The more illustrative figure is therefore Fig. 3.5B which shows the quasiparticle characteristics as a function of k_F/T. We find that the quasiparticle velocities decrease slightly with

[1] In our original paper we misidentified the location of the maximum peak height with E_F. The correct identification is when the pole hit the real axis in the complex frequency space. We explain this bellow in the last section of this chapter.

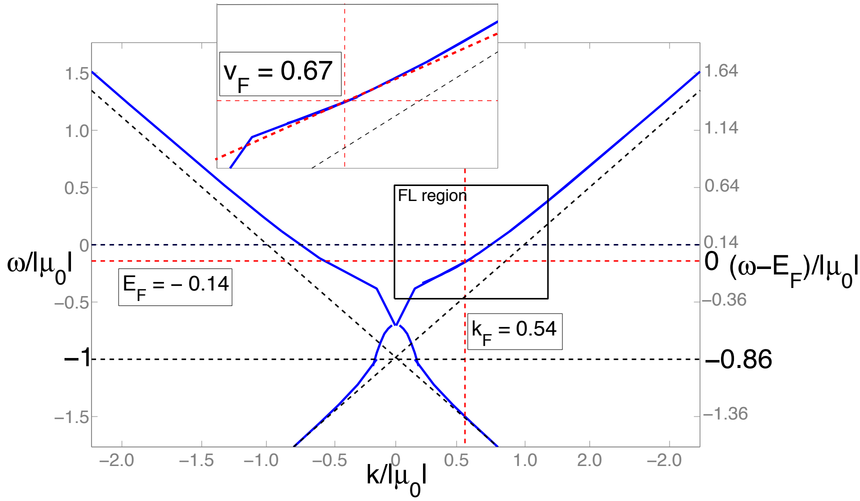

Figure 3.3: Maxima in the spectral function as a function of k/μ_0 for $\Delta_\Psi = 1.35$ and $\mu_0/T = -30.9$. Asymptotically for large k the negative k branch cut recovers the Lorentz-invariant linear dispersion with unit velocity, but with the zero shifted to $-\mu_0$. The peak location of the positive k branch cut that changes into the quasiparticle peak changes significantly. It gives the dispersion relation of the quasiparticle near (E_F, k_F). The change of the slope from unity shows renormalization of the Fermi velocity. This is highlighted in the inset. Note that the Fermi energy E_F is not located at $\omega_{AdS} = 0$. The AdS calculation visualizes the renormalization of the bare UV chemical potential $\mu_0 = \mu_{AdS}$ to the effective chemical potential $\mu_F = \mu_0 - E_F$ felt by the low-frequency fermions.

increasing k_F, rapidly leveling off to a finite constant less than the relativistic speed. Thus the quasiparticles become increasingly heavy as their mass $m_F \equiv k_F/v_F$ asymptotes to linear growth with k_F. The Fermi energy E_F also shows linear growth. Suppose the heavy Fermi-quasiparticle system has the underlying canonical non-relativistic dispersion relation $E = k^2/(2m_F) = k_F^2/(2m_F) + v_F(k - k_F) + ...$, then the observed Fermi energy E_F should equal the renormalized Fermi-energy $E_F^{(ren)} \equiv k_F^2/(2m_F)$. Fig. 3.5B shows that these energies E_F and $E_F^{(ren)}$ track each other remarkably well. We therefore infer that the true zero of energy of the Fermi-quasiparticle is set by the renormalized Fermi-energy as deduced from the Fermi-velocity and -momentum.

Although the true quasiparticle behavior disappears at $T > T_c$, Fig. 3.5A indicates that in the limit $k_F/T \to 0$ the quasiparticle pole strength

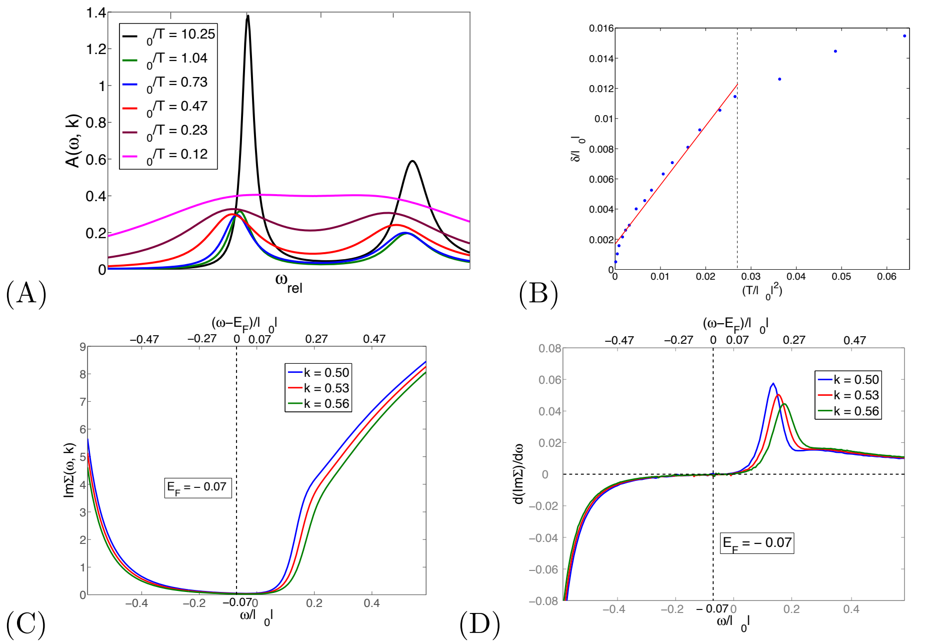

Figure 3.4: (A) Temperature dependence of the quasiparticle peak for $\Delta_\Psi = 5/4$ and $k/k_F \simeq 0.5$; all curves have been shifted to a common peak center. (B) The quasiparticle peak width $\delta \sim \mathrm{Re}\Sigma(\omega, k = k_F)$ for $\Delta_\Psi = 5/4$ as a function of T^2: it reflects the expected behavior $\delta \sim T^2$ up to a critical temperature T_c/μ_0, beyond which the notion of a quasiparticle becomes untenable. (C) The imaginary part of the self-energy $\Sigma(\omega, k)$ near E_F, k_F for $\Delta_\Psi = 1.4$, $\mu_0/T = -30.9$. The defining $\mathrm{Im}\Sigma(\omega, k) \sim (\omega - E_F)^2 + \ldots$-dependence for Fermi-liquid quasiparticles is faint in panel (C) but obvious in panel (D). It shows that the intercept of $\partial_\omega \mathrm{Im}\Sigma(\omega, k)$ vanishes at E_F, k_F.

vanishes, $Z_k \to 0$, while the Fermi-velocity v_F remains finite; v_F approaches the bare velocity $v_F = 1$. This is seemingly at odds with the heavy Fermi liquid wisdom $Z_k \sim m_{micro}/m_F = m_{micro} v_F/k_F$. The resolution is the restoration of Lorentz invariance at zero density. From general Fermi liquid considerations it follows that $v_F = Z_k(1 + \partial_k \mathrm{Re}\Sigma|_{E_F,k_F})$ and $Z_k = 1/(1 - \partial_\omega \mathrm{Re}\Sigma|_{E_F,k_F})$ where $\partial_{k,\omega}\mathrm{Re}\Sigma$ refers to the momentum and energy derivatives of the real part of the fermion self-energy $\Sigma(\omega, k)$ at k_F, E_F. Lorentz invariance imposes $\partial_\omega \Sigma' = -\partial_k \Sigma'$ which allows for vanishing Z_k with $v_F \to 1$. Interestingly, the case has been made that such a relativistic fermionic behavior might be underlying the physics of cuprate

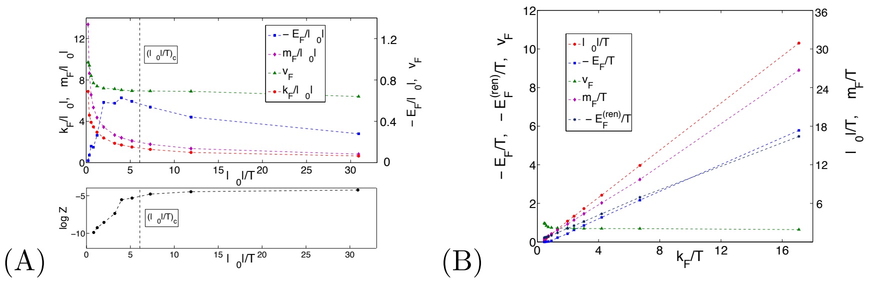

Figure 3.5: The quasiparticle characteristics as a function of μ_0/T for $\Delta_\Psi = 5/4$. Panel (A) shows the change of k_F, v_F, m_F, E_F and the pole strength Z (the total weight between half-maxima) as we change μ_0/T. Beyond a critical value $(\mu_0/T)_c$ we lose the characteristic T^2 broadening of the peak and there is no longer a real quasiparticle, though the peak is still present. For the Fermi-liquid k_F/T rather than μ_0/T is the defining parameter. We can invert this relation and panel (B) shows the quasiparticle characteristics as a function of k_F/T. Note the linear relationships of m_F, E_F to k_F and that the renormalized Fermi energy $E^{(ren)} \equiv k_F^2/(2m_F)$ matches the empirical value E_F remarkably well.

high T_c superconductors [90].

Finally, we address the important question what happens when we vary the conformal dimension Δ_Ψ of the fermionic operator. Fig. 3.6 shows that the Fermi momentum k_F stays constant as we increase Δ_Ψ. This completes our identification of the new phase as the Fermi-liquid: it indicates that the AdS dual obeys Luttinger's theorem, if we can interpret the conformal dimension of the fermionic operator as a proxy for the interaction strength. We find furthermore that the quasiparticle pole strength vanishes as we approach $\Delta_\Psi = 3/2$. This confirms our assumption made earlier that it is essential to study the system for $\Delta_\Psi < d/2$ and that the point $\Delta_\Psi = d/2$ where the naive fermion bilinear becomes marginal signals the onset of a new regime. Because the fermion bilinear is marginal at that point this ought to be an interesting regime in its own right and we refer to the recent article [79] for a discussion thereof. Highly remarkable is that the pole strength vanishes in an exponential fashion rather than the anticipated algebraic behavior [99, 72]. This could indicate that an essential singularity governs the critical point at $\Delta_\Psi = d/2$ and we note that such a type of behavior was identified by Lawler et al. in their analysis of the Pomeranchuk instability in $d = 2+1$ dimensions using the Haldane patching bosonization procedure [75]. Interestingly this finite μ_0/T transition as we vary Δ_Ψ has no clear symmetry change, similar to

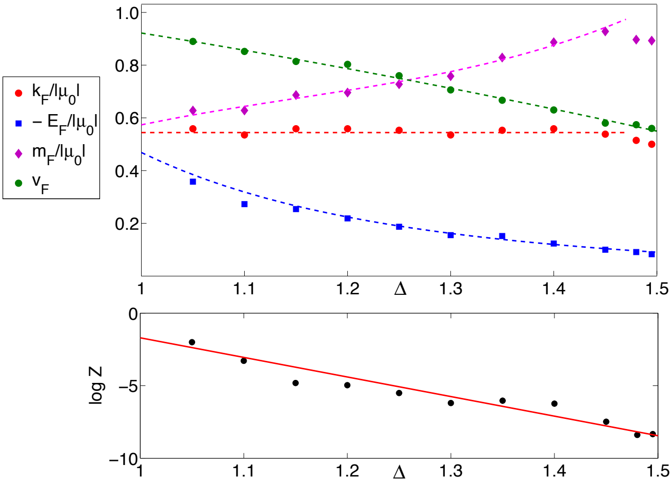

Figure 3.6: The quasiparticle characteristics as a function of the Dirac fermion mass $-1/2 < m < 0$ corresponding to $1 < \Delta_\Psi < 3/2$ for $\mu_0/T = -30.9$. The upper panel shows the independence of k_F of the mass. This indicates Luttinger's theorem if the anomalous dimension Δ_Ψ is taken as an indicator of the interaction strength. Note that v_F, E_F both asymptote to finite values as $\Delta_\Psi \to 3/2$. The lower panel shows the exponential vanishing pole strength Z (the integral between the half-maxima) as $m \to 0$.

[72]. However, this may be an artifact of the fact that our theory is not quantum mechanically complete. Note also that the quasiparticle velocity and the renormalized Fermi energy $E_F = v_F(k - k_F) - E$ stay finite at the $\Delta_\Psi = 3/2$ transition with $Z \to 0$, which could indicate an emergent Lorentz invariance for the reasons discussed in the previous paragraph.

3.3 Concluding remarks

We have presented evidence that the AdS dual description of strongly coupled field theories can describe the emergence of the Fermi-liquid from a quantum critical state — both as a function of density and interaction strength as encoded in the conformal dimension of the fermionic operators. From the AdS gravity perspective, it was unclear whether this would happen. Sharp peaks in the CFT spectral function correspond to so-called quasinormal modes of black holes [68], but Dirac quasinormal modes have received little study (see e.g. [14]). It is remarkable that the AdS calculation processes the Fermi-Dirac statistics essential to the Fermi-liquid correctly. This is manifested by the emergent renormalized Fermi-energy and the validity of Luttinger's theorem. The AdS gravity computation, however, is completely classical without explicit quantum statistics, although we do probe the system with a fermion. It would therefore be interesting to fully understand the AdS description of what is happening, in particular how the emergent scales E_F and k_F feature in the geometry. An early indication of such scales was seen in [101, 94] in a variant of the story that geometry is not universal in string theory: the geometry depends on the probe used and different probes experience different geometric backgrounds. The absence of these scales in the general relativistic description of the AdS black hole could thus be an artifact of the Riemannian metric description of spacetime.

Regardless of these questions, AdS/CFT has shown itself to be an powerful tool to describe finite density Fermi systems. The description of the emergent Fermi liquid presented here argues that AdS/CFT is uniquely suited as a computational device for field-theory problems suffering from fermion sign-problems. AdS/CFT represents a rich mathematical environment and a new approach to investigate qualitatively and quantitatively important questions in quantum many-body theory at finite fermion density.

3.4 Formal background for the calculation of the spectral functions

3.4.1 The AdS set up and AdS/CFT Fermion Green's functions.

The deviation from the strongly coupled 2+1 dimensional quantum critical point from which we wish to see the Fermi surface emerge is characterized by a temperature and background $U(1)$ chemical potential. The phenomenological AdS dual to such a finite-temperature system with chemical potential is a charged AdS$_4$ black hole. Including fermionic excitations, this system is described by the minimal action

$$S_{bulk} = \frac{1}{2\kappa_4^2}\int d^4x\sqrt{-g}\left[R + \frac{6}{L^2} + L^2\left(-\frac{1}{4}F^2 - \bar{\Psi}e_A^M\Gamma^A D_M\Psi - m\bar{\Psi}\Psi\right)\right] \tag{3.4.1}$$

Here e_A^M is the inverse vielbein, $\Gamma^A = \left\{\gamma^a, \gamma^4\right\}$ are 4d Dirac matrices obeying $\{\Gamma^A, \Gamma^B\} = 2\eta^{AB}$ (hermitian except Γ^0), and Ψ is a four-component

Dirac spinor with $\bar{\Psi} = \Psi^\dagger i\Gamma^0$. This spinor is charged under a $U(1)$ gauge field and the covariant derivative equals

$$D_M\Psi = \left(\partial_M + \frac{1}{8}\omega_M^{AB}[\Gamma_A, \Gamma_B] + igA_M\right)\Psi \ . \tag{3.4.2}$$

On its own this action is not a consistent quantum theory. It must be embedded in a string dual, e.g. for appropriate choices of m and g it is a subsector of the $\mathcal{N} = 8$ AdS$_4 \times S_7$ dual to the conformal fixed point of large N_c, $d = 3$ $\mathcal{N} = 8$ SYM and generically such a completion will have a number of $U(1)$ charged fields in addition to the fermions. For our considerations, specifically the two point function of fermions, the quantum completion is not relevant. At leading order in the gravitational coupling constant, the action (5.2.5) will yield the same two-point correlators independently of the non-linear supergravity couplings. It does mean, that we cannot equate the $U(1)$ chemical potential μ_0 directly with the density of fermions μ_F as we emphasize in the main article.

The charged AdS$_4$ black hole is a solution to the equations of motion of this action. In a gauge where $A_z = 0$ and A_0 is regular at the horizon the metric and gauge potential are given by [92, 44]

$$\begin{aligned} ds^2 &= \frac{L^2\alpha^2}{z^2}\left(-f(z)dt^2 + dx^2 + dy^2\right) + \frac{L^2}{z^2}\frac{dz^2}{f(z)} \ , \\ A_0 &= 2q\alpha(z-1) \ , \\ f(z) &= (1-z)(z^2 + z + 1 - q^2z^3) \ . \end{aligned} \tag{3.4.3}$$

For $z \to 0$ the metric asymptotes to AdS$_4$ in Poincaré coordinates with the boundary at $z = 0$ and there is a black hole horizon at the first zero, $z = 1$, of the function $f(z)$. In this parametrization the black hole temperature and $U(1)$ chemical potential — equal to the CFT temperature and bare chemical potential — are

$$T_{CFT} = T_{BH} = \frac{\alpha}{4\pi}(3 - q^2) \ , \quad \mu_0 = \mu_{BH} = -2q\alpha \ . \tag{3.4.4}$$

The parameter q is bounded between $0 \leq q^2 \leq 3$ interpolating between AdS-Schwarzschild and the extremal AdS black hole. For the equation of motion of fermions in this background we shall need the spin connection belonging to this metric. The nonzero components are

$$\omega_0^{ab} = -\delta_0^{[a}\delta_z^{b]}\alpha f\left(\frac{1}{z} - \frac{\partial_z f}{2f}\right) \quad , \quad \omega_i^{ab} = -\delta_i^{[a}\delta_z^{b]}\frac{\alpha\sqrt{f}}{z} \ . \tag{3.4.5}$$

Applying the AdS$_{d+1}$/CFT$_d$ dictionary the CFT fermion-fermion correlation function is computed from the action S_{bulk} (5.2.5) supplemented by appropriate boundary terms, S_{bdy}. One constructs the on-shell action given an arbitrary set of fermionic boundary conditions and the latter are then interpreted as sources of fermionic operators in the CFT:

$$Z_{CFT}(J) = \langle e^{J\mathcal{O}}\rangle_{CFT} \;\;=\;\; \exp\left[i(S_{bulk}+S_{bdy})^{on-shell}(\phi(J))\right]\Big|_{\phi|_{\partial AdS}=J} \quad (3.4.6)$$

The issue of which boundary terms ought to be added to the bulk action tends to be subtle. For fermionic systems it is critical as the bulk action (5.2.5) identically vanishes on-shell [57, 84, 56, 16, 66]. Because the field equations for the fermions are first order and half the components of the spinor correspond to the conjugate momenta of the other half, we can in fact only choose a boundary source for half the components of Ψ. Projecting onto eigenstates of Γ^z, $\Gamma^z\Psi_\pm = \pm\Psi_\pm$, we will choose a boundary source $\Psi_+^0 \equiv \lim_{z_0\to 0}\Psi_+(z=z_0)$ (to regulate the theory we impose the boundary conditions at a small distance z_0 away from the formal boundary $z=0$ and take $z_0\to 0$ at the end). The boundary value Ψ_-^0 is not independent but related to that of Ψ_+^0 by the Dirac equation. We should therefore not include it as an independent degree of freedom when taking functional derivatives with respect to the source. Adding a boundary action,

$$S_{bdy} \;=\; \frac{L^2}{2\kappa_4^2}\int_{z=z_0} d^3x\,\sqrt{-h}\,\bar{\Psi}_+\Psi_- \quad (3.4.7)$$

with $h_{\mu\nu}$ the induced metric ensures a proper variational principle [16]. The variation of $\delta\Psi_-$ from the boundary action,

$$\delta S_{bdy} \;=\; \frac{L^2}{2\kappa_4^2}\int_{z=z_0} d^3x\sqrt{-h}\,\bar{\Psi}_+\delta\Psi_-\Big|_{\Psi_+^0\,\text{fixed}}\;, \quad (3.4.8)$$

now cancels the boundary term from variation of the bulk action

$$\begin{aligned}\delta S_{bulk} \;=\;& \frac{L^2}{2\kappa_4^2}\int\sqrt{-g}\left[-\delta\bar{\Psi}(\not{D}+m)\Psi_+ - \overline{((\not{D}+m)\Psi)}\delta\Psi\right]\\ &+\frac{L^2}{2\kappa_4^2}\int_{z=z_0}\sqrt{-h}\left[-\bar{\Psi}_+\delta\Psi_- - \bar{\Psi}_-\delta\Psi_+\right]\Big|_{\Psi_+^0\,\text{fixed}}\,. \quad (3.4.9)\end{aligned}$$

3.4.2 The Fermion Green's function.

To compute the fermion Green's function, we thus solve the field-equation for $\Psi(z)$ with $\Psi_+^0 \equiv \lim_{z_0\to 0}\Psi_+(z=z_0)$ as the boundary condition, substitute this solution back into the combined action $S_{bulk}+S_{bdy}$ and functionally differentiate twice. As $\Psi_{sol}(\Psi_+^0)$ obeys the field-equation — the Dirac Equation —

$$(\not{D}+m)\Psi^{sol}(\Psi_+^0)=0\ , \tag{3.4.10}$$

the contribution to the on-shell action is solely due to the boundary action S_{bdy} in eq. (3.4.7). To solve the Dirac equation, we Fourier transform along the boundary,

$$\Psi(z,x^i,t)=\int\frac{d\omega d^2k}{(2\pi)^3}\ \Psi(z,k_i,\omega)e^{ik_ix^i-i\omega t}\ , \tag{3.4.11}$$

and project onto the eigenstates of Γ^z, $\Gamma^z\Psi_\pm=\pm\Psi_\pm$. Choosing the basis of Dirac matrices

$$\Gamma^z=\sigma^3\otimes 1\!\!1\ ,\quad \Gamma^i=\sigma^1\otimes\sigma^i\ ,\quad \Gamma^t=\sigma^1\otimes\sigma^t=\sigma^1\otimes i\sigma^3, \tag{3.4.12}$$

we can consider $\Psi_\pm$ to be two-component Dirac spinors appropriate for $d=3$ from here on. In the charged AdS black hole background with non-zero gauge field from eq. (6.3.43), the Dirac equation decomposes into the two equations

$$(\partial_z+\mathcal{A}^\pm)\Psi_\pm=\mp\mathcal{T}\Psi_\mp\ , \tag{3.4.13}$$

with

$$\begin{aligned}\mathcal{A}^\pm &= -\frac{1}{2z}\left(3-\frac{z\partial_z f}{2f}\right)\pm\frac{Lm}{z\sqrt{f}}\ ,\\ \mathcal{T} &= \frac{i}{\alpha f}\left[\left(-\omega+2gq\alpha(z-1)\right)\sigma^t+\sqrt{f}k_i\sigma^i\right]\ .\end{aligned} \tag{3.4.14}$$

We can eliminate either Ψ_+ or Ψ_- and readily derive a second order dynamical equation for $\Psi_\pm$. Using that

$$\mathcal{T}\mathcal{T}=-T_tT_t+T_1T_1+T_2T_2\equiv T^2\ , \tag{3.4.15}$$

we can invert $\mathcal{T}$ to rewrite

$$\frac{\mathcal{T}}{T^2}\left(\partial_z+\mathcal{A}^+\right)\Psi_+=-\Psi_- \tag{3.4.16}$$

and use the Ψ_- equation to obtain

$$(\partial_z + \mathcal{A}^-)\frac{\mathcal{T}}{T^2}(\partial_z + \mathcal{A}^+)\Psi_+ = -\mathcal{T}\Psi_+ \ . \tag{3.4.17}$$

Using the identity eq. (5.2.4) repeatedly, this is equivalent to

$$\left(\partial_z^2 + P(z)\partial_z + Q(z)\right)\Psi_+ = 0 \tag{3.4.18}$$

with

$$\begin{aligned} P(z) &= (\mathcal{A}^- + \mathcal{A}^+) - [\partial_z, \mathcal{T}]\frac{\mathcal{T}}{T^2} \ , \\ Q(z) &= \mathcal{A}^-\mathcal{A}^+ + (\partial_z\mathcal{A}^+) - [\partial_z, \mathcal{T}]\frac{\mathcal{T}}{T^2}\mathcal{A}^+ + T^2 \ . \end{aligned} \tag{3.4.19}$$

Note that both $P(z)$ and $Q(z)$ are two-by-two matrices. The equation for Ψ_- is simply obtained by switching $\mathcal{A}^+$ with $\mathcal{A}^-$ and $\mathcal{T}$ with $-\mathcal{T}$; it is the CPT conjugate obtained by sending $m \to -m$ and $\{\omega, k_i, q\} \to \{-\omega, -k_i, -q\}$.

We can now derive a formal expression for the propagator in terms of the solutions to the second-order equation. We write the on-shell bulk field as

$$\Psi_+^{sol}(z) \quad = \quad F_+(z)F_+^{-1}(z_0)\Psi_+^0(z_0) \tag{3.4.20}$$

where $F_\pm(u)$ is the two-by-two matrix satisfying the second order equation (4.2.11) [16] subject to a boundary condition in the interior of AdS. We will discuss the appropriate interior boundary condition below. There are two independent solutions $\Psi_+^{(1)}(z)$, $\Psi_+^{(2)}(z)$ that obey the interior boundary condition, one for each component of the spinor. In terms of this solution the matrix $F_+(z)$ equals

$$F_+(z) = \left(\Psi_+^{(1)}(z) \ , \quad \Psi_+^{(2)}(z)\right) \ . \tag{3.4.21}$$

Similarly for $\Psi_-^{sol}(z)$ we write

$$\Psi_-^{sol}(z) = F_-(z)F_-^{-1}(z_0)\Psi_-^0(z_0) \ . \tag{3.4.22}$$

However, Ψ_-^0 is not independent as we emphasized earlier. It is related to Ψ_+^0 through the Dirac equation in its projected form (4.3.13). Acting with $\partial_z + A^+$ on both sides of (5.2.11) we see that [16]

$$\begin{aligned} (\partial_z + A^+)\Psi_+^{sol} &= (\partial_z + A^+)F_+(z)F_+^{-1}(z_0)\Psi_+^0 \\ \Leftrightarrow \qquad -\mathcal{T}\Psi_-^{sol} &= -\mathcal{T}F_-(z)F_+^{-1}(z_0)\Psi_+^0 \ . \end{aligned} \tag{3.4.23}$$

We have used that all the z dependence of $\Psi_{\pm}^{sol}(z)$ is encoded in the matrices $F_{\pm}(z)$ and therefore $F_{\pm}(z)$ obey the same projected Dirac equations. Thus we find that Ψ_{-}^{0} equals

$$\Psi_{-}^{0} \;=\; F_{-}(z_0)F_{+}^{-1}(z_0)\Psi_{+}^{0} \; . \qquad (3.4.24)$$

Substituting this constraint into the boundary action, we obtain an expression for the full on-shell action in terms of the solutions $F_{\pm}(z)$:

$$S^{on-shell} = \frac{L^2}{2\kappa_4^2}\int_{z=z_0}\frac{d\omega d^2k}{(2\pi)^3}\sqrt{-h}\;\bar{\Psi}_{+}^{0}\,F_{-}(z_0)F_{+}^{-1}(z_0)\,\Psi_{+}^{0} \; . \qquad (3.4.25)$$

Up to a normalization $\mathcal{N}$ the two-point function is therefore

$$G(\omega,k) = \frac{1}{\mathcal{N}}F_{-}(z_0)F_{+}^{-1}(z_0) \; . \qquad (3.4.26)$$

This is the time-ordered two-point function. For the spectral function we shall need the imaginary part of the retarded propagator. At finite temperature the AdS background is no longer regular in the interior but has a horizon. In principle one should also consider its boundary contribution. The retarded propagator prescription of [105] — verified in [58]— is to ignore this contribution and to impose infalling boundary conditions at the horizon instead of regularity at the center of AdS. This is what we shall do.

The retarded Green's function for fermions is still a matrix. Parity and rotational invariance dictate that it can be decomposed as

$$G_R(\omega,k) = \Pi_s + \sigma^t\Pi_t + \sigma^i\Pi_i \; . \qquad (3.4.27)$$

Our main interest, the spectral function, proportional to $\mathrm{Im}\langle\Psi^\dagger\Psi\rangle$, is the imaginary part of Π_t. Specifically

$$A(\omega,k) = -\frac{1}{\pi}\mathrm{Im}(\mathrm{Tr}\, i\sigma^t G_R(\omega,k)) \; . \qquad (3.4.28)$$

As a consequence of the underlying conformal symmetry both the Green's function and the spectral function possess a scaling symmetry. Eq. (5.2.14) shows that the frequency ω and momenta k are naturally expressed in units of an effective temperature $T_{eff}(\mu_0) \equiv 3\alpha/4\pi$ which depends on the chemical potential μ_0

$$T_{eff}(\mu_0) = T\left(\frac{1}{2}+\frac{1}{2}\sqrt{1+\frac{(\mu_0\sqrt{3})^2}{(4\pi T)^2}}\right) \; .$$

The spectral function computed from AdS is therefore naturally of the form

$$A^{\frac{\mu_0}{T}}_{\Delta_\Psi}(\omega,k) = \frac{1}{T^{d-2\Delta_\Psi}}\tilde{f}\left(\frac{\omega}{T_{eff}(\mu_0)},\frac{k}{T_{eff}(\mu_0)};\Delta_\Psi,\frac{\mu_0}{T}\right) .$$

Any rescaling of T_{eff} can be compensated by a rescaling of the frequencies and momenta and μ_0/T is the single independent parameter determining the characteristics of the fermion spectral function. The results in the main text have been converted to units of k/T or k/μ_0 for clarity of the presentation.

3.4.3 Masses and Dimensions.

A final crucial step is the establish the aforementioned relation between the mass of the AdS fermion and the scaling dimension of the dual fermionic operator in the CFT. For generality we shall work in d dimensions in this subsection. This subsection recapitulates [16].

The scaling behavior can be read off from the asymptotic behavior of the solution near the boundary $z=0$. In this limit the second order equation (4.2.11) diagonalizes: (setting $L=1$)

$$\left(\partial_z^2 - \frac{d}{z}\partial_z + \frac{d(d+2)-4m(1+m)}{4z^2}\right)\Psi_+ = 0 + \dots \tag{3.4.29}$$

Clearly the temperature or chemical potential of the black-hole is immaterial to the asymptotic scaling behaviour at $z=0$; in terms of the CFT $z=0$ is the UV of the theory and it should be insensitive to the infrared physics at the horizon. The leading powers of the two independent solutions to this equation are

$$\Psi_+(z) = z^{\frac{d+1}{2}-|m+\frac{1}{2}|}(\psi_+ + \dots) + z^{\frac{d+1}{2}+|m+\frac{1}{2}|}(A_+ + \dots) . \tag{3.4.30}$$

(we may drop the absolute value signs in principle, but as it emphasizes the special value $m=-1/2$ it will be instructive to keep them.) Similarly for $\Psi_-(z)$ the leading singularities are obtained by sending $m \to -m$

$$\Psi_-(z) = z^{\frac{d+1}{2}-|m-\frac{1}{2}|}(\psi_- + \dots) + z^{\frac{d+1}{2}+|m-\frac{1}{2}|}(A_- + \dots). \tag{3.4.31}$$

However, recall that the Dirac equation relates the two asymptotic behaviors and that the boundary value of Ψ_- is not independent. Near $z=0$

$$(\partial_z - \frac{d/2-m}{z})\Psi_+ = -\not{T}|_{z=0}\Psi_- + \dots \tag{3.4.32}$$

Thus $\psi_- \propto \psi_+$ and $A_- \propto A_+$.

Because the equation diagonalizes, each component of $\Psi_\pm(z)$ can be considered independently and the matrices $F_\pm(z)$ diagonalize in the limit $z \to 0$. The scaling behavior of the Green's function is then readily read off from its definition

$$G(\omega, k) = \frac{1}{\mathcal{N}} F_- F_+^{-1} \sim \frac{z^{\frac{d+1}{2} - |m - \frac{1}{2}|}(\psi_- + \ldots) + z^{\frac{d+1}{2} + |m - \frac{1}{2}|}(A_- + \ldots)}{z^{\frac{d+1}{2} - |m + \frac{1}{2}|}(\psi_+ + \ldots) + z^{\frac{d+1}{2} + |m + \frac{1}{2}|}(A_+ + \ldots)} \quad (3.4.33)$$

The dominant scaling behavior depends on the value of m and there are three different regimes (I): $m > \frac{1}{2}$, (II): $\frac{1}{2} > m > -\frac{1}{2}$, and (III): $-\frac{1}{2} > m$. In these regimes the Green's function behaves as

$$G(\omega, k) \sim \begin{cases} z\left(\frac{\psi_-}{\psi_+} + \ldots\right) + z^{2m}\left(\frac{A_-}{\psi_+} + \ldots\right) & m > \frac{1}{2} \\ z^{2m}\left(\frac{\psi_-}{\psi_+} + \ldots\right) + z\left(\frac{A_-}{\psi_+} + \ldots\right) & \frac{1}{2} > m > -\frac{1}{2} \\ \frac{1}{z}\left(\frac{\psi_-}{\psi_+} + \ldots\right) + \frac{1}{z^{2m}}\left(\frac{A_-}{\psi_+} + \ldots\right) & -\frac{1}{2} > m. \end{cases} \quad (3.4.34)$$

In regime (I) the contribution proportional to z yields a contact term [16]. Recall that at zero-temperature and chemical potential each power of z is accompanied by a power of momentum: the dimensionless arguments of the solutions $\Psi_\pm^{sol}(z)$ are kz and ωz. Discarding the term analytic in z and thus analytic in momenta, the second term proportional to z^{2m} yields a Green's function

$$G(\omega, k) \sim (z_0 \omega)^{2m} \quad (3.4.35)$$

corresponding to the two-point function of a conformal operator of weight $\Delta_\Psi = \frac{d}{2} + m$. In regime (II) there is no contact term and one immediately finds the same relation between the AdS fermion mass and the scaling dimension of the conformal operator. In regime (III), however, one finds an explicit pole $(\omega z)^{-1}$ independent of the AdS fermion mass or the space-time dimension. It signals an inconsistency in the theory and one cannot consider this regime as physical [16]. This is reminiscent of the situation for scalars where for $m^2_{scalar} > -d^2/4 + 1$ one finds analytic terms in the two-point correlator; for $-d^2/4 + 1 > m^2_{scalar} > -d^2/4$ both solutions are normalizable; and for $-d^2/4 > m^2_{scalar}$ the theory is inconsistent. The analogy with scalars may appear strange since a negative mass-squared for scalars clearly can be problematic, whereas the sign of the fermion-mass term does not have any physical consequences normally. Recall, however, that the same AdS bulk action can describe several CFTs depending on the boundary terms added to the action [67]. We have chosen a very specific boundary action such that $\Psi_+(z)$ is the independent variable which breaks the degeneracy between (bulk) theories with $m > 0$ and $m < 0$. In this theory m is bounded below by $-1/2$. We could have chosen a different theory with $\Psi_-(z)$ the independent variable. One would find then that m is bounded from above by $1/2$. The regime $1/2 > m > -1/2$ is present in both theories; it is the range where both solutions are normalizable and choosing either $\Psi_+(z)$ or $\Psi_-(z)$ as the independent variable corresponds to switching the "sources" and "expectation values" in the usual way (see also [62]).

This analysis also teaches us that the normalization $\mathcal{N}$ should go as z_0^{2m} to obtain a finite answer in the limit $z_0 \to 0$.[2]

3.4.4 The retarded propagator boundary conditions at the horizon.

The final component of our set-up will be the boundary conditions at the horizon of the the black hole. To compute the retarded propagator in thermal settings/black hole the appropriate b.c. are those infalling into the horizon. Near the horizon at $z = 1$, the second order equation for $\Psi_\pm$ becomes the same for both Ψ_+ and Ψ_- and moreover diagonalizes:

$$\left(\partial_z^2 - \frac{3}{2(1-z)}\partial_z + \frac{\tilde{\omega}^2 + \frac{1}{16}}{(1-z)^2}\right)\Psi_\pm + \mathcal{O}((z-1)) = 0. \tag{3.4.36}$$

with $\tilde{\omega} \equiv \frac{\omega}{a(3-q^2)} = \frac{\omega}{4\pi T}$. This equation has solutions of the form

$$\Psi_\pm = (1-z)^{i\tilde{\omega}-\frac{1}{4}}(c_r + ...) + (1-z)^{-i\tilde{\omega}-\frac{1}{4}}(c_i + ...) \tag{3.4.37}$$

The second solution has the incoming boundary condition we seek.[3]

---

[2]Note that the factor $L^2/2\kappa_4^2$ in the on-shell action (5.2.10) follows from an unconventional normalization of the fields in the action (5.2.5). It would be absent for conventional normalization.

[3]A technical detail is that due to the factors $\sqrt{f}$ in the field equation, there is no standard Frobenius solution $\Psi_\pm = (1-z)^{\pm i\tilde{\omega}-\frac{1}{4}}\sum_{n=0}^{\infty} a_n^{(\pm)}(1-z)^n$. Rather half-integer powers of $(1-z)$ appear as well. We need the Frobenius method for the numerics: we use it to construct a second b.c. for the derivative of Ψ_+ — see e.g. [12]. Changing coordinates to $z = 1 - s^2$ solves this problem.

3.5 Finite temperature and the position of the Fermi surface

With some hindsight from the chapters to follow, as well as in the light of the detailed analysis performed in [79, 27] we will now comment on our finding that *at finite temperature* the zero of energy in field theory, i.e. the position of the Fermi surface lies at finite ω, i.e. differs from the AdS zero of energy $\omega = 0$. In our original paper reproduced in the previous sections, we identified the zero of energy at finite temperature with the maximum of the peak height. Our assumption was clearly that the peak maximum closely corresponds to the definition of zero energy: a pole for real ω at $T = 0$. For small T/μ thus the pole should not move much as the temperature is changed, and therefore neither should the position of the maximum peak height. We can test this hypothesis by plotting the position of the maximum of the spectral function $A(\omega, k = k_F)$ for three different temperatures (Figure 3.7A). Surprisingly, we see that the position of the maximum $E_F(T)$ drastically depends on T and moves toward $\omega = 0$ as the temperature is lowered. This suggests (in agreement with the arguments given in [79, 27]) that the sharp Fermi surface, which only exists at $T = 0$, is indeed at zero energy. This strong dependence of the peak position on temperature is not known in field theory models, and in the following chapter we will see that it suggests an inconsistency in the probe limit calculations presented in this section. The changing position $E_F(T)$ is due to the instability of the black hole background in the presence of Fermi surface (in the next chapter we will see that gravity dual of a Fermi surface always has finite fermion density, which backreacts on the gauge field and the metric).

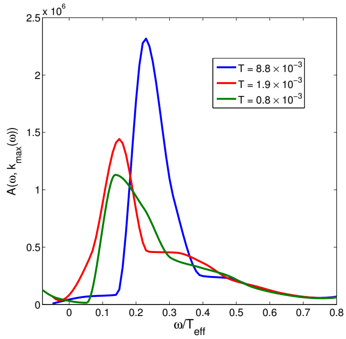

Figure 3.7: Spectral weight at its maximum, i.e. at the position of the peak for three different values of temperature and $\Delta_\Psi = 5/4$. We see that the maximum moves toward zero energy as the temperature is lowered. This suggests that the true zero temperature ground state is indeed at $\omega = 0$. However, the fact that the "Fermi energy" is strongly temperature-dependent is in fact a signal that we are looking at the false vacuum, i.e. that a self-consistent calculation with backreaction would yield a background different from the Reissner-Nordström black hole. (B) The relation between the linearly dispersing quasiparticle peak and the $\omega = 0$ peak with slow (sublinear) dispersion as $\Delta_\Psi \to 3/2$ for $k/\mu_0 = 0.35$ and $\mu_0/T = -30.9$.

Chapter 4

AdS dual of a Fermi liquid: Dirac hair [18]

4.1 Introduction

Fermionic quantum criticality is thought to be an essential ingredient in the full theory of high T_c superconductivity [112, 102]. The cleanest experimental examples of quantum criticality occur in heavy-fermion systems rather than high T_c cuprates, but the experimental measurements in heavy fermions raise equally confounding theoretical puzzles [80]. Most tellingly, the resistivity scales linearly with the temperature from the onset of superconductivity up to the crystal melting temperature [42] and this linear scaling is in conflict with single correlation length scaling at criticality [86]. The failure of standard perturbative theoretical methods to describe such behavior is thought to indicate that the underlying quantum critical system is strongly coupled [117, 78].

The combination of strong coupling and scale-invariant critical dynamics makes these systems an ideal arena for the application of the AdS/CFT correspondence: the well-established relation between strongly coupled conformal field theories (CFT) and gravitational theories in anti-de Sitter (AdS) spacetimes. An AdS/CFT computation of single-fermion spectral functions — which are directly experimentally accessible via Angle-Resolved Photoemission Spectroscopy [11, 21, 121] — bears out this promise of addressing fermionic quantum criticality [79, 17, 27, 28] (see also [76, 91]). The AdS/CFT single fermion spectral function exhibits distinct sharp quasiparticle peaks, associated with the formation of a Fermi surface, emerging from a scale-free state. The fermion liquid which this Fermi surface captures is generically singular: it has either a non-linear dispersion or non-quadratic pole strength [79, 27]. The precise details depend on the parameters of the AdS model.

From the AdS gravity perspective, peaks with linear dispersion correspond to the existence of a stable charged fermionic quasinormal mode in the spectrum of a charged AdS black hole. The existence of a stable charged bosonic quasinormal mode is known to signal the onset of an instability towards a new ground state with a pervading Bose condensate extending from the charged black hole horizon to the boundary of AdS. The dual CFT description of this charged condensate is spontaneous symmetry breaking as in a superfluid and a conventional superconductor [40, 47, 49]. For fermionic systems empirically the equivalent robust $T = 0$ groundstate is the Landau Fermi Liquid — the quantum groundstate of a system with a finite number of fermions. The existence of a stable fermionic quasinormal mode suggests that an AdS dual of a finite fermion density state exists.

Here we shall make a step towards the set of AdS/CFT rules for CFTs with a finite fermion density. The essential ingredient will be Migdal's theorem, which relates the characteristic jump in fermion occupation number at the energy ω_F of the highest occupied state to the pole strength of the quasiparticle. The latter we know from the spectral function analysis and its AdS formulation is therefore known. Using this, we can show that the fermion number discontinuity is encoded in the *probability density* of the normalizable wavefunction of the dual AdS fermion field.

This shows that the AdS dual of a Fermi liquid is given by a system with occupied fermionic states in the bulk. The Fermi liquid is clearly not a scale invariant state, but any such states will have energy, momentum/pressure and charge and will change the interior geometry from AdS to something else. Which particular (set of) state(s) is the right one, it does not yet tell us, as this conclusion relies only on the asymptotic behavior of fermion fields near the AdS boundary. Here we shall take the simplest such state: a single fermion.[1] Constructing first a set of equations in terms of the spatially averaged density, we find the associated backreacted asymptotically AdS solution. This approximate solution is already good enough to solve several problems of principle:

- A charged AdS black hole in the presence of charged fermionic modes

[1]These solutions are therefore the AdS extensions of [30–33].

has a critical temperature below which fermionic Dirac "hair" forms. For our effective single fermion solution, the derivative of the free energy has the characteristic discontinuity of a first order transition. In AdS/CFT this has to be the case: In contrast to bosonic quasinormal modes, a fermionic quasinormal mode can never cause a linear instability indicative of a continuous phase transition. In the language of spectral functions, the pole of the retarded Green's function can never cross to the upper-half plane [27].[2] The absence of a perturbative instability between this conjectured Dirac "black hole hair" solution and the "bald" charged AdS black hole can be explained if the transition is a first order gas-liquid transition. The existence of first order transition follows from a thermodynamic analysis of the free energy rather than a spectral analysis of small fluctuations.

- This solution with finite fermion profile is the preferred ground state at low temperatures compared to the bare charged AdS black hole. The latter is therefore a false vacuum in a theory with charged fermions. Confusing a false vacuum with the true ground state can lead to anomalous results. Indeed the finite temperature behavior of fermion spectral functions in AdS Reissner-Nordström, exhibited in the combination of the results of [79, 27] and [17], shows strange behavior. The former [79, 27] found sharp quasiparticle peaks at a frequency $\omega_F = 0$ in natural AdS units, whereas the latter [17] found sharp quasiparticle peaks at finite Fermi energy $\omega_F \neq 0$. As we will show, both peaks in fact describe the same physics: the $\omega_F \neq 0$ peak is a finite temperature manifestation of (one of the) $\omega = 0$ peaks in [27]. Its shift in location at finite temperature is explained by the existence of the nearby true finite fermion density ground state, separated by a potential barrier from the AdS Reissner-Nordström solution.

- The solution we construct here only considers the backreaction on the electrostatic potential. We show, however, that the gravitational energy density diverges at the horizon. This ought to be, as one expects the infrared geometry to change due to fermion profile. The charged AdS-black hole solution corresponds to a CFT system in a state with large ground state entropy. This is the area of the extremal black-hole horizon at $T = 0$. Systems with large ground-

[2] Ref. [10] argues that the instability can be second order.

state entropy are notoriously unstable to collapse to a low-entropy state, usually by spontaneous symmetry breaking. In a fermionic system it should be the collapse to the Fermi liquid. The final state will generically be a geometry that asymptotes to Lifschitz type, i.e. the background breaks Lorentz-invariance and has a double-pole horizon with vanishing area, as expounded in [50]. Indeed the gravitational energy density diverges at the horizon in a similar way as other systems that are known to gravitationally backreact to a Lifshitz solution. The fully backreacted geometry includes important separate physical aspects — it is relevant to the stability and scaling properties of the Fermi liquid — and will be considered in a companion article.

The Dirac hair solution thus captures the physics one expects of the dual of a Fermi liquid. We have based its construction on a derived set of AdS/CFT rules to describe systems at finite fermion density. Qualitatively the result is as expected: one also needs occupied fermionic states in the bulk. Next to our effective single fermion approximation, another simple candidate is the backreacted AdS-Fermi-gas [50]/electron star [51] which appeared during the course of this work.[3] The difference between the two approaches are the assumptions used to reduce the interacting Fermi system to a tractable solution. Ideally, one should carefully track all the fermion wavefunctions as in the recent article [96]. As explained in [19] the Fermi-gas and the single Dirac field are the two "local" approximations to the generic non-local multiple fermion system in the bulk, in very different regimes of applicability. The electron-star/Fermi-gas is considered in the Thomas-Fermi limit where the microscopic charge of the constituent fermions is sent to zero keeping the overall charge fixed, whereas the single Dirac field clearly is the 'limit' where the microscopic charge equals the total charge in the system. This is directly evident in the spectral functions of both systems. The results presented here show that each pole in the CFT spectral function corresponds to a unique occupied Fermi state in the bulk; the electron star spectra show a parametrically large number of poles [53, 63, 19], whereas the Dirac hair state has a single quasiparticle pole by construction. The AdS-Dirac-hair black hole derived here therefore has the benefit of a direct connection with a unique Fermi liquid state in the CFT. This is in fact the starting point of our derivation.

[3] See also [23, 6]. An alternative approach to back-reacting fermions is [64].

In the broader context, the existence of both the Dirac hair and backreacted Fermi gas solution is not a surprise. It is a manifestation of *universal* physics in the presence of charged AdS black holes. The results here, and those of [79, 27, 50, 51], together with the by now extensive literature on holographic superconductors, i.e. Bose condensates, show that at sufficiently low temperature in units of the black-hole charge, the electric field stretching to AdS-infinity causes a spontaneous discharge of the bulk vacuum outside of the horizon into the charged fields of the theory — whatever their nature. The positively charged excitations are repelled by the black hole, but cannot escape to infinity in AdS and they form a charge cloud hovering over the horizon. The negatively charged excitations fall into the black-hole and neutralize the charge, until one is left with an uncharged black hole with a condensate at finite T or a pure asymptotically AdS-condensate solution at $T = 0$. As [50, 51] and we show, the statistics of the charged particle do not matter for this condensate formation, except in the way it forms: bosons superradiate and fermions nucleate. The dual CFT perspective of this process is "entropy collapse". The final state therefore has negligible ground state entropy and is stable. The study of charged black holes in AdS/CFT is therefore a novel way to understand the stability of charged interacting matter which holds much promise.

4.2 From Green's function to AdS/CFT rules for a Fermi Liquid

We wish to show how a solution with finite fermion number — a Fermi liquid — is encoded in AdS. The exact connection and derivation will require a review of what we have learned of Dirac field dynamics in AdS/CFT through Green's functions analysis. The defining signature of a Fermi liquid is a quasi-particle pole in the (retarded) fermion propagator,

$$G_R = \frac{Z}{\omega - \mu_R - v_F(k - k_F)} + \text{regular} \qquad (4.2.1)$$

Phenomenologically a non-zero residue at the pole, Z, also known as the pole strength, is the indicator of a Fermi liquid state. Migdal famously related the pole strength to the occupation number discontinuity at the pole $\omega = 0$.

$$Z = \lim_{\epsilon \to 0} [n_F(\omega - \epsilon) - n_F(\omega + \epsilon)] \qquad (4.2.2)$$

where

$$n_F(\omega) = \int d^2k f_{FD}\left(\frac{\omega}{T}\right)\mathrm{Im}G_R(\omega,k).$$

with f_{FD} the Fermi-Dirac distribution function. Vice versa, a Fermi liquid with a Fermi-Dirac jump in occupation number at the Fermi energy $\omega_F = 0$ has a low-lying quasiparticle excitation. Using our knowledge of fermionic spectral functions in AdS/CFT we shall first relate the pole-strength Z to known AdS quantities. Then using Migdal's relation, the dual of a Fermi liquid is characterized by an asymptotically AdS solution with non-zero value for these very objects.

The Green's functions derived in AdS/CFT are those of charged fermionic operators with scaling dimension Δ, dual to an AdS Dirac field with mass $m = \Delta - \frac{d}{2}$. We shall focus on $d = 2+1$ dimensional CFTs. In its gravitational description this Dirac field is minimally coupled to 3+1 dimensional gravity and electromagnetism with action

$$S = \int d^4x\sqrt{-g}\left[\frac{1}{2\kappa^2}\left(R + \frac{6}{L^2}\right) - \frac{1}{4}F^2_{MN} - \bar{\Psi}(\not{D} + m)\Psi\right] . \quad (4.2.3)$$

For zero background fermions, $\Psi = 0$, a spherically symmetric solution is a charged AdS$_4$ black-hole background

$$\begin{aligned} ds^2 &= \frac{L^2\alpha^2}{z^2}\left(-f(z)dt^2 + dx^2 + dy^2\right) + \frac{L^2}{z^2}\frac{dz^2}{f(z)} , \\ f(z) &= (1-z)(1+z+z^2-q^2z^3) , \\ A_0^{(bg)} &= 2q\alpha(z-1) . \end{aligned} \quad (4.2.4)$$

Here $A_0^{(bg)}$ is the time-component of the $U(1)$-vector-potential, L is the AdS radius and the temperature and chemical potential of the black hole equal

$$T = \frac{\alpha}{4\pi}(3-q^2) , \quad \mu_0 = -2q\alpha, \quad (4.2.5)$$

where q is the black hole charge.

To compute the Green's functions we need to solve the Dirac equation in the background of this charged black hole:

$$e^M_A\Gamma^A(D_M + iegA_M)\Psi + m\Psi = 0 , \quad (4.2.6)$$

where the vielbein e_A^M, covariant derivative D_M and connection A_M correspond to the fixed charged AdS black-hole metric and electrostatic potential (6.2.4)Denoting $A_0 = \Phi$ and taking the standard AdS-fermion projection onto $\Psi_\pm = \frac{1}{2}(1 \pm \Gamma^Z)\Psi$, the Dirac equation reduces to

$$(\partial_z + \mathcal{A}_\pm)\,\Psi_\pm \;=\; \mp \not{\mathcal{T}}\Psi_\mp \tag{4.2.7}$$

with

$$\begin{aligned}\mathcal{A}_\pm &= -\frac{1}{2z}\left(3 - \frac{zf'}{2f}\right) \pm \frac{mL}{z\sqrt{f}}\;,\\ \not{\mathcal{T}} &= \frac{i(-\omega + g\Phi)}{\alpha f}\gamma^0 + \frac{i}{\alpha\sqrt{f}}k_i\gamma^i\;.\end{aligned} \tag{4.2.8}$$

Here γ^μ are the 2+1-dimensional Dirac matrices, obtained after decomposing the 3+1 dimensional Γ^μ-matrices.

Explicitly the Green's function is extracted from the behavior of the solution to the Dirac equation at the AdS-boundary. The boundary behavior of the bulk fermions is

$$\begin{aligned}\Psi_+(\omega, k; z) &= A_+ z^{\frac{3}{2}-m} + B_+ z^{\frac{5}{2}+m} + \ldots,\\ \Psi_-(\omega, k; z) &= A_- z^{\frac{5}{2}-m} + B_- z^{\frac{3}{2}+m} + \ldots,\end{aligned} \tag{4.2.9}$$

where $A_\pm(\omega, k),\ B_\pm(\omega, k)$ are not all independent but related by the Dirac equation at the boundary

$$A_- = -\frac{i\mu}{(2m-1)}\gamma^0 A_+\;,\quad B_+ = -\frac{i\mu}{(2m+1)}\gamma^0 B_-\;. \tag{4.2.10}$$

The CFT Green's function then equals [17, 62, 79]

$$G_R = \lim_{z\to 0} z^{-2m}\frac{\Psi_-(z)}{\Psi_+(z)} - \text{singular} = \frac{B_-}{A_+}\;. \tag{4.2.11}$$

In other words B_- is the CFT response to the (infinitesimal) source A_+. Since in the Green's function the fermion is a fluctuation, the functions $\Psi_\pm(z)$ are now probe solutions to the Dirac equation in a fixed gravitational and electrostatic background (for ease of presentation we are considering $\Psi_\pm(z)$ as numbers instead of two-component vectors). The boundary conditions at the horizon/AdS interior determine which Green's function one considers, e.g. infalling horizon boundary conditions yield the retarded Green's function. For non-zero chemical potential this fermionic Green's function can have a pole signalling the presence of a Fermi surface. This pole occurs precisely for a (quasi-)normalizable mode, i.e. a specific energy ω_F and momentum k_F where the external source $A_+(\omega, k)$ vanishes (for infalling boundary conditions at the horizon).

Knowing that the energy of the quasinormal mode is always $\omega_F = 0$ [79] and following [27], we expand G_R around $\omega = 0$ as:

$$G_R(\omega) = \frac{B^{(0)} + \omega B^{(1)} + \dots}{A_+^{(0)} + \omega A_+^{(1)} + \dots}. \tag{4.2.12}$$

A crucial point is that in this expansion we are assuming that the pole will correspond to a stable quasiparticle, i.e. there are no fractional powers of ω less than unity in the expansion around $\omega_F = 0$ [27]. Fermions in AdS/CFT are of course famous for allowing more general pole-structures corresponding to Fermi-surfaces without stable quasiparticles [27], but those Green's functions are not of the type (4.2.1) and we shall therefore not consider them here. The specific Fermi momentum k_F associated with the Fermi surface is the momentum value for which the first ω-independent term in the denominator vanishes $A_+^{(0)}(k_F) = 0$ — for this value of $k = k_F$ the presence of a pole in the Green's functions at $\omega = 0$ is manifest. Writing $A_+^{(0)} = a_+(k - k_F) + \dots$ and comparing with the standard quasiparticle propagator,

$$G_R = \frac{Z}{\omega - \mu_R - v_F(k - k_F)} + \text{regular} \tag{4.2.13}$$

we read off that the pole-strength equals

$$Z = B_-^{(0)}(k_F)/A_+^{(1)}(k_F).$$

We thus see that a non-zero pole-strength is ensured by a non-zero value of $B_-(\omega = 0, k = k_F)$ — the "response" *without* corresponding source as $A^{(0)}(k_F) \equiv 0$. Quantitatively the pole-strength also depends on the value of $A_+^{(1)}(k_F) \equiv \partial_\omega A_+(k_F)|_{\omega=0}$, which is always finite. This is not a truly independent parameter, however. The size of the pole-strength has only a relative meaning w.r.t. to the integrated spectral density. This normalization of the pole strength is a global parameter rather than an AdS boundary issue. We now show this by proving that $A_+^{(1)}(k_F)$ is inversely proportional to $B_-^{(0)}(k_F)$ and hence Z is completely set by $B_-^{(0)}(k_F)$, i.e.

$Z \sim |B_-^{(0)}(k_F)|^2$. Consider a transform $\widetilde{W}(\Psi_{+,A}, \Psi_{+,B})$ of the Wronskian $W(\Psi_{+,A}, \Psi_{+,B}) = \Psi_{+,A}\partial_z\Psi_{+,B} - (\partial_z\Psi_{+,A})\Psi_{+,B}$ for two solutions to the second order equivalent of the Dirac equation for the field Ψ_+

$$\left(\partial_z^2 + P(z)\partial_z + Q_+(z)\right)\Psi_+ = 0 \tag{4.2.14}$$

that is conserved (detailed expressions for $P(z)$ and $Q_+(z)$ will be given later):

$$\widetilde{W}(\Psi_{+,A}(z), \Psi_{+,B}(z), z; z_0) = \exp\left(\int_{z_0}^{z} P(z)\right) W(\Psi_{+,A}(z), \Psi_{+,B}(z)) \tag{4.2.15}$$

For this quantity it holds $\partial_z\widetilde{W} = 0$. Here z_0^{-1} is the infinitesimal distance away from the boundary at $z = 0$ which is equivalent to the UV-cutoff in the CFT. Setting $k = k_F$ and choosing for $\Psi_{+,A} = A_+ z^{3/2-m}\sum_{n=0}^{\infty} a_n z^n$ and $\Psi_{+,B} = B_+ z^{5/2+m}\sum_{n=0}^{\infty} b_n z^n r$ the real solutions which asymptote to solutions with $B_+(\omega, k_F) = 0$ and $A_+(\omega, k_F) = 0$ respectively, but for a value of ω infinitesimally away from $\omega_F = 0$, we can evaluate $\widetilde{W}$ at the boundary to find,[4]

$$\widetilde{W} = z_0^3(1 + 2m)A_+B_+ = \mu z_0^3 A_+B_- \tag{4.2.16}$$

The last step follows from the constraint (5.2.2) where the reduction from two-component spinors to functions means that γ^0 is replaced by one of its eigenvalues $\pm i$. Taking the derivative of $\widetilde{W}$ at $\omega = 0$ for $k = k_F$ and expanding $A_+(\omega, k_F)$ and $B_-(\omega, k_F)$ as in (4.2.12), we can solve for $A_+^{(1)}(k_F)$ in terms of $B_-^{(0)}(k_F)$ and arrive at the expression for the pole strength Z in terms of $|B_-^{(0)}(k_F)|^2$:

$$Z = \frac{\mu z_0^3}{\partial_\omega\widetilde{W}|_{\omega=0,k=k_F}} |B_-^{(0)}(k_F)|^2 \ . \tag{4.2.17}$$

Because $\partial_\omega\widetilde{W}$, as $\widetilde{W}$, is a number that is independent of z, this expression emphasizes that it is truly the nonvanishing subleading term $B_-^{(0)}(\omega_F, k_F)$ which sets the pole strength, up to a normalization $\partial_\omega\widetilde{W}$ which is set by the fully integrated spectral density. This integration is always UV-cut-off dependent and the explicit z_0 dependence should therefore not

[4] $P(z) = -3/z + \ldots$ near $z = 0$

surprise us.[5] We should note that, unlike perturbative Fermi liquid theory, Z is a dimensionful quantity of mass dimension $2m+1 = 2\Delta - 2$, which illustrates more directly its scaling dependence on the UV-energy scale z_0. At the same time Z is real, as it can be shown that both $\partial_\omega \widetilde{W}|_{\omega=0,k=k_F} = \mu z_0^3 A_+^{(1)} B_-^{(0)}$ and $B_-^{(0)}$ are real [27].

4.2.1 The AdS dual of a stable Fermi Liquid: Applying Migdal's relation holographically

We have thus seen that a solution with nonzero $B_-(\omega_F, k_F)$ whose corresponding external source vanishes (by definition of $\omega_F,\ k_F$), is related to the presence of a quasiparticle pole in the CFT. Through Migdal's theorem its pole strength is related to the presence of a discontinuity of the occupation number, and this discontinuity is normally taken as the characteristic signature of the presence of a Fermi Liquid. Qualitatively we can already infer that an AdS gravity solution with non-vanishing $B_-(\omega_F, k_F)$ corresponds to a Fermi Liquid in the CFT. We thus seek solutions to the Dirac equation with vanishing external source A_+ but non-vanishing response B_- coupled to electromagnetism (and gravity). The construction of the AdS black hole solution with a finite single fermion wavefunction is thus analogous to the construction of a holographic superconductor [47] with the role of the scalar field now taken by a Dirac field of mass m.

This route is complicated, however, by the spinor representation of the Dirac fields, and the related fermion doubling in AdS. Moreover, relativistically the fermion Green's function is a matrix and the pole strength Z appears in the time-component of the vector projection $\mathrm{Tr} i\gamma^i G$. As we take this and the equivalent jump in occupation number to be the signifying characteristic of a Fermi liquid state in the CFT, it would be

[5] Using that $\widetilde{W}$ is conserved, one can e.g. compute it at the horizon. There each solution $\Psi_{+,A}(\omega, k_F; z)$, $\Psi_{+,B}(\omega, k_F; z)$ is a linear combination of the infalling and outgoing solution

$$\begin{aligned}\Psi_{+,A}(z) &= \bar{\alpha}\,(1-z)^{-1/4+\imath\omega/4\pi T} + \alpha\,(1-z)^{-1/4-\imath\omega/4\pi T} + \ldots \\ \Psi_{+,B}(z) &= \bar{\beta}\,(1-z)^{-1/4+\imath\omega/4\pi T} + \beta\,(1-z)^{-1/4-\imath\omega/4\pi T} + \ldots \end{aligned} \tag{4.2.18}$$

yielding a value of $\partial_\omega \widetilde{W}$ equal to ($P(z) = 1/2(1-z) + \ldots$ near $z=1$)

$$\partial_\omega \widetilde{W} = \frac{i}{2\pi T}\mathcal{N}(z_0)(\bar{\alpha}\beta - \bar{\beta}\alpha) \tag{4.2.19}$$

with $\mathcal{N}(z_0) = \exp \int_{z_0}^{z} dz \left[P(z) - \frac{1}{2(1-z)}\right]$.

much more direct if we can derive an AdS radial evolution equation for the vector-projected Green's function and hence the occupation number discontinuity directly. From the AdS perspective is also more convenient to work with bilinears such as Green's functions, since the Dirac fields always couple pairwise to bosonic fields.

To do so, we start again with the two decoupled second order equations equivalent to the Dirac equation (4.2.7)

$$\left(\partial_z^2 + P(z)\partial_z + Q_\pm(z)\right)\Psi_\pm = 0 \tag{4.2.20}$$

with

$$\begin{aligned} P(z) &= (\mathcal{A}_- + \mathcal{A}_+) - [\partial_z, \mathcal{T}]\frac{\mathcal{T}}{T^2} \ , \\ Q_\pm(z) &= \mathcal{A}_-\mathcal{A}_+ + (\partial_z \mathcal{A}_\pm) - [\partial_z, \mathcal{T}]\frac{\mathcal{T}}{T^2}\mathcal{A}_\pm + T^2 \ . \end{aligned} \tag{4.2.21}$$

Note that both $P(z)$ and $Q_\pm(z)$ are matrices in spinor space. The general solution to this second order equation — with the behavior at the horizon/interior appropriate for the Green's function one desires — is a matrix valued function $(M_\pm(z))^\alpha{}_\beta$ and the field $\Psi_\pm(z)$ equals $\Psi_\pm(z) = M_\pm(z)\Psi_\pm^{(hor)}$. Due to the first order nature of the Dirac equation the horizon values $\Psi_\pm^{(hor)}$ are not independent but related by a z-independent matrix $S\Psi_+^{(hor)} = \Psi_-^{(hor)}$, which can be deduced from the near-horizon behavior of (5.2.2); specifically $S = \gamma^0$. One then obtains the Green's function from the on-shell boundary action (see e.g. [16, 17])

$$S_{bnd} = \oint_{z=z_0} d^dx \bar{\Psi}_+\Psi_- \tag{4.2.22}$$

as follows: Given a boundary source ζ_+ for $\Psi_+(z)$, i.e. $\Psi_+(z_0) \equiv \zeta_+$, one concludes that $\Psi_+^{(hor)} = M_+^{-1}(z_0)\zeta_+$ and thus $\Psi_+(z) = M_+(z)M_+^{-1}(z_0)\zeta_+$, $\Psi_-(z) = M_-(z)SM_+^{-1}(z_0)\zeta_+$. Substituting these solutions into the action gives

$$S_{bnd} = \oint_{z=z_0} d^dx\, \bar{\zeta}_+ M_-(z_0)SM_+^{-1}(z_0)\zeta_+ \tag{4.2.23}$$

The Green's function is obtained by differentiating w.r.t. $\bar{\zeta}_+$ and ζ_+ and discarding the conformal factor z_0^{2m} with m the AdS mass of the Dirac field (one has to be careful for $mL > 1/2$ with analytic terms [16])

$$G = \lim_{z_0 \to 0} z_0^{-2m} M_-(z_0)SM_+^{-1}(z_0) \ . \tag{4.2.24}$$

Since $M_{\pm}(z)$ are determined by evolution equations in z, it is clear that the Green's function itself is also determined by an evolution equation in z, i.e. there is some function $G(z)$ which reduces in the limit $z \to 0$ to $z_0^{2m} G$. One obvious candidate is the function

$$G^{(0)}(z) = M_-(z) S M_+^{-1}(z)\ . \tag{4.2.25}$$

Using the original Dirac equations one can see that this function obeys the non-linear evolution equation

$$\partial_z G^{(0)}(z) = -A_- G^{(0)}(z) - \not{T} M_+ S M_+^{-1} + A_+ G^{(0)}(z) + G^{(0)}(z) \not{T} G^{(0)}(z) \tag{4.2.26}$$

This is the approach used in [79], where a specific choice of momenta is chosen such that M_+ commutes with S. For a generic choice of momenta, consistency requires that one also considers the evolution equation for $M_+(z) S M_+^{-1}(z)$.

There is, however, another candidate for the extension $G(z)$ which is based on the underlying boundary action. Rather than extending the kernel $M_-(z_0) M_+^{-1}(z_0)$ of the boundary action we extend the constituents of the action itself, based on the individual fermion wavefunctions $\Psi_{\pm}(z) = M_{\pm}(z) S^{\frac{1}{2} \mp \frac{1}{2}} M_+^{-1}(z_0)$. We define an extension of the matrix $G(z)$ including an expansion in the complete set $\Gamma^I = \{\mathbb{1}, \gamma^i, \gamma^{ij}, \ldots, \gamma^{i_1, i_d}\}$ (with $\gamma^4 = i\gamma^0$)

$$\begin{aligned} G^I(z) &= \bar{M}_+^{-1}(z_0) \bar{M}_+(z) \Gamma^I M_-(z) S M_+^{-1}(z_0) \\ G^I(z_0) &= \Gamma^I G(z_0) \end{aligned} \tag{4.2.27}$$

where $\bar{M} = i\gamma^0 M^\dagger i\gamma^0$. Using again the original Dirac equations, this function obeys the evolution equation

$$\begin{aligned} \partial_z G^I(z) = -(\bar{A}_+ + A_-) G^I(z) - \bar{M}_{+,0}^{-1} \bar{M}_-(z) \bar{\not{T}} \Gamma^I M_-(z) S M_{+,0}^{-1} + \\ + \bar{M}_{+,0}^{-1} \bar{M}_+(z) \Gamma^I \not{T} M_+(z) S M_{+,0}^{-1} \end{aligned} \tag{4.2.28}$$

Recall that $\not{T} \gamma^{i_1 \cdots i_p} = \mathcal{T}^{[i_1} \gamma^{\cdots i_p]} + \mathcal{T}_j \gamma^{j i_1 \cdots i_p}$. It is then straightforward to see that for consistency, we also need to consider the evolution equations of

$$\mathcal{J}_+^I = \bar{M}_{+,0}^{-1} \bar{M}_+(z) \Gamma^I M_+(z) S M_{+,0}^{-1}\ , \quad \mathcal{J}_-^I = \bar{M}_{+,0}^{-1} \bar{M}_-(z) \Gamma^I M_-(z) S M_{+,0}^{-1}$$

and

$$\bar{G}^I = \bar{M}_{+,0}^{-1} \bar{M}_-(z) \Gamma^I M_+(z) S M_{+,0}^{-1}.$$

The significant advantage of these functions $G^I,\ \bar{G}^I,\ \mathcal{J}^I_\pm$ is that the evolution equations are now linear. This approach may seem overly complicated. However, if the vector $\mathcal{T}^i$ happens to only have a single component nonzero, then the system reduces drastically to the four fields $\mathcal{J}^i_\pm, G^{\mathbb{1}}, \bar{G}^{\mathbb{1}}$.We shall see below that a similar drastic reduction occurs, when we consider only spatially and temporally averaged functions $J^I = \int dtd^2x\mathcal{J}^I_\pm$.

Now the two extra currents $\mathcal{J}^I_\pm$ have a clear meaning in the CFT. The current $G^I(z)$ reduces by construction to Γ^I times the Green's function $G^{\mathbb{1}}(z_0)$ on the boundary, and clearly $\bar{G}^I(z)$ is its hermitian conjugate. The current $\mathcal{J}^I_+$ reduces at the boundary to $\mathcal{J}^I_+ = \Gamma^I M_{+,0}SM^{-1}_{+,0}$. Thus $\mathcal{J}^I_+$ sets the normalization of our linear system. The interesting current is the current $\mathcal{J}^I_-$. Using that $\bar{S} = \bar{S}^{-1}$, it can be seen to reduce on the boundary to the combination $\bar{\mathcal{J}}^{\mathbb{1}}_+\bar{G}^{\mathbb{1}}\Gamma^I G^{\mathbb{1}}$. Thus, $\left(\bar{\mathcal{J}}^{\mathbb{1}}_+\right)^{-1}\mathcal{J}^{\mathbb{1}}_-$ is the norm squared of the Green's function, i.e. the probability density of the off-shell process.

For an off-shell process or a correlation function the norm-squared has no real functional meaning. However, we are specifically interested in solutions in the absence of an external source, i.e. the *on-shell* correlation functions. In that case the analysis is quite different. The on-shell condition is equivalent to choosing momenta to saturate the pole in the Green's function, i.e. it is precisely choosing dual AdS solutions whose leading external source $A_\pm$ vanishes. Then M_+ and M_- are no longer independent, but $M_{+,0} = \delta B_+/\delta\Psi^{(hor)}_+ = -\frac{i\mu\gamma^0}{2m+1}M_{-,0}S$. As a consequence all boundary values of $\mathcal{J}^I_-(z_0), G^I(z_0), \bar{G}^I(z_0)$ become proportional; specifically using $S = \gamma^0$ one has that

$$\mathcal{J}^0_-(z_0)|_{on-shell} = \frac{(2m+1)}{\mu}\gamma^0 G^{\mathbb{1}}(z_0)|_{on-shell} \tag{4.2.29}$$

is the "on-shell" Green's function. Now, the meaning of the on-shell correlation function is most evident in thermal backgrounds. It equals the density of states $\rho(\omega(k)) = -\frac{1}{\pi}\mathrm{Im}G_R$ times the Fermi-Dirac distribution [77]

$$\mathrm{Tr}i\gamma^0 G^t_F(\omega_{bare}, k)\Big|_{\text{on-shell}} = 2\pi f_{FD}\left(\frac{\omega_{bare}-\mu}{T}\right)\rho(\omega_{bare}) \tag{4.2.30}$$

For a Fermi liquid with the defining off-shell Green's function (4.2.1) $\omega_{bare}(k_F) - \mu \equiv \omega = 0$ and $\rho(\omega_{bare}(k)) = Z_{z_0}\delta^2(k-k_F)\delta(\omega) + \ldots$. Thus we see that the boundary value of $\mathcal{J}_-^{(0)}(z_0)|_{on-shell} = Zf_{FD}(0)\delta^3(0)$ indeed captures the pole strength directly times a product of distributions. This product of distributions can be absorbed in setting the normalization. An indication that this is correct is that the determining equations for G^I, $\bar{G}^I$, $\mathcal{J}_\pm^I$ remain unchanged if we multiply G^I, $\bar{G}^I$, $\mathcal{J}_\pm^I$ on both sides with $M_{+,0}$. If $M_{+,0}$ is unitary it is just a similarity transformation. However, from the definition of the Green's function, one can see that this transformation precisely removes the pole. This ensures that we obtain finite values for G^I, $\bar{G}^I$, $\mathcal{J}_\pm^I$ at the specific pole-values ω_F, k_F where the distributions would naively blow up.

Boundary conditions and normalizability

We have shown that a normalizable solution to $\mathcal{J}_-^0$ correctly captures the pole strength directly. However, 'normalizable' is still defined in terms of an absence of a source for the fundamental Dirac field $\Psi_\pm$ rather than the composite fields $\mathcal{J}_\pm^I$ and G^I. One would prefer to determine normalizability directly from the boundary behavior of the composite fields. This can be done. Under the assumption that the electrostatic potential Φ is regular, i.e.

$$\Phi = \mu - \rho z + \dots \tag{4.2.31}$$

the "connection" $\mathcal{T}^I$ is subleading to the connection $\mathcal{A}$ near $z = 0$. Thus the equations of motion near $z = 0$ do not mix the various $\mathcal{J}_\pm^I$, G^I and the composite fields behave as

$$\begin{aligned}
\mathcal{J}_+^I &= j^I_{3-2m} z^{3-2m} + j^I_{4_+} z^4 + j^I_{5+2m} z^{5+2m} + \dots, \\
\mathcal{J}_-^I &= j^I_{5-2m} z^{5-2m} + j^I_{4_-} z^4 + j^I_{3+2m} z^{3+2m} + \dots, \\
G^I &= I^I_{4-2m} z^{4-2m} + I^I_3 z^3 + I^I_{4+2m} z^{4+2m} + I^I_5 z^5 + \dots,
\end{aligned} \tag{4.2.32}$$

with the identification

$$\begin{aligned}
&j^I_{3-2m} = \bar{A}_+\Gamma^I A_+, \quad j^I_{4_+} = \bar{A}_+\Gamma^I B_+ + \bar{B}_+\Gamma^I A_+, \quad j^I_{5+2m} = \bar{B}_+\Gamma^I B_+ \ , \\
&j^I_{3+2m} = \bar{A}_-\Gamma^I A_-, \quad j^I_{4_-} = \bar{A}_-\Gamma^I B_- + \bar{B}_-\Gamma^I A_-, \quad j^I_{5-2m} = \bar{B}_-\Gamma^I B_- \ , \\
&I^I_{4-2m} = \bar{A}_+\Gamma^I A_-, \qquad I^I_3 = \bar{A}_+\Gamma^I B_-, \qquad I_{4+2m} = \bar{B}_+\Gamma^I B_-, \\
&I^I_5 = \bar{B}_+\Gamma^I A_- \ .
\end{aligned} \tag{4.2.33}$$

A 'normalizable' solution in $\mathcal{J}_-^I$ and thus $\mathcal{J}_-^0$ is therefore defined by the vanishing of *both* the leading *and* the subleading term.

4.3 An AdS Black hole with Dirac Hair

Having determined a set of AdS evolution equations and boundary conditions that compute the pole strength Z directly through the currents $\mathcal{J}_{-}^{(0)}(z)$ and $G^{I}(z)$, we can now try to construct the AdS dual of a system with finite fermion density, including backreaction. As we remarked in the beginning of section 4.2.1, the demand that the solutions be normalizable means that the construction of the AdS black hole solution with a finite single fermion wavefunction is analogous to the construction of a holographic superconductor [47] with the role of the scalar field now taken by the Dirac field. The starting point therefore is the charged AdS_4 black-hole background (6.2.4) and we should show that at low temperatures this AdS Reissner-Nordström black hole is unstable towards a solution with a finite Dirac profile. We shall do so in a simplified "large charge" limit where we ignore the gravitational dynamics, but as is well known from holographic superconductor studies (see e.g. [47, 49]) this limit already captures much of the essential physics. In a companion article [20] we will construct the full backreacted groundstate including the gravitational dynamics.

In this large charge non-gravitational limit the equations of motion for the action (4.2.3) reduce to those of $U(1)$-electrodynamics coupled to a fermion with charge g in the background of this black hole:

$$\begin{aligned} D_M F^{MN} &= ige_A^N \bar{\Psi}\Gamma^A\Psi \ , \\ 0 &= e_A^M \Gamma^A (D_M + iegA_M)\Psi + m\Psi \ . \end{aligned} \tag{4.3.1}$$

Thus the vielbein e_A^M and and covariant derivative D_M remain those of the fixed charged AdS black hole metric (6.2.4), but the vector-potential now contains a background piece $A_0^{(bg)}$ plus a first-order piece $A_M = A_M^{(bg)} + A_M^{(1)}$, which captures the effect of the charge carried by the fermions.

Following our argument set out in previous section that it is more convenient to work with the currents $\mathcal{J}_{\pm}^{I}(z), G^{I}(z)$ instead of trying to solve the Dirac equation directly, we shall first rewrite this coupled non-trivial set of equations of motion in terms of the currents while at the same time using symmetries to reduce the complexity. Although a system at finite fermion density need not be homogeneous, the Fermi liquid ground state is. It therefore natural to make the ansatz that the final AdS solution is static and preserves translation and rotation along the boundary. As the Dirac field transforms non-trivially under rotations and boosts, we cannot make this ansatz in the strictest sense. However, in some average sense which we will make precise, the solution should be static and translationally invariant. Then translational and rotational invariance allow us to set $A_i = 0$, $A_z = 0$, whose equations of motions will turn into contraints for the remaining degrees of freedom. Again denoting $A_0 = \Phi$, the equations reduce to the following after the projection onto $\Psi_\pm = \frac{1}{2}(1 \pm \Gamma^Z)\Psi$.

$$\begin{aligned} \partial_z^2 \Phi &= \frac{-gL^3\alpha}{z^3\sqrt{f}} \left(\bar{\Psi}_+ i\gamma^0 \Psi_+ + \bar{\Psi}_- i\gamma^0 \Psi_- \right) , \\ \left(\partial_z + \mathcal{A}_\pm\right) \Psi_\pm &= \mp \mathcal{T} \Psi_\mp \end{aligned} \tag{4.3.2}$$

with

$$\begin{aligned} \mathcal{A}_\pm &= -\frac{1}{2z}\left(3 - \frac{zf'}{2f}\right) \pm \frac{mL}{z\sqrt{f}} , \\ \mathcal{T} &= \frac{i(-\omega + g\Phi)}{\alpha f}\gamma^0 + \frac{i}{\alpha\sqrt{f}} k_i \gamma^i . \end{aligned} \tag{4.3.3}$$

as before.

The difficult part is to "impose" staticity and rotational invariance for the non-invariant spinor. This can be done by rephrasing the dynamics in terms of fermion current bilinears, rather than the fermions themselves. We shall first do so rather heuristically, and then show that the equations obtained this way are in fact the flow equations for the Green's functions and composites $\mathcal{J}^I(z)$, $G^I(z)$ constructed in the previous section. In terms of the local vector currents[6]

$$J_+^\mu(x,z) = \bar{\Psi}_+(x,z) i\gamma^\mu \Psi_+(x,z) , \quad J_-^\mu(x,z) = \bar{\Psi}_-(x,z) i\gamma^\mu \Psi_-(x,z) , \tag{4.3.4}$$

or equivalently

$$\begin{aligned} J_+^\mu(p,z) &= \int d^3k \bar{\Psi}_+(-k,z) i\gamma^\mu \Psi_+(p+k,z), \\ J_-^\mu(p,z) &= \int d^3k \bar{\Psi}_-(-k,z) i\gamma^\mu \Psi_-(p+k,z) . \end{aligned} \tag{4.3.5}$$

rotational invariance means that spatial components $J_\pm^i$ should vanish on the solution — this solves the constraint from the A_i equation of motion, and the equations can be rewritten in terms of $J_\pm^0$ only. Staticity and

[6] In our conventions $\bar{\Psi} = \Psi^\dagger i\gamma^0$.

rotational invariance in addition demand that the bilinear momentum p_μ vanish. In other words, we are only considering temporally and spatially averaged densities: $J^\mu_\pm(z) = \int dtd^2x\bar{\Psi}(t,x,z)i\gamma^\mu\Psi(t,x,z)$. Analogous to the bilinear flow equations for the Green's function, we can act with the Dirac operator on the currents to obtain an effective equation of motion, and this averaging over the relative frequencies ω and momenta k_i will set all terms with explicit k_i-dependence to zero.[7] Restricting to such averaged currents and absorbing a factor of g/α in Φ and a factor of $g\sqrt{L^3}$ in $\Psi_\pm$, we obtain effective equations of motion for the bilinears directly

$$\begin{aligned} (\partial_z + 2\mathcal{A}_\pm)\, J^0_\pm &= \mp\frac{\Phi}{f} I \ , \\ (\partial_z + \mathcal{A}_+ + \mathcal{A}_-)\, I &= \frac{2\Phi}{f}(J^0_+ - J^0_-) \ , \\ \partial_z^2\Phi &= -\frac{1}{z^3\sqrt{f}}(J^0_+ + J^0_-) \ , \end{aligned} \tag{4.3.8}$$

with $I = \bar{\Psi}_-\Psi_+ + \bar{\Psi}_+\Psi_-$, and all fields are real. The remaining constraint from the A_z equation of motion decouples. It demands $\mathrm{Im}(\bar{\Psi}_+\Psi_-) = \frac{i}{2}(\bar{\Psi}_-\Psi_+ - \bar{\Psi}_+\Psi_-) = 0$. What the equations (4.3.8) tell us is that for nonzero $J^0_\pm$ there is a charged electrostatic source for the vector potential Φ in the bulk.

Momentarily we will motivate the effective equations (4.3.8) at a more fundamental level. Before that there are several remarks to be made

- These equations contain more information than just current conservation $\partial_\mu J^\mu = 0$. In an isotropic and static background current conservation is trivially true as $\partial_\mu J^\mu = \partial_0 J^0 = -i\int d\omega e^{-i\omega t}\omega J^0(\omega) = 0$ as $J^0(\omega \neq 0) = 0$.

[7] To see this consider

$$(\partial + 2\mathcal{A}_\pm)\Psi^\dagger_\pm(-k)\Psi_\pm(k) = \mp\frac{\Phi}{f}\left(\Psi^\dagger_- i\gamma^0\Psi_+ + \Psi^\dagger_+ i\gamma^0\Psi_-\right) + \frac{ik_i}{\sqrt{f}}\left(\Psi^\dagger_-\gamma^i\Psi_+ - \Psi^\dagger_+\gamma^i\Psi_-\right) \tag{4.3.6}$$

The term proportional to Φ is relevant for the solution. The dynamics of the term proportional to k_i is

$$(\partial + \mathcal{A}_+ + \mathcal{A}_-)(\Psi^\dagger_-\gamma^i\Psi_+ - \Psi^\dagger_+\gamma^i\Psi_-) = -2i\frac{k^i}{\sqrt{f}}(\Psi^\dagger_+\gamma^0\Psi_+ + \Psi^\dagger_-\gamma^0\Psi_-) \ . \tag{4.3.7}$$

The integral of the RHS over k^i vanishes by the assumption of translational and rotational invariance. Therefore the LHS of (5.2.14) and thus the second term in eq. (5.2.13) does so as well.

- We have scaled out the electromagnetic coupling. AdS_4/CFT_3 duals for which the underlying string theory is known generically have $g = \kappa/L$ with κ the gravitational coupling constant as defined in (4.2.3). Thus, using standard AdS_4/CFT_3 scaling, a finite charge in the new units translates to a macroscopic original charge of order $L/\kappa \propto N^{1/3}$. This large charge demands that backreaction of the fermions in terms of its bilinear is taken into account as a source for Φ.

- The equations are local. From the fundamental point of view, that one considers finite density in the bulk, this is strange to say the least. Generic multi-fermion configurations are non-local, see e.g. [96]. These equations can therefore never capture the full bulk fermion dynamics. Our starting point has been a single fermion perspective, where the Pauli blocking induced non-locality is absent. In that context local equations are fine. We have also explicitly averaged over all directions parallel to the boundary and, as we have shown in the previous section (see also footnote 7), it is this averaging that tremendously simplifies the equations. The most curious part may be that this unaveraged set of equations — and therefore also eqs (4.3.8) — are all local in the radial direction z. From the AdS perspective a many-fermion system should be non-local democratically and thus also exhibit non-locality in z, yet from the CFT perspective where z-dynamics encode RG-flow, it is eminently natural. We leave the resolution of this paradox to future work.

The justification of using (4.3.8) to construct the AdS dual of a regular Fermi liquid is the connection between local fermion bilinears and the CFT Green's function. The complicated flow equations reduce precisely to the first two equations in (4.3.8) upon performing the spacetime averaging and the trace, i.e. $J^0_\pm = \int d^3k \mathrm{Tr} \mathcal{J}^0_\pm$ and $I = \int d^3k \mathrm{Tr}\left(G^{\mathbb{1}} + \bar{G}^{\mathbb{1}}\right)$. Combined with the demand that we only consider normalizable solutions and the proof that $\mathcal{J}^0_-$ is proportional to the pole-strength, the radial evolution equations (4.3.8) are the (complicated) AdS recasting of the RG-flow for the pole-strength. This novel interpretation ought to dispel some of the a priori worries about our unconventional treatment of the fermions through their semi-classical bilinears. There is also support from the gravity side, however. Recall that for conventional many-body systems and fermions in particular one first populates a certain set of states and then tries to compute the macroscopic properties of the collective. In a certain sense the equations (4.3.8) formulate the same program but in opposite order: one computes the generic wavefunction charge density with and by imposing the right boundary conditions, i.e normalizability, one selects only the correct set of states. This follows directly from the equivalence between normalizable AdS modes and quasiparticle poles that are characterized by well defined distinct momenta k_F (for $\omega = \omega_F \equiv 0$). The demand that any non-trivial Dirac hair black hole is constructed from normalizable solutions of the composite operators (i.e. their leading and subleading asymptotes vanish[8]) thus means that one imposes a superselection rule on the spatial averaging in the definition of $J^I_\pm$:

$$\begin{aligned} J^0_\pm(z)|_{norm} &\equiv \int d^3k \bar{\Psi}_\pm(-k) i\gamma^0 \Psi_\pm(k)|_{norm} \\ &= \int d^3k\, \delta^2(|k| - |k_F|)|B^{(0)}_\pm(k)|^2 z^{4+2m\pm 1} + \ldots \end{aligned} \quad (4.3.9)$$

We see that the constraint of normalizability from the bulk point of the view, implies that one selects precisely the on-shell bulk fermion modes as the building blocks of the density $J^0_\pm$.

In turn this means that the true system that eqs. (4.3.8) describe is somewhat obscured by the spatial averaging. Clearly even a single fermion wavefunction is in truth the full set of two-dimensional wavefunctions whose momentum k^i has length k_F. However, the averaging could just as well be counting more, as long as there is another set of normalizable states once the isotropic momentum surface $|k| = |k_F|$ is filled. Pushing this thought to the extreme, one could even speculate that the system (4.3.8) gives the correct quantum-mechanical description of the many-body Fermi system: the system which gravitational reasoning suggests is the true groundstate of the charged AdS black hole in the presence of fermions.

To remind us of the ambiguity introduced by spatial averaging, we shall give the boundary coefficient of normalizable solution for $J^0_- = \int d^3k \mathcal{J}^0_-$ a separate name. The quantity $\mathcal{J}^0_-(z_0)$ is proportional to the

[8]One can verify that the discussion in section 4.2.1 holds also for fully backreacted solutions. The derivation there builds on the assumption that the boundary behavior of the electrostatic potential is regular. It is straightforward to check in (4.3.8) that indeed precisely for normalizable solutions, i.e. in the absence of explicit fermion-sources, when both the leading and subleading terms in $J^0_\pm$ and I vanish, the boundary behavior the scalar potential remains regular, as required.

pole strength, which via Migdal's relation quantifies the characteristic occupation number discontinuity at $\omega_F \equiv 0$. We shall therefore call the coefficient $\int d^3k|B_-|^2|_{normalizable} = \Delta n_F$.

Thermodynamics

At a very qualitative level the identification $J^0_-|_{norm}(z) \equiv \Delta n_F z^{3+2m} + \dots$ can be argued to follow from thermodynamics as well. From the free energy for an AdS dual solution to a Fermi liquid, one finds that the charge density directly due to the fermions is

$$\rho_{total} = -2\frac{\partial}{\partial\mu}F \;\; = \;\; \frac{-3}{2m+1}\frac{\Delta n_F}{z_0^{-1-2m}} + \rho + \dots \;, \qquad (4.3.10)$$

with z_0^{-1} the UV-cutoff as before. The cut-off dependence is a consequence of the fact that the system is interacting, and one cannot truly separate out the fermions as free particles. Were one to substitute the naive free fermion scaling dimension $\Delta = m + 3/2 = 1$, the cutoff dependence would vanish and the identification would be exact.

We can thus state that in the interacting system there is a contribution to the charge density from a finite number of fermions proportional to

$$\rho_F = \frac{-3}{2\Delta - 2}\frac{\Delta n_F}{z_0^{2-2\Delta}} + \dots \;, \qquad (4.3.11)$$

although this contribution formally vanishes in the limit where we send the UV-cutoff z_0^{-1} to infinity.

To derive eq. (5.2.16), recall that the free energy is equal to minus the on-shell action of the AdS dual theory. Since we disregard the gravitational backreaction, the Einstein term in the AdS theory will not contain any relevant information and we consider the Maxwell and Dirac term only. We write the action as,

$$\begin{aligned} S = \int_{z_0}^{1} \sqrt{-g}\left[\frac{1}{2}A_N D_M F^{MN} - \bar{\Psi}\not{D}\Psi - m\bar{\Psi}\Psi\right] + \\ + \oint_{z=z_0}\sqrt{-h}\left(\bar{\Psi}_+\Psi_- + \frac{1}{2}A_\mu n_\alpha F^{\alpha\mu}\right) \;, \end{aligned} \qquad (4.3.12)$$

where we have included an explicit fermionic boundary term that follows from the AdS/CFT dictionary [17] and n_α is a normal vector to the boundary. The boundary action is not manifestly real, but its on-shell value which contributes to the free energy is real. Recall that the imaginary part of $\bar{\Psi}_+\Psi_-$ decouples from eqs. (4.3.8). The boundary Dirac term in (5.2.10) is therefore equal to $I = 2\mathrm{Re}(\bar{\Psi}_+\Psi_-)$.

To write the free energy in terms of the quantities μ, ρ and Δn_F, note that the on-shell bulk Dirac action vanishes. Importantly the bulk Maxwell action does contribute to the free energy. Its contribution is

$$\begin{aligned} F_{bulk} &= \lim_{z_0\to 0}\int_{z_0}^{1} dz d^3x \left[\frac{1}{2}\Phi\partial_{zz}\Phi\right]_{on-shell} \\ &= -\lim_{z_0\to 0}\int_{z_0}^{1} dz d^3x \left[\frac{1}{2z^3\sqrt{f}}\Phi(J_+^0+J_-^0)\right]_{on-shell}, \end{aligned} \tag{4.3.13}$$

where we have used the equation of motion (4.3.8). This contribution should be expected, since the free energy should be dominated by infrared, i.e. near horizon physics. Due to the logarithmic singularity in the electrostatic potential (Eq. (4.3.17) this bulk contribution diverges, but this divergence should be compensated by gravitational backreaction. At the same time the singularity is so mild, however, that the free energy, the integral of the Maxwell term, remains finite in the absence of the Einstein contribution.

Formally, i.e. in the limit $z_0 \to 0$, the full free energy arises from this bulk contribution (4.3.13). The relation (5.2.16) between the charge density and Δn_F follows only from the regularized free energy, and is therefore only a qualitative guideline. Empirically, as we will show, it is however, a very good one (see Fig 4.1 in the next section). Splitting the regularized bulk integral in two

$$\begin{aligned} F_{bulk} = &\int_{z^*}^{1} dz d^3x \left[\frac{1}{2z^3\sqrt{f}}\Phi(J_+^0+J_-^0)\right]_{on-shell} + \\ &+\lim_{z_0\to 0}\int_{z_0}^{z_*} dz d^3x \left[\frac{1}{2z^3\sqrt{f}}\Phi(J_+^0+J_-^0)\right]_{on-shell}, \end{aligned} \tag{4.3.14}$$

we substitute the normalizable boundary behavior of $\Psi_+ = B_+ z^{5/2+m} + \ldots$, $\Psi_- = B_- z^{3/2+m} + \ldots$ and $\Phi = \mu - \rho z + \ldots$, and obtain for the regularized free energy

$$\begin{aligned} F = F_{horizon}(z_*) + &\lim_{z_0\to 0}\int_{z_0}^{z_*} d^3x dz \left[\frac{-1}{2z^3}\mu|B_-|^2 z^{3+2m} + \ldots\right] + \\ &+\oint \frac{d^3x}{z_0^3}\left[-\bar{B}_+B_- z_0^{4+2m} + \frac{1}{2}\mu\rho z_0^3\right]. \end{aligned} \tag{4.3.15}$$

Using that $B_+ = -i\mu\gamma^0 B_-/(2m+1)$ (eq. (5.2.2)), the second bulk term and boundary contribution are proportional, and the free energy schematically equals

$$F = F^{horizon} + \lim_{z_0\to 0}\int d^3x \left[\frac{3\mu}{2(2m+1)}\bar{B}_- i\gamma^0 B_- z_0^{1+2m} - \frac{1}{2}\mu\rho\right]. \quad (4.3.16)$$

With the UV-regulator z_0^{-1} finite, this yields the charge density in Eq. (5.2.16) after one recalls that $\bar{B}_- = B_-^\dagger i\gamma^0$.

With the derived rule that the AdS dual to a Fermi liquid has a nonzero normalizable component in the current J_-^0, we will now construct an AdS solution that has this property: an AdS black hole with Dirac hair. Ignoring backreaction, these are solutions to the density equations (4.3.8). In its simplest form the interpretation is that of the backreaction due to a single fermion wavefunction, but as explained the spatial averaging of the density combined with the selection rule of normalizability could be capturing a more general solution.

4.3.1 At the horizon: Entropy collapse to a Lifshitz solution

Before we can proceed with the construction of non-trivial Dirac hair solutions to Eqs. (4.3.8), we must consider the boundary conditions at the horizon necessary to solve the system. Insisting that the right-hand-side of the dynamical equations (4.3.8) is subleading at the horizon, the near-horizon behavior of $J_\pm^0$, I, Φ is:

$$\begin{aligned} J_\pm^0 &= J_{hor,\pm}(1-z)^{-1/2} + \dots, \\ I &= I_{hor}(1-z)^{-1/2} + \dots, \\ \Phi &= \Phi_{hor}^{(1)}(1-z)\ln(1-z) + (\Phi_{hor}^{(2)} - \Phi_{hor}^{(1)})(1-z) + \dots \end{aligned} \quad (4.3.17)$$

If we insist that Φ is regular at the horizon $z = 1$, i.e. $\Phi_{hor}^{(1)} = 0$, so that the electric field is finite, the leading term in $J_\pm^0$ must vanish as well, i.e. $J_{hor,\pm} = 0$, and the system reduces to a free Maxwell field in the presence of an AdS black hole and there is no fermion density profile in the bulk. Thus in order to achieve a nonzero fermion profile in the bulk, we must have an explicit source for the electric-field on the horizon. Strictly speaking, this invalidates our neglect of backreaction as the electric field and its energy density at the location of the source will be infinite. As we argued above, this backreaction is in fact expected to resolve the finite ground-state entropy problem associated with the presence of a horizon. The backreaction should remove the horizon completely, and the background should resemble the horizonless metrics found in [50, 37, 51]; the same horizon logarithmic behavior in the electrostatic potential was noted there. Nevertheless, as the divergence in the electric field only increases logarithmically as we approach the horizon, and our results shall hinge on the properties of the equations at the opposite end near the boundary, we shall continue to ignore it here. We shall take the sensibility of our result after the fact, as proof that the logarithmic divergence at the horizon is indeed mild enough to be ignored.

The identification of the boundary value of J^0_- with the Fermi liquid characteristic occupation number jump Δn_F rested on the insistence that the currents are built out of AdS Dirac fields. This deconstruction also determines a relation between the horizon boundary conditions of the composite fields $J^0_\pm$, I. If $\Psi_\pm(z) = C_\pm(1-z)^{-1/4} + \dots$ then $J_{hor,\pm} = C^2_\pm$ and $I_{hor} = C_+C_-$. As the solution $\Phi^{(1)}_{hor}$ is independent of the solution $\Phi^{(2)}_{hor}$ which is regular at the horizon, we match the latter to the vector-potential of the charged AdS black hole: $\Phi^{(2)}_{hor} = -2gq \equiv g\mu_0/\alpha$. Recalling that $\Phi^{(1)}_{hor} = -(J_{hor,+} + J_{hor,-})$, we see that the three-parameter family of solutions at the horizon in terms of $C_\pm$, $\Phi^{(2)}_{hor}$ corresponds to the three-parameter space of boundary values A_+, B_- and μ encoding a fermion-source, the fermion-response/expectation value and the chemical potential.

We can now search whether within this three-parameter family a finite normalizable fermion density solution with vanishing source $A_+ = 0$ exists for a given temperature T of the black hole.

4.3.2 A BH with Dirac hair

The equations are readily solved numerically with a shooting method from the horizon. We consider both an uncharged AdS-Schwarzschild solution and the charged AdS Reissner-Nordström solution. Studies of bosonic condensates in AdS/CFT without backreaction have mostly been done in the AdS-Schwarzschild (AdSS) background ([46, 47] and references therein). An exception is [3], which also considers the charged RN black hole. As is explained in [3], they correspond to two different limits of the exact solution: the AdSS case requires that $\Delta n_F \gtrsim \mu$ that is, the total charge of the matter fields should be dominant compared to the charge of the black hole. On the other hand, the RN limit is appropriate if $\Delta n_F \ll \mu$. It ignores the effect of the energy density of the charged matter sector on the charged black hole geometry. The AdS Schwarzschild background is only reliable near T_c, as at low temperatures the finite charged fermion density is comparable to μ. The RN case is under better control for low temperatures, because near $T = 0$ the chemical potential can be tuned to stay larger than fermion density.

We shall therefore focus primarily on the solution in the background of an AdS RN black hole, i.e. the system with a heat bath with chemical potential μ — non-linearly determined by the value of $\Phi^{(2)}_{hor} = \mu_0$ at the horizon — which for low T/μ should show the characteristic Δn_F of a Fermi liquid. The limit in which we may confidently ignore backreaction is $\Phi^{(1)}_{hor} \ll \mu_0$ for $T \lesssim \mu_0$ — for AdSS the appropriate limit is $\Phi^{(1)}_{hor} \ll T$ for $\mu_0 \ll T$.

Finite fermion density solutions in AdS-RN

Fig. 4.1 shows the behavior of the occupation number discontinuity $n_F \equiv |B_-|^2$ and the fermion free-energy contribution I as a function of temperature in a search for normalizable solutions to Eqs (4.3.8) with the aforementioned boundary conditions. We clearly see a first order transition to a finite fermion density, as expected. The underlying Dirac field dynamics can be recognized in that the normalizable solution for $J^0_-(z)$ which has no leading component near the boundary by construction, also has its subleading component vanishing (Fig. 4.2).[9]

Analyzing the transition in more detail in Fig. 4.3, we find:

1. The dimensionless number discontinuity $\Delta n_F/\mu^{2\Delta}$ scales as $T^{-\delta}$ in a certain temperature range $T_F < T < T_c$, with $\delta > 0$ depending on g and Δ, and T_F typically very small. At $T = T_c > T_F$ it drops to zero discontinuously, characteristic of a first order phase transition.

2. At low temperatures, $0 < T < T_F$, the power-law growth comes to a halt and ends with a plateau where $\Delta n_F/\mu^{2\Delta} \sim$ const. (Fig. 4.3A).

[9] Although the Dirac hair solution has charged matter in the bulk, there is no Higgs effect for the bulk gauge field, and thus there is no direct spontaneous symmetry breaking in the boundary. Indeed one would not expect it for the Fermi liquid groundstate. There will be indirect effect on the conductivity similar to [51]. We thank Andy O'Bannon for his persistent inquiries to this point.

It is natural to interpret this temperature as the Fermi temperature of the boundary Fermi liquid.

3. The fermion free energy contribution $I/\mu^{2\Delta+1}$ scales as $T^{1/\nu}$ with $\nu > 1$ for $0 < T < T_c$, and drops to zero discontinuously at T_c. As I empirically equals minus the free energy per particle, it is natural that $I(T = 0) = 0$, and this in turn supports the identification of $\Delta n_F(T = 0)$ as the step in number density at the Fermi energy.

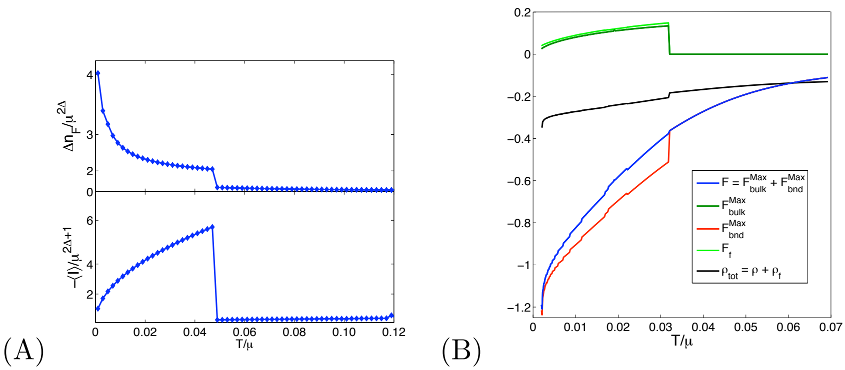

Figure 4.1: (A) Temperature dependence of the Fermi liquid occupation number discontinuity Δn_F and operator I for a fermionic field of mass $m = -1/4$ dual to an operator of dimension $\Delta = 5/4$. We see a large density for T/μ small and discontinuously drop to zero at $T \approx 0.05\mu$. At this same temperature, the proxy free energy contribution per particle (the negative of I) vanishes. (B) The free energy $F = F^{fermion} + F^{Maxwell}$ (Eq. (5.2.10)) as a function of T/μ ignoring the contribution from the gravitational sector. The blue curve shows the total free energy $F = F^{Maxwell}$, which is the sum of a bulk and a boundary term. The explicit fermion contribution $F_{fermion}$ vanishes, but the effect of a non-zero fermion density is directly encoded in a non-zero $F^{Maxwell}_{bulk}$. The figure also shows this bulk $F^{Maxwell}_{bulk}$ and the boundary contribution $F^{Maxwell}_{bulk}$ separately and how they sum to a continuous F_{total}. Although formally the explicit fermion contribution $F_f \sim I$ in equation (5.2.11) vanishes, the bulk Maxwell contribution is captured remarkably well by its value when the cut-off is kept finite. The light-green curve in the figure shows F_f for a finite $z_0 \sim 10^{-6}$. For completeness we also show the total charge density, Eq. (5.2.16). The dimension of the fermionic operator used in this figure is $\Delta = 1.1$.

One expects that the exponents δ, ν are controlled by the conformal dimension Δ.[10] The dependence of the exponent δ on the conformal di-

[10]The charge g of the underlying conformal fermionic operator scales out of the so-

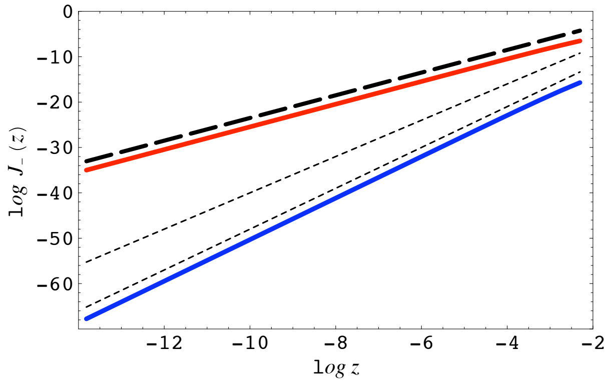

Figure 4.2: The boundary behavior of $J_{-}(0)$ in for a generic solution (blue) to Eqs. (4.3.8) and a normalizable Dirac-hair solution (red) for $m = -1/4$ in the background of an AdS-RN black hole with $\mu/T = 128.8$. The dotted lines show the scaling $z^{11/2}$ and z^4 of the leading and subleading terms in an expansion of $J^0_{-}(z)$ near $z = 0$; the dashed line shows the scaling $z^{5/2}$ of the subsubleading expansion whose coefficient is $|B_{-}(\omega_F, k_F)|^2$. That the Dirac hair solution (red) scales as the subsubleading solution indicates that the current J^0_{-} faithfully captures the density of the underlying normalizable Dirac field.

mension is shown in Fig. 4.3A. While a correlation clearly exists, the data are not conclusive enough to determine the relation $\delta = \delta(\Delta)$. The clean power law $T^{-\delta}$ scaling regime is actually somewhat puzzling. These values of the temperature, $T_F < T < T_c$, correspond to a crossover between the true Fermi liquid regime for $T < T_F$ and the conformal phase for $T > T_c$, hence there is no clear ground for a universal scaling relation for δ, which seems to be corroborated by the data (Fig. 4.3B). At the same time, the scaling exponent ν appears to obey $\nu = 2$ with great precision (Fig. 4.3B, inset) independent of Δ and g.

A final consideration, needed to verify the existence of a finite fermion density AdS solution dual to a Fermi liquid, is to show that the ignored backreaction stays small. In particular, the divergence of the electric field at the horizon should not affect the result. The total bulk electric field $E_z = -\partial_z \Phi$ is shown in Fig. 4.4A, normalized by its value at $z = 1/2$. The logarithmic singularity at the horizon is clearly visible. At the same time, the contribution to the total electric field from the charged fermions is

lution.

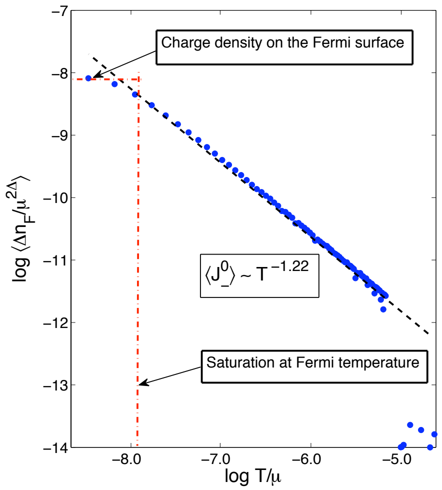

(A)

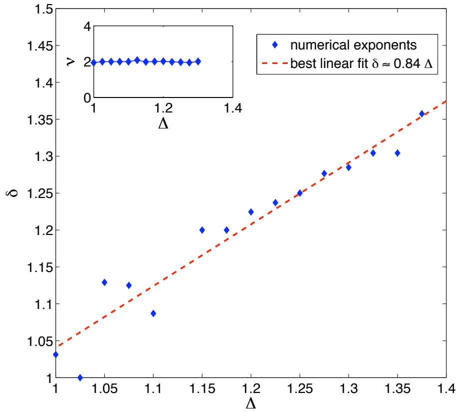

(B)

Figure 4.3: (A) Approximate power-law scaling of the Fermi liquid characteristic occupation number discontinuity $\Delta n_F/\mu^{2\Delta} \sim T^{-\delta}$ as a function of T/μ for $\Delta = 5/4$. This figure clearly shows the saturation of the density at very low T/μ. The saturation effect is naturally interpreted as the influence of the characteristic Fermi energy. (B) The scaling exponent δ for different values of the conformal dimension Δ. There is a clear correlation, but the precise relation cannot be determined numerically. The scaling exponent of the current $I/\mu^{2\Delta+1} \sim T^{-1/\nu}$ obeys $\nu = 2$ with great accuracy, on the other hand (Inset).

negligible even very close to the horizon.[11] This suggests that our results are robust with respect to the details of the IR divergence of the electric field.

The diverging backreaction at the horizon is in fact the gravity interpretation of the first order transition at T_c: an arbitrarily small non-zero density leads to an abrupt change in the on shell bulk action. As the latter is the free energy in the CFT, it must reflect the discontinuity of a first order transition. A full account of the singular behavior at the horizon requires self-consistent treatment including the Einstein equations. At this level, we can conclude that the divergent energy density at the horizon implies that the near-horizon physics becomes substantially different

[11]It is of the order 10^{-4}, starting from $z = 0.9999$. We have run our numerics using values between $1 - 10^{-6}$ and $1 - 10^{-2}$ and found no detectable difference in quantities at the boundary.

from the AdS_2 limit of the RN metric. It is natural to guess that the RN horizon disappears completely, corresponding to a ground state with zero entropy, as hypothesized in [50]. This matches the expectation that the finite fermi-density solution in the bulk describes the Fermi-liquid. The underlying assumption in the above reasoning is that the total charge is conserved.

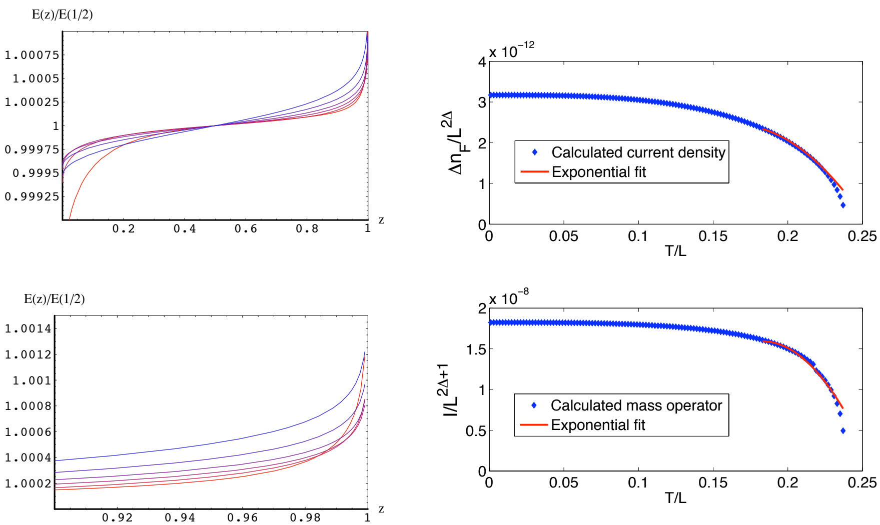

(A) (B)

Figure 4.4: (A) The radial electric field $-E_z = \partial\Phi/\partial z$, normalized to the midpoint value $E_z(z)/E_z(1/2)$ for whole interior of the finite fermion density AdS-RN solution (upper) and near the horizon (lower). One clearly sees the soft, log-singularity at the horizon. The colors correspond to increasing temperatures from $T = 0.04\mu$ (lighter) to $T = 0.18\mu$ (darker), all with $\Delta = 1.1$. (B) The occupation number jump Δn_F and free energy contribution I as a function of temperature in AdS-Schwarzschild. We see the jump Δn_F saturate at low temperatures and fall off at high T. An exponential fit to the data (red curve) shows that in the critical region the fall-off is stronger than exponential, indicating that the transition is first order. The conformal dimension of the fermionic operator is $\Delta = 1.1$. (C) The radial electric field $-E_z = \partial\Phi/\partial z$, normalized to the midpoint value $(E_z(z)/E_z(1/2))$ for the finite fermion density AdS-Schwarzschild background. The divergence of the electric field E_z is again only noticeable near the horizon and can be neglected in most of the bulk region.

Finite fermion density in AdSS

For completeness, we will describe the finite fermion-density solutions in the AdS Schwarzschild geometry as well. In these solutions the charge density is set by the density of fermions alone. They are therefore not reliable at very low temperatures $T \ll T_c$ when gravitational backreaction becomes important. The purpose of this section is to show the existence of finite density solutions does not depend on the presence of a charged black-hole set by the horizon value $\Phi^{(2)}_{hor} = \mu_0$, but that the transition to a finite fermion density can be driven by the charged fermions themselves.

Fig. 4.4B shows the nearly instantaneous development of a non-vanishing expectation value for the occupation number discontinuity Δn_F and I in the AdS Schwarzschild background. The rise is not as sharp as in the RN background. It is, however, steeper than exponential, and we may conclude that the system undergoes a discontinuous first order transition to a AdS Dirac hair solution. The constant limit reached by the fermion density as $T \to 0$ has no meaning as we cannot trust the solution far away from T_c.

The backreaction due to the electric field divergence at the horizon can be neglected, for the same reason as before (Fig. 4.4C).

4.3.3 Confirmation from fermion spectral functions

If, as we surmised, the finite fermion density phase is the true Fermi-liquid-like ground state, the change in the fermion spectral functions should be minimal as the characteristic quasi-particle peaks are already present in the probe limit, i.e. pure AdS Reissner-Nordström [79, 17]. Fig. 4.5 shows that quasiparticle poles near $\omega = 0$ with similar analytic properties can be identified in both the probe pure AdS-RN case and the AdS-RN Dirac-hair solution. The explanation for this similarity is that the electrostatic potential Φ almost completely determines the spectrum, and the change in Φ due to the presence of a finite fermion density is quite small. Still, one expects that the finite fermion density system is a more favorable state. This indeed follows from a detailed comparison between the spectral functions $A(\omega; k)$ in the probe limit and the fermion-liquid phase (Fig. 4.5). We see that:

1. All quasiparticle poles present in the probe limit are also present in the Dirac hair phase, at a slightly shifted value of k_F. This shift is a consequence of the change in the bulk electrostatic potential Φ

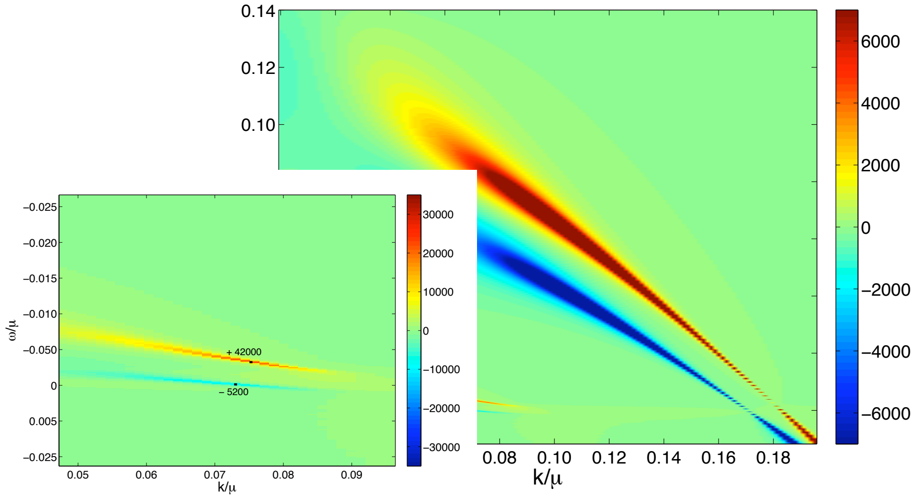

Figure 4.5: The single-fermion spectral function in the probe limit of pure AdS Reissner-Nordström (red/yellow) *minus* the spectrum in the finite density system (blue). The conformal dimension is $\Delta = 5/4$, the probe charge $g = 2$, and $\mu/T = 135$. We can see two quasiparticle poles near $\omega = 0$, a non-FL pole with $k_F^{probe} \simeq 0.11\mu$ and $k_F^{\Delta n_F} \simeq 0.08\mu$ respectively and a FL-pole with $k_F^{probe} \simeq 0.18\mu$ and $k_F^{\Delta n_F} \simeq 0.17\mu$. The dispersion of both poles is visibly similar between the probe and the finite density background. At the same time, the non-FL pole has about 8 times less weight in the finite density background, whereas the FL-pole has gained about 6.5 times more weight.

due to the presence of the charged matter. For a Fermi-liquid-like quasiparticle corresponding to the second pole in the operator with $\Delta = 5/4$ and $g = 2$ we find $k_F^{probe} - k_F^{\Delta n_F} = 0.07\mu$. The non-Fermi-liquid pole, i.e. the first pole for the same conformal operator, has $k_F^{probe} - k_F^{\Delta n_F} = 0.03\mu$.

2. The dispersion exponents ν defined through $(\omega - E_F)^2 \sim (k - k_F)^{2/\nu}$, also maintain roughly the same values as both solutions. This is visually evident in the near similar slopes of the ridges in Fig. 4.5. In the AdS Reissner-Nordström background, the dispersion coefficients are known analytically as a function of the Fermi momentum: $\nu_{k_F} = \sqrt{2\frac{k_F^2}{\mu^2} - \frac{1}{3} + \frac{1}{6}(\Delta - 3/2)^2}$ [27]. The Fermi-liquid-like quasiparticle corresponding to the second pole in the operator with $\Delta = 5/4$ and

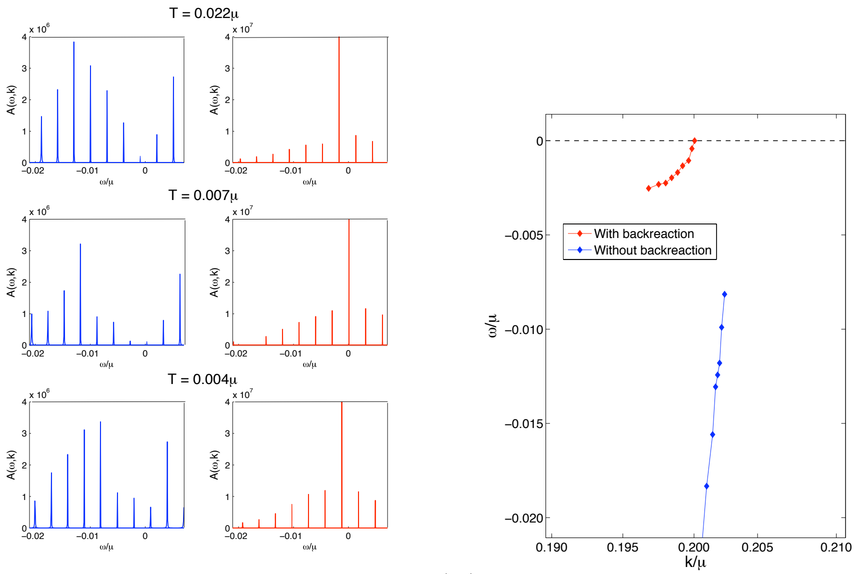

(A) (B)

Figure 4.6: (A) Single fermion spectral functions near $\omega = 0$ in pure AdS Reissner-Nordström (blue) and in the finite fermion density background (red). In the former the position of the maximum approaches $\omega = 0$ as T is lowered whereas in the latter the position of the maximum stays close to $T = 0$ for all values of T. (B) Position of the maximum of the quasiparticle peak in k-ω plane, for different temperatures and $\Delta = 5/4$. The probe limit around a AdS-RN black hole (blue) carries a strong temperature dependence of the ω_{max} value, with $\omega_{max,T\neq 0} \neq 0$. In the finite fermion density background, the position of the maximum (red) is nearly independent of temperature and stays at $\omega = 0$.

$g = 2$ has $\nu_{k_F}^{probe} = 1.02$ vs. $\nu^{\Delta n_F} = 1.01$. The non-Fermi-liquid pole corresponding to the first pole for the same conformal operator, has $\nu_{k_F}^{probe} \approx 0.10$, and $\nu^{\Delta n_F} = 0.12$.

3. The most distinct property of the finite density phase is the redistributed spectral weight of the poles. The non-Fermi liquid pole reaches its maximum height about 10^4, an order of magnitude less than in the probe limit, whereas the second, Fermi liquid-like pole, increases by an order of magnitude. This suggests that the finite density state corresponds to the Fermi-liquid like state, rather than a non-Fermi liquid.

4. As we mentioned in the introduction, part of the reason to suspect the existence of an AdS-RN Dirac-hair solution is that a detailed study of spectral functions in AdS-RN reveals that the quasiparticle peak is anomalously sensitive to changes in T. This anomalous temperature dependence disappears in the finite density solution. Specifically in pure AdS-RN the position ω_{max} where the peak height is maximum, denoted E_F in [17], does not agree with the value ω_{pole}, where the pole touches the real axis in the complex ω-plane, for any finite value of T, and is exponentially sensitive to changes in T (Fig 4.6). In the AdS-RN Dirac hair solution the location ω_{max} and the location ω_{pole} do become the same. Fig. 4.6B shows that the maximum of the quasiparticle peak always sits at $\omega \simeq 0$ in finite density Dirac hair solution, while it only reaches this as $T \to 0$ in the probe AdS-RN case.

4.4 Discussion and Conclusion

Empirically we know that the Fermi liquid phase of real matter systems is remarkably robust and generic. This is corroborated by analyzing effective field theory around the Fermi surface, but as it assumes the ground state it cannot explain its genericity. If the Fermi liquid ground state is so robust, this must also be a feature of the recent holographic approaches to strongly interacting fermionic systems. Our results here indicate that this is so. We have used Migdal's relation to construct AdS/CFT rules for the holographic dual of a Fermi liquid: the characteristic occupation number discontinuity Δn_F is encoded in the normalizable subsubleading component of the spatially averaged fermion density $J^0_-(z) \equiv \int d^3k\bar{\Psi}(\omega = 0, -k, z)i\gamma^0\Psi(\omega = 0, k, z)$ near the AdS boundary. This density has its own set of evolution equations, based on the underlying Dirac field, and insisting on normalizability automatically selects the on-shell wavefunctions of the underlying Dirac-field.

The simplest AdS solution that has a non-vanishing expectation value for the occupation number discontinuity Δn_F is that of a single fermion wavefunction. Using the density approach — which through the averaging appears to describe a class of solutions rather than one specific solution — we have constructed the limit of this solution where gravitational backreaction is ignored. At low black hole temperatures this solution with fermionic "Dirac hair" is the preferred ground state. Through an analysis of the free-energy, we argue that this gravitational solution with a non-zero fermion profile precisely corresponds to a system with a finite density of fermions. A spectral analysis still reveals a zoo of Fermi-surfaces in this ground state, but there are indications that in the full gravitationally backreacted solution only a Landau Fermi-liquid type Fermi surface survives. This follows in part from the relation between the spectral density and the Fermi momentum of a particular Landau liquid-like Fermi surface; it also agrees with the prediction from Luttinger's theorem. Furthermore, the spectral analysis in the finite density state shows no anomalous temperature dependence present in the pure charged black-hole single spectral functions. This also indicates that the finite density state is the true ground state.

The discovery of this state reveals a new essential component in the study of strongly coupled fermionic systems through gravitational duals, where one should take into account the expectation values of fermion bilinears. Technically the construction of the full gravitationally backreacted solution is a first point that is needed to complete our finding. A complete approach to this problem will have to take into account the many-body physics in the bulk. Within the approach presented in this paper, it means the inclusion of additional fermion wavefunctions, filling the bulk Fermi surface. The realization, however, that expectation values of fermion bilinears can be captured in holographic duals and naturally encode phase separations in strongly coupled fermion systems should find a large set of applications in the near future.

Chapter 5

From the Dirac hair to the electron star [19]

5.1 Introduction

The insight provided by the application of the AdS/CFT correspondence to finite density Fermi systems has given brand new perspectives on the theoretical robustness of non-Fermi liquids [79, 17, 27]; on an understanding of the non-perturbative stability of the regular Fermi liquid equivalent to order parameter universality for bosons [18, 20], and most importantly on the notion of fermionic criticality: Fermi systems with no scale. In essence strongly coupled conformally invariant fermi systems are one answer to the grand theoretical question of fermionic condensed matter: *Are there finite density Fermi systems that do not refer at any stage to an underlying perturbative Fermi gas?*

It is natural to ask to what extent AdS/CFT can provide a more complete answer to this question. Assuming, almost tautologically, that the underlying system is strongly coupled and there is in addition some notion of a large N limit, the Fermi system is dual to classical general relativity with a negative cosmological constant coupled to charged fermions and electromagnetism. As AdS/CFT maps quantum numbers to quantum numbers, finite density configurations of the strongly coupled large N system correspond to solutions of this Einstein-Maxwell-Dirac theory with finite charge density. Since the AdS fermions are the only object carrying charge, and the gravity system is weakly coupled, one is immediately inclined to infer that the generic solution is a weakly coupled charged Fermi gas coupled to AdS gravity: in other words an AdS electron star [50, 51], the charged equivalent of a neutron star in asymptotically anti-de Sitter space [23, 6].

Nothing can seem more straightforward. Given the total charge density Q of interest, one constructs the free fermionic wavefunctions in this system, and fills them one by one in increasing energy until the total charge equals Q. For macroscopic values of Q these fermions themselves will backreact on the geometry. One can compute this backreaction; it changes the potential for the free fermions at subleading order. Correcting the wavefunctions at this subleading order, one converges on the true solution order by order in the gravitational strength $\kappa^2 E^2_{full\ system}$. Here $E_{full\ system}$ is the energy carried by the Fermi system and κ^2 is the gravitational coupling constant $\kappa^2 = 8\pi G_{Newton}$ in the AdS gravity system. Perturbation theory in κ is dual to the $1/N$ expansion in the associated condensed matter system.

The starting point of the backreaction computation is to follow Tolman-Oppenheimer-Volkov (TOV) and use a Thomas-Fermi (TF) approximation for the lowest order one-loop contribution [23, 50, 51, 6]. The Thomas-Fermi approximation applies when the number of constituent fermions making up the Fermi gas is infinite. For neutral fermions this equates to the statement that the energy-spacing between the levels is neglible compared to the chemical potential associated with Q, $\Delta E/\mu \to 0$. For charged fermions the Thomas-Fermi limit is more direct: it is the limit $q/Q \to 0$ where q is the charge of each constituent fermion. [1]

This has been the guiding principle behind the approaches [23, 50, 6, 51, 89, 52] and the recent papers [53, 63], with the natural assumption that all corrections beyond Thomas-Fermi are small quantitative changes rather than qualitative ones. On closer inspection, however, this completely natural TF-electron star poses a number of puzzles. The most prominent perhaps arises from the AdS/CFT correspondence finding that every normalizable fermionic wavefunction in the gravitational bulk corresponds to a fermionic quasiparticle excitation in the dual condensed matter system. In particular occupying a particular wavefunction is dual to having a particular Fermi-liquid state [18]. In the Thomas Fermi limit the gravity dual thus describes an infinity of Fermi liquids, whereas the generic condensed matter expectation would have been that a been that

[1] For a fermion in an harmonic oscillator potential $E_n = \hbar(n - 1/2)\omega$: thus $\Delta E/E_{total} = 1/\sum_1^N (n - 1/2) = 2/N^2$.

a single(/few) liquid(s) would be the generic groundstate away from the strongly coupled fermionic quantum critical point at zero charge density. This zoo of Fermi surfaces is already present in the grand canonical approaches at fixed μ (extremal AdS-Reissner-Nordström (AdS-RN) black holes) [27] and a natural explanation would be that this is a large N effect. This idea, that the gravity theory is dual to a condensed matter system with N species of fermions, and increasing the charge density "populates" more and more of the distinct species of Fermi liquids, is very surprising from the condensed matter perspective. Away from criticality one would expect the generic groundstate to be a single Fermi-liquid or some broken state due to pairing. To pose the puzzle sharply, once one has a fermionic quasiparticle one should be able to adiabatically continue it to a free Fermi gas, which would imply that the free limit of the strongly coupled fermionic CFT is not a single but a system of order N fermions with an ordered distribution of fermi-momenta. A possible explanation of the multitude of Fermi surfaces that is consistent with a single Fermi surface at weak coupling is that AdS/CFT describes so-called "deconfined and/or fractionalized Fermi-liquids" where the number of Fermi surfaces is directly tied to the coupling strength [54, 97, 55, 53, 63]. It would argue that fermionic quantum criticality goes hand in hand with fractionalization for which there is currently scant experimental evidence.

The second puzzle is more technical. Since quantum numbers in the gravity system equal the quantum numbers in the dual condensed matter system, one is inclined to infer that each subsequent AdS fermion wavefunction has incrementally higher energy than the previous one. Yet analyticity of the Dirac equation implies that all normalizable wavefunctions must have strictly vanishing energy [27]. It poses the question how the order in which the fermions populate the Fermi gas is determined.

The third puzzle is that in the Thomas Fermi limit the Fermi gas is gravitationally strictly confined to a bounded region: famously, the TOV-neutron star has an edge. In AdS/CFT, however, all information about the dual condensed matter system is read off at asymptotic AdS infinity. Qualitatively, one can think of AdS/CFT as an "experiment" analogous to probing a spatially confined Fermi gas with a tunneling microscope held to the exterior of the trap. Extracting the information of the dual condensed matter system is probing the AdS Dirac system confined by a gravitoelectric trap instead of a magneto-optical trap for cold atoms. Although the Thomas-Fermi limit should reliably capture the charge and energy densities in the system, its abrupt non-analytic change at the edge (in a trapped system) and effective absence of a density far away from the center are well known to cause qualitative deficiencies in the description of the system. Specifically Friedel oscillations — quantum interference in the outside tails of the charged fermion density, controlled by the ratio q/Q and measured by a tunneling microscope — are absent. Analogously, there could be qualitative features in the AdS asymptotics of both the gravito-electric background and the Dirac wavefunctions in that adjusted background that are missed by the TF-approximation. The AdS asymptotics in turn *specify* the physics of the dual condensed matter system and since our main interest is to use AdS/CFT to understand quantum critical fermion systems where q/Q is finite, the possibility of a qualitative change inherent in the Thomas Fermi limit should be considered.

There is another candidate AdS description of the dual of a strongly coupled finite density Fermi system: the AdS black hole with Dirac hair [18, 20]. One arrives at this solution when one starts one's reasoning from the dual condensed matter system, rather than the Dirac fields in AdS gravity. Insisting that the system collapses to a generic single species Fermi-liquid ground state, the dual gravity description is that of an AdS Einstein-Dirac-Maxwell system with a single nonzero normalizable Dirac wavefunction. To have a macroscopic backreaction the charge of this single Dirac field must be macroscopic. The intuitive way to view this solution is as the other simplest approximation to free Fermi gas coupled to gravity. What we mean is that the full gravito-electric response is in all cases controlled by the total charge Q of the solution: as charge is conserved it is proportional to the constituent charge q times the number of fermions $n_{F_{AdS}}$ and the two simple limits correspond to $n_F \to \infty, q \to 0$ with $Q = qn_F$ fixed or $n_F \to 1, q \to Q$. The former is the Thomas-Fermi electron star, the latter is the AdS Dirac hair solution. In the context of AdS/CFT there is a significant difference between the two solutions in that the Dirac Hair solution clearly does not give rise to the puzzles 1, 2 and 3: there is by construction no zoo of Fermi-surfaces and therefore no ordering. Moreover since the wavefunction is demanded to be normalizable, it manifestly encodes the properties of the system at the AdS boundary. On the other hand the AdS Dirac hair solution does pose the puzzle that under normal conditions the total charge Q is much larger than the constituent charge q both from the gravity/string theory point of view and the condensed matter perspective. Generically one would expect a Fermi gas electron star rather than Dirac hair.

In this article we shall provide evidence for this point of view that the AdS electron star and the AdS Dirac hair solution are two limits of the same underlying system. Specifically we shall show that (1) the electron star solution indeed has the constituent charge as a free parameter which is formally sent to zero to obtain the Thomas-Fermi approximation. (2) The number of normalizable wavefunctions in the electron star depend on the value of the constituent charge q. We show this by computing the electron star spectral functions. They depend in similar way on q as the first AdS/CFT Fermi system studies in an AdS-RN background. In the formal limit where $q \to Q$, only one normalizable mode remains and the spectral function wavefunction resembles the Dirac Hair solution, underlining their underlying equivalence. Since both approximations have qualitative differences as a description of the AdS dual to strongly coupled fermionic systems, it argues that an improved approximation which has characteristics of both is called for.

The results here are complimentary to and share an analysis of electron star spectral functions with the two recent articles [53] and [63] that appeared in the course of this work (see also [61] for fermion spectral functions in general Lifshitz backgrounds). Our motivation to probe the system away from the direct electron star limit differs: we have therefore been more precise in defining this limit and in the analysis of the Dirac equation in the electron star background.

5.2 Einstein-Maxwell theory coupled to charged fermions

The Lagrangian that describes both the electron star and Dirac Hair approximation is Einstein-Maxwell theory coupled to charged matter

$$S = \int d^4x\sqrt{-g}\left[\frac{1}{2\kappa^2}\big(R+\frac{6}{L^2}\big)-\frac{1}{4q^2}F^2+\mathcal{L}_{\mathtt{mat}}(e^A_\mu, A_\mu)\right], \quad (5.2.1)$$

where L is the AdS radius, q is the electric charge and κ is the gravitational coupling constant. It is useful to scale the electromagnetic interaction to be of the same order as the gravitational interaction and measure all lengths in terms of the AdS radius L:

$$g_{\mu\nu} \to L^2 g_{\mu\nu}\ , \quad A_\mu \to \frac{qL}{\kappa}A_\mu. \quad (5.2.2)$$

The system then becomes

$$S = \int d^4x\sqrt{-g}\left[\frac{L^2}{2\kappa^2}\left(R+6-\frac{1}{2}F^2\right)+L^4\mathcal{L}_{\mathtt{mat}}(Le^A_\mu,\frac{qL}{\kappa}A_\mu)\right] \quad (5.2.3)$$

Note that in the rescaled variables the effective charge of charged matter now depends on the ratio of the electromagnetic to gravitational coupling constant: $q_{\mathtt{eff}} = qL/\kappa$. For the case of interest, charged fermions, the Lagrangian in these variables is

$$L^4\mathcal{L}_{\mathtt{f}}(Le^A_\mu,\frac{qL}{\kappa}A_\mu) = -\frac{L^2}{\kappa^2}\bar{\Psi}\left[e^\mu_A\Gamma^A(\partial_\mu+\frac{1}{4}\omega^{BC}_\mu\Gamma_{BC}-i\frac{qL}{\kappa}A_\mu)-mL\right]\Psi \quad (5.2.4)$$

where $\bar{\Psi}$ is defined as $\bar{\Psi} = i\Psi^\dagger\Gamma^0$. Compared to the conventional normalization the Dirac field has been made dimensionless $\Psi = \kappa\sqrt{L}\psi_{\text{conventional}}$. With this normalization all terms in the action have a factor L^2/κ^2 and it will therefore scale out of the equations of motion

$$\begin{aligned} R_{\mu\nu}-\frac{1}{2}g_{\mu\nu}R-3g_{\mu\nu} &= \left(F_{\mu\rho}F_\nu{}^\rho-\frac{1}{4}g_{\mu\nu}F_{\rho\sigma}F^{\rho\sigma}+T^{\mathtt{f}}_{\mu\nu}\right), \\ D_\mu F^{\mu\nu} &= -q_{\mathtt{eff}}J^\nu_{\mathtt{f}} \end{aligned} \quad (5.2.5)$$

with

$$T^{\mathtt{f}}_{\mu\nu} = \frac{1}{2}\bar{\Psi}e_{A(\mu}\Gamma^A\left[\partial_{\nu)}+\frac{1}{4}\omega^{BC}_{\nu)}\Gamma_{BC}-i\frac{qL}{\kappa}A_{\nu)}\right]\Psi-\frac{\kappa^2L^2}{2}g_{\mu\nu}\mathcal{L}_{\mathtt{f}} \quad (5.2.6)$$

$$J^\nu_{\mathtt{f}} = i\bar{\Psi}e^\nu_A\Gamma^A\Psi, \quad (5.2.7)$$

where the symmetrization is defined as $B_{(\mu}C_{\nu)} = B_\mu C_\nu + B_\nu C_\mu$ and the Dirac equation

$$\left[e^\mu_A\Gamma^A(\partial_\mu+\frac{1}{4}\omega^{BC}_\mu\Gamma_{BC}-i\frac{qL}{\kappa}A_\mu)-mL\right]\Psi = 0. \quad (5.2.8)$$

The stress-tensor and current are to be evaluated in the specific state of the system. For a single excited wavefunction, obeying (5.2.8), this gives the AdS Dirac hair solution constructed in [18]. (More specifically, the Dirac hair solution consists of a radially isotropic set of wavefunctions with identical momentum size $|\vec{k}| = \sqrt{k_x^2+k_y^2}$, such that the Pauli principle plays no role.) For multiple occupied fermion states, even without backreaction due to gravity, adding the contributions of each separate solution to (5.2.8) rapidly becomes very involved. In such a many-body-system, the collective effect of the multiple occupied fermion states is better captured in a "fluid" approximation

$$T_{\mu\nu}^{\texttt{fluid}} = (\rho + p)u_\mu u_\nu + p g_{\mu\nu}, \qquad N_\mu^{\texttt{fluid}} = n u_\mu \tag{5.2.9}$$

with

$$\rho = \langle u^\mu T_{\mu\nu} u^\nu \rangle_{\texttt{matter only}} \ , \quad n = -\langle u_\mu J^\mu \rangle_{\texttt{matter only}}. \tag{5.2.10}$$

In the center-of-mass rest frame of the multiple fermion system ($u_\mu = (e_{t\underline{0}}, 0, 0, 0)$), the expressions for the stress-tensor and charge density are given by the one-loop equal-time expectation values (as opposed to time-ordered correlation functions)

$$\rho = \langle \bar{\Psi}(t) e^t_{\underline{0}} \Gamma^{\underline{0}} (\partial_t + \frac{1}{4}\omega_t^{AB}\Gamma_{AB} - i q_{\texttt{eff}} A_t)\Psi(t)\rangle. \tag{5.2.11}$$

By the optical theorem the expectation value is equal to twice imaginary part of the Feynman propagator[2]

$$\rho = \lim_{t\to t'} 2\mathrm{ImTr}\left[e^t_{\underline{0}} \Gamma^{\underline{0}} (\partial_t + \frac{1}{4}\omega_t^{AB}\Gamma_{AB} - i q_{\texttt{eff}} A_t) G_F^{AdS}(t', t)\right]. \tag{5.2.12}$$

In all situations of interest, all background fields will only have dependence on the radial AdS direction; in that case the spin connection can be absorbed in the normalization of the spinor wavefunction.[3] In an adiabatic approximation for the radial dependence of $e_{t\underline{0}}$ and A_t — where $\mu_{\texttt{loc}}(r) = q_{\texttt{eff}} e^t_{\underline{0}}(r) A_t(r)$ and $\omega(r) = -i e^t_{\underline{0}}(r)\partial_t$; — this yields the known expression for a many-body-fermion system at finite chemical potential

$$\begin{aligned} \rho(r) &= \lim_{\beta\to\infty} 2 \int \frac{d^3k d\omega}{(2\pi)^4} \left[\omega(r) - \mu_{\texttt{loc}}(r)\right] \mathrm{ImTr}\, i\Gamma^{\underline{0}} G_F^\beta(\omega, k) \\ &= \frac{1}{\pi^2}\frac{\kappa^2}{L^2}\int_{mL}^{\mu_{\mathrm{loc}}} dE E^2 \sqrt{E^2 - (mL)^2}\ . \end{aligned} \tag{5.2.13}$$

[2]From unitarity for the S matrix $S^\dagger S = 1$ one obtains the optical theorem $T^\dagger T = 2\mathrm{Im}T$ for the transition matrix T defined as $S \equiv 1 + iT$.

[3]i.e. one can redefine spinors $\chi(r) = f(r)\Psi(r)$ such that the connection term is no longer present in the equation of motion.

The normalization κ^2/L^2 follows from the unconventional normalization of the Dirac field in eq. (5.2.4).[4] Similarly

$$n = \frac{1}{\pi^2}\frac{\kappa^2}{L^2}\int_{mL}^{\mu_{\rm loc}} dEE\sqrt{E^2-(mL)^2} = \frac{1}{3\pi^2}\frac{\kappa^2}{L^2}({\mu_{\rm loc}}^2-(mL)^2)^{3/2} \quad (5.2.14)$$

The adiabatic approximation is valid for highly localized wavefunctions, i.e. the expression must be dominated by high momenta (especially in the radial direction). The exact expression on the other hand will not have a continuum of solutions to the harmonic condition $-\Gamma^0\omega + \Gamma^i k_i + \Gamma^z k_z - \Gamma^0\mu_{\rm loc} - imL = 0$. Normalizable solutions to the AdS Dirac equations only occur at discrete momenta — one can think of the gravitational background as a potential well. The adiabatic approximation is therefore equivalent to the Thomas-Fermi approximation for a Fermi-gas in a box.

To get an estimate for the parameter range where the adiabatic approximation holds, consider the adiabatic bound $\partial_r\mu_{\tt loc}(r) \ll \mu_{\tt loc}(r)^2$. Using the field equation for $A_{\underline{0}} = \mu_{\tt loc}/q_{\tt eff}$:

$$\partial_r^2\mu_{\tt loc} \sim q_{\tt eff}^2 n, \quad (5.2.15)$$

this bound is equivalent to requiring

$$\partial_r^2\mu_{\tt loc} \ll \partial_r\mu_{\tt loc}^2 \;\Rightarrow\; (\frac{qL}{\kappa})^2 n \ll 2\mu_{\tt loc}\partial_r\mu_{\tt loc} \;\Rightarrow\; (\frac{qL}{\kappa})^2 n \ll \mu_{\tt loc}^3 \quad (5.2.16)$$

where in the last line we used the original bound again. If the chemical potential scale is considerably higher than the mass of the fermion, we may use (5.2.14) to approximate $n \sim \frac{\kappa^2}{L^2}\mu_{\tt loc}^3$. Thus the adiabatic bound is equivalent to,

$$q = \frac{q_{\tt eff}\kappa}{L} \ll 1 \quad (5.2.17)$$

the statement that the constituent charge of the fermions is infinitesimal. Note that in the rescaled action (6.3.43, 5.2.4), L/κ plays the role of $1/\hbar$,

[4] One can see this readily by converting the dimensionless definition of ρ, eq (5.2.11), to the standard dimension. Using capitals for dimensionless quantities and lower-case for dimensionful ones

$$\rho \;\sim\; \langle\Psi\partial_T\Psi\rangle \sim \kappa^2L^2\langle\psi\partial_t\psi\rangle \sim \kappa^2L^2\int_m^\mu d\epsilon\epsilon^2\sqrt{\epsilon^2-m^2} \sim \frac{\kappa^2}{L^2}\int_{mL}^{\mu L} dEE^2\sqrt{E^2-(mL)^2}$$

with $\mu L = \mu_{\tt loc}$ above.

and eq. (5.2.17) is thus equivalent to the semiclassical limit $\hbar \to 0$ with $q_{\mathtt{eff}}$ fixed. Since AdS/CFT relates $L/\kappa \sim N_c$ this acquires the meaning in the context of holography that there is a large N_c scaling limit [53, 63] of the CFT with fermionic operators where the RG-flow is "adiabatic". Returning to the gravitational description the additional assumption that the chemical potential is much larger than the mass is equivalent to

$$\begin{aligned}\frac{Q^{\mathtt{total}}_{\mathtt{phys}}}{V_{\mathtt{spatial\ AdS}}} &= \frac{LQ^{\mathtt{total}}_{\mathtt{eff}}}{\kappa V_{\mathtt{spatial\ AdS}}} \equiv \frac{L}{\kappa V_{\mathtt{spatial\ AdS}}}\int dr\sqrt{-g_{\text{induced}}}\,(q_{\mathtt{eff}}n) \quad (5.2.18)\\ &\simeq \frac{1}{V_{\mathtt{spatial\ AdS}}}\int dr\sqrt{-g}\frac{q_{\mathtt{eff}}\kappa}{L}\mu^3_{\mathtt{loc}}(r) \quad \gg \quad q(mL)^3\ .\end{aligned}$$

This implies that the total charge density in AdS is much larger than that of a single charged particle (as long as $mL \sim 1$). The adiabatic limit is therefore equivalent to a thermodynamic limit where the Fermi gas consists of an infinite number of constituents, $n \to \infty$, $q \to 0$ such that the total charge $Q \sim nq$ remains finite.

The adiabatic limit of a many-body fermion system coupled to gravity are the Tolman-Oppenheimer-Volkov equations. Solving this in asymptotically AdS gives us the charged neutron or electron star constructed in [51]. Knowing the quantitative form of the adiabatic limit, it is now easy to distinguish the electron star solution from the "single wavefunction" Dirac Hair solution. The latter is trivially the single particle limit $n \to 1$, $q \to Q$ with the total charge Q finite. The electron star and Dirac Hair black hole are opposing limit-solutions of the same system. We shall now make this connection more visible by identifying a formal dialing parameter that interpolates between the two solutions.

To do so we shall need the full adiabatic Tolman-Oppenheimer-Volkov equations for the AdS electron star [51]. Since the fluid is homogeneous and isotropic, the background metric and electrostatic potential will respect these symmetries and will be of the form (recall that we are already using "dimensionless" lengths, eq. (5.2.2))

$$ds^2 = -f(r)dt^2 + g(r)dr^2 + r^2(dx^2 + dy^2), \quad A = h(r)dt, \qquad (5.2.19)$$

where $f(r), g(r), h(r)$ are functions of r; the horizon is located at $r = 0$ and the boundary is at $r = \infty$. Combining this ansatz with a rescaling

$mL = q_{\mathtt{eff}}\hat{m}$ the bosonic background equations of motion become [51]

$$
\begin{aligned}
\frac{1}{r}\left(\frac{f'}{f}+\frac{g'}{g}\right)-\frac{gh\sigma}{\sqrt{f}} &= 0, & \rho &= \frac{q_{\mathtt{eff}}^4\kappa^2}{\pi^2L^2}\int_{\hat{m}}^{\frac{h}{\sqrt{f}}} d\epsilon\epsilon^2\sqrt{\epsilon^2-\hat{m}^2}\ , \\
\frac{f'}{rf}+\frac{h'^2}{2f}-g(3+p)+\frac{1}{r^2} &= 0, & \sigma &= \frac{q_{\mathtt{eff}}^4\kappa^2}{\pi^2L^2}\int_{\hat{m}}^{\frac{h}{\sqrt{f}}} d\epsilon\epsilon\sqrt{\epsilon^2-\hat{m}^2}\ , \\
h''+\frac{2}{r}h'-\frac{g\sigma}{\sqrt{f}}\left(\frac{rhh'}{2}+f\right) &= 0, & -p &= \rho-\frac{h}{\sqrt{f}}\sigma\ ,
\end{aligned}
\tag{5.2.20}
$$

where we have used that $\mu_{\mathtt{loc}} = q_{\mathtt{eff}}h/\sqrt{f}$ and $\sigma = nq_{\mathtt{eff}}$ is the rescaled local charge density. What one immediately notes is that the Tolman-Oppenheimer-Volkov equations of motion for the background only depend on the parameters $\hat{\beta} \equiv \frac{q_{\mathtt{eff}}^4\kappa^2}{\pi^2L^2}$ and $\hat{m}$, whereas the original Lagrangian and the fermion equation of motion also depend on $q_{\mathtt{eff}} = \left(\frac{\pi^2L^2\hat{\beta}}{\kappa^2}\right)^{1/4}$. It is therefore natural to guess that the parameter $q_{\mathtt{eff}} = qL/\kappa$ will be the interpolating parameter away from the adiabatic electron star limit towards the Dirac Hair BH.

Indeed in these natural electron star variables the adiabatic bound (5.2.17) translates into

$$
\hat{\beta} \ll \frac{L^2}{\kappa^2} = \frac{q_{\mathtt{eff}}^2}{q^2}\ . \tag{5.2.21}
$$

Thus we see that for a given electron star background with $\hat{\beta}$ fixed decreasing κ/L improves the adiabatic fluid approximation whereas increasing κ/L makes the adiabatic approximation poorer and poorer. “Dialing κ/L up/down” therefore *interpolates* between the electron star and the Dirac Hair BH. Counterintuitively improving adiabaticity by decreasing κ/L corresponds to increasing $q_{\mathtt{eff}}$ for fixed q, but this is just a consequence of recasting the system in natural electron star variables. A better way to view improving adiabaticity is to decrease the microscopic charge q but while keeping $q_{\mathtt{eff}}$ fixed; this shows that a better way to think of $q_{\mathtt{eff}}$ is as the total charge rather than the efffective constituent charge.

The parameter $\kappa/L = q/q_{\mathtt{eff}}$ parametrizes the gravitational coupling strength in units of the AdS curvature, and one might worry that “dialing κ/L up” pushes one outside the regime of classical gravity. This is not the case. One can easily have $\hat{\beta} \gg 1$ and tune κ/L towards or away from the adiabatic limit within the regime of classical gravity. From eq. (5.2.17) we see that the edge of validity of the adiabatic regime $\hat{\beta} \simeq L^2/\kappa^2$ is simply equivalent to a microscopic charge $q = 1$ which clearly has a classical gravity description. It is not hard to see that the statement above is the equivalent of changing the level splitting in the Fermi gas, while keeping the overall energy/charge fixed. In a Fermi gas microscopically both the overall energy and the level splitting depends on $\hbar$. Naively increasing $\hbar$ increases both, but one can move away from the adiabatic limit either by decreasing the overall charge density, keeping $\hbar$ fixed or by keeping the charge density fixed and raising $\hbar$. Using again the analogy between κ/L and $\hbar$, the electron star situation is qualitatively the same where one should think of $\hat{\beta} \sim q^4 L^2/\kappa^2$ parametrizing the microscopic charge. One can either insist on keeping κ/L fixed and *increase* the microscopic charge $\hat{\beta}$ to increase the level splitting or one can keep $\hat{\beta}$ fixed and increase κ/L. In the electron star, however, the background geometry changes with $\hat{\beta}$ in addition to the level splitting, and it is therefore more straightforward to keep $\hat{\beta}$ and the geometry fixed, while dialing κ/L.

We will now give evidence for our claim that the electron star and Dirac Hair solution are two opposing limits. To do so, we need to identify an observable that goes either beyond the adiabatic background approximation or beyond the single particle approximation. Since the generic intermediate state is still a many-body fermion system, the more natural starting point is the electron star background and perturb away from there. Realizing then that the fermion equation of motion already depends directly on the dialing parameter $q_{\texttt{eff}}$ the obvious observables are the single fermion spectral functions in the electron star background. Since one must specify a value for $q_{\texttt{eff}}$ to compute these, they directly probe the microscopic charge of the fermion and are thus always beyond the strict electron star limit $q \to 0$. In the next two sections we will compute these and show that they indeed reflect the interpretation of $q_{\texttt{eff}}$ as the interpolating parameter between the electron star and Dirac Hair BH.

5.3 Fermion spectral functions in the electron star background

To compute the fermion spectral functions in the electron star background we shall choose a specific representative of the family of electron stars parametrized by $\hat{\beta}$ and $\hat{m}$. Rather than using $\hat{\beta}$ and $\hat{m}$ the metric of an electron star is more conveniently characterized by its Lifshitz-scaling behavior near the interior horizon $r \to 0$. From the field equations (5.2.20) the limiting interior behavior of $f(r), g(r), h(r)$ is

$$f(r) = r^{2z} + \dots\ , \quad g(r) = \frac{g_\infty}{r^2} + \dots\ , \quad h(r) = h_\infty r^z + \dots \tag{5.3.22}$$

The scaling behavior is determined by the dynamical critical exponent z, which is a function of $\hat{\beta}$, $\hat{m}$ [51] and it is conventionally used to classify the metric instead of $\hat{\beta}$. The full electron star metric is then generated from this horizon scaling behavior by integrating up an irrelevant RG-flow [39, 37]

$$\begin{aligned} f &= r^{2z}\left(1 + f_1 r^{-\alpha} + \dots\right) \\ g &= \frac{g_\infty}{r^2}\left(1 + g_1 r^{-\alpha} + \dots\right) \\ h &= h_\infty r^z\left(1 + h_1 r^{-\alpha} + \dots\right). \end{aligned} \tag{5.3.23}$$

with

$$\alpha = \frac{2+z}{2} - \frac{\sqrt{9z^3 - 21z^2 + 40z - 28 - \hat{m}^2 z(4-3z)^2}}{2\sqrt{(1-\hat{m}^2)z - 1}}. \tag{5.3.24}$$

Scaling $f_1 \to b f_1$ is equal to a coordinate transformation $r \to b^{1/\alpha} r$ and $t \to b^{z/\alpha} t$, and the sign of f_1 is fixed to be negative in order to be able to match onto an asymptotically AdS$_4$ solution. Thus $f_1 = -1$ and g_1 and h_1 are then uniquely determined by the equations of motion.

Famously, integrating the equations of motion up the RG-flow outwards towards the boundary fails at a finite distance r_s. This is the edge of the electron star. Beyond the edge of the electron star, there is no fluid present and the spacetime is that of an AdS$_4$-RN black hole with the metric

$$f = c^2 r^2 - \frac{\hat{M}}{r} + \frac{\hat{Q}^2}{2r^2}, \quad g = \frac{c^2}{f}, \quad h = \hat{\mu} - \frac{\hat{Q}}{r}. \tag{5.3.25}$$

Demanding the full metric is smooth at the radius of electron star r_s determines the constants c, $\hat{M}$ and $\hat{Q}$. The dual field theory is defined on the plane $ds^2 = -c^2 dt^2 + dx^2 + dy^2$.

The specific electron star background we shall choose without loss of generality is the one with $z = 2, \hat{m} = 0.36$ (Fig. 5.1)[5], smoothly matched at $r_s \simeq 4.25252$ onto a AdS-RN black-hole.

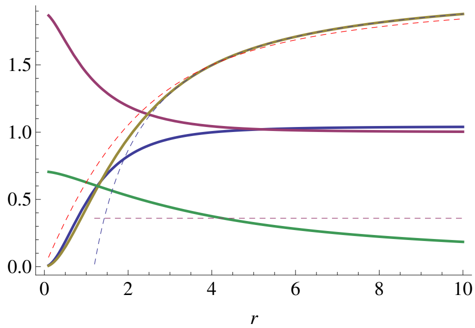

Figure 5.1: Electron star metric for $z = 2, \hat{m} = 0.36$, $c \simeq 1.021, \hat{M} \simeq 3.601, \hat{Q} \simeq 2.534, \hat{\mu} \simeq 2.132$ compared to pure AdS. Shown are $f(r)/r^2$ (Blue), $r^2 g(r)$ (Red) and $h(r)$ (Orange). The asymptotic AdS-RN value of $h(r)$ is the dashed blue line. For future use we have also given $\mu_{\texttt{loc}} = h/\sqrt{f}$ (Green) and $\mu_{q_{\texttt{eff}}} = \sqrt{g^{ii}}h/\sqrt{f}$ (Red Dashed) At the edge of the star $r_s \simeq 4.253$ (the intersection of the purple dashed line setting the value of $m_{\texttt{eff}}$ with $\mu_{\texttt{loc}}$) one sees the convergence to pure AdS in the constant asymptotes of $f(r)/r^2$ and $r^2 g(r)$.

The CFT fermion spectral functions now follow from solving the Dirac equation in this background [79, 17]

$$\left[e^{\mu}_{A}\Gamma^{A}\left(\partial_{\mu} + \frac{1}{4}\omega_{\mu AB}\Gamma^{AB} - iq_{\texttt{eff}}A_{\mu}\right) - m_{\texttt{eff}}\right]\Psi = 0 \qquad (5.3.26)$$

where $q_{\texttt{eff}}$ and $m_{\texttt{eff}}$ in terms of the parameters of the electron star equal

$$q_{\texttt{eff}} = \left(\frac{\pi^2 L^2 \hat{\beta}}{\kappa^2}\right)^{1/4}, \quad m_{\texttt{eff}} = q_{\texttt{eff}}\hat{m} = \hat{m}\left(\frac{\pi^2 L^2 \hat{\beta}}{\kappa^2}\right)^{1/4} \qquad (5.3.27)$$

For a given electron star background, i.e. a fixed $\hat{\beta}$, $\hat{m}$ the fermion spectral function will therefore depend on the ratio L/κ. For $L/\kappa \gg \hat{\beta}^{1/2}$ the poles in these spectral functions characterize the occupied states in a many-body gravitational Fermi system that is well approximated by the electron star.

[5]This background has $c \simeq 1.021, \hat{M} \simeq 3.601, \hat{Q} \simeq 2.534, \hat{\mu} \simeq 2.132$, $\hat{\beta} \simeq 19.951$, $g_\infty \simeq 1.887$, $h_\infty = 1/\sqrt{2}$, $\alpha \simeq -1.626$, $f_1 = -1$, $g_1 \simeq -0.4457$, $h_1 \simeq -0.6445$.

As L/κ is lowered for fixed $\hat{\beta}$ the electron star background becomes a poorer and poorer approximation to the true state and we should see this reflected in both the number of poles in the spectral function and their location.

Projecting the Dirac equation onto two-component $\Gamma^{\underline{r}}$ eigenspinors

$$\Psi_{\pm} = (-gg^{rr})^{-\frac{1}{4}} e^{-i\omega t + ik_i x^i} \begin{pmatrix} y_{\pm} \\ z_{\pm} \end{pmatrix} \tag{5.3.28}$$

and using isotropy to set $k_y = 0$, one can choose a basis of Dirac matrices where one obtains two decoupled sets of two simple coupled equations [79]

$$\begin{aligned} \sqrt{g_{ii}g^{rr}}(\partial_r \mp m_{\mathtt{eff}}\sqrt{g_{rr}})y_{\pm} &= \mp i(k_x - u)z_{\mp}, & (5.3.29) \\ \sqrt{g_{ii}g^{rr}}(\partial_r \pm m_{\mathtt{eff}}\sqrt{g_{rr}})z_{\mp} &= \pm i(k_x + u)y_{\pm} & (5.3.30) \end{aligned}$$

where $u = \sqrt{\frac{g_{ii}}{-g_{tt}}}(\omega + q_{\text{eff}}h)$. In this basis of Dirac matrices the CFT Green's function $G = \langle \bar{\mathcal{O}}_{\psi_+} i\gamma^0 \mathcal{O}_{\psi_+} \rangle$ equals

$$G = \lim_{\epsilon \to 0} \epsilon^{-2mL} \begin{pmatrix} \xi_+ & 0 \\ 0 & \xi_- \end{pmatrix} \Bigg|_{r=\frac{1}{\epsilon}}, \quad \text{where} \quad \xi_+ = \frac{iy_-}{z_+}, \ \xi_- = -\frac{iz_-}{y_+} \tag{5.3.31}$$

Rather than solving the coupled equations (5.3.29) it is convenient to solve for $\xi_{\pm}$ directly [79],

$$\sqrt{\frac{g_{ii}}{g_{rr}}}\partial_r \xi_{\pm} = -2m_{\mathtt{eff}}\sqrt{g_{ii}}\xi_{\pm} \mp (k_x \mp u) \pm (k_x \pm u)\xi_{\pm}^2. \tag{5.3.32}$$

For the spectral function $A = \text{ImTr}G_R$ we are interested in the retarded Green function. This is obtained by imposing in-falling boundary conditions near the horizon $r = 0$. Since the electron star is a "zero-temperature" solution this requires a more careful analysis than for a generic horizon. To ensure that the numerical integration we shall perform to obtain the full spectral function has the right infalling boundary conditions, we first solve eq. (5.3.32) to first subleading order around $r = 0$. There are two distinct branches. When $\omega \neq 0$ and $k_x r/\omega, r^2/\omega$ is small, the in-falling boundary condition near the horizon $r = 0$ is (for $z = 2$)

$$\begin{aligned} \xi_+(r) &= i - i\frac{k_x r}{\omega} + i\frac{(k_x^2 - 2im_{\mathtt{eff}}\omega)r^2}{2\omega^2} - i\frac{f_1 k_x r^{1-\alpha}}{2\omega} + \ldots \\ \xi_-(r) &= i + i\frac{k_x r}{\omega} + i\frac{(k_x^2 - 2im_{\mathtt{eff}}\omega)r^2}{2\omega^2} + i\frac{f_1 k_x r^{1-\alpha}}{2\omega} + \ldots \end{aligned} \tag{5.3.33}$$

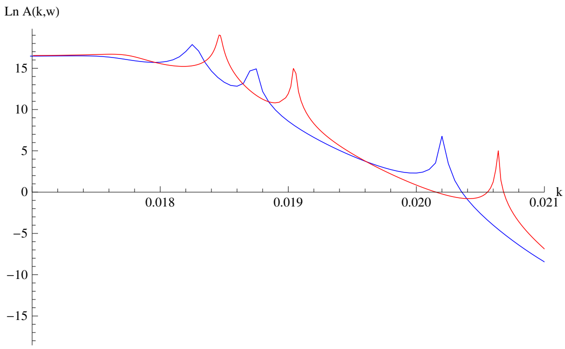

Figure 5.2: Electron star MDF spectral functions with multiple peaks as a function of k for $\omega = 10^{-5}, z = 2, \hat{m} = 0.36$. The blue curve is for $\kappa = 0.091$; the red curve is for $\kappa = 0.090$. Note that the vertical axis is logarithmic. Visible is the rapidly decreasing spectral weight and increasingly narrower width for each successive peak as k_F increases.

When $\omega = 0$, i.e. $k_x r/\omega$ is large, and $r/k_x \to 0$,

$$\begin{aligned} \xi_+(r) &= -1 + \frac{(q_{\text{eff}} h_\infty + m_{\texttt{eff}})r}{k_x} + \left(\frac{\omega}{k_x r} - \frac{\omega}{2\sqrt{g_\infty} k_x^2}\right) + \ldots \\ \xi_-(r) &= 1 + \frac{(q_{\text{eff}} h_\infty - m_{\texttt{eff}})r}{k_x} + \left(\frac{\omega}{k_x r} - \frac{\omega}{2\sqrt{g_\infty} k_x^2}\right) + \ldots, \end{aligned} \tag{5.3.34}$$

the boundary conditions (5.3.34) become real. As (5.3.32) are real equations, the spectral function vanishes in this case. This is essentially the statement that all poles in the Green's function occur at $\omega = 0$ [27]. Note that the fact that the electron star $\omega = 0$ boundary conditions (5.3.32) are real for all values of k is qualitatively different from the AdS-RN $\omega = 0$ boundary conditions (eq. (26) in [79]). In the AdS-RN "quantum-critical" infrared governed by the near horizon $\text{AdS}_2 \times \mathbb{R}_2$ geometry, in general there is a special scale k_o below which the boundary condition turns complex. This scale k_o is related to the surprising existence of an oscillatory region in the spectral function. One therefore infers that in a scaleful Lifshitz infrared this oscillatory region is no longer present [63]. We will confirm this in section 5.4.

5.3.1 Numerical results and discussion

We can now solve for the spectral functions numerically. In Fig. 5.3 we plot the momentum-distribution-function (MDF) (the spectral function as a function of k) for fixed $\omega = 10^{-5},\ z = 2,\ \hat{m} = 0.36$ while changing the value of κ. Before we comment on the dependence on $q_{\mathtt{eff}} \sim \kappa^{-1/2}$ which studies the deviation away from the adiabatic limit of a given electron star background (i.e. fixed dimensionless charge and fixed dimensionless energy density), there are several striking features that are immediately apparent:

- As expected, there is a multitude of Fermi surfaces. They have very narrow width and their spectral weight decreases rapidly for each higher Fermi-momentum k_F (Fig. 5.2). This agrees with the exponential width $\Gamma \sim \exp(-\left(\frac{k^z}{\omega}\right)^{1/(z-1)})$ predicted by [26] for gravitational backgrounds that are Lifshitz in the deep interior, which is the case for the electron star. This prediction is confirmed in [61, 53, 63] and the latter two articles also show that the weight decreases in a corresponding exponential fashion. This exponential reduction of both the width and the weight as k_F increases explains why we only see a finite number of peaks, though we expect a very large number. In the next section we will be able to count the number of peaks, even though we cannot resolve them all numerically.

- The generic value of k_F of the peaks with visible spectral weight is *much* smaller than the effective chemical potential μ in the boundary field theory. This is quite different from the RN-AdS case where the Fermi momentum and chemical potential are of the same order. A numerical study cannot answer this, but the recent article [63] explains this.[6]

- Consistent with the boundary value analysis, there is no evidence of an oscillatory region.

The most relevant property of the spectral functions for our question is that as κ is increased the peak location k_F decreases orderly and peaks *disappear* at various threshold values of k. This is the support for our argument that changing κ changes the number of microscopic constituents in the electron star. Comparing the the behavior of the various Fermi momenta k_F in the electron star with the results in the extremal AdS-RN black-hole, they are qualitatively identical when one equates $\kappa^{-1/2} \sim q_{\mathtt{eff}}$ with the charge of the probe fermion. We may therefore infer from our

[6] In view of the verification of the Luttinger count for electron star spectra in [53, 63], this had to be so.

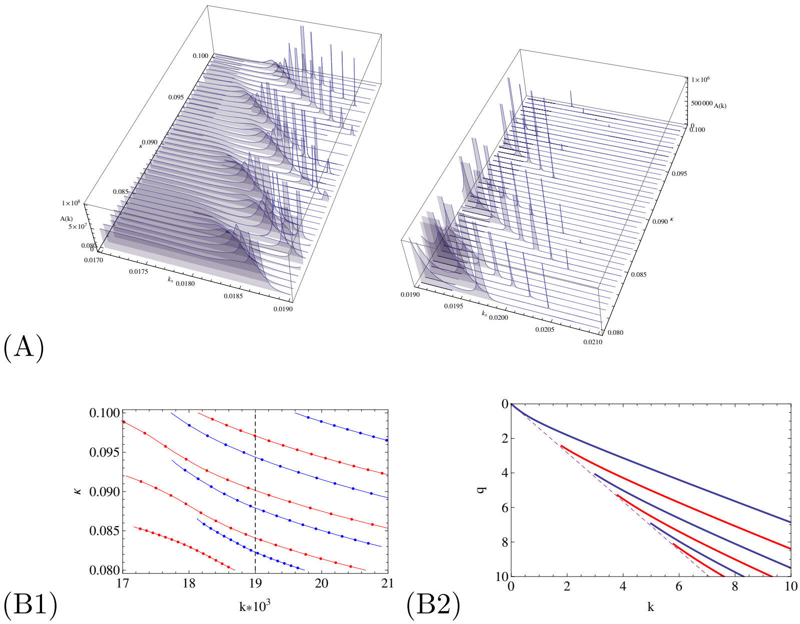

Figure 5.3: (A) Electron-star MDF spectral functions as a function of κ for $z = 2, \hat{m} = 0.36, \omega = 10^{-5}$. Because the peak height and weights decrease exponentially, we present the adjacent ranges $k \in [0.017, 0.019]$ and $k \in [0.019, 0.021]$ in two different plots with different vertical scale. (B1/B2) Locations of peaks of spectral functions as a function of κ: comparison between the electron star (B1) for $z = 2, \hat{m} = 0.36, \omega = 10^{-5}$ (the dashed gray line denotes the artificial separation in the 3D representations in (A)) and AdS-RN (B2) for $m = 0$ as a function of q in units where $\mu = \sqrt{3}$ These two Fermi-surface 'spectra' are qualitatively similar.

detailed understanding of the behavior of k_F for AdS-RN that also for the electron star as k_F is lowered peaks truly disappear from the spectrum until by extrapolation ultimately one remains: this is the AdS Dirac hair solution [18].

We can only make this inference qualitatively as the rapid decrease in spectral weight of each successive peak prevents an exact counting of Fermi surfaces in the numerical results for the electron star spectral functions. One aspect that we can already see is that as κ decreases all present peaks shift to higher k, while new peaks emerging from the left for smaller kappa. This suggests a fermionic version of the UV/IR correspondence where the peak with *lowest* k_F corresponds to the last occupied level, i.e. highest "energy" in the AdS electron star. We will now address both of these points in more detail.

5.4 Fermi surface ordering: k_F from a Schrödinger formulation

Our analysis of the behavior of boundary spectral functions as a function of κ relies on the numerically quite evident peaks. Stricly speaking, however, we have not shown that there is a true singularity in the Green's function at $\omega = 0, k = k_F$. We will do so by showing that the AdS Dirac equation, when recast as a Schrödinger problem has quasi-normalizable solutions at $\omega = 0$ for various k. As is well known, in AdS/CFT each such solution corresponds to a true pole in the boundary Green's function. Using a WKB approximation for this Schrödinger problem we will in addition be able to estimate the number of poles for a fixed κ and thereby provide a quantitative value for the deviation from the adiabatic background.

We wish to emphasize that the analysis here is general and captures the behavior of spectral functions in all spherically symmetric and static backgrounds backgrounds alike, whether AdS-RN, Dirac hair or electron star.

The $\omega = 0$ Dirac equation (5.3.26) for one set of components (5.3.29, 5.3.30) with the replacement $iy_- \to y_-$, equals

$$\begin{aligned} \sqrt{g_{ii}g^{rr}}\partial_r y_- + m_{\mathtt{eff}}\sqrt{g_{ii}}y_- &= -(k - \hat{\mu}_{q_{\mathtt{eff}}})z_+, \\ \sqrt{g_{ii}g^{rr}}\partial_r z_+ - m_{\mathtt{eff}}\sqrt{g_{ii}}z_+ &= -(k + \hat{\mu}_{q_{\mathtt{eff}}})y_-, \end{aligned} \tag{5.4.35}$$

where $\hat{\mu}_{q_{\mathtt{eff}}} = \sqrt{\frac{g_{ii}}{-g_{tt}}} q_{\mathtt{eff}} A_t$ and we will drop the subscript x on k_x. In our conventions z_+ (and y_+) is the fundamental component dual to the source of the fermionic operator in the CFT [79, 17]. Rewriting the coupled first order Dirac equations as a single second order equation for z_+:

$$\partial_r^2 z_+ + \mathcal{P}\partial_r z_+ + \mathcal{Q} z_+ = 0 \tag{5.4.36}$$

where the coefficients are

$$\begin{aligned} \mathcal{P} &= \frac{\partial_r(g_{ii}g^{rr})}{2g_{ii}g^{rr}} - \frac{\partial_r\hat{\mu}_{q_{\mathtt{eff}}}}{k+\hat{\mu}_{q_{\mathtt{eff}}}}, \\ \mathcal{Q} &= -\frac{m_{\mathtt{eff}}\partial_r\sqrt{g_{ii}}}{\sqrt{g_{ii}g^{rr}}} + \frac{m_{\mathtt{eff}}\sqrt{g_{rr}}\partial_r\hat{\mu}_{q_{\mathtt{eff}}}}{k+\hat{\mu}_{q_{\mathtt{eff}}}} - m_{\mathtt{eff}}^2 g_{rr} - \frac{k^2-\hat{\mu}_{q_{\mathtt{eff}}}^2}{g_{ii}g^{rr}}. \end{aligned} \tag{5.4.37}$$

the first thing one notes is that both $\mathcal{P}$ and $\mathcal{Q}$ diverge at some $r = r_*$ where $\hat{\mu}_{q_{\mathtt{eff}}} + k = 0$. Since $\hat{\mu}_{q_{\mathtt{eff}}}$ is (chosen to be) a positive semidefinite function which increases from $\hat{\mu}_{q_{\mathtt{eff}}} = 0$ at the horizon, this implies that for negative k (with $-k < \hat{\mu}_{q_{\mathtt{eff}}}|_\infty$) the wavefunction is qualitatively different from the wavefunction with positive k which experiences no singularity.The analysis is straightforward if we transform the first derivative away and recast it in the form of a Schrödinger equation by redefining the radial coordinate:

$$\frac{ds}{dr} = \exp\left(-\int^r dr'\mathcal{P}\right) \quad \Rightarrow \quad s = c_0 \int_{r_\infty}^r dr' \frac{|k + \hat{\mu}_{q_{\mathtt{eff}}}|}{\sqrt{g_{ii}g^{rr}}} \tag{5.4.38}$$

where c_0 is an integration constant whose natural scale is of order $c_0 \sim q_{\mathtt{eff}}^{-1}$. This is a simpler version of the generalized k-dependent tortoise coordinate introduced in [27]. In the new coordinates the equation (5.4.37) is of the standard form:

$$\partial_s^2 z_+ - V(s) z_+ = 0 \tag{5.4.39}$$

with potential

$$V(s) = -\frac{g_{ii}g^{rr}}{c_0^2|k + \hat{\mu}_{q_{\mathtt{eff}}}|^2}\mathcal{Q}. \tag{5.4.40}$$

The above potential (5.4.40) can also be written as

$$V(s) = \frac{1}{c_0^2(k + \hat{\mu}_{q_{\mathtt{eff}}})^2}\left[(k^2 + m_{\mathtt{eff}}^2 g_{ii} - \hat{\mu}_{q_{\mathtt{eff}}}^2) + m_{\mathtt{eff}} g_{ii}\sqrt{g^{rr}}\partial_r \ln \frac{\sqrt{g_{ii}}}{k + \hat{\mu}_{q_{\mathtt{eff}}}}\right]. \tag{5.4.41}$$

We note again the potential singularity for negative k, but before we discuss this we first need the boundary conditions. The universal boundary behavior is at spatial infinity and follows from the asymptotic AdS geometry. In the adapted coordinates $r \to \infty$ corresponds to $s \to 0$ as follows from $ds/dr \simeq c_0(k + \hat{\mu}_{q_{\mathtt{eff}}}|_\infty)/r^2$. The potential therefore equals

$$V(s) \simeq \frac{1}{s^2}\left(m_{\mathtt{eff}} + m_{\mathtt{eff}}^2\right) + \ldots \tag{5.4.42}$$

and the asymptotic behavior of the two independent solutions equals $z_+ = a_1 s^{-m_{\mathrm{eff}}} + b_1 s^{1+m_{\mathrm{eff}}} + \ldots$. The second solution is normalizable and we thus demand $a_1 = 0$.

In the interior, the near-horizon geometry generically is Lifshitz

$$ds^2 = -r^{2z}dt^2 + \frac{1}{r^2}dr^2 + r^2(dx^2 + dy^2) + \ldots, \quad A = h_\infty r^z dt + \ldots \tag{5.4.43}$$

with finite dynamical critical exponent z — AdS-RN, which can be viewed as a special case where $z \to \infty$, will be given separately. In adapted coordinates the interior $r \to 0$ corresponds to $s \to -\infty$ and it is easy to show that in this limit potential behaves as

$$V(s) \simeq \frac{1}{c_0^2} + \frac{1}{s^2}\left(m_{\mathtt{eff}}\sqrt{g_\infty} + m_{\mathtt{eff}}^2 g_\infty - h_\infty^2 q_{\mathtt{eff}}^2 g_\infty\right) + \dots. \tag{5.4.44}$$

Near the horizon the two independent solutions for the wavefunction z_+ therefore behave as

$$z_+ \to a_0 e^{-s/c_0} + b_0 e^{s/c_0}. \tag{5.4.45}$$

The decaying solution $a_0 = 0$ is the normalizable solution we seek.

Let us now address the possible singular behavior for $k < 0$. To understand what happens, let us first analyze the potential qualitatively for positive k. Since the potential is positive semi-definite at the horizon and the boundary, the Schrödinger system (5.4.39) only has a zero-energy normalizable solution if $V(s)$ has a range $s_1 < s < s_2$ where it is negative. This can only at locations where $k^2 < \hat{\mu}_{q_{\mathtt{eff}}}^2 - m_{\mathtt{eff}}^2 g_{ii} - m_{\mathtt{eff}} g_{ii}\sqrt{g^{rr}}\partial_r \ln \frac{\sqrt{g_{ii}}}{k+\hat{\mu}_{q_{\mathtt{eff}}}}$. Defining a "renormalized" position dependent mass $m_{\mathtt{ren}}^2 = m_{\mathtt{eff}}^2 g_{ii} + m_{\mathtt{eff}} g_{ii}\sqrt{g^{rr}}\partial_r \ln \frac{\sqrt{g_{ii}}}{k+\hat{\mu}_{q_{\mathtt{eff}}}}$ this is the intuitive statement that the momenta must be smaller than the local chemical potential $k^2 < \hat{\mu}_{q_{\mathtt{eff}}}^2 - m_{\mathtt{ren}}^2$. For positive k the saturation of this bound $k^2 = \hat{\mu}_{q_{\mathtt{eff}}}^2 - m_{\mathtt{ren}}^2$ has at most two solutions, which are regular zeroes of the potential. This follows from the fact that $\hat{\mu}_{q_{\mathtt{eff}}}^2$ decreases from the boundary towards the interior. If the magnitude $|k|$ is too large the inequality cannot be satisfied, the potential is strictly positive and no solution exists. For negative k, however, the potential has in addition a triple pole at $k^2 = \hat{\mu}_{q_{\mathtt{eff}}}^2$; two poles arise from the prefactor and the third from the $m_{\mathtt{eff}}\partial_r \ln(k + \hat{\mu}_{q_{\mathtt{eff}}})$ term. This pole always occurs closer to the horizon than the zeroes and the potential therefore qualitatively looks like that in Fig. 5.4 (Since $\hat{\mu}_{q_{\mathtt{eff}}}$ decreases as we move inward from the boundary, starting with $\hat{\mu}_{q_{\mathtt{eff}}}^2 > \hat{\mu}_{q_{\mathtt{eff}}}^2 - \mu^2 > k^2$, one first saturates the inequality that gives the zero in the potential as one moves inward.) Such a potential cannot support a zero-energy bound state, i.e. eq. (5.4.39) has no solution for negative k. In the case $m_{\mathtt{eff}} = 0$ a double zero changes the triple pole to a single pole and the argument still holds. This does not mean that there are no $k < 0$ poles in the CFT spectral function. They arise from the other physical polarization

y_+ of the bulk fermion Ψ. From the second set of decoupled first order equations for the other components of the Dirac equation (after replacing $iz_- \to z_-$,)

$$\begin{aligned} \sqrt{g_{ii}g^{rr}}\partial_r y_+ - m_{\texttt{eff}}\sqrt{g_{ii}}y_+ &= -(k-\hat{\mu}_{q_{\texttt{eff}}})z_-, \\ \sqrt{g_{ii}g^{rr}}\partial_r z_- + m_{\texttt{eff}}\sqrt{g_{ii}}z_- &= -(k+\hat{\mu}_{q_{\texttt{eff}}})y_+, \end{aligned} \tag{5.4.46}$$

and the associated second order differential EOM for y_+:

$$\partial_r^2 y_+ + \mathcal{P}\partial_r y_+ + \mathcal{Q}y_+ = 0,$$

with the coefficients

$$\begin{aligned} \mathcal{P} &= \frac{\partial_r(g_{ii}g^{rr})}{2g_{ii}g^{rr}} - \frac{\partial_r\hat{\mu}_{q_{\texttt{eff}}}}{-k+\hat{\mu}_{q_{\texttt{eff}}}}, \\ \mathcal{Q} &= -\frac{m_{\texttt{eff}}\partial_r\sqrt{g_{ii}}}{\sqrt{g_{ii}g^{rr}}} + \frac{m_{\texttt{eff}}\sqrt{g_{rr}}\partial_r\hat{\mu}_{q_{\texttt{eff}}}}{-k+\hat{\mu}_{q_{\texttt{eff}}}} - m_{\texttt{eff}}^2 g_{rr} - \frac{k^2-\hat{\mu}_{q_{\texttt{eff}}}^2}{g_{ii}g^{rr}} \end{aligned} \tag{5.4.47}$$

one sees that the Schrödinger equation for y_+ is the $k \to -k$ image of the equation (5.4.39) for z_+ and thus y_+ will only have zero-energy solutions for $k < 0$. For simplicity we will only analyze the z_+ case. Note that this semi-positive definite momentum structure of the poles is a feature of any AdS-to-Lifshitz metric different from AdS-RN, where one can have negative k solutions [27].

(A) 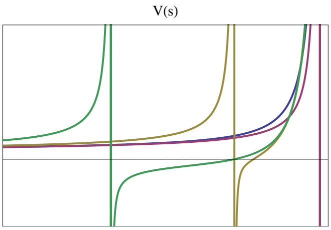

(B) 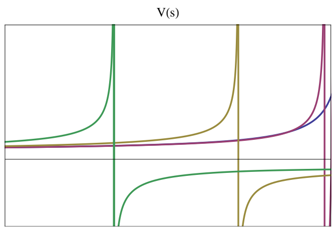

Figure 5.4: The behavior of the Schrödinger potential $V(s)$ for z_+ when k is negative. Such a potential has no zero-energy bound state. The potential is rescaled to fit on a finite range. As $|k|$ is lowered below k_{max} for which the potential is strictly positive, a triple pole appears which moves towards the horizon on the left (Fig A. The Blue,Red,Orange,Green curves are decreasing in $|k|$). The pole hits the horizon for $k=0$ and disappears. Fig B. shows the special case $m_{\texttt{eff}} = 0$ where two zeroes collide with two of the triple poles to form a single pole.

The exact solution of (5.4.39) with the above boundary conditions corresponding to poles in the CFT spectral function is difficult to find. By construction the system is however equivalent to a Schrödinger problem of finding a zero energy solution z_+ in the potential (5.4.40) and can be solved in the WKB approximation (see e.g. [27]). The WKB approximation holds when $|\partial_s V| \ll |V|^{3/2}$. Notice that this is more general than the background adiabacity limit $m_{\texttt{eff}} \gg 1, q_{\texttt{eff}} \gg 1$ with $\hat{\beta},\ \hat{m}$ fixed . Combining background adiabaticity with a scaling limit $k \gg 1, m_{\texttt{eff}} \gg 1, q_{\texttt{eff}} \gg 1$ with $c_0 k$ fixed and k is parametrically larger than $\hat{\mu}_{q_{\texttt{eff}}}$ one recovers the WKB potential solved in [53, 63]. As our aim is to study the the deviation away from the background adiabatic limit we will be more general and study the WKB limit of the potential itself, without direct constraints on $q_{\texttt{eff}}, m_{\texttt{eff}}$. And rather than testing the inequality $|\partial_s V| \ll |V|^{3/2}$ directly, we will rely on the rule of thumb that the WKB limit is justified when the number of nodes in the wave-function is large. We will therefore estimate the number n of bound states and use $n \gg 1$ as an empirical justification of our approach.[7] With this criterion we will be able to study the normalizable solutions to the Dirac equation/pole structure of the CFT spectral functions as a function of κ/L.

The potential is bounded both in the AdS boundary and at the horizon, and decreases towards intermediate values of r. We therefore have a standard WKB solution consisting of three regions:

- In the regions where $V > 0$, the solution decays exponentially:
$$z_+ = c_{1,2} V^{-1/4} \exp\left(\pm \int_{r_{1,2}}^{r} dr' \left[c_0 \sqrt{g^{ii} g_{rr}} \left(k + \hat{\mu}_{q_{\texttt{eff}}}\right) \sqrt{V} \right] \right). \quad (5.4.48)$$
Here $r_1,\ r_2$ are the turning points where $V(r_1) = 0 = V(r_2)$.

- In the region $r_1 < r < r_2$, i.e. $V < 0$, the solution is
$$z_+ = c_3 (-V)^{-1/4} \mathrm{Re}\left[\exp\left(i \int_{r_1}^{r} dr' [c_0 \sqrt{g^{ii} g_{rr}} \left(k + \hat{\mu}_{q_{\texttt{eff}}}\right) \sqrt{-V}] - i\pi/4 \right) \right], \quad (5.4.49)$$
with the constant phase $-i\pi/4$ originating in the connection formula at the turning point r_1.

Finding a WKB solution shows us that the peaks seen numerically are true poles in the spectral function. But it also allows us to estimate

[7] A large number of bound states n implies $|\partial_s V| \ll |V|^{3/2}$ if the potential has a single minimum, but as is well known there are systems, e.g. the harmonic oscillator, where the WKB approximation holds for small n as well.

the number of peaks that the numerical approach could not resolve. The WKB quantization condition

$$\int_{r_1}^{r_2} dr' \left[c_0 \sqrt{g^{ii} g_{rr}} (k + \hat{\mu}_{q_{\text{eff}}}) \sqrt{-V} \right] = \pi(n + 1/2) \tag{5.4.50}$$

counts the number of bound states with negative semi-definite energy. Note that n does not depend on the integral constant as there is also a factor $1/c_0$ in $\sqrt{-V}$. Since V depends on k, we will see that as we increase k this number decreases. The natural interpretation in the context of a bulk many-body Fermi system is that this establishes the ordering of the the filling of all the $\omega = 0$ momentum shells in the electron star. For a fixed k one counts the modes that have been previously occupied and, consistent with our earlier deduction, the lowest/highest k_F corresponds to the last/first occupied state. Though counterintuitive from a field theory perspective where normally $E \sim k_F$, this UV/IR correspondence is very natural from the AdS-bulk, if one thinks of the electron star as a trapped electron gas. The last occupied state should then be the outermost state from the center, but this state has the lowest effective chemical potential and hence lowest k_F.

Let us now show this explicitly by analyzing the potential and the bound states in the electron star and AdS-RN.

Electron star

The potential (5.4.41) for the electron star is given in Fig. 5.5 and the number of bound states as a function of k in Fig. 5.6. As stated the number of states decreases with increasing k, consistent with the analogy of the pole distribution of the spectral functions compared with AdS-RN. Moreover, we clearly see the significant increase in the number of states as we decrease κ/L thereby improving the adiabaticity of the background. This vividly illustrates that the adiabatic limit corresponds to a large number of constituents. As all numbers of states are far larger than one, the use of the WKB is justified.

The Reissner-Nordström case

For AdS-RN the Schrödinger analysis requires a separate discussion of the near horizon boundary conditions, which we present here for completeness

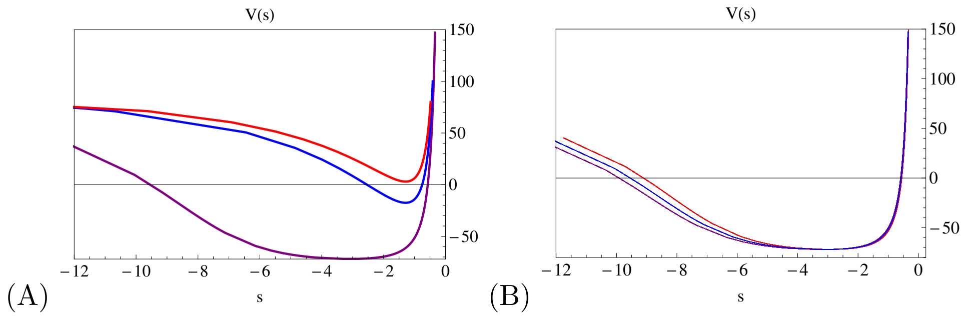

Figure 5.5: The Schrödinger potential $V(s)$ for the fermion component z_+ of in the ES background $\hat{m} = 0.36, z = 2, c_0 = 0.1$. Fig. A. shows the dependence on the momentum $k = 0.0185$ (Purple), $k = 5$ (Blue), $k = 10$ (Red) for $\kappa = 0.092$. Fig. B. shows the dependence on $\kappa = 0.086$ (Purple), $\kappa = 0.092$ (Blue), $\kappa = 0.1$ (Red) for $k = 0.0185$. Recall that $s = 0$ is the AdS boundary and $s = -\infty$ is the near-horizon region.

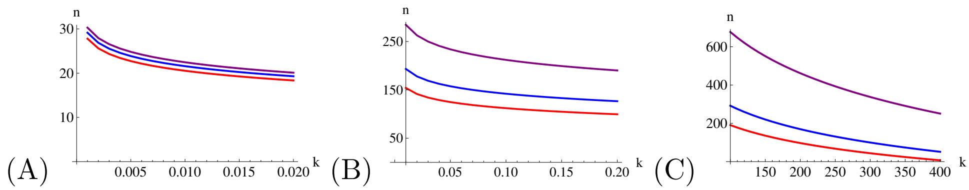

Figure 5.6: The WKB estimate of the number of bound states n as a function of the momentum k for $\kappa = 0.086$(Purple), 0.092(Blue), 0.1(Red) (Fig A.); for $\kappa = 0.001$(Purple), 0.002(Blue), 0.003(Red) (Fig B.) and for $\kappa = 10^{-5}$(Purple), 3×10^{-5}(Blue), 5×10^{-5}(Red) (Fig C.). Note the parametric increase in number of states as the adiabaticity of the background improves for smaller κ. Both figures are for the electron star background with $\hat{m} = 0.36, z = 2$. Since $n \gg 1$ in all cases, WKB gives a valid estimate.

and comparison. Part of this analysis is originally worked out in [27]. The

AdS-RN black hole with metric

$$ds^2 = L^2\left(-f(r)dt^2 + \frac{dr^2}{f(r)} + r^2(dx^2+dy^2)\right), \qquad (5.4.51)$$

$$f(r) = r^2\left(1+\frac{3}{r^4}-\frac{4}{r^3}\right), \qquad (5.4.52)$$

$$A = \mu\left(1-\frac{1}{r}\right)dt, \qquad (5.4.53)$$

has near horizon geometry $\mathrm{AdS}_2 \times \mathbb{R}^2$

$$ds^2 = -6(r-1)^2dt^2 + \frac{dr^2}{6(r-1)^2} + (dx^2+dy^2), \qquad (5.4.54)$$

$$A = \sqrt{3}\left(r-1\right)dt. \qquad (5.4.55)$$

A coordinate redefinition of r in eq. (5.4.43) to $r = (r_{AdS_2}-1)^{1/z}$ shows that this corresponds to a dynamical critical exponent $z=\infty$ and is outside the validity of the previous analysis.

Before we proceed, recall that the existence of $\mathrm{AdS}_2\times\mathbb{R}^2$ near-horizon region allows for a semi-analytic determination of the fermion spectral functions with the self-energy $\Sigma \sim \omega^{2\nu_{k_F}}$ controlled by the IR conformal dimension $\delta_k = 1/2+\nu_k$ with

$$\nu_k = \frac{1}{\sqrt{6}}\sqrt{m^2+k^2-\frac{q^2}{2}}\ . \qquad (5.4.56)$$

When ν_k is imaginary, which for $q^2 > 2m^2$ always happens for small k, the spectral function exhibits oscillatory behavior, but generically has finite weight at $\omega=0$. When ν_k is real, there are poles in the spectral functions at a finite number of different Fermi momenta k_F. The associated quasiparticles can characterize a non-FL ($\nu_{k_F}<1/2$), a marginal FL ($\nu_{k_F}=1/2$) or irregular FL ($\nu_{k_F}>1/2$) with linear dispersion but width $\Gamma \neq \omega^2$ [27].

The analytic form of the near-horizon metric allows us to solve exactly for the near horizon potential V in terms of $s = \frac{c_0}{\sqrt{6}}(k+q/\sqrt{2})\ln(r-1)+\ldots$. As noted in [27] one remarkably obtains that the near-horizon potential for $s\to-\infty$ is proportional to the self-energy exponent:

$$V(s) \simeq \frac{6}{c_0^2(k+q/\sqrt{2})^2}\nu_k^2 + \ldots. \qquad (5.4.57)$$

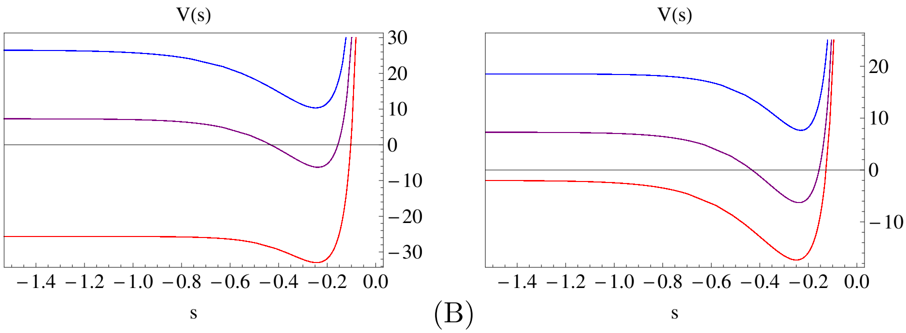

(A) (B)

Figure 5.7: The Schrödinger potential $V(s)$ for the fermion component z_+ of in the AdS-RN background $r_+ = 1, \mu = \sqrt{3}, g_F = 1, mL = 0.4, c_0 = 0.1$. Fig. A. shows the dependence on the momentum $k = 1$ (Red), $k = 2$ (Purple), $k = 3$ (Blue) for charge $q = 2.5$. Fig. B. shows the dependence on the charge q — analogous to κ in the ES background —. Shown are the values $q = 2$ (Blue), $q = 2.5$ (Purple), $q = 3$ (Red) for the momentum $k = 2$. In both figures the Red potentials correspond to the oscillatory region $\nu_k^2 < 0$, the Purple potentials show the generic shape that can support an $\omega = 0$ bound state, and the Blue potentials are strictly positive and no zero-energy bound state is present. Recall that $s = 0$ is the AdS boundary and $s = -\infty$ is the near-horizon region.

One immediately recognizes the oscillatory region $\nu_k^2 < 0$ of the spectral function as an $\omega = 0$ Schrödinger potential which is "free" at the horizon $s = -\infty$ (Fig. 5.7) and no bound state can form. Comparing with our previous results, we see that this oscillatory region is a distinct property of AdS-RN. For any Lifshitz near-horizon metric the potential is always positive-definite near the horizon and all $\omega = 0$ solutions will be bounded. (see also [53, 63]). As we increase k, ν_k^2 becomes positive, then the AdS-RN potential is also positive at the horizon and bound zero-energy states can form. Increasing k further, one reaches a maximal k_{max}, above which the potential is always positive and no zero-energy bound state exists anymore.

Because the near-horizon boundary conditions for AdS-RN differ from the general analysis, the possible singularity in the potential for $k < 0$ also requires a separate study. This is clearly intimately tied to the existence of an oscillatory regime in the spectral function, as the previous analysis does apply for $\nu_k^2 > 0$. The clearest way to understand what happens for $\nu_k^2 < 0$ is to analyze the potential explicitly. Again if $|k| > k_{max}$

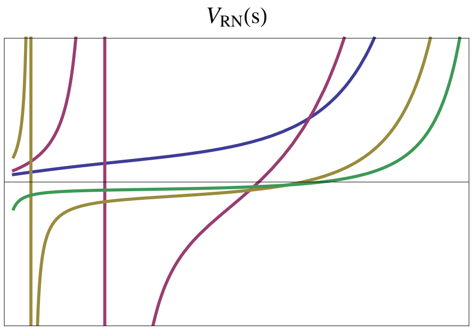

Figure 5.8: The qualitative behavior for negative k of the Schrödinger potential $V(s)$ for the fermion component z_+ of in the AdS-RN background $r_+ = 1, \mu = \sqrt{3}, g_F = 1, mL = 0.1$. The radial coordinate has been rescaled to a finite domain such that the full potential can be represented in the figure; on the right is the AdS boundary and left is the near-horizon region and the range is slightly extended beyond the true horizon, which is exactly at the short vertical line-segments on the right. Potentials are given for $q = 12/\sqrt{3}$, $k = -15$ (Blue) for which the potential is strictly positive, $k = -10$ (Red), $k = -7$ (Orange), which both have triple poles and the pole can be seen to move towards the horizon on the left as k decreases, and $k = -4$ (Green) which has no pole and a finite negative value at the horizon. The pole disappears for $|k| < q/\sqrt{2}$ leaving a regular bounded potential which can support zero-energy bound states.

the potential is strictly positive definite, and no zero-energy bound state exists. As we decrease the magnitude of $k < 0$, a triple pole will form near the boundary when $k = -\hat{\mu}_{q_{\mathtt{eff}}}(s)$, soon followed by a zero at $k = -\sqrt{\hat{\mu}_{q_{\mathtt{eff}}}(s)^2 - m_{\mathtt{ren}}(s)^2}$ (see Fig. 5.4). As we approach the horizon, in the general case where $\lim_{r\to 0} \hat{\mu}_{q_{\mathtt{eff}}} = h_\infty q_{\mathtt{eff}} r + \ldots$, this pole at $r_* = -k/(h_\infty q_{\mathtt{eff}})$ hits the horizon and disappears precisely when $k = 0$. In AdS-RN, however, where $\lim_{r\to 1} \hat{\mu}_{q_{\mathtt{eff}}} = \frac{q}{\sqrt{2}} + \frac{\sqrt{2}q}{3}(r-1) + \ldots$, the pole at $r_*^{RN} - 1 = \frac{3}{\sqrt{2}q}(k + \frac{q}{\sqrt{2}})$ hits the horizon and disappears at $k = -\frac{q}{\sqrt{2}}$. For negative values of k whose magnitude is less than $|k| < \frac{q}{\sqrt{2}}$, the potential is regular and bounded and can and does have zero-energy solutions. Fig. 5.4 shows this disappearance of the pole for the AdS-RN potential.

Counting solutions through WKB is also more complicated for AdS-RN. For $\mathcal{O}(1)$ values of q there are only few Fermi surfaces and the WKB

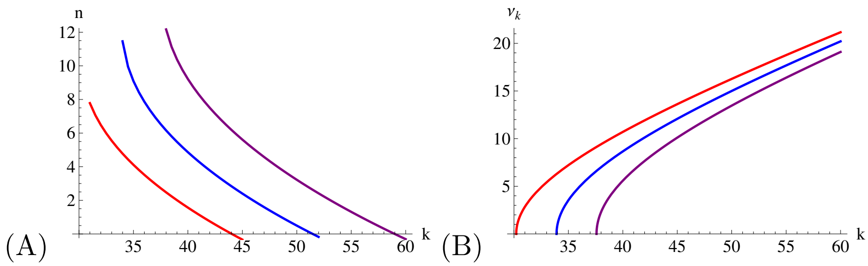

Figure 5.9: The WKB estimate of the number of bound states n in the AdS-RN Schrödinger potential for z_+ with $mL = 10$. The WKB approximation only applies to large values of the charge $q = 45$ (Red), $q = 50$ (Blue), $q = 55$ (Purple). Fig B. gives the associated values of the IR conformal dimension $\nu_k = \frac{1}{\sqrt{6}}\sqrt{m^2 + k^2 - \frac{q^2}{2}}$. Both figures are for the extremal AdS-RN background with $\mu = \sqrt{3}, r_+ = 1, g_F = 1$.

approximation does not apply. For large q it does, however. For completeness we show the results in Fig. 5.9.

5.5 Conclusion and Discussion

These electron star spectral function results answer two of the three questions raised in the introduction directly.

- They show explicitly how the fermion wavefunctions in their own gravitating potential well are ordered despite the fact that they all have strictly vanishing energy: In a fermionic version of the UV-IR correspondence they are ordered *inversely* in k, with the "lowest"/first occupied state having the highest k and the "highest"/last occupied state having the lowest k. With the qualitative AdS/CFT understanding that scale corresponds to distance away from the interior, one can intuitively picture this as literally filling geometrical shells of the electron star, with the outermost/highest/last shell at large radius corresponding to the wavefunction with lowest local chemical potential and hence lowest k.

- The decrease of the number of bound states — the number of occupied wavefunctions in the electron star — as we decrease $q_{\texttt{eff}} = \hat{\beta}^{1/4}\sqrt{\frac{\pi L}{\kappa}}$ for a fixed electron star background extrapolates naturally to a limit where the number of bound states is unity. This extrapolation pushes the solution beyond its adiabatic regime of validity. In principle we know what the correct description in this limit is: it is the AdS Dirac Hair solution constructed in [18]. The dependence of the number of bound states on κ/L therefore illustrates that the electron star and Dirac Hair solutions are two limiting cases of the gravitationally backreacted Fermi gas.

With this knowledge we can schematically classify the groundstate solutions of AdS Einstein-Maxwell gravity minimally coupled to charged fermions at finite charge density. For large mass mL in units of the constituent charge q, the only solution is a charged AdS-Reissner-Nördstrom black hole. For a low enough mass-to-charge ratio, the black hole becomes unstable and develops hair. If in addition the total charge density Q is of the order of the microscopic charge q this hairy solution is the Dirac Hair configuration constructed in [18], whereas in the limit of large total charge density Q one can make an adiabatic Thomas Fermi approximation and arrives a la Tolman-Oppenheimer-Volkov at an electron star (Fig. 5.10).

Translating this solution space through the AdS/CFT correspondence one reads off that in the dual strongly coupled field theory, one remains in the critical state if the ratio of the scaling dimension to the charge Δ/q is too large. For a small enough value of this ratio, the critical state is unstable and forms a novel scaleful groundstate. The generic condensed matter expectation of a unique Fermi liquid is realized if the total charge density is of the same order as the constituent charge. Following [53, 63] and [54, 97, 55] the state for $Q \gg q$ is some deconfined Fermi liquid.

The gravity description of either limit has some deficiencies, most notably the lack of an electron star wavefunction at infinity and the unnatural restriction to $Q = q$ for the Dirac Hair solution. A generic solution for $Q \geq q$ with wavefunction tails extending to infinity as the Dirac hair would be a more precise holographic dual to the strongly interacting large N Fermi system. Any CFT information can then be cleanly read off at the AdS boundary. A naive construction could be to superpose Dirac Hair onto the electron star; in principle one can achieve this solution by a next order Hartree-Fock or Local Density Approximation computation.

This best-of-both-worlds generic solution ought to be the true holographic dual of the strongly interacting Fermi ground state. If one is able to answer convincingly how this system circumvents the wisdom that the groundstate of an interacting many-body system of fermions is a generic

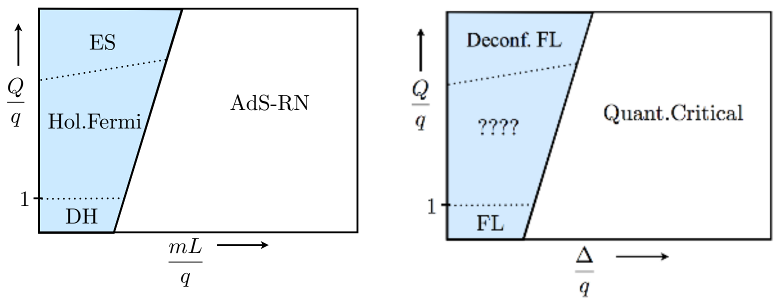

Figure 5.10: Schematic diagram of the different groundstate solutions of strongly coupled fermions implied by holography for fixed charge density Q. Here q is the constituent charge of the fermions and $mL \sim \Delta$ the mass/conformal scaling dimension of the fermionic operator. One has the gravitational electron star (ES)/Dirac Hair (DH) solution for large/small Q/q and small mL/q dual a deconfined Fermi liquid/regular Fermi liquid in the CFT. For $mL/q \sim \Delta/q$ large the groundstate remains the fermionic quantum critical state dual to AdS-RN.

single quasiparticle Landau Fermi liquid, then one would truly have found a finite density Fermi system that does not refer at any stage to an underlying perturbative Fermi gas.

Chapter 6

The phase diagram: electron stars with Dirac hair [83]

6.1 Introduction

The problem of fermionic quantum criticality has proven hard enough for the condensed matter physics to keep seeking new angles of attack. The main problem we face is that the energy scales vary by orders of magnitude between different phases. The macroscopic, measurable quantities emerge as a result of complex collective phenomena and are difficult to relate to the microscopic parameters of the system. An illustrative example present the heavy fermion materials [80] which still behave as Fermi liquids but with vastly (sometimes hundredfold) renormalized effective masses. On the other hand, the strange metal phase of cuprate-based superconducting materials [118], while remarkably stable over a range of doping concentrations, shows distinctly non-Fermi liquid behavior. Holography (AdS/CFT correspondence) [81, 38, 114] has become a well-established treatment of strongly correlated electrons by now, but it still has its perplexities and shortcomings. Since the existence of holographic duals to Fermi surfaces has been shown in [79, 17], the next logical step is to achieve the understanding of the phase diagram: what are the stable phases of matter as predicted by holography, how do they transform into each other and, ultimately, can we make predictions on quantum critical behavior of real-world materials based on AdS/CFT.

The condensed matter problems listed all converge toward a single main question in field-theoretical language. It is the classification of ground states of interacting fermions at finite density. In this paper we attempt to understand these ground states in the framework of AdS/CFT, the duality between the strongly coupled field theories in d dimensions and a string configuration in $d+1$ dimension. The classification of ground states now translates into the following question: classify the stable asymptotically AdS geometries with charged fermionic matter in a black hole background. Most of the work done so far on AdS/CFT for strongly interacting fermions relies on bottom-up toy gravity models and does not employ a top-down string action. We stay with the same reasoning and so will work with Einstein gravity in $3+1$ dimensions. We note, however, that a top-down construction of holographic fermions has been derived in [35]. While expectedly more complicated, it confirms the robustness of some features seen in 3+1-dimensional classical gravity, such as the emergent scale invariance of the field theory propagators in the IR.

So far three distinct models aiming at capturing the stable phases of holographic fermionic matter have appeared: the electron star [51], Dirac hair [18] and a confined Fermi liquid model [96]. The electron star is essentially a charged fermion rewriting of the well-known Oppenheimer-Volkov equations for a neutron star in AdS background. The bulk is thus modeled as a semiclassical fluid. The mystery is its field theory dual: it is a hierarchically ordered multiplet of fermionic liquids with stable quasiparticles [53]. On the other end of the spectrum is Dirac hair, which reduces the bulk fermion matter to a single quantum-mechanical wave function. As a consequence the field theory dual is a single Fermi liquid, however its gravitational consistency properties are not yet fully understood. In [19] we have shown that Dirac hair and electron star can be regarded as the extreme points of a continuum of models, dialing from deep quantum – a single occupied state — to a classical regime — a very large occupation number — in the bulk. They correspond to two extreme "phases" in the field theory phase diagram: a multiplet of a very large number of Fermi liquids and a single Fermi liquid. The confined Fermi liquid model [96] introduces confinement through modifying the bulk geometry and solves for quantum-mechanical wave functions adding them up to compute the full bulk density. This latter step is more general then the single-particle approach of [18] and it naturally extends a Dirac hair state with single Fermi surface to a state with multiple Fermi surfaces. Our main motivation is to construct a complementary model that extends from the other end — the classical regime — down to a state with few Fermi surfaces.

We aim for a system which is general enough to encompass the middle ground between extreme quantum and extreme classical regimes in the original deconfined setup.

In addition to simply improving the mathematical treatment of the many-body-bulk fermion system, the guiding principle in our analysis will be to rest on the advantages and disadvantages of the current models. On the one hand, the Dirac hair is a fully quantum-mechanical model which shows its strength in particular near the boundary (the ultraviolet of the field theory) but becomes worse in the interior, i.e.close to the horizon (the infrared of the field theory) where density is high and the resulting state of matter cannot be well described by a single-particle wave function. On the other hand, the electron star yields a very robust description of high-density matter in the interior but its sharp boundary at some radius r_c means that it has zero density at the boundary of the AdS space. This is a crucial drawback as the holographic dictionary *defines* densities and thermodynamic quantities on the CFT side in terms of the asymptotics of the bulk fields at infinity. It is thus obvious that the physically interesting model lies somewhere in-between the two approaches. This is why what we try to achieve will essentially be an "electron star with Dirac hair".

We will reproduce the results of the electron star/Dirac hair models in the limit of infinitely large/small fermion charge but also get a look at what is in-between. Importantly, our model incorporates the quantum corrections to the leading WKB approximation for the bulk electron density. Our system therefore does not terminate at some finite radius like the electron star, allowing direct calculation of the CFT quantities at the boundary. This will allow us to sketch the phase diagram as a whole. We do not aim at quantitative accuracy in this paper: in a follow-up publication we will present a more accurate calculation making use of density functional formalism for interacting fermions in the bulk. Here, we use a simple WKB formalism with quantum tails which adds quantum corrections to the Thomas-Fermi (fluid) approximation by taking into account finite level spacing. While not highly accurate, it is able to penetrate deep in the quantum regime thus giving at least a qualitative look in the intermediate regime. In particular, we are able to detect the instability of the RN black hole leading to its discharge and formation of finite density phase in the bulk. The precursor os this instability is known as oscillatory or log-oscillatory region [27, 50, 63]. All calculations are self-consistent and include the backreaction on the gauge field by fermions and on the geometry by both.

The physical task of understanding the various states and their instabilities is clearly still ahead of us. The obvious question to ask is, what is the nature of the phase transitions and to what degree is it universal? A partial answer is provided by our finding that the finite density phases with fermionic quasiparticles at high enough temperatures always exhibit a first order transition into the zero density phase. Intuitively, this can be interpreted as a universal van der Waals liquid-gas transition. In the fluid limit however, returning to the semiclassical description, the transition becomes continuous as predicted in [52]. At zero temperature, we detect a continuous transition whereby the AdS-RN system develops finite bulk density of fermions, driving the instability of the black hole toward a finite density phase, which in the fluid limit is just the electron star. It is here that our method is especially useful as it allows us to probe the "electron star at birth", i.e. to observe the instability of the black hole when only few fermion levels are filled. The instability mechanism was discussed in [50, 63] in the framework of electron star. We again find that finite level spacing matters and the transition is shifted compared to the electron star model. Finally, we find also a crossover between the low density (Dirac hair) and high density (electron star) regime. The crossover is not a transition and thus there is no clear transition point. However, looking at the two extremes, with $N \sim 1$ levels and with $N \sim \infty$ levels we will see that they bring a characteristic difference in the behavior of the system in field theory.

The nature of the zero temperature phase transition and the crossover between the finite density phases is complex and we will not be able to offer a complete description of these phenomena. Hopefully any gain of understanding in these questions will give us some insight into the crucial question: *are there any stable phases of fermion matter that cannot be adiabatically continued to a Fermi gas*?

The outline of the paper is as follows. In the Section II we describe the field content and geometry of our gravity setup, an Einstein-Maxwell-Dirac system in $3+1$ dimension, and lay out the single-particle solution to the bulk Dirac equation. In Section III we start from that solution and apply the WKB approximation to derive the Dirac wave function of a many-particle state in the bulk. Afterwards we calculate density and pressure of the bulk fermions – the semiclassical estimate and the quantum corrections, thus arriving at the equation of state. Section IV contains the solution of the self-consistent set of equations for fermions, gauge field and the metric. There we also describe our numerical procedure. Section V is the core of the matter, where we analyze thermodynamics and spectra of the field theory side and identify different phases as a function of the three parameters of the system: chemical potential μ, fermion charge e and conformal dimension Δ. Section VI sums up the conclusions and offers some insight into possible broader consequences of our work and into future steps.

6.2 Holographic fermions in charged background

We wish to construct the gravity dual to a field theory at finite fermion density. Dimensionality is not of crucial importance at this stage. While some interesting condensed matter systems live in $2+1$ dimensions, the heavy fermion materials are for instance all three-dimensional. We will specialize to $2+1$-dimensional conformal systems of electron matter, dual to AdS_4 gravities. We consider a Dirac fermion of charge e and mass m in an electrically charged gravitational background with asymptotic AdS geometry. Adopting the AdS radius as the unit length, we can rescale the metric $g_{\mu\nu}$ and the gauge field A_μ:

$$g_{\mu\nu} \mapsto g_{\mu\nu} L^2, \quad A_\mu \mapsto L A_\mu. \tag{6.2.1}$$

In these units, the action of the system is:

$$S = \int d^4x \sqrt{-g} \left[\frac{1}{2\kappa^2} L^2 (R+6) + \frac{L^2}{4} F^2 + L^3 \mathcal{L}_f \right] \tag{6.2.2}$$

where κ is the gravitational coupling and $F_{\mu\nu} = \partial_\mu A_\nu - \partial_\nu A_\mu$ is the field strength tensor. The fermionic Lagrangian is:

$$\mathcal{L}_f = \bar{\Psi} \left[e^\mu_A \Gamma^A \left(\partial_\mu + \frac{1}{4} \omega_\mu^{BC} \Gamma_{BC} - ieLA_\mu \right) - mL \right] \Psi \tag{6.2.3}$$

where $\bar{\Psi} = i\Psi^\dagger \Gamma^0$, e^μ_A is the vierbein and ω_μ^{AB} is the spin connection. Since the magnetic field is absent, the $U(1)$ gauge field is simply $A = \Phi dt$. We parametrize our (spherically symmetric asymptotically AdS) metric in four spacetime dimensions as:

$$ds^2 = \frac{f(z)e^{-h(z)}}{z^2} dt^2 - \frac{1}{z^2} \left(dx^2 + dy^2 \right) - \frac{1}{f(z) z^2} dz^2 \tag{6.2.4}$$

The radial coordinate is defined for $z \geq 0$, where $z = 0$ is the location of AdS boundary. All coordinates are dimensionless, according to (6.2.1). This form of the metric is sufficiently general to model any configuration of static and isotropic charged matter. Development of a horizon at finite z is signified by the appearance of a zero of the function $f(z)$, $f(z_H) = 0$. From now on we will set $L = 1$.

We will now proceed to derive the equation of motion for the Dirac field. From (6.2.3), the equation reads:

$$e^{\mu}_{A}\Gamma^{A}\left(\partial_{\mu} + \frac{1}{4}\omega_{\mu}^{BC}\Gamma_{BC} - ieA_{\mu}\right)\Psi = m\Psi. \tag{6.2.5}$$

In the metric (6.2.4) we can always eliminate the spin connection [79] by transforming:

$$\Psi \mapsto (gg^{zz})^{-\frac{1}{4}}\Psi = \frac{e^{h(z)/4}z^{3/2}}{f(z)^{1/4}}\Psi \equiv a^{-1}(z)\Psi \tag{6.2.6}$$

After decomposing into radial projections $\Psi_{\pm}$, defined as:

$$\Psi_{\pm} = \frac{1}{2}\left(1 \pm \Gamma^{Z}\right)\Psi, \tag{6.2.7}$$

in a basis where $\Gamma^{Z} = \mathrm{diag}(1, 1, -1, -1)$, the Dirac equation in matrix form becomes:

$$\sqrt{f}\partial_z \begin{pmatrix}\Psi_+\\ \Psi_-\end{pmatrix} = \hat{D}\begin{pmatrix}\Psi_+\\ \Psi_-\end{pmatrix}\ . \tag{6.2.8}$$

Here the matrix $\hat{D}$ is the differential operator along the transverse coordinates (x, y) and time, which we will specify shortly.

We will give the solution of the Dirac equation in the cylindrical coordinates, which will serve as the input to the calculation of bulk fermion density in WKB approximation. Introducing the cylindrical coordinates as $(t, x, y, z) \mapsto (t, \rho, \phi, z)$ we make the separation ansatz:

$$\begin{pmatrix}\Psi_+(z,\rho,\phi)\\ \Psi_-(z,\rho,\phi)\end{pmatrix} = \int \frac{d\omega}{2\pi}\begin{pmatrix}F(z)K_1(\rho,\phi)\\ -G(z)K_2(\rho,\phi)\end{pmatrix}e^{-i\omega t} \tag{6.2.9}$$

where, unlike previous approaches, the F, G are are taken as scalars and the modes $K_{1,2}$ are in-plane spinors. The Dirac equation then takes the form:

$$\begin{pmatrix}\partial_z FK_1\\ -\partial_z GK_2\end{pmatrix} = \begin{pmatrix}-\hat{\partial}/\sqrt{f(z)} & \left(\tilde{E}\left(\omega,z\right) + \tilde{M}\left(z\right)\right)\sigma_3\\ \left(\tilde{E}\left(\omega,z\right) - \tilde{M}\left(z\right)\right)\sigma_3 & -\hat{\partial}/\sqrt{f(z)}\end{pmatrix}\begin{pmatrix}FK_1\\ -GK_2\end{pmatrix} \tag{6.2.10}$$

We recognize the matrix at the right hand side as $\hat{D}/\sqrt{f}$. The terms $\tilde{E}$ and $\tilde{M}$ have the meaning of local energy and mass terms, respectively:

$$\tilde{E}(z) = -\frac{e^{h(z)/2}}{f(z)}(\omega + q\Phi(z)), \ \tilde{M}(z) = \frac{m}{z\sqrt{f(z)}}. \tag{6.2.11}$$

The in-plane operator $\hat{\partial}$ acts on each in-plane spinor as:

$$\hat{\partial} = \begin{pmatrix} 0 & i\bar{\partial} \\ -i\partial & 0 \end{pmatrix} \tag{6.2.12}$$

with $\partial \equiv e^{i\phi}(\partial_\rho + \partial_\phi/\rho)$. To maintain the separation of variables in (6.2.10), we require $\hat{\partial}K_i = \lambda_i K_i$, where $|\lambda_i|^2$ corresponds the momentum-squared of the in-plane motion of the particle. The solution of the cylindrical eigenvalue problem for each in-plane spinor K_i gives:

$$K_i(\rho, \phi) = \begin{pmatrix} J_{l-1/2}(\lambda_i \rho) e^{i(l-1/2)\phi} \\ J_{l+1/2}(\lambda_i \rho) e^{-i(l+1/2)\phi} \end{pmatrix}. \tag{6.2.13}$$

Of the two linearly independent solutions, only the Bessel function of the first kind $J(x)$ is chosen in order to satisfy the normalizability condition of the wave function at $\rho \longrightarrow 0$ (for linear independent Bessel function Y this condition is not fulfilled). Remembering that $|\lambda_i|^2$ is the squared in-plane momentum, the physical requirement that this momentum be the same for both radial projections translates into the condition $|\lambda_2| = |\lambda_1|$. Consistency of the separation of variables then shows us that $K_2 = \sigma_3 K_1$ and thus $\lambda_1 = -\lambda_2 = k$ and the reduced radial equation becomes:

$$\begin{pmatrix} \partial_z F \\ \partial_z G \end{pmatrix} = \begin{pmatrix} -\tilde{k} & \tilde{E} + \tilde{M} \\ \tilde{M} - \tilde{E} & \tilde{k} \end{pmatrix} \begin{pmatrix} F \\ G \end{pmatrix} \tag{6.2.14}$$

with $\tilde{k} = k/\sqrt{f}$ (let us note that Eq. (6.2.14) is for the pair (F, G), whereas the initial equation (6.2.10) is written for the bispinor $(FK_1, -GK_2)$). For the WKB calculation of the density, it is useful to remind that the wave function Ψ in Eq. (6.2.9) has two quantum numbers corresponding to the motion in the (ρ, ϕ) plane: λ, l (or equivalently the momenta k_x, k_y in Cartesian coordinates). The radial eigenfunctions in z-direction will provide a third quantum number n.

6.3 Equation of state of the bulk fermion matter

In this section we construct the model of the bulk fermions in an improved semiclassical approximation. In the next section we will complement it with the equations for the Einstein-Maxwell sector. We will start by estimating the bulk fermion density in the semiclassical case. The Dirac equation is solved in the WKB approximation, and the density is computed assuming a large number of energy levels. This is in the spirit of WKB approximation. However, we sum the exact quantum-mechanical solutions for the wave functions rather than immediately taking the fluid limit. In this respect our method goes beyond Thomas-Fermi and in fact corresponds to calculating the vacuum density in the Hartree approximation. The resulting estimate has sharp bounds along the radial direction, at some points z_1 and z_2 ($0 < z_1 < z_2 \leq 1$), similar to electron star [51] and its finite-temperature generalization [52]. As we have already argued, sharp bounds fail to capture several essential phenomena on the CFT side. To overcome this shortcoming, we will improve on the WKB approximation and continue our bulk density profile outside the classical region by making use of Airy corrections to WKB in the interior, and the Dirac hair formalism near the boundary. The reason for the latter is that Airy or decaying WKB approximations rapidly fail beyond the naive exterior sharp edge. Compared to other models of holographic fermions at finite density this quantum improvement on the semiclassical WKB limit bridges the gap between the all-classical electron star [51] and single-particle quantum mechanical calculation of Dirac hair [18].

6.3.1 WKB hierarchy and semiclassical calculation of the density

In the framework of WKB calculations, the first task is to construct the effective potential as a functional of the induced charge density $n(z)$. Physically, the origin of the induced charge in our model is the pair production in the strong electromagnetic field of the black hole. To remind the reader, a (negatively) charged black hole in AdS space is unstable at low temperatures, and spontaneously discharges the vacuum [60]. This means that there will be a non-zero net density of electrons n. Within the semiclassical approximation it is consistent to calculate n as density of non-interacting electrons. We will thus employ the semiclassical gas model and add up all possible states enumerated by good quantum numbers. For this we choose the set (λ, l, n).

We now give the algorithm for the WKB expansion of the wave function for Dirac equation, adopted from [113]. Even though every single step is elementary, altogether it seems to be less well known than its Schrödinger equivalent. We consider the Dirac equation in the form (6.2.8) and introduce the usual WKB phase expansion for it:

$$\Psi(z) = e^{\int_{z_0}^{z} dz y(z)\sqrt{f(z)}}\chi(z) \tag{6.3.15}$$

with the spinor part $\chi(z)$. The phase $y(z)$ can be expressed as the semi-classical expansion in $\hbar$ [1]

$$y(z) = \left(y_{-1}(z) + y_0(z) + y_1(z) + \ldots\right). \tag{6.3.16}$$

The equations for the perturbative corrections now follow from (6.3.15-6.3.16):

$$\begin{aligned}
\hat{D}\chi_0 &= y_{-1}\chi_0, && (6.3.17)\\
\hat{D}\chi_1 &= y_{-1}\chi_1 + y_0\chi_0 + \sqrt{f}\partial_z\chi_0, && (6.3.18)\\
&\ldots \\
\hat{D}\chi_n &= y_{-1}\chi_n + \sqrt{f}\partial_z\chi_{n-1} + \sum_{i=0}^{n-1} y_{n-i-1}\chi_i. && (6.3.19)
\end{aligned}$$

Notice in particular that y_{-1}/χ_0 is an eigenvalue/eigenvector of $\hat{D}$. In our case the matrix $\hat{D}$ has rank two, so there are two eigenvalues/eigenvectors for y_{-1}/χ_0: $y_{-1}^{\pm}$ and $\chi_0^{\pm}$. To find the first order correction to the phase of the wave function y_0, we multiply (6.3.18) from the left by the left eigenvalue $\tilde{\chi}_0^{\pm}$ of the matrix $\hat{D}$ ($\hat{D}$ is in general not symmetric, so the right and left eigenvalues are different):

$$y_0 = -\frac{(\partial_z\chi_0^{\pm}, \tilde{\chi}_0^{\pm})}{(\tilde{\chi}_0^{\pm}, \chi_0^{\pm})}. \tag{6.3.20}$$

so we can now construct the usual WKB solution of the form $\Psi_{\pm} = e^{i\theta_{\pm}}/\sqrt{q}$, where q is the WKB momentum and $\theta_{\pm}$ the phase. The term y_0 is just the first order correction to $\theta_{\pm}$.

[1] From the very beginning we put $\hbar = 1$. However, to elucidate the semi-classical nature of the expansion we give it here with explicit $\hbar$. Dirac equation becomes $\hbar\sqrt{f}\partial_z\hat{\Psi} = \hat{D}\hat{\Psi}$, where $\hat{\Psi} = (\Psi_+, \Psi_-)$, yielding the expansion $y(z) = \hbar^{-1}\left(y_{-1}(z) + \hbar y_0(z) + \hbar^2 y_1(z) + \ldots\right)$.

Finally, let us recall the applicability criterion of the WKB calculation. It is known that WKB approximation fails in the vicinity of turning points. The condition of applicability comes from comparing leading and the next to leading term in the expansion (6.3.16):

$$\frac{y_0(z)}{y_{-1}(z)} \ll 1. \tag{6.3.21}$$

In terms of $\tilde{E}(z)$ and $\tilde{M}(z)$ introduced in Eq. (6.2.11) it gives at $k = 0$:

$$\frac{\tilde{M}(z)\partial_z \tilde{E}(z) - \tilde{E}(z)\partial_z \tilde{M}(z)}{\tilde{E}(z)(\tilde{E}(z) - \tilde{M}(z))} \ll 1. \tag{6.3.22}$$

We will use this expression later on to estimate the point where we need to replace the WKB density and pressure with their full quantum estimates.

WKB wave function

According to (6.3.17), the leading effective WKB momentum for the motion in z direction $q \equiv |y_{-1}^{\pm}|$ is:

$$q^2(z) = \tilde{E}^2(z) - \tilde{M}^2(z) - \tilde{k}^2(z). \tag{6.3.23}$$

The wave function in radial direction, $\Psi = (F, -G)$, is given by the superposition of two linear independent solutions

$$\Psi(z) = C_+ \chi_+(z) e^{i\theta(z)} + C_- \chi_-(z) e^{-i\theta(z)}, \tag{6.3.24}$$

with the phase determined by

$$\theta(z) = \int^z \left(q(z') + \delta\theta(z')\right) dz' \tag{6.3.25}$$

$$\delta\theta(z) = \int^z \frac{\tilde{k}\partial_z \tilde{k} - q\partial_z q + \left(\tilde{E} - \tilde{M}\right)\left(\partial_z \tilde{E} + \partial_z \tilde{M}\right)}{2\tilde{k}q} dz. \tag{6.3.26}$$

The constants C_+ and C_- are related by invoking the textbook boundary conditions for the behavior of WKB wave function at the boundary of the classically allowed region ($q^2(z) > 0$) and the classically forbidden region

($q^2(z) < 0$). The wave function in the classically allowed then reads:

$$\Psi(z) = \frac{C}{\sqrt{q(z)}} \begin{pmatrix} \sqrt{\tilde{E}(z)+\tilde{M}(z)}\sin\left(\theta(z)-\delta\theta(z)\right) \\ \sqrt{\tilde{E}(z)-\tilde{M}(z)}\sin\theta\left(z\right) \end{pmatrix}, \quad (6.3.27)$$

$$\delta\theta(z) = \mathrm{ArcSin}\frac{q(z)}{\sqrt{\tilde{E}^2(z)-\tilde{M}^2(z)}}, \quad (6.3.28)$$

and C is the only remaining undetermined normalization constant. For the classically forbidden region we will use a different wave function, to be described in the subsequent subsections. Integrating the probability density over all coordinates in classically allowed region (z_1, z_2) gives the normalization condition:

$$C^2 \int_{z_1}^{z_2} dz \frac{\sqrt{g_{3d}(z)}}{a(z)^2} \int \rho d\rho \int d\phi C_{2d}^2 \Psi_{nl\lambda}(z,\rho,\phi)\Psi^\dagger_{n'l'\lambda'}(z,\rho,\phi) = 1. \quad (6.3.29)$$

The metric factor is $g_{3d}(z) = g(z)g^{tt}(z)$, and $a(z)$ is the conversion factor from (6.2.6). In the left-hand side of the equality we took into account the normalization of the continuous spectrum in the (ρ, ϕ) plane. The integration over ϕ is trivial. The orthogonality relation for Bessel functions (which encapsulates the (ρ, ϕ) solution) gives the definition of C_{2d}^2:

$$C_{2d}^{-2} \int_0^\infty J(\lambda\rho)J(\lambda'\rho)\rho d\rho = \frac{\delta(\lambda-\lambda')}{\lambda} \quad (6.3.30)$$

and it allows us to express the normalization constant as:

$$C = \left(4\pi \int dz \frac{\sqrt{g^{tt}}}{\sqrt{g^{zz}}} \frac{\tilde{E}(z)}{q(z)}\right)^{-1/2}, \quad (6.3.31)$$

where a factor of 2π comes from the integration over ϕ and an additional factor of 2 from the summation over the full four-component wave function, i.e. bispinor (each spinor gives $\tilde{E}(z)/q(z)$ after averaging over the fast oscillating phase θ). This completes the derivation of WKB wave function and allows us to compute the density.

WKB density

The key input for WKB approximation is the self-consistent bulk electron density $n(z)$. As in [113] we find the total density by summing single-particle wave functions in the classically allowed region. The WKB wave function is characterized by the quantum numbers (λ, l, n) with λ being the linear momentum in the $x-y$ plane, l – the orbital momentum in the $x-y$ plane and n – the energy level of the central motion in the potential well along z direction. The bulk density can be expressed as the sum over the cylindrical shells of the bulk Fermi surface. This suggests to work in the cylindrical geometry as the natural choice (remember that we use the $SO(2)$ invariant in-plane spinors). Each shell satisfies the Luttinger theorem in the transverse $(x-y)$ direction and so the density carried by each shell $n_{xy}(z)$ can easily be found. We can then sum over all shells to arrive at the final answer which reads simply $\int dz n_z(z) n_{xy}(z)$. A similar qualitative logic for summing the Luttinger densities in the $x-y$ plane was used also in [96] although the model used in that paper is overall very different.

Let us start by noticing that the end points of the classically allowed region determine the limits of summation over n and λ: $q^2(\omega_n, \lambda) \geq 0$. Thus, the density in the WKB region is:

$$n(z) = \frac{1}{a(z)^2} \sum_{l=0}^{\infty} \int_0^{2\pi} d\phi \sum_{n:q^2(\omega_n,\lambda)\geq 0} \int_0^{\lambda_0} \lambda d\lambda \int_0^{\infty} d\rho \rho C_{2d}^2 |\Psi(z,\rho,\phi)|^2, \tag{6.3.32}$$

where $\lambda_0 = \sqrt{f(z)(\tilde{E}^2(\omega,z) - \tilde{M}^2(z))}$. The limit of the sum over the level number n is determined by the requirement that WKB momentum be positive; in other words, we sum over occupied level inside the potential well only. The sum over the orbital quantum number l extends to infinity as the (x,y) plane is homogenous and the orbital number does not couple to the non-trivial dynamics along the radial direction. For large occupation numbers the normalization condition (6.3.31) and the (local) Bohr-Sommerfeld quantization rule ($\int dz \sqrt{q(z)} = N\pi$) then give:

$$C_n = \left(\frac{1}{4\pi^2} \frac{\partial \omega_n}{\partial n} \right)^{1/2}, \text{ for } q(z) \gg \delta\theta(z), \ z \approx 1. \tag{6.3.33}$$

Now we turn the summation over the quantum number n into the integration over energy and obtain for the *bulk* electron density (here we also performed the integration over ρ using the explicit expression for the wave function (6.2.10) and the normalization condition (6.3.30) for the Bessel functions):

$$n(z) = \frac{2}{a(z)^2} \sum_{l=0}^{\infty} \int_0^{2\pi} d\phi \int_0^{\sqrt{f(z)(\tilde{E}^2(\omega,z)-\tilde{M}^2(z))}} d\lambda\lambda \int_0^{\mu_{loc}} d\omega \frac{\tilde{E}(\omega,z)}{4\pi^2 q(\omega,\lambda,z)}. \tag{6.3.34}$$

After performing first integral over ω and then over λ we get[2]:

$$n(z) = z^3 \frac{p_{max}^3(z) f^{3/2}(z)}{3\pi^2} \tag{6.3.35}$$

with p_{max} determined by

$$p_{max}^2 = \tilde{E}^2(0,z) - \tilde{M}^2(z). \tag{6.3.36}$$

Notice that this result corresponds with common knowledge on the density of electron star [51].

6.3.2 Airy correction to semiclassical density

The semiclassical density profile has sharp cutoffs in the classically forbidden regions, that is, for $p_{max}^2 < 0$, i.e. $\tilde{E}(z) < \tilde{M}(z)$ (Fig. 6.1, dashed curves). Generically, there will be such two turning points, z_* and z_{**}, so that $0 < z_* < z_{**} < z_H$ where $z_H = \infty$ in pure AdS or equals the horizon radius at finite temperature. The semiclassical density is only nonzero for $z_* < z < z_{**}$. Leaving out the quantum "tails" outside this region misses even some qualitative features of the system, as we have discussed in the introduction. Moreover, the WKB approximation ceases to be valid close to the turning points (Eq. 6.3.22), at some $z_{1,2}$ ($0 < z_* < z_1 < z_2 < z_{**} < z_H$). We thus account for the quantum corrections for $z < z_1$ and $z > z_2$. We first treat the latter case, i.e. the quantum corrections in the near-horizon IR region.

To this end it is convenient to rewrite the Dirac equation in the Schrödinger (second order) form for the Ψ_+ component. Following the

[2] The given result for n can be compared to the charge density in the electron star limit given in [53]. The metric functions used there are related to ours as $f \mapsto fe^{-h}/z^2$ and $g \mapsto 1/fz^2$, where our metric functions are on the right hand side. Likewise, our definition of p_{max} is related to k_F of [53] as $p_{max} = k_F/\sqrt{f}$. Now the *total* bulk charge is expressed in [53] as $Q = \int dz \tilde{n}_e(z)$ where $\tilde{n}_e(z) \sim n(z)e^{h/2}$. In our conventions $Q = \int dz\sqrt{-g}g^{zz}g^{tt}n = \int dz n(z)e^{h/2}$ thus giving the same result as in [53].

textbook, the lowest order correction to the WKB solution is obtained by expanding the potential,

$$V_{eff}(z) = \tilde{E}^2(z) - \tilde{M}^2(z) - 3\left(\partial_z \log\left(\tilde{E}(z) + \tilde{M}(z)\right)\right)^2 + \frac{1}{2}\frac{\partial_{zz}(\tilde{E}(z) + \tilde{M}(z))}{\tilde{E}(z) + \tilde{M}(z)}, \tag{6.3.37}$$

in the vicinity of the turning point. Naively the logical extension of our formalism into the classically forbidden region would be to solve the Dirac equation or the corresponding Schrödinger equation in WKB form with imaginary WKB momentum. The result would be a set of exponentially decaying wave functions. This is, however, not the optimal approach. Firstly, the summation of all exponentially decaying wave functions would be an overkill as the contributions of all but the highest amplitude exponential correction are negligible and do not have a measurable influence on the result. Secondly, the summation of wave functions with imaginary WKB momenta turns out to be much more difficult in practice. We thus perform the series expansion of the potential (6.3.37)around $z = z_2$ as our approximation scheme. The lowest order (linear) term in the expansion of the potential yields a solution in terms of an Airy function which coincides with the WKB solution as we approach the turning point, i.e. for $z = z_2 - 0$.

In principle, also for Airy corrections such a continuation should be made for each of the wave functions (6.3.24), and the corrections then should be summed up. However, the Airy corrections for excited levels are also exponentially suppressed outside the classically allowed region. It is therefore a good approximation to only match the squared module of one single, suitably chosen, Airy function to the total WKB density. This should be the solution at the Fermi level $\omega = 0$. Exponentially small corrections are in any case beyond the scope of a Hartree-based method and require a density functional approach.

We first expand the potential V_{eff} in $z - z_{**}$, where z_{**} is the (second) turning point, i. e. $q(z_{**}) = 0$. The resulting second-order equation for Ψ_+ is schematically of the form:

$$\left(\partial_{zz} + \left(P_0 + P_1\left(z - z_{**}\right)\right)\partial_z + Q_0 + Q_1\left(z - z_{**}\right)\right)\Psi_+ = 0. \tag{6.3.38}$$

We transform to a Schrödinger-type equation (without a first derivative term) but consistently keep only linear correction in the potential, giving the equation:

$$\left(\partial_{zz} + Q_0 + (Q_1 - 2P_0)(z - z_{**})\right)\Psi_+ = 0 \tag{6.3.39}$$

with

$$
\begin{aligned}
Q_0 &= \tilde{k}\frac{\partial_z\tilde{E}+\partial_z\tilde{M}}{\tilde{E}+\tilde{M}} - \partial_z\tilde{k}|_{z=z_{**}} \\
Q_1 &= 2\tilde{M}\partial_z\tilde{M} + 2\tilde{k}\partial_z\tilde{k} - 2\tilde{E}\partial_z\tilde{E} + \frac{\partial_z\tilde{E}B+\partial_z\tilde{M}}{(\tilde{E}+\tilde{M})^2}\Big[(\tilde{E}+\tilde{M})\partial_z\tilde{k} - (\partial_z\tilde{E}+\partial_z\tilde{M})\tilde{k}\Big] \\
P_0 &= -\frac{\partial_z E+\partial_z\tilde{M}}{\tilde{E}+\tilde{M}}|_{z=z_{**}}
\end{aligned}
\tag{6.3.40}
$$

The decaying normalizable solution to the above equation is (non-normalizable solution would imply instability of the interior):

$$
\Psi_+(z) = \mathcal{N}\mathrm{Ai}\left(-\frac{(2P_0-Q_1)(z-z_{**})}{(2P_0-Q_1)^{2/3}}\right) \tag{6.3.41}
$$

where $\mathcal{N}$ is the normalization constant. There is a similar equation for Ψ_- with the same normalization $\mathcal{N}$ for consistency with the first order Dirac equation. The density is now simply

$$
n^{IR}(z) = |\Psi_+(z)|^2 + |\Psi_-(z)|^2. \tag{6.3.42}
$$

where in our approximation the only contribution comes from the single wavefunction with $\omega = 0$. We match this to the WKB density at the point where it fails, i.e. at the point z_2 in the interior where $y_0/y_{-1} = 1$:

$$
n^{WKB}(z_2 - 0) = n^{IR}(z_2 + 0). \tag{6.3.43}
$$

This determines the normalization $\mathcal{N}$.

This approximation for the quantum tail becomes better and better at z_H as $z_{**} \to z_H$. It is exactly there, in deep interior, where the Airy correction is most critical for gravitational backreaction. The presence of a nonzero density for $z \to z_H$ implies backreaction at the horizon as we shall see in the next section.

6.3.3 Dirac hair correction to semiclassical density

In principle, the Airy expansion can also be applied to the UV non-classical region near the AdS boundary ($0 < z < z_1$). This approach, however, has both practical problems and problems of principle when applied in the near-boundary region:

- The convergence of the Airy expansion is poor near the boundary. Airy expansion is nothing but the linear approximation of the effective potential, as in Eq. (6.3.38). Typically, however, the AdS boundary is too far away from the turning point and the rate of change of the effective potential V_{eff} for $z \approx 0$ is large enough to require higher-order terms in the expansion of V_{eff}. These would, however, make the calculations much more complicated and go beyond the accuracy of the current model.

- More importantly, expanding away from z_* toward the boundary inevitably means that the resulting approximation will not reproduce the exact asymptotics of the fermion field at the AdS boundary. The holographic dictionary identifies expectation values on the field theory side by considering the asymptotics of the bulk fields at the AdS boundary ($z \to 0$). In particular, the correct asymptotics are necessary to have the correct fermionic contribution to thermodynamics. With an Airy expansion around z_*, the behavior at $z = 0$ is completely uncontrolled.

Therefore, in the context of the AdS/CFT correspondence one needs to start the expansion at $z = 0$ in the UV region and glue it to the semiclassical region at $z = z_*$ and not vice versa. The natural framework for this task is the Dirac hair formalism [18]. In the region $0 < z < z_*$ the density rapidly decreases toward zero and it is increasingly dominated by the long range wave functions with $\omega = 0$ and $k \approx 0$ [19]. These facts are precisely the necessary conditions for Dirac hair to be a good approximation. We will thus glue the Dirac hair wave function to the semiclassical result to obtain the quantum tail at small z. The quantum correction in the UV is especially crucial, since otherwise all holographic dictionary entries related to fermions (density, currents, response functions) are all, according to the holographic dictionary, equal to zero.

We will start with a very concise review of Dirac hair. As argued in [18], a very good approximation to the bulk fermion profile at low densities is to describe it through a single collective wave function which encapsulates the nonzero VEV of the fermion density. The right quantity to consider is just the spacetime average of the bulk density $J(z)$:

$$J(z; E, p) = \int d\omega \int d^2k \Psi^\dagger(z; -\omega, -k)\Psi(z; E + \omega, p + k) \qquad (6.3.44)$$

In the bulk, this is just the probability density associated with the quantum-mechanical state Ψ. Analogously to the Airy correction in the IR region, one should, strictly speaking, construct a separate density bilinear for every bulk excitation (filled level) and add up all the bilinears. Analogously to the Airy correction, we do not implement this procedure, but approximate the density with only a single wave function, as we did in the original Dirac hair approximation [18] essentially neglecting the multi-particle nature of the system in the classically forbidden region. The justification is less rigorous than for the Airy correction: the subleading Dirac hair corrections are not damped exponentially but only as a power law. In practice, however we have shown that the numerical value of the amplitude of the excited wave functions with $k \neq 0$ is small enough to be neglected [19].

In the single-particle Dirac hair approximation the expectation value of $J(z; E, p)$ at the boundary at zero energy and momentum $\langle J(z = E = p = 0)\rangle$ translates into the density discontinuity in the vicinity of the Fermi surface [18]:

$$\langle J(E = p = 0)\rangle = \int_{k_F - 0}^{k_F + 0} d^2 k N(k) \sim Z, \tag{6.3.45}$$

where through Migdal's theorem Z corresponds with the quasiparticle pole strength in the spectral function. Especially in the single particle approximation, it is convenient to directly deduce effective equations of motion for $J(z, E, p)$ from the Dirac equation, rather than solving the Dirac equation and squaring. Since the dominant Fermi momentum in the UV is $k_F \simeq 0$ the contribution of the Fermi momentum to the effective equations of motion for J can be ignored. In this simplification its equations of motion only contain the explicit density momentum p. The Fermi momentum is still implicitly present in the integration over the internal momentum k. To write the evolution equation directly for the density $J(\omega = k = 0)$, it is convenient to consider separately the radial projections $\Psi_\pm$ and construct the bilinears

$$J_\pm(z) = \int d\omega \int d^2 k \Psi_\pm^\dagger \Psi_\pm, \quad \text{with} \quad J = J_+ + J_- \tag{6.3.46}$$

together with the auxiliary quantity

$$I(z) = \int d\omega \int d^2 k \Psi_+^\dagger \Psi_- + \text{h.c.} \tag{6.3.47}$$

which we need to close the system of equations. The coupled equations for $J_\pm, I$ implied by the Dirac equation read:

$$\left(\partial_z + \frac{\partial_z f}{2f} - \frac{3}{z} \pm \frac{2m}{z\sqrt{f}} - \frac{2\partial_z h}{h}\right) J_\pm \pm \frac{e\Phi}{f} I = 0 \tag{6.3.48}$$

$$\left(\partial_z + \frac{\partial_z f}{2f} - \frac{3}{z} - \frac{2\partial_z h}{h}\right) I - \frac{2e\Phi}{f}(J_+ - J_-) = 0. \tag{6.3.49}$$

Here we just need the Dirac hair solution to correct the semiclassical model near the boundary, not in the whole space. We find it easiest to seek the solution near $z = 0$ in the form of a series in z:

$$J_-(z) = j_-^0 z^{\alpha_-}(1 + j_-^1 z + j_-^2 z^2 + \ldots) \tag{6.3.50}$$

$$J_+(z) = -\frac{\mu^2}{(2m+1)^2} z^{\alpha_+}(j_+^0 + j_+^1 z + j_+^2 z^2 + \ldots) \tag{6.3.51}$$

$$I(z) = \frac{i\mu}{2m+1} z^{\alpha_0}(i^0 + i^1 z + i^2 z^2 + \ldots). \tag{6.3.52}$$

The exponents $\alpha_{0,\pm}$ are determined by the lowest order of the near-boundary expansion of the Dirac equation. As usual, one gets two families of solutions and, according to the dictionary, the one with faster decay at $z \to 0$ corresponds to a VEV. This is the family with $\alpha_\pm = 4 + 2m \pm 1$, $\alpha_0 = 4 + 2m$. Since we will only use this solution in the UV region, it is convenient to solve directly for the coefficients in this power series, rather than a full numerical determination. We have explicitly checked the convergence of the series using the D'Alembert criterion.

The density obtained in this way is

$$n^{UV}(z) = J_+(z) + J_-(z). \tag{6.3.53}$$

This single particle density is now matched to the WKB density at the point z_1 where $y_0/y_{-1} = 1$ in the exterior:

$$n^{UV}(z_1 - 0) = n^{WKB}(z_1 + 0). \tag{6.3.54}$$

In this way we determine the amplitude j_-^0 (from Eq. (6.3.50)). Together with the Airy matching in the interior we end up with a continuous density in the whole space.

To complete our setup, we would like to have a quick and easy way to quantify the "classicality" of the system, i.e. the proximity to the electron star limit and the smallness of the quantum corrections. A very good estimate is provided by the number of energy levels N in the potential well: the classical limit corresponds to $N \to \infty$ and vanishing spacing between the levels. Provided N is large, it can be well approximated by the textbook WKB formula. The estimate reads

$$N = \frac{1}{4\pi} \int_{z_*}^{z_{**}} dz \sqrt{g_{zz}} V_{eff}(z) \tag{6.3.55}$$

where V_{eff} is the effective Schrödinger potential, Eq. (6.3.37), derived in the context of the Airy function tails. From now on we will frequently use N to characterize the system at certain values of the parameters (μ, q, m).

In Fig. 6.1 we show the full quantum corrected WKB densities obtained with the matching outlined above. These are obtained upon solving the whole self-consistent system of equations (including electromagnetic and gravitational backreaction) described in later sections. We show this here already just to illustrate of our method. In Figs. 6.1A and 6.1B, the semiclassical estimates $n_e^{WKB}(z)$ in the whole classically allowed region ($z_* < z < z_{**}$) are shown as dotted lines compared to the actual (quantum-corrected) density. Fig. 6.1C shows explicitly that N is the correct parameter that controls the size of the quantum corrections. As already argues in [19], for low N which is equivalent to the statement that the total charge density becomes of the order of the charge of the constituent fermion, the WKB approximation fails. Here we see visually that quantum corrections become dominant in this limit.

6.3.4 Pressure and equation of state in the semiclassical approximation

Following the logic behind the density calculation, we will now calculate the pressure. It will actually prove easier to write the equation of state first and then derive the pressure. We can start by computing the energy density of the bulk fermions. By definition, it reads

$$\mathcal{E}(z) = \sum_{\lambda,l} \int_0^{2\pi} d\phi \int_0^{\infty} d\rho \int_0^{\mu_{loc}} d\omega \omega \Psi^\dagger(z)\Psi(z) =$$
$$= \sum_{\lambda,l} \int_0^{2\pi} d\phi \int_0^{\infty} d\rho \int_0^{\mu_{loc}} d\omega \omega \frac{\tilde{E}(z)}{4\pi^2 q(z)} \tag{6.3.56}$$

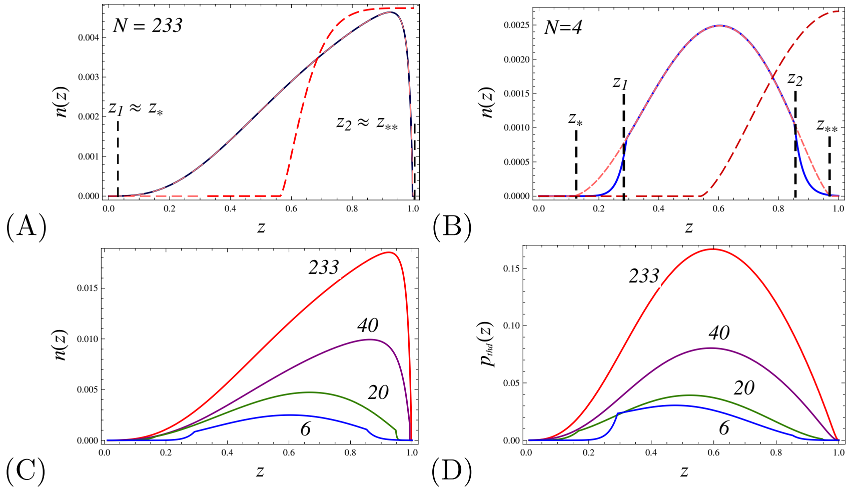

Figure 6.1: Semiclassical bulk density $n^{WKB}(z)$ (Eq. 6.3.35, dashed pink lines) and full density $n(z)$ with quantum corrections – Airy tails for large $z > z_2$ in the interior and Dirac hair for small $z < z_1$ near the AdS boundary (Eqs. 6.3.42, 6.3.53, solid blue lines). Parameter values (A) $(\mu, e, m) = (1.7, 100, 0.1)$, (B) $(\mu, e, m) = (1.7, 10, 1)$. The classically allowed region lies between the turning points z_* and z_{**}, determined by the the condition of vanishing WKB momentum ($q(z_*) = q(z_{**}) = 0$). The gluing of the quantum tails to the semiclassical part is implemented according to the condition of applicability of WKB approximation, $y_0/y_{-1} = 1$, at the point z_2 for the Airy correction (Eq. 6.3.41), and at the point z_1 for the Dirac hair correction (Eq. 6.3.44). The parameters for (A) are in the classical (electron star) regime, the quantum corrections are manifestly small and the classical region almost coincides with the WKB region: $z_1 \approx z_*, z_2 \approx z_{**}$. The plot (B) is given to show that when the system is closer to the single particle Dirac hair approximation, $N \sim 1$, the WKB approximation fails and the quantum corrections are of the same order as the WKB part. (C) Bulk density with quantum corrections, for a range of values $(\mu, e, m) = (1.7, 100, 0.1)$ (red), $(\mu, e, m) = (1.7, 30, 0.1)$ (violet), $(\mu, e, m) = (1.7, 10, 0.1)$ (green) and $(\mu, e, m) = (1.7, 5, 1)$ (blue). For large specific charge of the fermion (and therefore a large number of WKB levels in the bulk) the solution is dominated by the classically allowed region. For smaller q/m values (and thus fewer WKB levels) the quantum correction in the near-boundary region becomes important and eventually dominates the density profile. (D) Thermodynamical pressure with quantum tails (Eq. 6.3.59), for the same parameter values as in (C).

where $\tilde{E}(z)$ is defined in (6.2.11) and the sum limits are the same as in (6.3.34). Performing the integration in a similar fashion as when computing $n(z)$ in (6.3.34-6.3.35), we obtain

$$\mathcal{E} = \frac{1}{2}e\Phi n + \frac{1}{2}f^2\tilde{M}^2\text{ArcSinh}\frac{\tilde{E}}{\tilde{M}}. \tag{6.3.57}$$

Notice that the first term exactly captures the electrostatic energy while the second is the one-loop term that encapsulates the quantum fluctuations. The above result is remarkably close to the Hartree vacuum polarization correction as it appears in various model energy functionals in literature. Now the calculation of pressure needs to be done very carefully in our semiclassical setup. It is possible to delineate two opposite regimes:

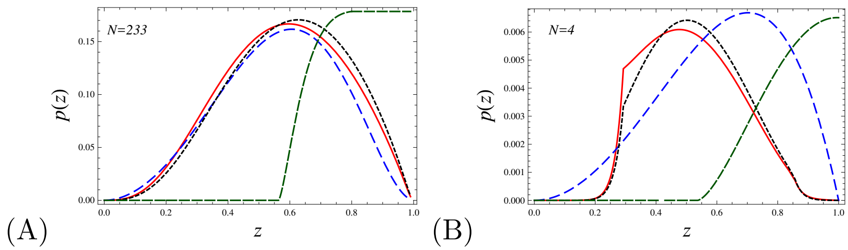

Figure 6.2: Comparison between full quantum pressure (dashed blue lines, Eq. 6.3.58) and thermodynamic pressure (solid red lines, Eq. 6.3.59) for two sets of parameters: $(\mu, e, m) = (1.7, 100, 0.1)$ (A) and $(\mu, e, m) = (1.7, 5, 1)$ (B). For comparison we plot also the fluid pressure $p = en\Phi/2$ (dashed green lines). Expectedly, all three models are close to each other for large N while for N small the level spacing is large and it is necessary to sum the contributions of individual levels: both the thermodynamic approximation and the simple fluid approximation deviate considerably from the exact sum.

1. In the deep quantum regime we can express the pressure from the microscopic fermionic Lagrangian (6.2.3). By definition it reads

$$p = \sum_{n,l,\lambda} \Psi_+^\dagger \partial_z \Psi_+ - \Psi_-^\dagger \partial_z \Psi_- + h.c. = \sum_{n,l} \frac{2l+1}{4\pi q} \frac{e^{-3h/2}}{z^2 f} C_n^2(\omega_n - \Phi) \tag{6.3.58}$$

The explicit calculation is tedious but straightforward and we leave it out. The end result involves the integral of a complicated function of

q and θ. Unlike for density case, we find ourselves unable to package it in a closed-form expression. Instead, we integrate numerically over the energy levels ω_n to obtain the function $p(z)$.

2. Deep in the classical regime, according to thermodynamics $p = \partial E/\partial V$ which generically results in a nonzero outcome. While the volume V is difficult to calculate exactly, we can obtain a crude estimate in the following way. At unit AdS radius, the volume equals the length ℓ of the classically allowed interval along z axis, i.e. the interval between the zeros of the WKB momentum $p_{max}(z) = \sqrt{\tilde{E}^2(z) - \tilde{M}^2(z)}$. From (6.2.11) we find $\ell \sim m/e\mu$, assuming neither of the two turning points is very close to the boundary or very deep in the interior. One further assumption we make is that, not too far in the interior, the gauge field is well described by the linear law $\Phi \sim \mu(1-z)$. We thus arrive at the estimate
$$p_{thd} = \frac{\partial \mathcal{E}}{\partial \Phi}\frac{\partial \Phi}{\partial \mu}\frac{\partial \mu}{\partial \ell} \sim \frac{e\mu^2}{2m}(1-z)\left(en + \frac{m^2 f e^{-h}}{z\sqrt{m^2 f + \Phi^2 e^{-2h} z^2}}\right) \tag{6.3.59}$$
where we have used (6.3.57). We will call this the thermodynamic pressure and denote it by p_{thd} to differentiate from the exact quantum expression (6.3.58). The expression (6.3.59) is also the equation of state of the system as it connects the pressure to the density.

The thermodynamical pressure is much more convenient calculationally. In spite of its approximate nature, it yields a remarkably accurate result when compared with the exact quantum pressure. We ascribe the quantitative proximity of the results in the two cases to the fact that the differences are small in the two key regions of deep UV and deep IR. Outside the classically allowed region, we approximate the system with a single quantum-mechanical particle and calculate the pressure from the quantum equation (6.3.58). The nonzero pressure obtained in this way for the classically forbidden region is *not* the Fermi pressure (which vanishes for a non-macroscopic number of particles). It is the pressure inherent to relativistic fluids.

Finally, it is illustrative to see how we reproduce the electron star pressure [51] in the limit of large density. For $n \to \infty$, the first term in $\mathcal{E}$ dominates and we obtain
$$p_{ES} = \frac{1}{2}\partial_z(e\Phi n) \tag{6.3.60}$$

as expected for an ideal fluid, which corresponds to the electron star approach. The physical interpretation of this result (and of the pressure inside the classically allowed region in general) is that of a Fermi gas pressure which, as we know, survives also in the limit of classical thermodynamics. The comparison of p, p_{thd} and p_{ES} is summarized in Fig. 6.2, for high and low number of levels. While all three approximations are good as $N \ll 1$, for small N both the fluid limit and the thermodynamic limit break down and the contributions of individual levels must be taken into account.

6.4 Maxwell-Dirac-Einstein system

We have now arrived at the point where we can solve our model self-consistently with the Einstein-Maxwell equations. Unavoidably, the solution is numerical, using an iterative procedure to converge toward the solution. Only in the IR region it is possible to use a scaling ansatz to estimate the scaling behavior of the metric and matter fields, akin to the procedure used in [50]. We will also see how the "quantum tails" in both IR and UV are crucial to capture at least qualitatively the full effect of backreaction. This is the first attempt at a self-consistent solution including backreaction on the geometry with holographic fermions which goes beyond the fluid picture of [51].

Fortunately, it is known how to calculate it in the fluid (i.e. electron star) approximation. The action principle for the relativistic fluid as put forward in [108] and used in [51, 52] gives the Lagrangian of the whole system (fluid plus Einstein and Maxwell background) as

$$S = \int d^4x \left[\frac{1}{2\kappa^2} (R + 6) - \frac{1}{2q^2} (\partial_z \Phi)^2 + p \right]. \qquad (6.4.61)$$

In other words, the contribution of fermions reduces to the pressure p. While we do not take the fluid limit in this paper, one can suspect that in the first approximation the influence of the corrections to fluid limit ($N \to \infty$) is fully encapsulated by the correction to the classical (or fluid) pressure we found in (6.3.57-6.3.58).

Starting from the exact action (6.2.2), we replace the fermionic terms with our model for the density and pressure of the bulk fermions. The total action is represented as $S = S_E + S_M + S_f$, the sum of Einstein, Maxwell and fermionic part. The only nonzero component of the gauge field is Φ and the only non-vanishing derivatives are the radial derivatives ∂_z (the others average out to zero for symmetry reasons). The fermion contribution is subtler. On-shell, the bulk action for the fermions vanishes because it is proportional to equations of motion. The boundary contribution is the bilinear $\bar{\Psi}\Psi$ but one can show that this vanishes too when properly regularized [19]. At the quantum level, however, there is a nonzero fermion pressure p, considered in Sec. 6.3.4, as well as nonzero (local) charge density is given by j_e^0 as

$$j_e^0 = qn\sqrt{g^{00}} = qn\frac{ze^{h/2}}{\sqrt{f}}, \tag{6.4.62}$$

The fermionic term in the effective action thus becomes

$$S_f = -\int d^4x\sqrt{-g}\left(j_e^0\Phi + p\right). \tag{6.4.63}$$

Packaging everything together, we arrive at the effective action:

$$S_{eff} = \int d^4x\sqrt{-g}\left[\frac{1}{2\kappa^2}(R+6) - \frac{z^4}{2}e^h\left(\frac{\partial\Phi}{\partial z}\right)^2 - j_e^0\Phi + \sqrt{g^{zz}}p\right]. \tag{6.4.64}$$

The only components of the stress tensor the fermion kinetic energy contributes to is T_{zz} and T_{00} ; the others vanish due to homogeneity and isotropy in time and in the $x-y$ plane. From (6.4.64) we get the equations for the energy-momentum tensor:

$$\begin{aligned} T_0^0 &= -\frac{1}{2}z^4e^h\left(\frac{\partial\Phi}{\partial z}\right)^2 + j_e^0\Phi & (6.4.65)\\ T_z^z &= -\frac{1}{2}z^4e^h\left(\frac{\partial\Phi}{\partial z}\right)^2 + j_e^0\Phi + mn + g_z^zp. & (6.4.66)\end{aligned}$$

We can now write down our equations of motion:

$$\begin{aligned} \frac{1}{\sqrt{-g}}\left(\partial_z e^{-h/2}\partial_z\Phi\right) &= -j_e^0 & (6.4.67)\\ 3f - z\partial_z f - 3 &= T_0^0 & (6.4.68)\\ 3f - z\partial_z f(z) - 3zf\partial_z h - 3 &= T_z^z. & (6.4.69)\end{aligned}$$

The boundary conditions for the gauge field are standard in AdS/CFT: $\Phi(z_0) = \mu$ fixes the chemical potential at the boundary ($z_0 \to 0$), while

$\partial_z \Phi(z_H) = 0$ ensures the stability of the horizon. Asymptotic AdS geometry implies $h(z_0) = 0$, while the redshift factor vanishes at the horizon, $f(z_H) = 0$ (the derivative is determined by the temperature as $\partial_z f(z_H) = T/4\pi$).[3] Finally, it remains to define the units used throughout the paper. The natural unit of energy and momentum is the chemical potential μ and we will express all quantities in units of μ whenever μ is kept constant. When varying μ, we will resort to using the temperature T as the unit. The two ways are essentially equivalent as in holographic systems only the ration μ/T has physical meaning.

Let us conclude with an outline of the numerical algorithm, which is not completely trivial. The boundary conditions to be implemented are given at different points: some are given at the AdS boundary and some at the horizon. Since the system is nonlinear, it is necessary to either linearize the system or to shoot for the correct boundary conditions with the full nonlinear system. After experimenting with both, we have decided to iterate the full, non-simplified system of equations, integrating from the horizon and shooting for the conditions at the boundary. We perform the procedure iteratively, gradually increasing the fermion charge in every iteration, and then iterating with fixed fermion charge until the convergence of the solution is achieved to the fixed set of functions, (f, h, Φ). More explicitly, the procedure is as follows: we start with the non-backreacted AdS/RN geometry and compute the density (semiclassical plus the quantum corrections) for the the electron charge equal to e/N (where e is the physical charge and N some positive integer), then we solve the system of Einstein-Maxwell equations (6.4.67-6.4.69), afterwards we increase the fermion charge to $2e/N$, calculate the charge density in the background (f, h, Φ) taken from previous iteration and solve for this density Einstein-Maxwell equations (6.4.67-6.4.69). We repeat this procedure for charge $3e/N$, $4e/N$ etc. After N iterations we have arrived at the physical value of the charge e. Then we do more iterations with fixed charge e to ensure that the solution has converged, checking that the set of functions (f, h, Φ) does not change from iteration to iteration. In this way we achieve the self-consistent numerical solution of the Maxwell-Dirac-Einstein system of

[3] At zero temperature, when the horizon vanishes due to fermionic backreaction (this includes also the case of Lifshitz geometry), the boundary condition for f guarantees also the smoothness of the solution on the horizon: $\partial_z f(z_H) = 0$. This condition ensures that we pick the correct branch of the solution as there are typically two families of functions $f(z)$ that satisfy the equations of motion and the condition $f(z) = 0$. One of them has a vanishing derivative whereas the other has finite derivative as $z \to 1$.

equations. The integration is always done from the horizon, shooting for the conditions for Φ and h at the boundary, since it is well known that integrating from the AdS boundary is a risky procedure as it is next to impossible to arrive at the correct branch of the solution at the horizon.

6.5 Phases of holographic fermions

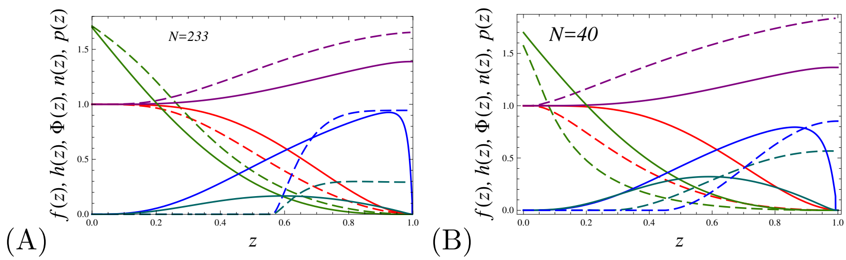

Figure 6.3: Profiles of the metric functions $f(z)$ (red) and $e^{h(z)}$ (violet), the gauge field $\Phi(z)$ (green), density $n(z)$ (blue) and the pressure $p(z)$ (cyan) at zero temperature, for $(\mu, e, m) = (1.7, 100, 0.1)$ (A) and for $(\mu, e, m) = (1.7, 10, 0.1)$ (B). Solid lines are calculated form our model while dashed lines are the electron star solution for the same parameter values. For better visibility density and pressure are rescaled by a constant factor. Near the boundary we always have $h(z) \to 0$ and $\Phi(z) = \mu + O(z)$, in accordance with the universal AdS asymptotics of the solution but in the interior the solutions start to deviate. Most striking is the absence of sharp classical edges in density and pressure. The difference in pressure will turn out to be crucial in moving away from the fluid limit. Here we have not shown the solution with $N = 4$: this case deviates from the electron star ($N \to \infty$) so strongly that it does not make sense to compare it. Indeed, $4 \ll \infty$!

We can now analyze the structure of both the bulk and the field theory side as a function of the parameters μ, e and m. We first shortly discuss the nature of the bulk solution for the geometry and gauge field and notice some qualitative properties. Afterwards we study the structure of the phase diagram using the thermodynamical quantities as the guiding principle, and corroborate these findings with spectral functions. As a result we will be able to draw the phase diagram.

The typical way that the solutions to the Dirac-Maxwell-Einstein system (6.4.67-6.4.69) look like, including the quantum tails in both UV and IR for the density $n(z)$, is illustrated in Fig. 6.3. The near-horizon scaling of the metric and gauge field is of Lifshitz type, as expected in the light of earlier models [50, 51]. It is illustrative to make a comparison with the simpler models of Dirac hair and electron star. The metric functions f and h of all three models converge toward each other near the boundary, and the gauge field Φ remains close to the non-backreacted RN setup [18, 51]. This gives hope that these approximations can provide a decent estimate of important quantities on the CFT side since these are not overly sensitive to the precise modeling of the fermionic condensate in the interior. In addition, the Dirac-hair-like quantum correction reproduces the finite density tail near the boundary, crucial for thermodynamics.

6.5.1 Thermodynamics

We can now use these full solutions to determine the macroscopic characteristics of the dual strongly coupled fermion system. Let us first derive the free energy of the boundary field theory. According to the dictionary, it is equal to the (Euclidean) on-shell action, which contains both bulk and boundary components:

$$F = S_{bulk}^{on-shell} + S_{bnd}^{on-shell}. \tag{6.5.70}$$

We have already discussed the bulk action in the previous section. We will approximate the fermionic contribution (6.4.63) by its leading term, pressure. Notice that we do not disregard backreaction to the metric and gauge field, i.e. we calculate the exact value of the gravitational and gauge field action, and then add the fermionic component approximating it with p.

The boundary action encapsulates the regularizing terms that eliminate the divergences and the von Neumann boundary condition for the gauge field:

$$S_{bnd} = \oint_{\partial AdS} \sqrt{-h} \left(\frac{1}{2} n_\nu F^{\mu\nu} A^\mu + \bar{\Psi}_+ \Psi_- \right), \tag{6.5.71}$$

with h being the induced metric on the boundary ($h = \frac{1}{z^2}(-1/f(z = 0), 1, 1)$) and Ψ_+ and Ψ_- are radial projections of the wave function as in Eq. (6.2.7). By ∂AdS we have denoted the boundary of the AdS space. Their asymptotics at the boundary are given by

$$\Psi_+ = \frac{i\mu\gamma^0}{2m+1} B_- z^{5/2+m} + \ldots, \qquad \Psi_- = B_- z^{3/2+m} + \ldots \tag{6.5.72}$$

as noticed in the subsection IIIE. In our system, the electromagnetic boundary term reduces to $\Phi\partial_z\Phi|_{z=0} = -\mu\rho$, where ρ is the total boundary (not only fermionic) charge density, read off from the subleading "response" of the bulk electrostatic potential $\lim_{z\to 0}\Phi(z) = \mu - \rho z + \ldots$. The regularized boundary action now reads

$$S_{bnd} = \lim_{z_0\to 0} S(z_0) + \lim_{z_0\to 0}\int d^3x \left[\frac{3\mu}{2(2m+1)}\bar{B}_- i\gamma^0 B_- z_0^{1+2m} - \frac{1}{2}\mu\rho\right], \tag{6.5.73}$$

and the total on-shell action, i.e. the free energy can be written as

$$F = \int_{z_0}^{z_H} dz d^3x\sqrt{-g}\left[R + 6 + \frac{ze^{h/2}qn\Phi}{2\sqrt{f}} + p\right] - \frac{1}{2}\mu\rho + \frac{\mu}{2(2m+1)} I(z_0) z_0^{1+2m}, \tag{6.5.74}$$

where we exploit the definition of the bilinear I from Eq. (6.3.47)[4]. Notice that the last term in the free energy (6.5.74), coming from the fermionic term in the boundary action (6.5.73), vanishes in the limit $z_0 \to 0$, i.e. at the boundary. Therefore, it does not influence the free energy and we include it only for completeness.

6.5.2 Constructing the phase diagram

Let us first briefly describe the role of different control parameters. One obvious parameter is the temperature T which drives the thermal phase transitions. In the limit $T \to 0$, we can determine the nature of the ground state and possible quantum phase transitions between them.[5] The parameters that determine the ground state are μ, e and m. Current wisdom suggests that the phases of the system are primarily sensitive to the ratio e/m [19]. Another convenient parameter is the "effective chemical potential"

$$\frac{\mu_{eff}}{T} \equiv \frac{e\mu}{mT} \tag{6.5.75}$$

motivated that only the combination $e\mu$ appears in the Dirac equation. We will also sometimes look at μ_0, the threshold chemical potential for nonzero

[4] In Eq. (6.5.74) the kinetic term for the Maxwell field $\sim \partial_z\Phi^2$ is transformed through partial integration into $\sim \Phi\partial_{zz}\Phi$ which is then transformed into $\sim n\Phi$ using the Poisson equation

[5] Our numerical approach is not convenient at strict zero temperature. However, it is known that quantum phase transitions can be detected also at small but finite temperatures.

bulk density and the formation of a Fermi surface on the field theory side. Its value at $T = 0$ is easily determined either by tracking the emergence of a solution with finite bulk density n, or by looking at the formation of a quasiparticle peak in the spectrum (see the next subsection). Finally, we have already argued that the parameter $N(\mu, e, m)$ that controls the classical/quantum regime is another convenient parameter. An alternate parametrization of the phase diagram is therefore μ_{eff}, N and m.

First order thermal phase transition to RN-AdS

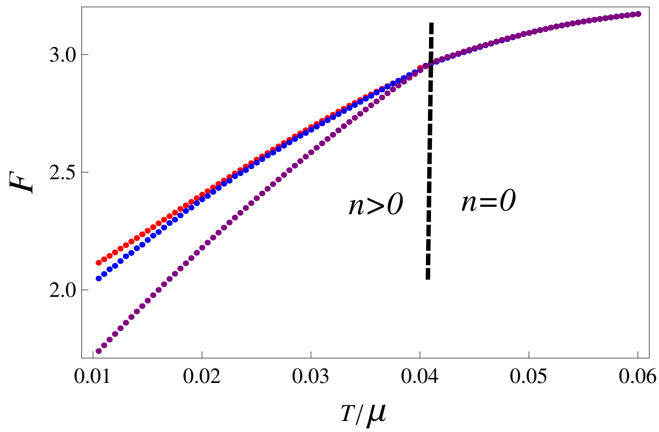

Figure 6.4: Free energy as a function of temperature $F(T)$. The abrupt change of the derivative signifies the first order transition between the finite density phase and the pure black hole (with zero bulk fermion density), in line with the analytical prediction of the first order transition from the second term in the bulk free energy in Sec. 6.5.2. We show the calculations for three different values (μ, e, m) of the system parameters: $(1.7, 30, 0.1)$, $N(T = 0) = 40$ in red, $(1.7, 10, 0.1)$, $N(T = 0) = 20$ in blue and $(1.7, 10, 0.7)$, $N(T = 0) = 11$ in violet. In the high temperature (RN) phase the curves $F(T)$ fall on top of each other as one expects for the RN black hole with $n = 0$. The behavior in the low-temperature phase (with non-zero density) is different for the three curves as the value of the charge affects the behavior of the bulk fermions. For presentation purposes, the curves have been rescaled to the same transition temperature; in general, however, $(T/\mu)_c$ is *not* universal and will differ for different corners of the parameter space.

At high temperature the preferred state of the system is the charged

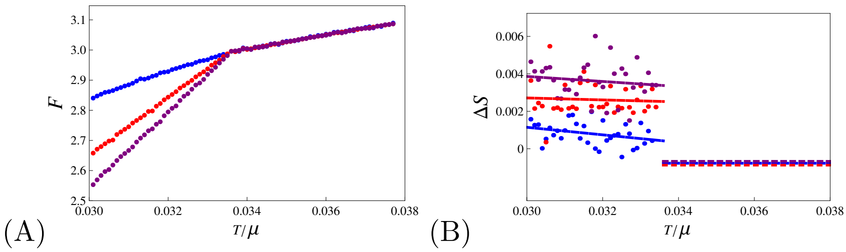

Figure 6.5: (A) Free energy (rescaled and centered to common value at the transition point) for the same parameters as in Fig. 6.4, in the vicinity of $T = T_c$ (*not* for the whole range of temperatures). The cusp characteristic of a first order transition is now clearly visible. The value of F on the RN side ($n = 0$) is without error bars as the thermodynamic functions of the black hole can be exactly calculated. Notice how the slope of F in the low-temperature phase decreases as the number of levels increases: for $N \to \infty$ we reach the electron star limit when the transition becomes continuous. (B) Difference between the entropy of the RN black hole and the entropy of the system $\Delta S = S_{RN} - S$, where entropy is obtained from free energy as $S = -\partial F/\partial T$, for the same parameters and in the same color schemes as in Fig. 6.4 and panel (A). The first order nature of the transition is recognized from the jump ΔS at the critical point. Notice that the difference is positive for $T < T_c$, and thus the high temperature phase has more entropy as expected. The entropies in the RN/local quantum critical phase are exact, as they are calculated from the exactly known RN solution at given chemical potential. They are thus represented by a single (black) set of data points. The entropy is in relative (computational) units.

AdS black hole rather than a finite bulk fermion density configuration. This AdS-RN black hole describes a local (momentum-independent) quantum critical phase which generically has no Fermi surfaces. At low T/μ one finds several non-Fermi-liquid Fermi surfaces [79, 17, 27, 63], but this should be where the instability to the finite density system sets in. Fig. 6.4 shows the behavior of the free energy $F(T)$ in a broad range of temperatures, encompassing both the low and the high temperature phases for different parameters e, μ, m. The cusps in the dependence $F(T)$ correspond to the points of a first order phase transition (where the derivative $\partial F/\partial T$ experiences a jump). In the high temperature phase the dependence $F(T)$ is the same for different electron charges at given chemical potential as there are no fermions in the bulk and the solution is determined only by the temperature and the chemical potential at the boundary. In low temperature phase the free energies, although close, are distinct. Fig. 6.5A shows the free energy in the vicinity of the phase transition and we can clearly see the cusp in the function $F(T)$ signalling the *first order phase transition*. To further corroborate the first order nature of the transition, we plot the entropy $S = -\partial F/\partial T$ in Fig. 6.5B for the same parameters as in Fig. 6.4 and 6.5A. To better show the transition, entropy is plotted with reference to its value for the black hole, as $\Delta S = S_{RN} - S$. Notice that the jump of the derivative $\Delta S(T)$ is positive for $T < T_c$, as it should be, as the system evolves toward maximizing its entropy.

A first order transition between a zero/nonzero bulk density can be explained from general analytical considerations. Starting from low temperatures, at the transition point the bulk density n vanishes. In our model that means that the turning points coincide: $z_* = z_{**}$. In this limit we are able to analytically predict the order of the transition in the following way. Assuming that the transition is dominated by the behavior of the fermions, the relevant part of the free energy of the system is given by $\mathcal{F} = \int_0^{z_H} dz \mathcal{E}(z)$. Since the bulk matter lives at zero temperature, all thermodynamical potentials are equal and the free energy is just the total (internal) energy of the system. The first ("electron star") term in the energy, $e\Phi n/2$ is analyzed in detail in [52] and is concluded to yield the scaling $\mathcal{F} \sim (T - T_c)^3$. We will now analyze the second, Hartree term, $f^2\tilde{M}^2\mathrm{ArcSinh}\left(\tilde{E}/\tilde{M}\right)$. The vanishing of the classically allowed region means $\tilde{E} \approx \tilde{M}$ in the whole (narrow) region $z_* < z < z_{**}$. One can thus expand $\tilde{E} = \tilde{M} + \delta z \times \delta\tilde{E}/\delta z + \ldots$ and analyze the leading terms in δz. It is easy to see that its expansion starts from a constant: $\mathrm{ArcSinh}\left(\tilde{E}/\tilde{M}\right) = \text{const.} + O(\delta z)$, where $\delta z = z_{**} - z_*$. Its integral thus scales as $\mathcal{F} \sim \delta z$. Now, for a vanishing bulk charged fluid/emerging charged black hole, the principle of detailed balance predicts that the charge of the former equals the charge of the latter: $n\delta z = n_{BH}\delta z_H$, where the charge densities of the bulk and the black hole are n and n_{BH}, respectively, and δz_H is the change in the position of the black hole horizon. The crucial insight is that the densities can be assumed constant for vanishing δz and δz_H. We thus find $\delta z \sim \delta z_H \sim T - T_c$. The conclusion is that

$$\mathcal{F} \sim T - T_c \tag{6.5.76}$$

and *the transition is always of first order.* The final subtlety is that we have now analyzed the bulk free energy: the boundary free energy F (evaluated as the bulk on-shell action) is distinct from it. However, the difference $F - \mathcal{F}$ cannot have terms of order lower than linear in $T - T_c$. We thus conjecture that the thermal transition from a bulk fermionic system to a black hole is generically of first order.

The numerics confirms the prediction of the first order phase transition. The field theory interpretation of the discontinuous nature of the transition to a phase with Fermi surfaces is simple: fermions do not break any symmetry but the discharge of the black hole does signify that the ground state is reconstructed due to formation of a rigid Fermi surface. The only way to reconstruct the ground state without breaking any symmetries is precisely the first order transition of the density van der Waals liquid-gas type. This is the interpretation put forward in [18] for the first order transition from Dirac hair to RN state. We find here that this conclusion stays valid even for large values of n, in contrast to [52]. These papers study the birth of a (classical) electron star upon reducing the temperature and find a continuous, third order, transition. The crucial Hartree term in $\mathcal{F}$ is absent in the classical electron star limit, leaving only the continuous transition from the electrostatic energy $en\Phi$. As the Hartree term will be present for any finite value of n, no matter how large, these results indicate that the physical transition in the strongly coupled fermion system is indeed of first order.

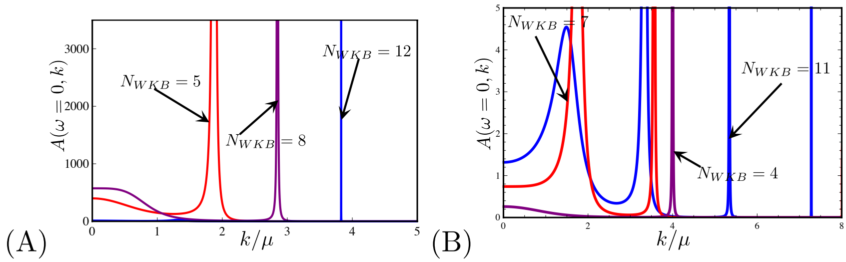

Figure 6.6: The emergence of Fermi surfaces seen in MDCs $A(\omega = 0, k)$ upon dialing $\mu = 0.8, 1.0, 1.2$ (red, violet, blue), in (A) for $(e, m) = (10, 1)$, and in (B) for $(e, m) = (30, 5)$. The sharp peaks at some $k = k_F$, present for higher values of the chemical potential reveals the Fermi surface with Fermi momentum k_F. Remarkably, the emergence of a Fermi surface coincides with critical values of μ for which the RN black hole is replaced by a finite density solution. The obvious difference between (A) and (B) is that in the former case only one (generically, few) Fermi surface can form while in the latter the number of Fermi surfaces grows rapidly with further increasing μ. The numbers in the figure (pointing on the curves) give the level count N.

In order to further explore the physical meaning of different phases on the field theory side, we will study also the spectra of the fermion in each of the phases. The central object here is the spectral weight $A(\omega, k)$ which can be defined in terms of the retarded propagator G_R:

$$A(\omega, k) = \mathrm{Tr}\Im G_R(\omega, k). \tag{6.5.77}$$

To obtain $A(\omega, k)$ we solve now the equations of motion for a probe fermion in the background obtained from the self-consistent solution of the bulk equations. From this one can construct the retarded propagator G_R on the field theory side and compute the spectral function. The appropriate procedure is well established by now [79, 17] and we will only briefly summarize it. The solution to the bulk Dirac equation (6.2.5) can be expanded near the boundary as

$$\Psi_+ = A_+ z^{3/2+m} + B_+ z^{5/2-m} + \dots, \tag{6.5.78}$$
$$\Psi_- = A_- z^{3/2-m} + B_- z^{5/2+m} + \dots \tag{6.5.79}$$

According to the holographic dictionary, the retarded propagator equals the ratio of the VEV (subleading term in Ψ_-) and the source (leading term in Ψ_+):

$$G_R = z_0^{2m} B_- A_+^{-1} \tag{6.5.80}$$

where the prefactor is just the regularization at some $z = z_0$. Following [79], we package the equation of motion into a single nonlinear equation for the ratio $B_- A_+^{-1}$. At zero temperature, Fermi surfaces are always located at $\omega = 0$ [79, 27]and they are most easily found by studying the momentum distribution curves (MDCs) at zero energy, $A(\omega = 0, k)$.

We can now confirm that finite/zero density phases are indeed roughly equivalent to presence/absence of Fermi surfaces. Extensive calculations of spectra in the vicinity of the critical μ/T or the critical temperature show that the finite density phase *always* has at least one Fermi surface on the field theory side while the zero density phase *generically* has no Fermi surfaces. This is expected: Fermi surfaces are signalled in the bulk by the existence of quasinormal modes, only if there are (quasi)normalizable modes in the spectrum can we have a finite bulk fermion density, a finite bulk fermion density implies also finite boundary density, and finite fermion density in field theory implies the existence of Fermi surfaces. Emergence of Fermi surfaces from the quantum critical (RN) phase is observed in Fig. 6.6 for the low- and high μ_{eff} case, or roughly for an electron star at birth and a Dirac hair at birth from a bald RN black hole. In the first case (Fig. 6.6A), a single Fermi surface emerges at μ_{eff}^{crit} and remains stable, while in Fig. 6.6B increasing μ_{eff} leads to the emergence of an ever increasing number of Fermi surfaces. Both cases belong to the low temperature phase from Figs. 6.4-6.5. The difference between the two regimes of this phase we will study later in this subsection.

Continuous quantum phase transition to RN-AdS

The second axis of the phase diagram is the conformal dimension Δ, i.e. the bulk mass m. Studies of the electron star [51, 53] suggest that the appropriate control parameter is actually the charge to mass ratio e/m: electron star is the thermodynamically preferred solution for high e/m values. We see from the expression for WKB density (6.3.35) that increasing the fermion mass or reducing fermion charge reduces the semiclassical region and the total bulk charge. The electron star reasoning likewise suggests that the finite density ground state corresponds to high values of e/m. For some threshold value $(e/m)_c$ the electron star vanishes [51] and the RN solution is preferred.

We will now consider in some detail the quantum phase transition from AdS-RN zero density regime to the finite density phase. Let us fist summarize what is known. The near-horizon geometry of the RN black hole is described by AdS_2 throat. The conformal dimension of the corresponding IR CFT is [27]:

$$\nu_k = \sqrt{\frac{m^2}{6} + \frac{1}{2}\left(\frac{k}{\mu}\right)^2 - \frac{e^2}{12}}, \tag{6.5.81}$$

For $e < m\sqrt{2}$ we have $\nu_k^2 > 0$ for any momentum value (including $k = 0$), implying that the bulk geometry is stable. For $e > m\sqrt{2}$, the conformal dimension ν_k becomes imaginary. According to [63, 87], this region is unstable due to pair creation near the horizon. Accordingly, one expects finite bulk density to form for $e > m\sqrt{2}$, leading to backreaction and disappearance of AdS_2 throat. However, to the best of our knowledge, this was not checked explicitly so far in the Einstein-Maxwell-Dirac setup. Using our WKB method we will now study the appearance of finite bulk density and its consequences on field theory side.

The dependence of the free energy on the conformal dimensions Δ with other parameters fixed is given at Fig. 6.7. We have marked with dashed lines the critical values of the conformal dimension Δ_c when a nonzero bulk density $n(z)$ appears. The free energy does not reveal any simgularity at these points. Nevertheless, they can be identified as the points where the dependence $\mathcal{F}(\Delta)$ deviates from the straight line $\mathcal{F}(\Delta)$ = const. – free energy of a pure RN black hole clearly does not depend on the fermion. In the zoom-in near Δ_c (Fig. 6.7(B)) we find that the behavior of free energy is consistent with the BKT form:

$$\mathcal{F}(\Delta) - \mathcal{F}(\Delta_c) = \text{const.} \times e^{-\frac{\text{const.}}{\sqrt{\Delta_c - \Delta}}}. \tag{6.5.82}$$

The BKT nature of the phase transition can be related to the RG interpretation of the oscillatory regime. The effective Schrödinger potential in AdS_2 regime is proportional to $1/r^2$ [28]. This form of potential gives rise to RG limit cycles [85]. Finally, it is known that the system generically experiences a BKT phase transition when the RG flow with a limit cycle becomes unstable [106]. One can therefore argue that the BKT transition we observe appears as a consequence of the exiting from RG limit cycle behavior in the bulk.

In order to understand what drives the instability of the RN regime and to what it corresponds in field theory, it is helpful to look at the spectra (Fig. 6.8). By stacking together MDCs for different Δ values we can easily follow their evolution: the sharp, narrow maximum corresponding to the quasiparticle peak vanishes at Δ_c simultaneously with disappearance of n. This again suggests the generic absence of critical Fermi surfaces immanent in the RN setup [17, 79]: the quantum phase transition separates the ES/DH phase with stable quasiparticles from AdS_2 metal with no quasiparticles at all.

Crossover between low and high density phases

Now we will take a closer look at the low temperature finite density phase. This is the parameter regime where earlier models [18, 51, 19] anticipate the emergence of regular Landau Fermi surfaces. These models predict a single Fermi surface for low fermion charge [19] while, according to [53], the regime of high fermion charge describes a "deconfined" phase with a multiplicity of Fermi surfaces, with fermions of different flavors. The question arises if the two regimes are thermodynamically distinct and if so, separated by a critical point or by a crossover. To that end we plot the free energy as a function of the effective chemical potential $\mu_{eff} = e\mu$.

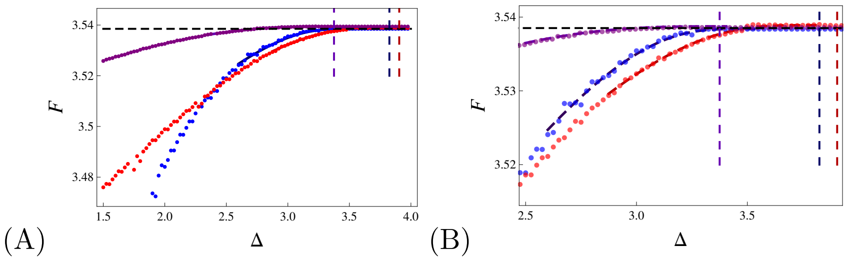

Figure 6.7: (A) Free energy as a function of the conformal dimension $\Delta = 3/2 + m$, for $(\mu, e) = (1.7, 20)$ – blue, $(1.0, 20)$ – red and $(1.0, 5)$ – violet. Numerically, the curves are smooth and all derivatives $\partial^k F/\partial^k \Delta$ are finite. We identify the transition points as the values Δ_c when the fermion density $n(z)$ vanishes identically and mark the corresponding values in the figure. Both the look of the curves and the analytical reasoning, i.e. the lack of two independent scales that could compete as in a crossover, are consistent with a BKT transition. (B) Zoom-in near the transition points with analytical plots of the BKT scaling relation $F \propto \exp(-\text{const.}/\sqrt{\Delta - \Delta_c})$. The numerical data are fully consistent with the BKT scaling.

Remarkably, all four curves fall on top of each other for small charges, where the background is close (though not identical) to AdS-RN. The curves are smooth in the whole region. The absence of a cusp in $F(\mu_{eff})$ definitely discards the possibility of a first order transition, the distinction between a continuous transition and a crossover is difficult to make. Analytical arguments however strongly suggest the crossover. To see why, remember that the (thermodynamically defined) density $n_{th} = \partial F/\partial \mu$ is an analytic function of the solutions to the Einstein-Maxwell system $(f(z), h(z), \Phi(z))$. We thus expect all higher derivatives $n = \partial^k F/\partial \mu_r^k$ $(k = 2, 3, \ldots)$ to be continuous as well. In addition, the simplest physical interpretation of increasing μ_{eff} is that of increasing the number of bulk fermions by filling increasingly higher levels in the effective potential well (6.3.37). One can expect a substantial change of the behavior of the system as the potential well is filled but not a discontinuity of the thermodynamical functions (e.g. [77]). We can thus conclude that *a crossover separates a Dirac-hair-like region from the electron-star-like region.*

At first sight just the change in the number of occupied states should not affect any thermodynamic properties. We will argue below that the cause of the crossover is the change of the scaling behavior of the quasiparticle width. Notice that the function $F(\mu_{eff}/T)$ keeps the same convexity

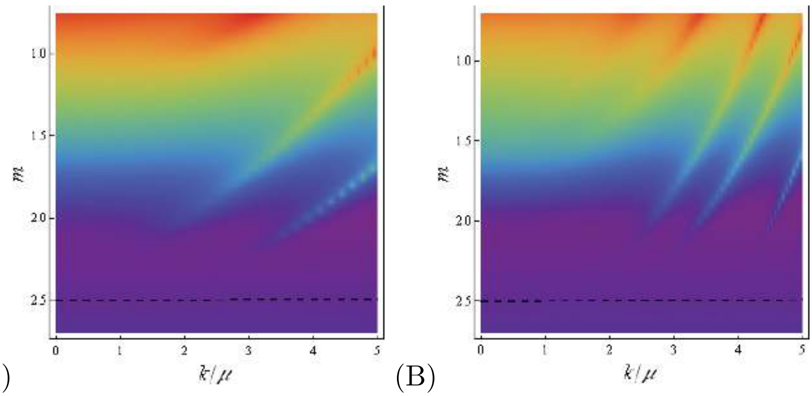

(A) (B)

Figure 6.8: (A) MDC spectra at $\omega = 0$ for $(\mu, e) = (1.0, 5)$ and varying Δ. Curves for different Δ values are stacked on top of each other to represent the evolution of the spectrum with Δ. To better show the Fermi surfaces we use the logarithmic color scale, i.e. the color value is proportional to $\log A(\omega = 0, k)$. Crucially, the Fermi surfaces (lines of lighter color) disappear at $\Delta = \Delta_c$, simultaneously with entering the RN phase. Dashed line delimits the area within which bulk density is nonzero and the system backreacts away from AdS-RN (it is parallel t0 the k axis as the presence of nonzero bulk density does not depend on the momentum of the probe fermion). We can conclude that the formation of a Fermi surface indeed drives the instability of the RN background to a new, finite density phase. In (B), we show for comparison the MDC curves for the same parameter values without backreaction, i.e. in the AdS-RN background. In RN background the number of Fermi surfaces is larger (we see four Fermi surfaces).Hoeve,r both in (A) and (B) there are no Fermi surfaces bellow the dashed line.

as in Fig. 6.4: the argument of the function is increasing in Fig. 6.4 and decreasing in Fig. 6.9, hence the increasing/decreasing trend in the function.

The dispersion of the energy distribution functions (EDCs) for momenta in the vicinity of the Fermi momentum yields a better insight into the physical meaning of the finite density phases. It is here that the crossover from Dirac hair to electron star becomes most obvious: the few Fermi surfaces of Dirac hair regime exhibit a broader power law scaling of self-energy $\Im\Sigma \sim \omega^{2\nu}$ with $\nu = 1$ to high accuracy while the many Fermi surfaces of the electron star are exponentially sharp: $\Im\Sigma \sim e^{-1/\omega}$ (Fig. 6.10). The latter scaling was predicted in [26] and confirmed in [53], while the former was postulated on general grounds in [18]. Importantly,

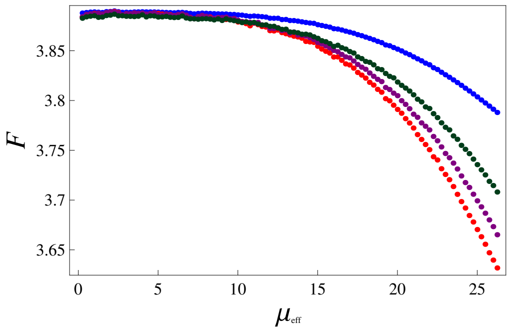

Figure 6.9: Free energy as a function of the fermion charge e in the crossover region for $(\mu, m) = (2.2, 0.5)$ – red, $(1.0, 0.5)$ – violet, $(1.7, 1.0)$ – green and $(1.7, 5.0)$ – blue curve and for a range of fermion charge values. On the abscise we plot the effective chemical potential $\mu_{eff} = e\mu$. The temperature is kept fixed at $T = 0.0005$. All four cases exhibit a crossover about the same value of μ_{eff}/T ($\mu_{eff}^{cross}/T \approx 20$), suggesting that μ_{eff} is indeed the key quantity that drives the changes of the Fermi surface. The low-μ_{eff} region is a few-Fermi-surfaces DH-like system while the high-μ_{eff} regime describes an ES-like multiplet of Fermi surfaces. We will later study in more detail the dispersion properties of the two regimes. Apart from the gradual and soft nature of the transition as seen from the numerical curves, the crossover (as opposed to phase transition) nature of the phenomenon also follows from analytical considerations. The dependence of the solution $(f(z), h(z), \Phi(z))$ on the parameters of the system (μ, q, m) is analytical, which strongly suggests that the derivatives of the free energy $\partial^k F/\partial\mu^k$ are continuous to all orders $k = 2, 3, \ldots$.

no unstable or underdamped Fermi surfaces (with self-energy scaling as $\Im\Sigma \propto \omega^{2\nu}$ with $\nu < 1/2$) are found: these seem to be the artifacts of the probe limit and will not arise in a self-consistent approach (with backreaction).

6.5.3 Phase diagram

We are now in the position to summarize our findings in the form of a phase diagram. In Fig. 6.11(A) we give three-dimensional phase diagram which includes all three independent parameters – μ/T, e and m, while the "reduced" phase diagram with only two parameters, $e\mu/T$ and Δ, is given in Fig. 6.11(B). At high temperatures the system is always in the zero density quantum critical AdS-RN phase. Dialing $e\mu$ at fixed temperature

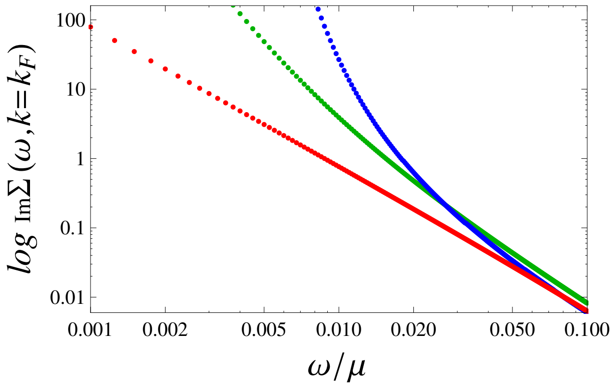

Figure 6.10: Imaginary part of the self-energy of the quasiparticle in the immediate vicinity of $\omega = 0$ for $e = 5, 15, 50$ (red, green, blue). It shows the crossover from power-law (solid line) (red line) to exponential The self-energy of the quasiparticle undergoes a transition from quadratically damped peaks ($\Im\Sigma \sim \omega^2$, red points) toward exponentially narrow poles ($\Im\Sigma \sim e^{-1/\omega}$, blue points). Notice that the all three peaks are stable: the power-law exponent is $\nu = 1$ with high accuracy, signalling a normal Fermi liquid phase.

toward larger and larger values, the Fermi surfaces proliferate until the point of crossover, when the peaks become exponentially sharp. The true nature of this system is not yet known in detail [6]. We have already suggested such a diagram in [19] based on the analysis of the two extreme limits. Here we have gone further and analyzed quantitatively also the intermediate regimes. The structure of the phase diagram can now be summarized as follows:

1. *Van der Waals transition*, Fig. 6.11(A), Fig. 6.5. There is universally a the first order (van der Waals) transition from finite to zero density phase upon dialing μ/T and thus filling the levels of the bulk fermionic system. In field theory, this means a liquid-gas transition between the Fermi liquid(s) and the disordered phase, devoid of quasiparticles and dominated by slow conformal dynamics. Interestingly, the quantum corrections to the density and pressure are crucial for the discontinuous nature of the transition: in the electron star limit, as shown in [52], the transition becomes continuous.

[6] Reference [97] interprets it as fractionalized Fermi liquid

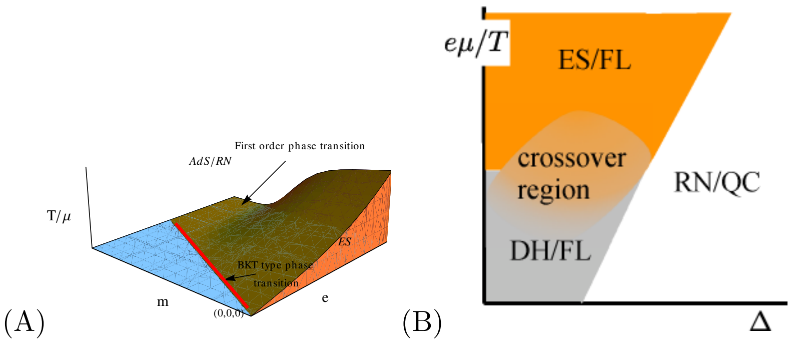

Figure 6.11: (A) Three dimmensional phase diagram $(e, m, T/\mu)$. The phase transition from finite density phase to AdS-RN phase is a first order phase transition in contrast to zero temperature BKT-type phase transition. (B) Phase diagram in $(e\mu/T, \Delta)$ plane, based on thermodynamics and spectra, at zero temperature. The two regimes with stable quasiparticles are denoted with different colors: electron star (ES), describing (likely) a "Russian doll" of stable Fermi-liquid-like quasiparticles (ES/FL), and Dirac hair which is closer to normal Fermi liquid (DH/FL). The third regime, for large Δ, is the RN black hole with its quantum critical Fermi surfaces and no quasiparticle.

2. *Quantum phase transition*, Fig. 6.11(B), Fig. 6.7. There is a continuous (likely BKT) transition from finite to zero density phase upon dialing the conformal dimension Δ at fixed fermion charge (or equivalently varying the ratio m/e, or equivalently varying the fermion charge e or the total charge Q at fixed Δ). The fact that the Fermi-liquid-like quasiparticles vanish in the high Δ/low e regime is known from the electron star limit and not surprising on basis of general arguments (bulk density in the classical approximation drops with increasing m/e). However, our finite level spacing correction to electron star makes it possible to study the transition region in detail, and shows a nontrivial outcome: the transition is of BKT type, and happens inside the oscillatory (pair-creation) region.

3. *No Fermi surfaces in AdS_2 metal phase.* The transition happens at such parameter values which, on the AdS-RN side of the transition, correspond to absence of Fermi surfaces, i.e. imaginary IR conformal dimension ν. The system thus passes directly from a Fermi-liquid-like phase into a profoundly different, exotic phase that we call AdS_2 metal, and which was studied in detail in [27].

At constant temperature, the finite density phase exhibits analytic behavior of the free energy and has no phase transitions but shows a clear crossover between the single-Fermi-surface, Dirac hair limit and the infinity of Fermi liquids in the electron star limit. Thermodynamically the crossover is explained by the change in quasi-particle width $\Im\Sigma$ from power-law behavior in the Dirac-hair-like quantum regime with $N_{WKB} \lesssim 10$ to exponential suppression in the semi-classical electron star like regime with $N \gg 10$.

We will finish this section with a look towards real-world examples of such phase diagrams. Condensed matter literature offers a vast landscape of strongly coupled Fermi liquids like our DH phase, e.g. in the context of heavy fermions [80]. However, the properties of the electron star ("Matryoshka" or "Russian doll") phase are not easy to relate to the real-world examples. In part, it is a consequence of the large-N limit in AdS/CFT which, for example, leads to an exponentially small self-energy. The hope is that finite-N corrections would eventually lead to a realistic picture of the ES phase, while the DH, perhaps with some modifications of the geometry, would correspond to normal metals.

6.6 Discussion and conclusions

In this paper we have constructed a semiclassical model with quantum tails of holographic fermions in AdS_4 space, aimed at understanding the phase diagram of strongly coupled Fermi and non-Fermi liquids. The model uses WKB approximation in the classically allowed region, complementing it with quantum-mechanical estimates of the fermionic wave function in the classically forbidden region. Introducing the pressure into the essentially quantum mechanical model we get the Hartree quantum correction ("vacuum polarization") of the classical model – the electron star. This approach has allowed us to address the intermediate fermion charges which cannot be modeled satisfyingly with any of the previously used models.

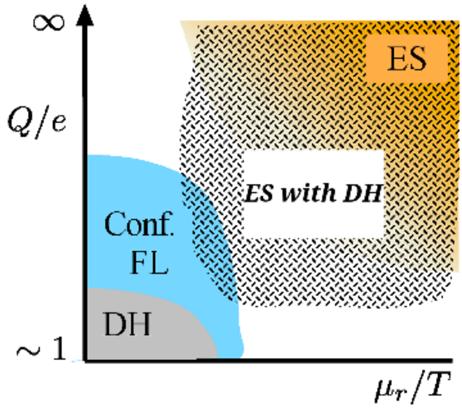

Figure 6.12: Applicability of various approximations as a function of $\mu_r \equiv e\mu/m$ and the ratio of the fermion charge and the total charge of the system, e/Q: Dirac hair, electron star, confined Fermi liquid and our present model. Dirac hair and electron star are the simplest and most flexible approximations but limited to extreme corners of the μ_r axis.

By studying the free energy of the system as well as the spectra and the number of Fermi surfaces we have contructed the phase diagram of the system and analyzed the phase transitions. Most importantly, we find a *universal first order phase transition from finite density to zero density (Reissner-Nordström, quantum critical) phase.* The discontinuity of the density comes from the quantum term in the internal energy. This term is always present but its relative contribution to the free energy decreases with the inverse of the fermion charge as $1/e$. The extreme limit $e \to \infty$ thus reproduces the continuous phase transition found in [52]. Nevertheless, in any real system with finite fermion charge the discontinuity will be present, which fits neatly into the general expectation that the thermal phase transition of a fermionic system should be of van der Waals (liquid-gas, Ising) type.

The finite density phase is further divided into two regimes corresponding to low and high values of the ratio $e\mu/m$ or, more precisely, level number N, that encompass the known limits of Dirac hair [18] and electron star [51]. The transition manifests itself as a line of crossover points which end with a BKT quantum phase transition to the RN phase. The BKT transition fits nicely in the RG interpretation of holography in the following way. Firstly, the log-oscillatory region studied in [27] can be understood as a limit cycle of RG describing a conformal quantum mechanical system (i.e. a conformal theory in $1+1$ dimensions) [106]. Then, instability of the limit cycle generically happens through a BKT transition.

It is illustrative to discuss our model in some more detail in the context of earlier work in the field: electron star [51], Dirac hair [18] and the confined Fermi liquid [96]. All models use the same microscopic action, however they differ in the approximations made in order to to solve it. It is helpful to introduce a combination of all parameters e, μ, m that one might dub "reduced chemical potential":

$$\mu_r \equiv \frac{e\mu}{m}. \tag{6.6.83}$$

Electron star is the fluid limit of the equations of motion, yielding the Openheimer-Volkov equations in the bulk. As explained in [19], this approximation is valid in the limit of large chemical potential: $\mu_r \to \infty$. Dirac hair makes the opposite assumption, treating the bulk fermion as a single collective excitation, which becomes exact in the limit $\mu_r \to 0$. Finally, the confined Fermi liquid of [96] is essentially a non-local version of Dirac hair, which models the bulk as a non-interacting Fermi gas, adding individual excitations up to the Fermi energy. This significantly increases the region of applicability but at the cost of substantial practical complications, in particular if one wishes to take into account the backreaction on the metric. This picture breaks down at high chemical potential but works well for reduced chemical potential of order unity (or smaller): $\mu_r \lesssim 1$. Our model makes use of the WKB approximation, thus assuming semiclassical dynamics and large number of energy levels in the bulk. Nevertheless, we do *not* make the assumption of zero energy spacing necessary for the fluid approximation: our model thus works well in the intermediate regime, $\mu_r > 1$. In Fig. 6.12 we give a schematic description of these findings, on a one-dimensional diagram with μ_r and e/Q as control parameters. The ratio of the fermion charge and the total charge, e/Q, is crucial for Dirac hair and for electron stars: the former requires it to be small (otherwise many energy levels are filled and the single-particle approximation is not valid), the latter to be large (otherwise the level separation is too small and the fluid limit does not apply). Our approach does not take the fluid limit and thus does not depend on e/Q. It is shifted toward high μ_r values because of the WKB approximation but – thanks to using the Dirac hair near the boundary – can still cope with lower μ_r

values to some extent.

The next step in our work will be the increase of quantitative accuracy by replacing the WKB approximation with a fully quantum-mechanical density functional method. It is, in fact, not a significant complication compared to the approach of this paper: the recipe for computing the density n will be replaced by a complicated functional of the gauge field and the metric. It needs to be computed iteratively, however our approach requires iterations in any case, to account for the backreaction. We do not expect qualitative changes but some quantitative aspects, e.g. the values of the scaling exponents and the scaling relations might benefit from increased accuracy.

Chapter 7

Discussion and conclusions

We have undertaken this research motivated by the the limitations of field theory and many-body physics to explain the collective behavior of strongly interacting fermions at finite density. Such a situation is not encountered in traditional areas of high energy physics – scattering of fermions is a few-body problem that is perfectly within the reach of perturbative field theory. Strongly correlated fermions at finite density are another story however. Through the lens of holography we have learned a few things about this problem. At best, this is just setting the stage to face the truly deep problems of the field. Still, we feel that even the modest insights we have obtained hinge crucially on the ability of the to penetrate deep into the workings of strongly coupled physics holographic principle and could not be found in another way. More than a calculational tool, AdS/CFT looks to us as a novel viewpoint, connecting many-body and field theory to gravity. Physics on the gravity side often offers not only quantitative results but also a clearer view of physics – for example, phase transition from a quantum critical phase to a stable phase is easily understood as the discharge of an unstable black hole due to the electrostatic repulsion of fermions. We find that the questions we ask are interesting not only for specific condensed matter problems but are also informative in a general field theory context.

The main achievements of this research can be summarized as follows:

1. *The Dirac hair formalism.* The Dirac hair formalism has been the backbone of this work in a formal sense. It not only provides us with a controlled and easy method to calculate various quantities but also a physical view of what we are doing: expectation values are dual

to various fermion currents (bilinears) in the bulk, and the flow equations for field theory propagators are natural bulk extensions of the boundary action. While rather technical, we find the DH important as it allows us to tackle any form of order parameter in principle, to model Cooper pairing, exciton formation, etc. in a unified way.

2. *The holographic Migdal theorem.* The extension of the holographic dictionary that captures the essence of the Fermi surface – a rigid localized object in momentum space, akin to a classical order parameters for bosons – is the holographic Migdal theorem. It leads to the precise conclusion that the Fermi surface after all can indeed be understood in a Landau-Ginzburg-like language: it is a condensate of a certain bulk operator ($\Psi^\dagger_- \Psi_-$) and the jump of the number density Z is the order parameter associated with such a transition.

3. *Phase diagram.* The main conclusion of direct relevance for condensed matter physics is the phase diagram for the Einstein-Maxwell-Dirac system we have found. It predicts a quantum critical region (as opposed to isolated quantum critical points familiar from field theory), which gives way to a FL-like phase with multiple stable fermion quasiparticles (as opposed to a single Fermi surface familiar from field theory). The diagram is thus different from what is usually seen in experiment but not unheard of. For example, multiple Fermi surfaces are indeed seen in heavy fermion systems, explained by the difference between valence and f-shell electrons [80].

4. *Fermi liquid stability.* The closest we have come to the original goal of understanding the fermionic physics in Fermi liquids is the finding of generic stability of Fermi liquids: NFL-like excitations are only present at the critical point, and generically give way either to AdS_2 metal phase where fermions do not condense into a Fermi surface at all or stable FL-like quasiparticles. In gravity, this is explained by the instability of the extremal RN black hole, which generically discharges into bulk fermions, forming a Lifshitz geometry.

As we have explained at the beginning, quantitative results such as values of critical temperatures etc. cannot be trusted. But qualitative insights are quite instructive already. From the very start we have encountered a zoo of scaling exponents – this is indeed the defining property of the quantum critical AdS-RN Fermi surfaces. But this zoo is replaced by a universal (exponentially narrow or quadratic, depending on if we are in Dirac hair or electron star regime) behavior of the self-energy in the stable phase. While relating the AdS-RN zoo to experiment might be hazardous, the stable phases are easy to identify as they predict quasiparticles which do not depend on microscopic details. The second qualitative lesson is the universal van der Waals first order thermal transition, present in the whole finite density regime. So far only detected in liquid helium, it seems to be a universal property of Fermi surfaces, in sharp contract with the wealth of phases at zero temperature. Thus the simplifying influence of temperature conjectured in the quantum criticality literature [15, 95] is supported by our results. On a more technical level, this result suggests that the fluid limit of the electron star is pathological – it predicts a continuous phase transition that becomes discontinuous in the presence of arbitrarily small but finite level spacing. This is an interesting example of how a model that is perfectly reasonable as a general picture of the bulk physics – the Thomas-Fermi limit which works out so well in a diverse array of situations such as atomic physics and astrophysics – might prove inadequate in a specifically holographic context where we wish to be accurate near the boundary rather than "everywhere" in the interior, and where crucial elements of the boundary physics might depend on seemingly unimportant details in the bulk. Dirac hair itself is another example. There we have an approximation which is in general of poor quantitative accuracy except for very low densities but which is doing well (actually becoming exact) in the UV where it matters most.

The Luttinger theorem has proved to be a central criterion for differentiation between FL and NFL systems. Again, AdS/CFT offers an intuitive picture: the Luttinger theorem is the consequence of the black hole discharge; when no charge hides behind the horizon all of it will show up in the Fermi surface at the boundary. Only what is inside the black hole cannot reach the boundary. The fact that the theorem is badly violated by the NFL-like Fermi surfaces in AdS-RN phase suggests that this system should not be viewed as a zero density system: even though quasiparticle density certainly is zero, it does represent a system with nonzero macroscopic number of fermions, which manage to organize themselves into a FS (except in the truly mysterious AdS_2 phase). We feel that the true nature of the RN phase is still unclear, despite the vast number of works devoted to it.

The first question we have originally asked – what is the gravity dual of a conventional Fermi liquid – we have not managed to answer with complete confidence. This question was fully worked out in [96], and it turns out that the crucial ingredient is to impose the confinement of the quasiparticles by imposing an IR cutoff. We have found the AdS-DH phase which captures the stability, robustness and the quasiparticle of FL systems, but it is just a small corner of the phase containing generically multiple FL-like quasiparticles, culminating in the electron star phase with an infinite tower of Fermi surfaces. The open issue is whether this picture, with many stable quasiparticle excitations, also represents realistic physics which is yet to be discovered experimentally. This is one direction for further work stemming from this thesis.

We were more successful in extending the dictionary. The holographic Migdal theorem is a solid dictionary entry, and it connects the unconventional "order" of the Fermi surface to the Landau-Ginzburg paradigm. In a similar fashion, one can couple the fermion to any order parameter and derive analogous relations for various properties. We regard this as the most promising continuation of our work and we plan to tackle it in near future. In particular, a number of approaches to the problem of high temperature superconductivity starts from the assumption that the ground state in the normal phase is something different from a FL, and unique enough to account both for robust superconductivity and the zoo of order parameters (current loops, stripes, spin dimers, etc) seen in the pseudogap phase [118]. It will be interesting to see what kind of superconductivity will arise from AdS-DH phase. A first step in that direction was accomplished in [29] in the probe limit. But a better chance of reproducing the simple and universal properties of the strange metal phase [111] lies with some stable, backreacted setup more akin to AdS-DH.

We would also like to know what is the role of top-down approaches in this context. We have not explored that at all in this thesis. A problem with AdS/CFT is that one is often not sure what the system one is studying actually is. Lacking the microscopic Hamiltonian means we can judge it only indirectly. Top-down models solve this problem, as the field content is constrained by string theory, and we know exactly the symmetries and operators on the field theory side. An important top-down insight is in [22] where the authors have shown that holographic Fermi surfaces generically exist in top-down approaches.

Another extension of our work will be in the direction of transport phenomena. Adding finite energy and momentum to the flow equations for DH one derives expressions for conductivity. This is of special importance for connecting our results to experiment as a straightforward way to characterize various materials remains the measurement of DC and optical conductivity. The ultimate goal here is the understanding of linear resistivity in the strange metal phase of cuprates and similar materials [118]. In principle, this can be achieved by making the scaling exponent ν os the quasiparticle self-energy a function of an external parameter. This can be achieved e.g. by coupling the fermion to a bosonic order parameter. In that case, there can be a quantum critical point corresponding to $\nu = 1/2$, i.e. with a marginal Fermi liquid scaling which leads to linear resistivity. A puzzle remains however to which degree the phenomenology of the strange metal is dependent on lattice physics which is harder to account for in AdS/CFT.

We close this thesis with a look into future development of the field. Holography seems to be moving away from "Lagrangian-based" physics – for the strongly correlated systems we study, the knowledge of microscopic degrees of freedom would anyway be of little value. We can therefore hope to understand the key qualitative issues in strongly correlated electron physics even though we will not be able to study lattice scale physics and microscopic workings of any material. It remains to be seen if these microscopic details always matter, or if many deep problems in the field can be understood through a simple emergent principle encoded by holography.

References

[1] A. Adams, K. Balasubramanian, J. McGreevy, JHEP **0811**, 059 (2008) [arXiv:0807.1111 [hep-th]].

[2] O. Aharony, S. S. Gubser, J. Maldacena, H. Ooguri, Y. Oz, Phys. Rep. **323**, 183 (1999). [arXiv:hep-th/9905111]

[3] T. Albash, C. V. Johnson, JHEP **0809**, 121 (2008) [arXiv:0804.3466 [hep-th]].

[4] A. Allais, J. McGreevy and X. Josephine Suh, Phys. Rev. Lett **108**, 231602 (2010). [arXiv:1202.5308[hep-th]]

[5] P. W. Anderson, *Basic notions of condensed matter physics*, The Benjamin/Cummings publishing company, Menlo Park, 1984.

[6] X. Arsiwalla, J. de Boer, K. Papadodimas and E. Verlinde, [arXiv:1010.5784 [hep-th]].

[7] G. E. Arutyunov, S. A. Frolov, Nuc. Phys. B **544**, 576 (1999). [arXiv:hep-th/9806216]

[8] K. Balasubramanian, J. McGreevy, Phys. Rev. Lett. **101**, 061601 (2008) [arXiv:0804.4053 [hep-th]].

[9] J. Bekenstein, Phys. Rev. **D7**, 2333 (1973).

[10] R. G. Cai, Z. Y. Nie, B. Wang, H. Q. Zhang, [arXiv:1005.1233 [gr-qc]].

[11] J. C. Campuzano, M. R. Norman, M. Randeria, in *Handbook of Physics: Physics of Conventional and Unconventional Superconductors*, edited by K. H. Benneman and J. B. Ketterson, (Springer Verlag, 2004); [arXiv:cond-mat/0209476]

[12] S. Caron-Huot, P. Kovtun, G. D. Moore, A. Starinets, L. G. Yaffe, JHEP **0612**, 015 (2006) [arXiv:hep-th/0607237].

[13] D. M. Ceperley, Phys. Rev. Lett. **69**, 331 (1992).

[14] H. T. Cho, A. S. Cornell, J. Doukas, W. Naylor, Phys. Rev. D **77**, 016004 (2008) [arXiv:0709.1661 [hep-th]].

[15] P. Coleman, A. J. Schofield, Nature **433** 226 (2005).

[16] R. Contino, A. Pomarol, JHEP **0411**, 058 (2004)

[17] M. Čubrović, J. Zaanen, K. Schalm, Science **325**, 439 (2009) [arXiv:0904.1993 [hep-th]].

[18] M. Čubrović, J. Zaanen, K. Schalm, JHEP **1110**, 017 (2011). [arXiv:1012.5681 [hep-th]].

[19] M. Čubrović, Y. Liu, K. Schalm, Y. W. Sun and J. Zaanen, Phys. Rev. **D84**, 086002 (2011). [arXiv:1106.1798 [hep-th]].

[20] M. Čubrović, J. Zaanen, K. Schalm (2012), to appear.

[21] A. Damascelli, Z. Hussain, Z. X. Shen, Rev. Mod. Phys. **75**, 473 (2003). [arXiv:cond-mat/0208504]

[22] O. De Wolfe, S. S. Gubser, C. Rosen, Phys. Rev. Lett. **108**, 251601 (2012). [arXiv:1112:.3036[hep-th]].

[23] J. de Boer, K. Papadodimas, E. Verlinde, [arXiv:0907.2695 [hep-th]].

[24] P. Di Francesco, P. Mathieu, D. Senechal, *Conformal field theory*, Springer, New York, 1997.

[25] E. D'Hoker, D. Z. Freedman, 2002. [arXiv:hep-th/0201253].

[26] T. Faulkner and J. Polchinski, (2010). arXiv:1001.5049 [hep-th].

[27] T. Faulkner, H. Liu, J. McGreevy, D. Vegh, Phys. Rev. **D83**, 125002 (2011). [arXiv:0907.2694 [hep-th]].

[28] T. Faulkner, N. Iqbal, H. Liu, J. McGreevy, D. Vegh, Science **329**, 1043 (2010). [arXiv:1003.1728 [hep-th]].

[29] T. Faulkner, G. Horowitz, J. McGreevy, M. Roberts, D. Vegh, JHEP **1003**, 121 (2010). [arXiv:0911.3402[hep-th]].

[30] F. Finster, J. Smoller, S. T. Yau, [arXiv:gr-qc/0211043].

[31] F. Finster, J. Smoller, S. T. Yau, Adv. Theor. Math. Phys. **4**, 1231 (2002). [arXiv:gr-qc/0005028].

[32] F. Finster, J. Smoller, S. T. Yau, Nucl. Phys. B **584**, 387 (2000). [arXiv:gr-qc/0001067].

[33] F. Finster, J. Smoller, S. T. Yau, Commun. Math. Phys. **205**, 249 (1999).

[34] E. Fradkin, *Field theories in condensed matter systems*, Addison-Wesley, 1991.

[35] A. Donos, J. P. Gauntlett, N. Kim, O. Varela, JHEP **1012**, 003 (2010). [arXiv:1009.3805[hep-th]]

[36] G. W. Gibbons and S. W. Hawking, Phys. Rev. D **15**, 2738 (1977).

[37] K. Goldstein, S. Kachru, S. Prakash, S. P. Trivedi, JHEP **1008**, 078 (2010). [arXiv:0911.3586 [hep-th]].

[38] S. S. Gubser, I. R. Klebanov, A. M. Polyakov, Phys. Lett. B **428**, 105 (1998). [arXiv:hep-th/9802109]

[39] S. S. Gubser and A. Nellore, *Ground states of holographic superconductors*, Phys. Rev. D **80**, 105007 (2009) [arXiv:0908.1972 [hep-th]].

[40] S. S. Gubser, Phys. Rev. D **78**, 065034 (2008). [arXiv:0801.2977 [hep-th]].

[41] S. S. Gubser, A. Karch, Ann. Rev. Nucl. Part. Sci. **59**, 145 (2009). [arXiv:0901.0935 [hep-th]].

[42] M. Gurvitch, A. T. Fiory, Phys. Rev. Lett. **59**, 1337 (1987).

[43] S. A. Hartnoll, P. K. Kovtun, M. Muller, S. Sachdev, Phys. Rev. B **76**, 144502 (2007). [arXiv:0706.3215 [cond-mat.str-el]].

[44] S. A. Hartnoll, P. Kovtun, Phys. Rev. D **76**, 066001 (2007). [arXiv:0704.1160 [hep-th]].

[45] S. A. Hartnoll, Science **322**, 1639.

[46] S. A. Hartnoll, C. P. Herzog, G. T. Horowitz, Phys. Rev. Lett. **101**, 031601 (2008). [arXiv:0803.3295 [hep-th]].

[47] S. A. Hartnoll, C. P. Herzog, G. T. Horowitz, JHEP **0812**, 015 (2008). [arXiv:0810.1563 [hep-th]].

[48] S. A. Hartnoll, Class. Quant. Grav. **26**, 224002 (2009). [arXiv:0903.3246 [hep-th]].

[49] S. A. Hartnoll, Class. Quant. Grav. **26**, 224002 (2009). [arXiv:0903.3246 [hep-th]].

[50] S. A. Hartnoll, J. Polchinski, E. Silverstein, D. Tong, JHEP **1004**, 120 (2010). [arXiv:0912.1061 [hep-th]].

[51] S. A. Hartnoll, A. Tavanfar, Phys. Rev. D **83**, 046003 (2011). [arXiv:1008.2828 [hep-th]].

[52] S. A. Hartnoll, P. Petrov, Phys. Rev. Lett. **106**, 121601 (2011). [arXiv:1011:6469[hep-th]]

[53] S. A. Hartnoll, D. M. Hofman and D. Vegh, JHEP **2011**, 096 (2011). [arXiv:1105.3197[hep-th]].

[54] S. A. Hartnoll, D. M. Hofman and A. Tavanfar, Europhys. Lett. **95**, 31002 (2011). [arXiv:1011.2502 [hep-th]].

[55] L. Huijse and S. Sachdev, [arXiv:1104.5022 [hep-th]].

[56] M. Henneaux, [arXiv:hep-th/9902137].

[57] M. Henningson, K. Sfetsos, Phys. Lett. B **431**, 63 (1998) [arXiv:hep-th/9803251].

[58] C. P. Herzog, D. T. Son, JHEP **0303**, 046 (2003). [arXiv:hep-th/0212072].

[59] C. P. Herzog, P. Kovtun, S. Sachdev, D. T. Son Phys. Rev. **D75**, 085020 (2007).

[60] G. Horowitz, A. Lawrence, E. Silverstein, JHEP **0907**, 057 (2009). [arXiv:0904.3922[hep-th]].

[61] N. Iizuka, N. Kundu, P. Narayan and S. P. Trivedi, (2011). arXiv:1105.1162 [hep-th].

[62] N. Iqbal, H. Liu, Fortsch. Phys. **57** 367 (2009). [arXiv:0903.2596 [hep-th]].

[63] N. Iqbal, H. Liu and M. Mezei, JHEP **1204**, 73. [arXiv:1105.4621 [hep-th]].

[64] L. Y. Hung, D. P. Jatkar and A. Sinha, Class. Quant. Grav. **28**, 015013 (2011). [arXiv:1006.3762 [hep-th]].

[65] A. Karch, D. T. Son, A. O. Starinets, Phys. Rev. Lett. **102**, 051602 (2009).

[66] I. Kirsch, JHEP **0609**, 052 (2006). [arXiv:hep-th/0607205].

[67] I. R. Klebanov, E. Witten, Nucl. Phys. B **556**, 89 (1999). [arXiv:hep-th/9905104].

[68] P. K. Kovtun, A. O. Starinets, Phys. Rev. D **72**, 086009 (2005). [arXiv:hep-th/0506184].

[69] M. Kulaxizi, A. Parnachev, Nucl. Phys. B **815**, 125 (2009). [arXiv:0811.2262 [hep-th]].

[70] M. Kulaxizi, A. Parnachev, Phys. Rev. D **78**, 086004 (2008). [arXiv:0808.3953 [hep-th]].

[71] H. Kleinert, *Gauge fields in condensed matter*, World Scientific, 1990.

[72] F. Krüger, J. Zaanen, Phys. Rev. **B78**, 035104 (2008). [arXiv:0804.2161[cond-mat]]

[73] L. D. Landau, Zh. Eksp. Teor. Fiz. **30**, 1058 (1956).

[74] R. B. Laughlin, Phys. Rev. Lett. **50**, 1395 (1983).

[75] M .J. Lawler, V. Fernandez, D. G. Barci, E. Fradkin, L. Oxman, Phys. Rev. B **73**, 085101 (2006). [arXiv:cond-mat/0508747v2].

[76] S. S. Lee, Phys. Rev. D **79**, 086006 (2009). [arXiv:0809.3402 [hep-th]].

[77] E. M. Lifshitz, L. P. Pitaevskii, *Statistical physics. Part 2*, Pergamon Press, Oxford, 1980.

[78] J. M. Luttinger, Phys. Rev. **119**, 1153 (1960).

[79] H. Liu, J. McGreevy, D. Vegh, Phys. Rev. **83**, 065029 (2011). arXiv:0903.2477 [hep-th].

[80] H. v. Löhneysen, A. Rosch, M. Vojta, P. Wölfle *Fermi-liquid instabilities at magnetic quantum phase transitions*, Rev. Mod. Phys. **79**, 1015 (2007). [arXiv:cond-mat/0606317 [cond-mat]].

[81] J. Maldacena, Adv. Theor. Math. Phys. **2**, 231 (1998). [arXiv:hep-th/9905111]

[82] J. McGreevy, (2010). [arXiv:0909.0518[hep-th]].

[83] M. Medvedyeva, M. Čubrović, K. Schalm, J. Zaanen, E. Gubankova (2012), to appear.

[84] W. Mueck, K. S. Viswanathan, Phys. Rev. D **58**, 106006 (1998). [arXiv:hep-th/9805145].

[85] E. Mueller, T.-L. Ho, (2004). [arxiv:cond-mat/0403283].

[86] P. Phillips, C. Chamon, Phys. Rev. Lett. **95**, 107002 (2005). [arXiv:cond-mat/0412179]

[87] B. Pioline et al, JHEP **03**, 043 (2005). [arXiv:hep-th/0501169].

[88] J. Polchinski, 1992. [arXiv:hep-th/9210046]

[89] V. G. M. Puletti, S. Nowling, L. Thorlacius and T. Zingg, JHEP **2012**, 73 (2012). [arXiv:1011.6261 [hep-th]].

[90] M. Randeria, A. Paramekanti, N. Trivedi, Phys. Rev. 69 **B**, 144509 (2004). [arXiv:cond-mat/0307217].

[91] S. J. Rey, Prog. Theor. Phys. Suppl. **177**, 128 (2009). [arXiv:0911.5295 [hep-th]].

[92] L. J. Romans, Nucl. Phys. B **383**, 395 (1992). [arXiv:hep-th/9203018].

[93] M. Rozali, L. Brits, (2008). [arXiv:0810.5321 [hep-th]].

[94] M. Rozali, H. H. Shieh, M. Van Raamsdonk, J. Wu, JHEP **0801**, 053 (2008). [arXiv:0708.1322 [hep-th]]. [arXiv:hep-th/0406257].

[95] S. Sachdev, *Quantum Phase Transitions*, Cambridge University Press, Cambridge, 2011.

[96] S. Sachdev, Phys. Rev. **D84**, 066009 (2011). [arXiv:1107.5321 [hep-th]].

[97] S. Sachdev, Phys. Rev. Lett. **105**, 151602 (2010). [arXiv:1006.3794 [hep-th]].

[98] H. J. Schulz, G. Cuniberti, P. Pieri, (1998). in *Field Theories for Low-Dimensional Condensed Matter Systems*, G. Morandi, P. Sodano, A. Tagliacozzo, V. Tognetti, Eds. (Springer, Berlin, 2000), chap. 2. [arXiv:cond-mat/9807366].

[99] T. Senthil, Phys. Rev. B **78**, 035103 (2008). [arXiv:0803.4009v2 [cond-mat.str-el]].

[100] R. Shankar, Rev. Mod. Phys. **66**, 129 (1994).

[101] H. H. Shieh, G. van Anders, JHEP **0903**, 019 (2009). [arXiv:0810.1661 [hep-th]].

[102] J.H. She, J. Zaanen, Phys. Rev. **B80**, 184518 (2009). [arXiv:0905.1225 [cond-mat]].

[103] D. T. Son, Phys. Rev. D **78**, 046003 (2008). [arXiv:0804.3972 [hep-th]].

[104] D. T. Son, A. O. Starinets, Ann. Rev. Nucl. Part. Sci. **57**, 95 (2007). [arXiv:0704.0240 [hep-th]].

[105] D. T. Son, A. O. Starinets, JHEP **0209**, 042 (2002). [arXiv:hep-th/0205051].

[106] D. B. Kaplan, J.-W. Lee, D. T. Son, M. A. Stephanov, Phys. Rev. D **80**, 125005 (2009). [arXiv:0905.4752[hep-th]].

[107] L. Susskind, J. Math. Phys **36**, 6377 (1995). [arXiv:hep-th/9409089].

[108] R. C. Tolman, Phys. Rev. D **55**, 364 (1939).

[109] M. Troyer, U. J. Wiese, Phys. Rev. Lett. **94**, 170201 (2005).

[110] A. M. Tsvelik, *Quantum field theory in condensed matter physics*, Cambridge University Press, Cambridge, 2003.

[111] D. van de Marel *et al.*, Nature **425** (2003) 271.

[112] C. M. Varma, Z. Nussinov, W. van Saarloos, Phys. Rep. **361**, 267 (2002). [arXiv:cond-mat/0103393].

[113] D. N. Voskresenskii and A. V. Senatorov, Sov. J. Nucl. Phys **36**, 208 (1982).

[114] E. Witten, Adv. Theor. Math. Phys. **2**, 253 (1998). [arXiv:hep-th/9802150].

[115] E. Witten, Adv. Theor. Math. Phys. **2**, 505 (1998). [arXiv:hep-th/9803131].

[116] J. Zaanen, Nature **430**, 512 (2004).

[117] J. Zaanen, Science **319**, 1205 (2008).

[118] J. Zaanen (2010), in *100 years of superconductivity*, (eds. H. Rochalla and P. H. Kes), Chapman and Hall, in press. [arXiv:1012.5461[cond-mat]].

[119] J. Zaanen, F. Krueger, J. H. She, D. Sadri, S. I. Mukhin, Ir. J. Phys. Res. **8**, 111 (2008). [arXiv:0802.2455[cond-mat]].

[120] A. B. Zamolodchikov, Pis'ma Zh. Eksp. Teor. Fiz. **43**, 565 (1986).

[121] X. J. Zhou, T. Cuk, T. Devereaux, N. Nagaosa, Z.-X. Shen, in *Handbook of High-Temperature Superconductivity: Theory and Experiment*, edited by J. R. Schrieffer, (Springer Verlag, 2007); [arXiv:cond-mat/0604284]

[122] G. 't Hooft, 1993. [arXiv:gr-qc/9310026]

Summary

This thesis is devoted to the physics of strongly interacting electron systems from the viewpoint of a string-theoretical paradigm known as the holographic principle. The idea is to bridge the gap between two seemingly disconnected areas: gravity and quantum fields. The arena of strongly interacting electrons is a prime example which could benefit from such a connection, for both fundamental and practical reasons. In order to understand how, let us first take a closer look at how gravity and quantum fields are related by the holographic principle.

Holography is motivated by the realization that the entropy of a black hole scales with its area. As the entropy determines the information content (and eventually the number of degrees of freedom) of a black hole, we can conclude that the information carried in a black hole can be "written" on its surface. In other words, all of its degrees of freedom are captured by a suitably defined object spanning its surface, not its volume. This has prompted 't Hooft and Susskind to conjecture that, quite generally, the dynamics in a curved spacetime, in the presence of gravity, can be equivalently thought of as a quantum field in flat spacetime with one dimension less. Finally, in 1997, Maldacena constructed an explicit example, showing that a conformal field theory (CFT – a highly symmetric field theory, invariant with respect to length rescaling at every point) is the "image" of gravity in a space with a certain specific geometry, known as Anti-de Sitter (AdS) space. The connection is in the form of a duality, meaning that the partition functions of D-dimensional CFT and $D+1$-dimensional AdS gravity are equal. That opens a way to calculate correlation functions, expectation values, stress tensors and other quantities on the CFT side. The list of such correspondences is known as the holographic dictionary. Importantly, AdS/CFT is a weak/strong duality, meaning that weakly coupled gravity in AdS_{D+1} is dual to a strongly coupled quantum field theory. Weakly coupled gravity is just its classical limit, i.e. general

relativity, which is relatively well studied and a wealth of exactly solvable models exists. On the other hand, strongly coupled field theory is out of reach of perturbative techniques and thus poorly known.

This goes double for fermion systems to which this thesis is devoted. The core issue comes from the simple fact that fermions obey Fermi-Dirac statistics – meaning that their wave functions are antisymmetric and the density matrix of a many-fermion system will contain negative contributions. This in turn leads to the so-called "fermion sign problem": the partition function acquires negative contributions, which ruins its probabilistic interpretation. Therefore, the formalism of statistical mechanics (or, equivalently, Euclidean field theory) is not applicable. At weak coupling, the Landau Fermi liquid theory provides a controlled approximation scheme: the interacting system behaves as a gas of quasiparticles. A wealth of interesting systems is however outside this weakly coupled regime. The prime example is the strange metal phase of high-temperature superconductors, which shows distinctly non-Fermi liquid behavior, with its universal scaling laws such as linear resistivity scaling with temperature. It is here that we see a great opportunity to apply the AdS/CFT correspondence: it is a unique tool which provides an insight into the problem of strongly interacting fermions in a controlled way. While we are not yet able to arrive at a realistic model of any condensed-matter system, we study the universal features characterizing the holographic fermions.

We start our research by looking at the quantum-critical fermion systems. These systems have a quantum phase transition – a zero temperature transition driven by quantum, not thermal fluctuations. Quite a number of materials is conjectured to slip from a Fermi liquid to a non-Fermi liquid by passing through a quantum critical point. The gravity dual turns out to be a charged black hole in AdS space, with zero fermion density in the bulk. We study in detail the spectrum of the the system, and find gapless excitations around specific values (E_F, k_F) of energy and momentum, which are clearly to be identified with the Fermi energy and Fermi momentum. We thus find holographic Fermi surfaces. Tuning the parameters of the system, we find both stable, narrow peaks corresponding to Fermi liquids, and unstable peaks with exotic and nonuniversal features such as particle-hole asymmetry, of distinctly non-Fermi liquid kind. This is in line with the expectation that the charged black hole describes a quantum critical point: it is a point from which the system might evolve either towards a Fermi or a non-Fermi liquid.

The natural step now is to see where the system flows away from the critical point, i.e. what happens when the black hole becomes unstable. The gravity picture is that of pair production in an electrostatic and gravitational field: some of the pair-produced fermions will orbit the black hole, making it unstable. The result is a novel geometry on the gravity side, and thus a novel system on the field theory side. We have dubbed this model a black hole with Dirac hair. We find that it contains only stable Fermi-liquid quasiparticles, while the unstable ones go away. After some algebra, one can obtain from the gravity side a number of results of the Fermi liquid theory. We therefore have a solid gravity dual to a Fermi liquid.

Our next goal is the exploration of the full parameter space and understanding of all possible ground states. It is found that this holographic Fermi liquid is unexpectedly robust: in the whole parameter space, the stable quasiparticles dominate the spectrum as soon as one moves away from the quantum critical (charged black hole) phase, which shows definite characteristics of a non-Fermi liquid. Somewhat unexpectedly, even in the strongly coupled setup of AdS/CFT, Fermi liquids are ubiquitous – and only disappear when quantum-critical behavior develops. It is conceivable that different, more involved gravity models would give a richer spectrum of non-Fermi liquid phases. The transition between the two phases is of the Berezhinsky-Kosterlitz-Thouless (BKT) type, i.e., of infinite order. Clearly, it has nothing to do with vortices but with a specific instability of the non-Fermi liquid (in technical terms, it manifests itself as the merger of two fixed points of the RG flow).

In conclusion, we have observed previously unknown forms of fermionic quantum criticality by employing the AdS/CFT correspondence, and obtained a proof of Fermi liquid stability from the theory of gravity. The former points to the ability of AdS/CFT to bring new developments into the field of many-body physics, while the latter is an important check, reproducing the best established result of conventional condensed-matter theory. We are still at the very beginning of holographic studies of quantum matter, but there is good reason to believe that these studies have the potential to bring entirely new results to the field.

Samenvatting

Dit proefschrift is gewijd aan de studie van sterk gecorreleerde elektron systemen vanuit een snaartheoretisch perspectief, via het zogenoemde holografisch principe. In essentie relateert dit principe twee onderwerpen uit de theoretische natuurkunde, die niets met elkaar te maken lijken te hebben; zwaartekracht en kwantumveldentheorie. Deze connectie is wellicht in het bijzonder van nut voor sterk gecorreleerde elektronsystemen, vanuit zowel fundamentele als praktisch oogpunt. Om dit te begrijpen, is het noodzakelijk om bovengenoemde correspondentie te verduidelijken.

Aan de basis van het holografisch principe ligt de studie van zwarte gaten. Aangezien de entropie van een zwart gat evenredig is met de oppervlakte van zijn horizon, en deze entropie kan worden opgevat als een hoeveelheid informatie (en uiteindelijk het aantal vrijheidsgraden), kan men concluderen dat de oppervlakte van de horizon codeert voor de informatie van het zwarte gat. Anders gezegd, de vrijheidsgraden worden bepaald door de oppervlakte en niet door het volume van het zwarte gat. Dit bewoog 't Hooft en Susskind ertoe om te postuleren dat, heel algemeen, de dynamica van een gekromde ruimtetijd (i.e. ruimtetijd in aanwezigheid van zwaartekracht) evengoed kan worden beschouwd als een kwantumveldentheorie in een Minkowski-ruimte in een dimensie lager. Uiteindelijk vond Maldacena in 1997 een expliciet voorbeeld van deze veronderstelling in de vorm van de AdS/CFT correspondentie. Hierin wordt aangetoond dat een conforme veldentheorie (CFT - een veldentheorie die invariant is onder hoekgetrouwe transformaties, i.e transformaties die lengtes herschalen maar hoeken gelijk houden) in verhouding staat tot een specifieke ruimtetijd geometrie, de Anti-de Sitter ruimte (AdS). Deze correspondentie betreft een vorm van dualiteit, hetgeen betekent dat de partitiefuncties in de D dimensionale veldentheorie en $D+1$ dimensionale AdS zwaartekrachttheorie gelijk zijn. Als gevolg kan men correlatiefuncties, verwachtingswaarden, de energie-impuls-tensor en andere grootheden via deze dualiteit berekenen. In feite heeft men een holografisch woordenboek van specifieke correspondenties. Een van de belangrijkste eigenschappen van de AdS-CFT correspondentie is het feit dat het een sterk/zwakke dualiteit betreft. Namelijk, een zwak gecorreleerd probleem in AdS_{D+1} is duaal aan een sterk gecorreleerde kwantumveldentheorie. Zwak wisselwerkende zwaartekracht, d.w.z. de algemene relativiteitstheorie, is uitgebreid bestudeerd en tal van gevallen zijn dan ook daadwerkelijk opgelost. Daarentegen zijn sterk gecorreleerde kwantumveldentheorien niet op te lossen met behulp van storingsrekening, en daardoor slechts oppervlakkig begrepen.

De situatie voor fermionsystemen, die het onderwerp van dit proefschrift vormen, is problematischer. Dit komt omdat fermionen een halftallige spin hebben en dus aan de Fermi-Dirac statistiek gehoorzamen. Hierdoor zijn de bijbehorende golffuncties antisymmetrisch en bevat de dichtheidsmatrix negatieve bijdragen, waardoor die niet probabilistisch geinterpreteerd kan worden. Het formalisme van de statistische mechanica (ofwel Euclidische veldentheorie) is dan niet langer van toepassing. Wanneer de interacties zwak zijn biedt Landau-Fermi-vloeistoftheorie uitkomst als gecontroleerd benaderingsschema: het wisselwerkende system gedraagt zich als een gas van quasideeltjes. Er zijn echter tal van interessante systemen die niet zwak gekoppeld zijn. Een van de bekendste voorbeelden is die van hoge-temperatuur supergeleiders, die zich niet als Fermi vloeistof gedragen. Voor dit soort systemen zien we veel mogelijke winst bij het toepassen van de AdS/CFT correspondentie; het is een geweldig instrument om sterk wisselwerkende fermion systemen te analyseren op een gecontroleerde manier. Hoewel we met AdS/CFT nog niet een realistisch model voor een probleem uit de gecondenseerde materie aankunnen, kunnen we wel kenmerkende universele eigenschappen van holografische fermionsystemen bestuderen.

In ons onderzoek kijken we allereerst naar kwantum-kritische fermionsystemen. Deze systemen hebben een kwantum-faseovergang – dat is een faseovergang bij nul temperatuur die veroorzaakt wordt door kwantum fluctuaties, en niet door thermische fluctuaties. Van veel materialen is gesuggereerd dat deze een kwantum-faseovergang kennen van een Fermi-vloeistof naar een niet-Fermi vloeistof. In de duale zwaartekracht-taal wordt dit beschreven met een geladen zwart gat in de AdS ruimte, met een fermionendichtheid in de bulk gelijk nul. We hebben in detail het spectrum van dit systeem bestudeerd. Wij vinden excitaties bij een specifieke energie E_F en impuls k_F die we duidelijk kunnen identificeren met de Fermi energie en Fermi impuls. Wij hebben dus holografisch Fermi-oppervlakken gevonden. Door met de parameters van het model te spelen vinden we zowel stabiele scherpe pieken die we kennen van de Fermi vloeistof, maar ook instabiele pieken met exotische en ongewone eigenschappen (zoals deeltjes-gat asymmetrie) die typerend zijn voor niet-Fermi vloeistoffen. Dit klopt met de verwachting die we hebben van het kwantum-kritische punt: van daar uit kan het systeem zowel een Fermi vloeistof alsook een niet-Fermi vloeistof worden.

De logische vervolgstap is om te onderzoeken hoe dit systeem zich gedraagt net voorbij het kwantum-kritische punt, dat wil zeggen: wat gebeurt er als het zwarte gat instabiel wordt? Aan de zwaartekrachtkant zien wij paar productie in een electrostatisch en zwaartekrachtsveld. Een deel van de fermionen die ontstaan in de paar-productie komt in een baan om het zwarte gat, waardoor dit instabiel wordt. Het resultaat is een nieuwe metriek aan de zwaartekrachtszijde, en dat komt overeen met een nieuw systeem aan de velden-theoretische kant. We hebben dit nieuwe model "een zwart gat met Dirac haar" genoemd. Het blijkt dat dit systeem alleen maar stabiele Fermi-vloeistof quasideeltjes bevat; de instabiele excitaties zijn verdwenen. Met wat wiskundige trucs kunnen we aan de zwaartekrachtskant een aantal resultaten vinden die gelijk zijn aan een Fermi-vloeistof. We hebben daarom een overtuigende duale beschrijving van de Fermi-vloeistof gevonden.

Ons volgende doel is om dit systeem te begrijpen voor alle mogelijke parameters in alle mogelijke grondtoestanden. Onze holografische Fermi vloeistof blijkt echter onverwacht robuust: voor alle parameters wordt het spectrum gedomineerd door de stabiele quasideeltjes zolang we niet in de kwantum-kritische fase (het geladen zwarte gat, dat duidelijk een niet-Fermi vloeistof signatuur heeft) zitten. Het is ietwat onverwacht dat zelfs in de sterke-koppelingstheorie de Fermi vloeistof overal opduikt – en alleen verdwijnt in het kwantum-kritisch regime. Overigens is het goed voor te stellen dat andere, meer gecompliceerde zwaartekrachtsmodellen meer mogelijke niet-Fermi vloeistof fases kunnen beschrijven. De overgang tussen de twee genoemde fases is van het Berezhinsky-Kosterlitz-Thouless type, oftewel een oneindige-orde faseovergang. De overgang heeft niets met vortices te maken maar eerder met een specifieke instabiliteit van de niet-Fermi vloeistof; in technische termen komt het neer op het samengaan van twee vaste punten in de renormalisatiegroep-stroom. We hebben daarmee een nieuw voorbeeld gevonden van een niet-topologische Berezhinsky-Kosterlitz-Thouless overgang binnen de holografische theorie.

Samenvattend: we hebben tot nu toe onbekende vormen van fermionische kwantum kritikaliteit in AdS/CFT bestudeerd, waarbij we een bewijs gevonden hebben voor de stabiliteit de Fermi vloeistof aan de zwaartekrachtskant. Het eerstgenoemde toont de mogelijkheden aan van het gebruik voor AdS/CFT om vooruitgang te boeken in het onderzoek naar veeldeeltjes fysica. Het tweede is een belangrijke toets waarbij het bestbekende resultaat van de gecondenseerde materie wordt gereproduceerd. We staan slechts aan het begin van het holografisch onderzoek naar kwantummaterie, maar er zijn goede redenen om te geloven dat dit onderzoek de potentie heeft om compleet nieuwe inzichten in de gecondenseerde materie te genereren.

List of Publications

- *Fractional kinetic model for chaotic transport in nonintegrable Hamiltonian systems*, M. Čubrović, Phys. Rev. **E72**, 025204 (2005).
- *Semistiff polymer model of unfolded proteins and its application to NMR residual dipolar couplings*, M. Čubrović, O. I. Obolensky, A. V. Solov'yov, Eur. Phys. Jour. **D51**, 41 (2009).
- *String theory, quantum phase transitions, and the emergent Fermi liquid*, M. Čubrović, J. Zaanen, K. Schalm, Science **325**, 439 (2009) [arXiv0904:1993 [hep-th]].
- *AdS Black Holes with Dirac Hair*, M. Čubrović, J. Zaanen, K. Schalm, JHEP **1110**, 017 (2011) [arXiv:1012.5681 [hep-th]].
- *Holographic fermions in external magnetic fields*, E. Gubankova, J. Brill, M. Čubrović, K. Schalm, P. Schijven and J. Zaanen, Phys. Rev. **D84**, 106003 (2011) [arXiv:1011.4051 [hep-th]].
- *Spectral probes of the holographic Fermi ground state: dialing between the electron star and AdS Dirac hair*, M. Čubrović, Y. Liu, K. Schalm, Y. W. Sun and J. Zaanen, Phys. Rev. **D84**, 086002 (2011) [arXiv:1106.1798 [hep-th]].

Curriculum Vitæ

On the 4th of May 1985 I was born in Belgrade, Serbia. From 1992 till 2004 I received my primary and secondary education. In the fall of 2004 I started my studies at the Department of Physics, University of Belgrade. In December 2008 I defended my diploma thesis in Theoretical Physics, in the field of topological defects in quantum critical spin systems.

My research training started at the Petnica Science Center (Valjevo, Serbia) during high school, as a participant of Astronomy seminars, doing research on asteriods and dynamical astronomy. During my university years I was attending Astronomy seminars as a junior associate but my research crossed into Physics, first towards nonlinear dynamics and chaos (in collaboration with the Institute of Physics, Belgrade), then to nanosystems and polymers (in collaboration with the Institute for Advanced Studies, Frankfurt), and finally to quantum matter (again at the Institute of Physics, Belgrade). The last field determined the choice of the topic for my PhD.

In February 2009 I started my PhD studies at the Lorentz Institute, Leiden University, on the AdS/CFT correspondence and strongly interacting fermions. During this time I also became interested in other aspects of holography, as well as in quantum criticality in general. During the PhD years I participated in several workshops and conferences where I presented my work, and gave seminars at universities in the Netherlands, Serbia and the United States. In addition to research I performed occasional teaching activities, as a teaching assistant on the course Condensed Matter Theory at Leiden University and as a lecturer at the Petnica Science Center.

Stellingen

behorende bij het proefschrift

Holography, Fermi surfaces and criticality

1. Wavefunction renormalization Z, i.e. the jump of number density $n(k)$ at the Fermi surface $k = k_F$ is the Landau-Ginzburg order parameter of a holographic Fermi liquid.

   This thesis, Chapter 4.

2. At high temperatures holographic Fermi liquids undergo a first order phase transition to the phase dual of a charged black hole.

   This thesis, Chapter 5.

3. In the phase diagram of holographic fermions a continuous phase transition separates the Fermi liquid phase from the quantum critical AdS_2 metal phase.

   This thesis, Chapter 5.

4. The empirical stability of Fermi liquids has its gravity dual in the fact that an extremely broad class of systems with bulk fermions develops a Lifshitz horizon in the interior of the AdS space.

5. The accuracy of calculations of field-theoretic quantities in AdS/CFT is not simply related or directly proportional to the accuracy of calculations on the gravity side.

6. Even if of little use for the understanding of high-T_c superconductivity, the many elaborate models proposed to explain it such as emergent gauge theories, resonant valence bonds etc. have contributed much to broadening the horizons and the arsenal of methodological tools available in many-body physics.

7. The importance of knowing the Lagrangian/Hamiltonian of a physical system is overrated. At strong coupling it doesn't help much.

8. The purpose of computational physics is not to replace analytical work but only to help it. The goal of science is insight, not numbers, and insight only comes from analytical considerations.

9. Quality of text is an example of a non-extensive property: improving several paragraphs individually might still *decrease* the quality of the whole.

Mihailo Čubrović,
27 February 2013